COLLECTED PAPERS on Off-shell Science

Vol. 33

January 2018 – December 2018

Motoichi OHTSU[1,2]

1 Chief Director,

(General Incorporated Association)

Research Origin for Dressed Photon

2 Prof. Emeritus, The University of Tokyo

MEMBERS

(From April 1, 2018)

[I] RESEARCH ORIGIN FOR DRESSED PHOTON (RODREP) *

Chief Director

Motoichi OHTSU**	(Dr. Eng.)

Directors

Hidefumi HORI	(Dr. Eng.)
Masayuki NAYA	(Dr. Eng.)
Hirofumi SAKUMA	(PhD.)
Teruo MURAKAMI	

Auditor

Satoshi SUGIURA

Advisors

Izumi OJIMA	(Dr. Sci.)
Junji MIYAHARA	(Dr. Eng.)
Masuo FUKUI	(Dr. Eng.)
Tadashi KAWAZOE	(Dr. Sci.)

Visiting Scientists

Hayato SAIGO	(Dr. Sci.) (Nagahama Inst. Bio-Sci. and Tech.)
Kazuya OKAMURA	(Dr. Sci.) (Nagoya Univ.)
Itsuki BANNO	(Univ. Yamanashi)
Hiroshi ANDO	(Dr. Sci.) (Chiba Univ.)
Suguru SANGU	(Dr. Eng.) (Ricoh Co. Ltd.)

Secretary

Mari KAZAMA

(*)（General Incorporated Association）Research Origin for Dressed Photon
(RODreP)
Phone: 090-1603-0562
E-mail: rodrep-general@rodrep.or.jp
URL: http://www.rodrep.or.jp
(Labs.)
c/o Yokohama Technology Center, NICHIA Corp.
3-13-19 Moriya-cho, Kanagawa-ku, Yokohama-shi, Kanagawa 221-0022, Japan
(Executive office)
Foundation for the Promotion of Engineering Research,
c/o Institute of Engineering Innovation, School of Engineering,
The University of Tokyo,
2-11-16 Yayoi, Bunkyo-ku, Tokyo 113-8656, Japan

（一般社団法人）ドレスト光子研究起点
Phone: 090-1603-0562
E-mail: ohtsu@nanophotonics.t.u-tokyo.ac.jp
URL: http://www.rodrep.or. jp
（研究所）
〒221-0022　神奈川県横浜市神奈川区守屋町 3－13－19
日亜化学工業（株）　横浜技術センター　1 階
（事務局）
一般財団法人　総合研究奨励会
〒113-8656　東京都文京区弥生 2-11-16　東京大学大学院工学系研究科
総合研究機構内

（**）Professor Emeritus, The University of Tokyo and Tokyo Institute of Technology
東京大学名誉教授、東京工業大学名誉教授

LIST OF PAPERS

[I] ORIGINAL PAPERS

N.A.

[II] PRESENTATIONS IN INTERNATIONAL CONFERENCES

[1] M. Ohtsu, “High-power Silicon Light-emitting Diodes and Lasers by Dressed Photons,” Proceedings and Abstract Book of the European Advanced Materials Congress (EAMC2018), August 20-23, 2018, Stockholm, Sweden, p.7
[IAAM Medal Lecture]

[2] T. Kawazoe and M. Ohtsu, “High power Si light emitting device using dressed photon,” Abstract of the 7th Advanced Lasers and Photon Sources (ALPS2018), April 24-27, 2018, Yokohama, Japan, paper number ALPS9-G1-2.

[III] REVIEW PAPERS

N.A.

[IV] PREPRINT DEPOSITORIES

[IV-1] OFF-SHELL ARCHIVE

[Original papers]

[1] I. Banno and M. Ohtsu, "Logical Fallacy of using the Electric Field in Non-resonant Near-field Optics", Off-shell Archive (August 2018), Offshell:1808O.001.v1.
DOI:10.14939/1808O.001.v1

[2] M. Ohtsu and T. Kawazoe, "High-Power Infrared Silicon Light-emitting Diodes Fabricated and Operated using Dressed Photons," Off-shell Archive (April 2018), Offshell:1804O.001.v1.
DOI:10.14939/1804O.001.v1

[Review papers]

[1] M. Ohtsu, "Embarking on theoretical studies for off-shell science," Off-shell Archive (November 2018), Offshell:1811R001.v1.
DOI:10.14939/1811R001.v1

[2] M. Ohtsu, T. Kawazoe, "Gigantic Ferromagnetic Magneto-Optical Effect in a SiC Light-emitting Diode Fabricated by Dressed-Photon–Phonon-Assisted Annealing," Off-shell Archive (September 2018), OffShell: 1809R.001.v1.
DOI:10.14939/1809R.001.v1

[3] M. Ohtsu and T. Kawazoe, "Principles and Practices of Si Light Emitting Diodes using Dressed Photons," Off-shell Archive (May 2018), Offshell:1805R.001.v1.
DOI:10.14939/1805R.001.v1

[4] M. Ohtsu and T. Kawazoe, "Experimental estimation of the maximum size of a dressed photon," Off-shell Archive (February 2018), Offshell:1802R.001.v1.
DOI:10.14939/1802R.001.v1

[IV-2] arXiv

[1] I. Banno and M. Ohtsu, "Logical Fallacy of using the Electric Field in Non-resonant Near-field Optics," arXiv:1807.10991v1 [phycisc.optics] 29 Jul 2018.

[V] PUBLISHED BOOKS

[1] M. Ohtsu, “Historical Review of Dressed Photons: Experimental Progress and Required Theories,” in *Progress in Nanophotonics* 5, ed. by T. Yatsui, Springer, Heidelberg, October 2018, pp.1-51.

[VI] PRESENTATIONS IN DOMESTIC CONFERENCES

[1] I. Banno and M. Ohtsu, “A Logical Fallacy of Electric Field in the Dressed-Photon Systems,” Abstracts of the 79th Jpn. Soc. Appl. Phys. Autumn Meeting, September 2018, Nagoya, Japan, paper number 19a-437-1.
【坂野斎、大津元一、「ドレスト光子系での電場の概念の破綻」、第 79 回応用物理学会秋季学術講演会予稿集（名古屋、2018 年 9 月）、講演番号 19a-437-1】

[2] I. Banno, T. Kawazoe, and M. Ohtsu, “Diamagnetic Current in the Dressed-Photon Systems, “Abstracts of the 79th Jpn. Soc. Appl. Phys. Autumn Meeting, September 2018, Nagoya, Japan, paper number 19a-437-2.
【坂野斎、川添忠、大津元一、「ドレスト光子系の反磁性電流」、第 79 回応用物理学会秋季学術講演会予稿集（名古屋、2018 年 9 月）、講演番号 19a-437-2】

[3] H. Sakuma, I. Ojima, and M. Ohtsu, “A mathematical expression of stationary dressed photon as a composite of timelike and spacelike fields,” Abstracts of the 79th Jpn. Soc. Appl. Phys. Autumn Meeting, September 2018, Nagoya, Japan, paper number 19a-437-3.
【佐久間弘文、小嶋泉、大津元一、「TimelikeとSpacelikeな場の合成による停留状態のドレスト光子の数学的表現」、第79回応用物理学会秋季学術講演会予稿集（名古屋、2018年9月）、講演番号19a-437-3】

[4] S. Sangu, H. Saigo, and M. Ohtsu, “Simulation of Dressed Photon Energy Transfer based on Quantum-Walk Model,” Abstracts of the 79th Jpn. Soc. Appl. Phys. Autumn Meeting, September 2018, Nagoya, Japan, paper number 19a-437-7.
【三宮俊、西郷甲矢人、大津元一、「量子ウォークモデルを用いたドレスト光子エネルギー移動シミュレーション」、第79回応用物理学会秋季学術講演会予稿集（名古屋、2018年9月）、講演番号19a-437-7】

[5] T. Kawazoe and M. Ohtsu, “Consideration of injection current dependence of Si-LED using Stefan-Boltzmann law,” Abstracts of the 79th Jpn. Soc. Appl. Phys. Autumn Meeting, September 2018, Nagoya, Japan, paper number 19a-437-8.
【川添忠、大津元一、「シュテファンボルツマン則によるSi-LED の注入電流依存性の考察」、第79回応用物理学会秋季学術講演会予稿集（名古屋、2018年9月）、講演番号19a-437-8】

[6] S. Sakuma, I. Ojima, and M. Ohtsu, “On the existence of dressed photon constant and its implication,” Abstracts of the 65th Jpn. Soc. Appl. Phys. Spring Meeting, March 2018, Tokyo, Japan, paper number 19p-F310-12.

【佐久間弘文、小嶋泉、大津元一、「ドレスト光子定数の存在可能性とその意味するもの」、第 65 回応用物理学会春季学術講演会予稿集（東京、2018 年 3 月）、講演番号 19p-F310-12】

[7] T. Kawazoe and M. Ohtsu, “Operation with 1W-optical output of Si-LED and current dependence,” Abstracts of the 65th Jpn. Soc. Appl. Phys. Spring Meeting, March 2018, Tokyo, Japan, paper number 19p-F310-13.
【川添忠、大津元一、「Si 発光ダイオードの光出力 1W 動作と電流依存性」、第 65 回応用物理学会春季学術講演会予稿集（東京、2018 年 3 月）、講演番号 19p-F310-13】

[8] I Banno and M. Ohtsu, “Theory of Non-resonant Effect in Near-field Optics Ⅲ: Approach to a Base of Dressed Photon employing Non-linear Response Theory under a Preferable Gauge Condition,” Abstracts of the 65th Jpn. Soc. Appl. Phys. Spring Meeting, March 2018, Tokyo, Japan, paper number 19p-F310-15.
【坂野斎、大津元一、「近接場光学における非線形共鳴効果の理論Ⅲ：非線形応答理論によるドレスト光子の基礎づけの試み、ゲージ条件の検討」、第 65 回応用物理学会春季学術講演会予稿集（東京、2018 年 3 月）、講演番号 19p-F310-15】

[VII] AWARDS

[1] M. Ohtsu, *IAAM Medal*, International Association of Advanced Materials (IAAM), August 22, 2018, Stockholm.

[VIII] APPENDIX

Publications and Presentations by RODreP members.

[II] PRESENTATIONS IN INTERNATIONAL CONFERENCES

[1] I. Ojima, “Micro-Macro duality for Inductions/ Reductions,” Abstract of the 18th Workshop "NONCOMMUTATIVE PROBABILITY, OPERATOR ALGEBLA, RANDOM MATRICES AND RELATED TOPICS, WITH APPLICATIONS", July 15-21, Bedlewo, Poland, date of presentation July 21, 2018.

[IV] PREPRINT DEPOSITORIES

[IV-1] OFF-SHELL ARCHIVE

[Original papers]

[1] I. Ojima, “Micro-Macro Duality for Inductions/ Reductions,” Off-shell Archive (September 2018), Offshell:1809O.001.v1.
DOI:10.14939/1809O.001.v1

[2] I. Banno, “Theory of Single Susceptibility for Near-field Optics Equally Associated with Scalar and Vector Potentials,” Offshell Archive (September 2018), Offshell: 1809O.002.v1.
DOI:10.14939/1809O.002.v1

[3] Izumi Ojima and Hayato Saigo, “Photon localization revisited,” Off-shell Archive (April 2018), Offshell:1804O.002.v1.
DOI:10.14939/1804O.002.v1

[IV-2] arXiv

[1] I. Banno, “Theory of Single Susceptibility for Near-field Optics Equally Associated with Scalar and Vector Potentials,” arXiv:1807.10992v1 [phycisc.optics] 29 Jul 2018.

[V] PUBLISHED BOOKS

[1] H. Sakuma, “Virtual Photon Model by Spatio-Temporal Vortex Dynamics,” in *Progress in Nanophotonics* 5, ed. by T. Yatsui, Springer, Heidelberg, October 2018, pp.53-77.

[2] H. Saigo, “Quantum Probability for Dressed Photons: The Archsine Law in Nanophotonics,” in *Progress in Nanophotonics* 5, ed. by T. Yatsui, Springer, Heidelberg, October 2018, pp.79-106.

[3] I. Ojima, “Control over Off-Shell QFT via Induction and Imprimitivity,” in *Progress in Nanophotonics* 5, ed. by T. Yatsui, Springer, Heidelberg, October 2018, pp.107-136.

[4] K. Okamura, “An Approach from Measurement Theory to Dressed Photon,” in *Progress in Nanophotonics* 5, ed. by T. Yatsui, Springer, Heidelberg, October 2018, pp.137-167.

[5] I. Banno, “Response Theory Supporting Dressed Photons,” in *Progress in Nanophotonics* 5, ed. by T. Yatsui, Springer, Heidelberg, October 2018, pp.169-200.

[VI] PRESENTATIONS IN DOMESTIC CONFERENCES

[1] K. Okamura, “An approach from measurement theory to dressed photon,” Abstracts of the 79th Jpn. Soc. Appl. Phys. Autumn Meeting, September 2018, Nagoya, Japan, paper number 19a-437-4.
【岡村和弥、「ドレスト光子への測定理論的アプローチ」、第79回応用物理学会秋季学術講演会予稿集（名古屋、2018年9月）、講演番号19a-437-4】

[2] H. Ando, “On a mathematical model describing the localization property of dressed photons,” Abstracts of the 79th Jpn. Soc. Appl. Phys. Autumn Meeting, September 2018, Nagoya, Japan, paper number 19a-437-5.
【安藤浩志、「ドレスト光子の局在性を理解する為の数理モデルの検討」、第79回応用物理学会秋季学術講演会予稿集（名古屋、2018年9月）、講演番号19a-437-5】

[3] H. Saigo, ”Dressed Photons from the Viewpoint of Quantum Probability,” Abstracts of the 79th Jpn. Soc. Appl. Phys. Autumn Meeting, September 2018, Nagoya, Japan, paper number 19a-437-6.
【西郷甲矢人、「量子確率論の見地からみたドレスト光子」、第79回応用物理学会秋季学術講演会予稿集（名古屋、2018年9月）、講演番号19a-437-6】

[4] W. Nomura, W. Yamagishi, and T. Kawazoe, ” Development of dispersing method of ZnO quantum dots and dye in EVA resin for wavelength conversion film,” Abstracts of the 79th Jpn. Soc. Appl. Phys. Autumn Meeting, September 2018, Nagoya, Japan, paper number 19a-437-9.
【野村航、山岸 亙、川添 忠、「波長変換膜を目的としたEVA 樹脂への酸化亜鉛量子ドット−色素分散手法の開発」、第79回応用物理学会秋季学術講演会予稿集（名古屋、2018年9月）、講演番号19a-437-9】

[5] T. Kawazoe, K. Hashimoto, and S. Sugiura, “Fabrication and demonstration of stacked Si-LED connected in series,” Abstracts of the 79th Jpn. Soc. Appl. Phys.

Autumn Meeting, September 2018, Nagoya, Japan, paper number 19a-437-13.
【川添 忠、橋本和信、杉浦聡、 「積層型Si-LEDの作製と評価」、第79回応用物理学会秋季学術講演会予稿集（名古屋、2018年9月）、講演番号19a-437-13】

[6] T. Kawazoe, K. Hashimoto, and S. Sugiura, “High Power Homojunction Silicon Laser,” Abstracts of the 65th Jpn. Soc. Appl. Phys. Spring Meeting, March 2018, Tokyo, Japan, paper number 19p-F310-14.
【川添忠、橋本和信、杉浦聡、「高出力ホモ接合シリコンレーザー」、第 65 回応用物理学会春季学術講演会予稿集（東京、2018 年 3 月）、講演番号 19p-F310-14】

[I] ORIGINAL PAPERS

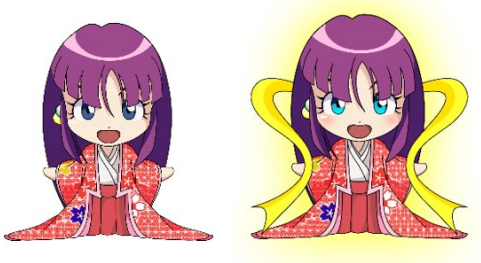

[II] PRESENTATIONS

IN INTERNATIONAL CONFERENCES

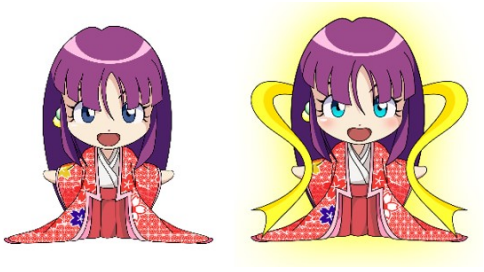

Published online by the VBRI Press

High-power Silicon Light-emitting Diodes and Lasers by Dressed Photons

M. Ohtsu[1,2]

[1](Director-in-chief) Research Origin for Dressed Photon, Yokohama 221-0022, Japan
[2](Professor Emeritus) The University of Tokyo, Tokyo 113-8656, Japan

Table of contents

This keynote talk includes 1. Introduction, 2. Dressed Photon (Fig.1),
3. Fabrication (Fig.2), 4, Operation (Figs.3-5), 5. Future outlook, and 6. Summary.

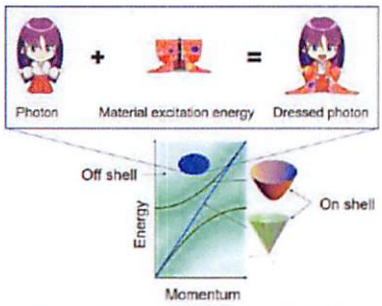

Fig.1 Dressed photon in off-shell.

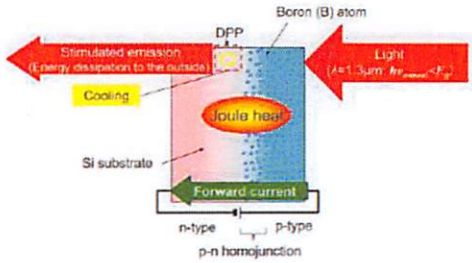

Fig.2 DPP-assisted annealing.

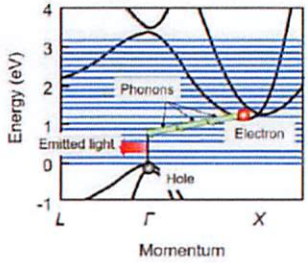

Fig.3 Mechanism of photon emission.

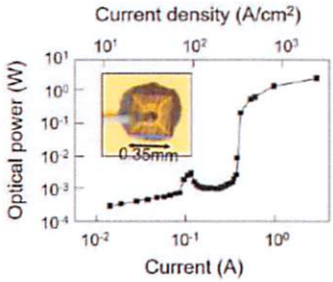

Fig.4 High-power LED.

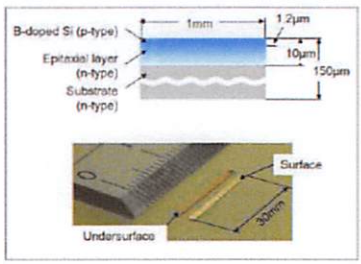

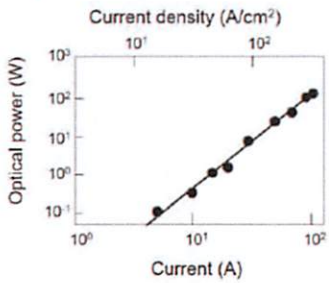

Fig.5 High-power laser.

Abstract

There is a long-held belief in material science and technology that a crystalline silicon (Si), an indirect-transition-type semiconductor, is not suitable for use in light emitting devices. The problem is that the probability of the interaction between an electron-hole pair and phonons is very low. However, it has been solved by using a dressed photon (DP) and a dressed-photon—phonon (DPP), which are novel off-shell quantum fields in a nanometric space[1]. This keynote talks reviews the use of a crystalline Si to construct high-power light emitting diodes (LED) and diode lasers. The spatial distribution of B atoms (p-type dopant) is controlled autonomously by the DPP-assisted annealing to satisfy the momentum conservation law[2]. Besides the fabrication step, DPs and DPPs are also used in the operation of the device. The fabricated devices exhibit a novel property called "photon breeding", which originates from the DPs and DPPs. In photon breeding, the photon energy and photon spin of the light emitted from the device are identical to those of the light that irradiates the crystal during the DPP-assisted annealing. The CW optical power emitted from the fabricated LED was as high as 1 W[3] at 1.3 micron-wavelength. By modifying the device structure of the previously fabricated Si-laser[4], high-power infrared laser device was successfully fabricated by utilizing the very low infrared absorption of crystalline Si. The cavity length was increased to 30 mm to realize high power. After the DPP-assisted annealing, a CW output power as high as 100 W was obtained at 1.9 micron-wavelength[5]. The last part of the speech is devoted to reviewing details of the features of DPs and future outlook of the DP research.

Keywords: Dressed photon, silicon, light emitting diode, laser.

The 7th Advanced Lasers and Photon Sources (ALPS2018), Yokohama, Japan, Apr. 23 - Apr. 27, 2018

High power Si light emission device using dressed photons

Tadashi Kawazoe [1], Motoichi Ohtsu[2]
[1] Institute of Advanced Laser Technology, Tokyo Denki University,
5 Senju Asahi-cho, Adachi-ku, Tokyo, 120-8551, Japan, +81-3-5284-5981.
[2] The University of Tokyo, 2-11-16 Yayoi, Bunkyo-ku, Tokyo 113-8656, Japan
E-mail: kawazoe@mail.dendai.ac.jp

Abstract: *We fabricated Silicon-electro-luminescence devices e.g., a Si-LED and a Si laser. Their optical output powers of them were more than 1 W (Si-LED) and 10 W (Si-LD).*

1. Introduction

Radiative recombination life time of the indirect-transition-type semiconductor between electrons and holes is very long. Therefore, a kind of indirect-transition-type semiconductor Silicon (Si) is not suitable for a light-emitting diode and a semiconductor laser. In spite of the disadvantage, the Si light emitter has been studied due to compatibility with electronics.

In recent years, we have succeeded to demonstrate several near-infrared Si light emitting devices at room temperature fabricated using a phonon-assisted process [1-3]. Their operation principle and fabrication method are based on the photon-phonon interaction via dressed photons [4]. However, some part of emission mechanisms are still not clear. Especially, the influence of the black body radiationrelation on the EL spectrum shuld be discussed. Therefore, I measuer the EL spectra of the Si-LED at low temperature. As a result, the optical output power and efficiency were increased with the decreasing the device temperature drastically. In the presentation, I discuss the temperature dependence of Si-LED. Finally, I review the high power Si-LED and Si-LD.

2. Dressed photon-phonon annealing

The fabrication methods of the Si light emitting device with the p-n junction have already reported [1-3]. First, the p-n homojunction was fabricated by the ion-implanting of a p-dopant (Boron:B) into an n-type Si substrate which was As-doped n-type Si wafer with an electrical resistivity of 5 Ω•cm. The energy of the ion-implantation for the B doping was 700 keV, and the dose density was 5×10^{13} cm^{-2}. Second, in order to optical activation of the Si p-n junction, the fabricated p-n homojunction is annealed by Joule heating causing the foreword injection current. During this annealing process, the p-n homojunction is irradiated by the infrared light. This annealing process has been named DPP (dressed photon-phonon) annealing.

3. Experimental results

Figure 1 shows the EL spectrum of the DPP annealed Si-LED with the device size of $1mm^2$ at 77K. Due to the temperature dependence of the Si band-gap, the emission peak coming from the inter-band transition shifts shorter wavelength. The EL intensity increased drastically with the decreasing the device temperature. This indicates that the emission from the Si-LED does not originates from thermal effect but the electron hole recombination.

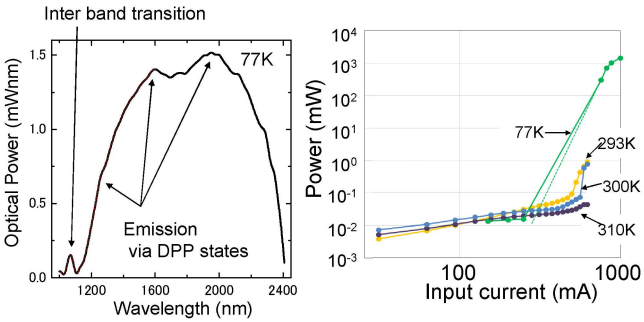

Fig.1. A EL spectrum of Si-LED at 77K and temperature dependence of the optical output power.

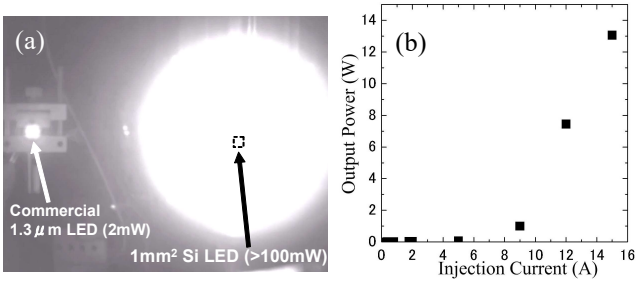

Fig.2. (a) A infrared photograph of emitting Si-LED. (b) Optical output power depending on the injection current of the Si-Laser.

Figure 2 (a) shows the infrared photograph of the Si-LED at the operation power of more than 100mW and the reference commercial 1.3 μm LED at the operation power of 2mW. This Si EL device is applicable to the Si-Laser. Figure 2 (b) shows the fabricate Si-laser by DPP annealing. Its operation output power was reached to more than 10W.

[1] T. Kawazoe, M. Ohtsu, K. Akahane, and N. Yamamoto, Appl. Phys. B 107, 659 (2012).
[2] H. Tanaka, T. Kawazoe, M. Ohtsu, K. Akahane, and N. Yamamoto, Appl. Phys. A 121, 1377 (2015).
[3] J. H. Kim, T. Kawazoe, and M. Ohtsu. Applied Physics A, 123.9 (2017): 606.
[4] Y. Tanaka, K. Kobayashi, Physica E 40, 297 (2007).

[III] REVIEW PAPERS

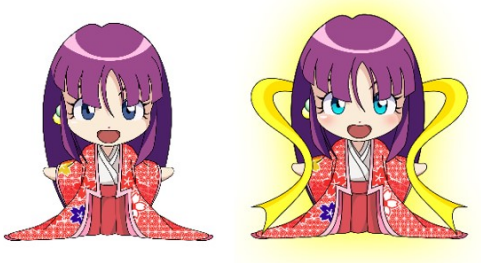

[IV] PREPRINT DEPOSITORIES

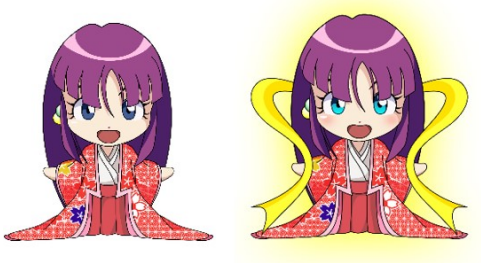

Logical Fallacy of using the Electric Field in Non-resonant Near-field Optics

Itsuki Banno*

Graduate Faculty of Interdisciplinary Research

Faculty of Engineering, University of Yamanashi,

*4-3-11 Takeda, Kofu, Yamanashi, 400-8511, Japan**

Motoichi Ohtsu

Research Origin for Dressed Photon,

c/o Yokohama Technology Center, NICHIA Corporation,

3-13-19 Moriya-cho Kanagawa-ku, Yokohama-shi, 221-0022, Japan

(Dated: July 29, 2018)

Abstract

We find that the electric field is not a suitable physical quantity to describe the response of *a non-metallic material* in the study of *non-resonant* near-field optics. In practice, we show the spin-less one-electron two-level system responds differently to longitudinal and transverse electric fields under the non-resonant condition. This difference originates from *the non-relativistic nature* of the system, and should exist in actual many-electron systems. For this type of system, it is a logical fallacy to use the constitutive equation in terms of the total electric field and the associated permittivity. Recognizing this fallacy, both experimental and theoretical progress is needed in the field of non-resonant near-field optics of non-metallic materials.

PACS numbers: 78.67.-n, 78.20.Bh, 41.20.-q, 42.25.Ja

Keywords: non-resonant condition, non-metallic material, optical near field, response function

*Electronic address: banno@yamanashi.ac.jp

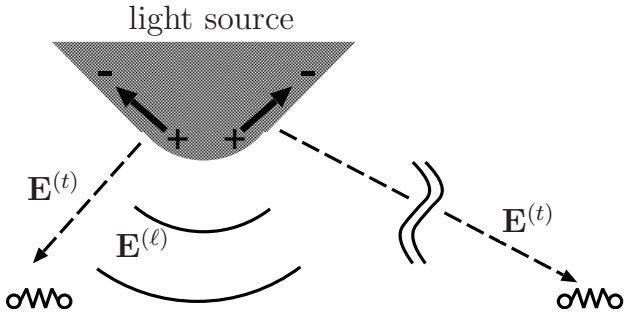

FIG. 1: Target materials under near- and far-field incidences: the former is exposed to the incident longitudinal and transverse electric fields simultaneously (the left side), whereas the latter is exposed to only the transverse field (the right side).

Under *non-resonant conditions* in the optical near field, *non-metallic materials* cause various phenomena not observed in conventional optics, such as highly efficient light emission from indirect-transition-type semiconductors (LED[1, 2] and Laser[2, 3]), chemical reaction with insufficient photon energy (chemical vapor deposition[4], optical near-field lithography[5], optical near-field etching[6]), frequency up-conversion[7, 8], non-adiabatic effect beyond forbidden transition (local energy concentration[9], nano-photonic gate device[10]), and gigantic magneto-optical rotation of the LED[2, 11, 12]. Theoretically, *dressed photons*, namely, the localized electromagnetic field easily coupled with phonons, were introduced to allow non-adiabatic transitions[13–15].

This Rapid communication focuses on another fundamental role of the non-resonant condition in near-field optics (NFO) with non-metallic materials. We examine the one-electron two-level system close to both the light source and the observation point under long wavelength approximation (LWA), and find it a logical fallacy to regard *the total electric field* as causing the response under the non-resonant condition. In contrast, under the resonant condition or the far-field observation condition, the electric field works as expected. These findings originate from *the non-relativistic nature* of the system and should be applicable in actual optical systems with non-metallic materials. For the readability, calculation details are given in the last part of this paper.

Suppose a small-scale material is placed in the vicinity of a nanostructure, which functions as a light source (Fig.1). In such a system, under the NF incidence condition, the target material is exposed to longitudinal and transverse electric fields simultaneously, whereas

in a system under the far-field incidence condition, the target material is exposed only to the transverse field, which survives far from the light source. Therefore, the coexistence of longitudinal and transverse electric fields distinguishes such a system under the NF incidence condition from that under the far-field incidence condition.

Here, the longitudinal electric field originates from the charge density on the nanostructure, obeys Coulomb's law, and has a non-radiative nature to localize around the nanostructure. On the other hand, the transverse electric field originates from the transverse current density on the nanostructure, obeys the Ampere-Maxwell law and Faraday's law, and has a radiative nature allowing it to propagate far from the light source, accompanied by the magnetic field. (The longitudinal current density is determined via the charge conservation law, once the charge density is known, and is not an independent source.) Therefore, the two incidences coexisting in an NF optical system have distinct properties.

Furthermore, owing to *the non-relativistic nature* of the system, the scalar and vector potentials appear in a different manner in the Hamiltonian, which governs the electron response, for example, (13) of *Calculation details* (i) in the last part of this paper. Considering that the scalar and vector potentials under the Coulomb gauge represent the longitudinal and transverse electric fields, respectively, one may confirm that the two types of incidences in NFO cause different responses. Now our question is the following: under what condition can we observe these differences?

Before proceeding with the analysis, let us first classify the optical systems. The two systems under near- and far-field incidence conditions in Fig.1 are subdivided into two classes depending on the near- or far-field observation condition. These four classes are listed in Table I, together with a summary of the results mentioned below. In particular, the systems of (I′) and (II′) are the limiting cases of null longitudinal incidence of the systems (I) and (II), respectively. Thus, in the systems (I′) and (II′), the longitudinal response vanishes and the difference in response may not be observed. In the following, therefore, we focus mainly on systems (I) and (II), in which longitudinal incidence exists.

Microscopic responses to longitudinal and transverse electric fields. Applying the linear response theory and the LWA to the electron system of the target material on a small scale, the induced charge and current densities (*as a result of the response*), $\Delta\rho(\mathbf{r},t)$ and $\Delta\mathbf{j}(\mathbf{r},t)$, are described as the total derivative with respect to the longitudinal and transverse electric fields (*as the cause of the response*), $\Delta\mathbf{E}^{(\ell)}(\mathbf{0},t)$ and $\Delta\mathbf{E}^{(t)}(\mathbf{0},t)$, where $\mathbf{0}$ is the

TABLE I: Classification of optical systems by distance from the target material to the light source and distance from that to the observation point, together with a summary of the results; the validity of the electric field as the cause of the response.

	Near-field observation Source:$\Delta\rho$ and $\Delta\mathbf{j}$	**Far-field observation** Source: $\overline{\Delta\mathbf{j}}$
Near-field incidence : $\Delta\mathbf{E}^{(\ell)} + \Delta\mathbf{E}^{(t)}$	**(I) NF optical system** non-resonant / resonant	**(II) NF optical system** non-resonant / resonant
Validity of the electric field	NG / OK	OK / OK
Far-field incidence : $\Delta\mathbf{E}^{(t)}$	**(I′) NF optical system** non-resonant / resonant	**(II′)conventional optical system** non-resonant / resonant
Validity of the electric field	OK / OK	OK / OK

representative position in the electron system under the LWA:

$$\Delta\rho(\mathbf{r},t) = \chi_j^{\rho\leftarrow(\ell)}(\mathbf{r},\omega)\,\Delta E_j^{(\ell)}(\mathbf{0},t) + \chi_j^{\rho\leftarrow(t)}(\mathbf{r},\omega)\,\Delta E_j^{(t)}(\mathbf{0},t)\,, \tag{1}$$

$$\Delta j_i(\mathbf{r},t) = \chi_{ij}^{\mathbf{j}\leftarrow(\ell)}(\mathbf{r},\omega)\,\Delta \dot{E}_j^{(\ell)}(\mathbf{0},t) + \chi_{ij}^{\mathbf{j}\leftarrow(t)}(\mathbf{r},\omega)\,\Delta \dot{E}_j^{(t)}(\mathbf{0},t)\,, \tag{2}$$

where the partial derivative coefficients, $\chi_{\cdots}^{\cdots}(\mathbf{r},\omega)$'s are susceptibilities (response functions), and Einstein's rule is used for the summation over the vector indices, for example, $\chi_j^{\rho\leftarrow(\ell)}(\mathbf{r},\omega)\,\Delta E_j^{(\ell)}(\mathbf{0},t) = \sum_{j=1}^{3} \chi_j^{\rho\leftarrow(\ell)}(\mathbf{r},\omega)\,\Delta E_j^{(\ell)}(\mathbf{0},t)$. In (2), the time derivatives of the two types of electric fields, namely, $\Delta\dot{E}_j^{(\ell)}(\mathbf{0},t)$ and $\Delta\dot{E}_j^{(t)}(\mathbf{0},t)$, are regarded as the causes, instead of the two types of electric fields themselves. The magnetic response vanishes in the leading order under the LWA ; see Ref.[16]. The derivation of (1) and (2) is given in *Calculation details* (i).

For simple evaluation of the susceptibilities in (1) and (2), suppose we have a spinless one-electron system with two levels, the ground and excited states in the non-perturbed system with eigenenergies, $\hbar\omega_0$ and $\hbar\omega_1$, and orbitals, $\varphi_0(\mathbf{r})$ and $\varphi_1(\mathbf{r})$, respectively. Those orbitals are assumed to be bound states expressed by real functions, carry well-defined and distinct spatial parities (even and odd parities), and form the normalized orthogonal complete set. The excitation energy is $\hbar\Delta\omega_1 \equiv \hbar\omega_1 - \hbar\omega_0 > 0$; this finite excitation energy means that the target is a non-metallic material, such as a molecule, nano-structured semiconductor

and insulator.

The susceptibilities in (1) and (2) are derived in *Calculation details* (ii), and those leading to the induced charge density result in the following:

$$\chi_j^{\rho\leftarrow(\ell)}(\mathbf{r},\omega) = \chi_j^{\rho\leftarrow(t)}(\mathbf{r},\omega) = 2q^2\,\frac{\eta}{\eta^2-1}\,\frac{1}{\hbar\omega}\,\mathcal{D}_j\,\varphi_0(\mathbf{r})\varphi_1(\mathbf{r})\,, \tag{3}$$

$$\text{where} \qquad \eta \equiv \frac{\hbar\Delta\omega_1}{\hbar\omega} = \frac{\text{excitation energy}}{\text{photon energy}}\,, \text{ and} \tag{4}$$

$$\mathcal{D}_i \equiv \int \mathrm{d}^3 r\;\varphi_1(\mathbf{r})\,r_i\,\varphi_0(\mathbf{r})\,. \tag{5}$$

This means that the responses to the longitudinal and transverse electric fields are common, such that the induced charge density has a linear relationship with *the total electric field*, namely, $\Delta\rho(\mathbf{r},t) = \chi_j^{\rho\leftarrow(\ell)\text{ or }(t)}(\mathbf{r},\omega)\left(\Delta E_j^{(\ell)}(\mathbf{0},t) + \Delta E_j^{(t)}(\mathbf{0},t)\right)$.

The susceptibilities leading to the induced current density are not so simple and result in the following:

$$\chi_{ij}^{\mathbf{j}\leftarrow(\ell)}(\mathbf{r},\omega) = \frac{q^2\hbar^2}{m}\,\frac{1}{\eta^2-1}\,\frac{1}{(\hbar\omega)^2}\,\mathcal{D}_j\,\left(\partial_i\varphi_1(\mathbf{r})\varphi_0(\mathbf{r}) - \varphi_1(\mathbf{r})\partial_i\varphi_0(\mathbf{r})\right)\,, \tag{6}$$

$$\chi_{ij}^{\mathbf{j}\leftarrow(t)}(\mathbf{r},\omega) = \eta^2\,\chi_{ij}^{\mathbf{j}\leftarrow(\ell)}(\mathbf{r},\omega) - \frac{q^2\hbar^2}{m}\,\frac{1}{(\hbar\omega)^2}\,\varphi_0(\mathbf{r})\varphi_0(\mathbf{r})\,. \tag{7}$$

The susceptibility to the transverse electric field, (7), is composed of two terms. The first term, namely, the resonant term, includes the energy denominator enhanced under the resonant condition, $\eta \simeq 1$, as in the susceptibility to the longitudinal electric field, (6). The second term, namely, the non-resonant term, does not include such a resonance factor.

Equal responses under the resonant condition. Under the condition $\eta \simeq 1$ in all cases in Table I, (7) is dominated by the resonant term (the first term) over the non-resonant term (the second term) and asymptotically equals (6).

$$\chi_{ij}^{\mathbf{j}\leftarrow(t)}(\mathbf{r},\omega) \simeq \chi_{ij}^{\mathbf{j}\leftarrow(\ell)}(\mathbf{r},\omega)\,. \tag{8}$$

Equation (8) together with (3) reveal the equivalency of the responses to the longitudinal and transverse electric fields, so that the total electric field is regarded as the cause of the response in *any* optical system under the resonant condition listed in Table I .

Equal responses under the far-field observation condition. In the system (Ⅱ) and (Ⅱ′) in Table I, the far field to be observed is insensitive to the details of the source but is determined by the spatial average of the source. Under the LWA, such an average can be

achieved by the spatial average of the susceptibilities. Detailed calculations are shown in *Calculation details* (iii); the results are as follows.

$$\overline{\chi_j^{\rho\leftarrow(\ell)}(\mathbf{r},\omega)} = \quad \overline{\chi_j^{\rho\leftarrow(t)}(\mathbf{r},\omega)} = 0\,, \tag{9}$$

$$\overline{\chi_{ij}^{\mathbf{j}\leftarrow(\ell)}(\mathbf{r},\omega)} = \overline{\chi_{ij}^{\mathbf{j}\leftarrow(t)}(\mathbf{r},\omega)} = \delta_{i\,j}\frac{q^2\hbar^2}{m\,\mathcal{V}}\frac{1}{(\hbar\Delta\omega_1)^{\,2}-(\hbar\omega)^2}\,, \tag{10}$$

where the overline represents the spatial average and $\mathcal{V}$ is the volume of the target material. From (9) and (10), one may not observe different responses to the two types of incidences under the far-field observation condition. The null response represented in (9) is reasonable because the induced charge density yields the longitudinal electric field, which has a non-radiative nature and vanishes in the far-field regime.

Unequal responses under the non-resonant, NF incidence, and NF observation conditions. The different responses claimed in the beginning of this Rapid communication may be detected only in the system (I) in Table I under the non-resonant condition, which is just the compliment to the popular optical systems under the resonant condition and/or the far-field observation condition. In the NF optical system (I) with a non-metallic material under the non-resonant condition, *the total electric field* is not the cause of the response; therefore, the response may not be described by the macroscopic constitutive equation (MCE), namely, the linear relationship between the polarization and "electric field" via permittivity, and the microscopic susceptibilities are essential to treat separately the longitudinal and transverse incidences.

In NFO, the response to the longitudinal electric field is discussed in Chap. 5 in Ref.[16] and Chap. 9 in Ref.[18]. The present work is a further comparison of the two responses, considering *the non-resonant condition*.

The present model is very simple and the responses may be modified in a many-electron system or a low-symmetry system. However, the difference in the responses to the two types of electric fields originates in *the non-relativistic nature* of the system (as stated in the beginning of this Rapid communication), and should survive in actual NF optical systems with non-metallic materials (the materials with finite excitation energy). Actually, there is no reason for equating the two responses in the many-electron and low-symmetry systems. Therefore, one may infer a guiding principle to highlight NF optical phenomena: under the non-resonant condition and simultaneous NF-incident and NF-observation conditions, non-metallic materials bring about NF-specific optical phenomena that may not be described

by the MCE in terms of the electric field and the permittivity. Some of the experiments mentioned in the beginning of this paper were performed under such conditions; thus, we will analyze them in detail in future investigation.

A remark on applying the finite differential time domain (FDTD) method to an NF optical system. The MCE in terms of the permittivity has been widely employed to calculate the optical near field in the FDTD method[17]. One may notice that the permittivity in the FDTD method carries a simple spatial dependence and leads to some quantitative error. Actually, the microscopic susceptibilities, for example, (3), (6), and (7), have rippling spatial distributions originating from the orbitals.

In the case of the NF optical system (I) in Table I with a non-metallic material under the non-resonant condition, the situation is more serious because the concept *electric field* is not available, such that it is a logical fallacy to use the MCE. Thus, a novel simulation method is necessary.

NFO and many-electron problem. Why has the comparison of responses to the two types of electric fields not been addressed in NF optical theory? First, in the long history of optics, the NF optical system (I) in Table I under a non-resonant condition has been out of focus. Such a system could not be resolved until the technical difficulty of NF observation was overcome. Additionally, resonance phenomena continue to attract attention. Furthermore, even in NFO, there has been less emphasis on non-metallic materials, as opposed to metallic materials, which are essential for plasmonics.

The second reason is that the ordinary Hamiltonian for a many-electron system does not include the longitudinal electric field, which is rewritten to the two-body Coulomb interaction and eliminated. With this Hamiltonian, the response to the longitudinal electric field incidence accompanies the Coulomb interaction, and is difficult to analyze. Therefore, NFO is inevitably related to the many-electron problem; however, this has not been well recognized for a long time. This study considered a one-electron system, avoiding the many-electron problem. In future studies, the present scenario will be extended to a many-electron system and nonlinear response, overcoming the many-electron problem, and applying the findings to various phenomena mentioned in the beginning of this Rapid communication.

To the best of our knowledge, the present near-field optical system with non-metallic material under the non-resonant condition is the third example that cannot be described in terms of electric field and/or magnetic field, after the superconductor system with the

Meissner effect and the electron system with the Aharonov-Bohm effect. The diversity of non-metallic materials including semiconductors, dielectrics, and magnetic materials has been utilized in conventional optics. We believe that focusing on non-metallic materials in NFO promotes further development both conceptually and technically.

Calculation details. Here we provide the calculation details, including the derivation of the unfamiliar relationship (28) between two types of dipole transition matrix elements.

(i) Derivation of the microscopic constitutive equations, (1) and (2). The incident scalar and vector potentials, $\Delta\phi(\mathbf{r},t)$ and $\Delta A_i(\mathbf{r},t)$, are assumed to be monochromatic with the angular momentum ω, and are expressed using the Coulomb gauge and LWA, as follows:

$$\Delta\phi(\mathbf{r},t) = \Delta\phi(\mathbf{r})\cos\omega t = \left(\Delta\phi(\mathbf{0}) - \Delta\mathbf{E}^{(\ell)}(\mathbf{0})\cdot\mathbf{r}\right)\cos\omega t\,, \tag{11}$$

$$\Delta\mathbf{A}(\mathbf{r},t) = \Delta\mathbf{A}(\mathbf{r})\sin(\omega t+\xi) = -\frac{1}{\omega}\Delta\mathbf{E}^{(t)}(\mathbf{0})\sin(\omega t+\xi)\,, \tag{12}$$

where and ξ is the phase difference between the two incident potentials. The nanostructure is assumed to be a robust light source, which is not affected by the target material, and the electromagnetic field is assumed to be a classical field.

Using a spinless one-electron system, let us evaluate the induced charge and current densities caused by the coexisting incidences of the scalar and vector potentials. The total Hamiltonian is as follows:

$$\hat{H} = \frac{1}{2m}\left(\frac{\hbar}{i}\frac{\partial}{\partial x_i(t)} - qA_i(\mathbf{x}(t),t)\right)\left(\frac{\hbar}{i}\frac{\partial}{\partial x_i(t)} - qA_i(\mathbf{x}(t),t)\right) + q\phi(\mathbf{x}(t),t)\,, \tag{13}$$

where t is time, $\mathbf{x}(t)$ is the position of the electron, and $q(=-e), m$ are the electron charge and mass, respectively. The perturbation Hamiltonian is given by

$$\int \mathrm{d}^3r\,\left(\hat{\rho}(\mathbf{r},t)\Delta\phi(\mathbf{r},t) - \hat{j}_i(\mathbf{r},t)\Delta A_i(\mathbf{r},t)\right), \tag{14}$$

where $\hat{\rho}(\mathbf{r},t), \hat{j}_i(\mathbf{r},t)$ are the Heisenberg operators of the charge and current densities defined as

$$\hat{\rho}(\mathbf{r},t) = q\delta^3(\mathbf{r}-\mathbf{x}(t))\,, \tag{15}$$

$$\hat{j}_i(\mathbf{r},t) = \frac{q}{2m}\left\{\left(\frac{\hbar}{i}\frac{\partial}{\partial x_i(t)} - qA_i(\mathbf{x}(t),t)\right)\delta^3(\mathbf{r}-\mathbf{x}(t)) + \delta^3(\mathbf{r}-\mathbf{x}(t))\left(\frac{\hbar}{i}\frac{\partial}{\partial x_i(t)} - qA_i(\mathbf{x}(t),t)\right)\right\}. \tag{16}$$

The linear response theory leads to the operators of the induced charge and current densities, as follows:

$$\Delta\hat{\rho}(\mathbf{r},t) = \int_{-\infty}^{t} \mathrm{d}t_1 \int \mathrm{d}^3 r_1 \left\{ \frac{1}{i\hbar} \left[\hat{\rho}^{(0)}(\mathbf{r},t)\,,\, \hat{\rho}^{(0)}(\mathbf{r}_1,t_1) \right] \Delta\phi(\mathbf{r}_1,t_1) \right. \\ \left. - \frac{1}{i\hbar} \left[\hat{\rho}^{(0)}(\mathbf{r},t)\,,\, \hat{j}_{i_1}^{(0)}(\mathbf{r}_1,t_1) \right] \Delta A_{i_1}(\mathbf{r}_1,t_1) \right\}, \tag{17}$$

$$\Delta\hat{j}_i(\mathbf{r},t) = \int_{-\infty}^{t} \mathrm{d}t_1 \int \mathrm{d}^3 r_1 \left\{ \frac{1}{i\hbar} \left[\hat{j}_i^{(0)}(\mathbf{r},t)\,,\, \hat{\rho}^{(0)}(\mathbf{r}_1,t_1) \right] \Delta\phi(\mathbf{r}_1,t_1) \right. \\ \left. - \frac{1}{i\hbar} \left[\hat{j}_i^{(0)}(\mathbf{r},t)\,,\, \hat{j}_{i_1}^{(0)}(\mathbf{r}_1,t_1) \right] \Delta A_{i_1}(\mathbf{r}_1,t_1) \right\} - \frac{q}{m} \hat{\rho}^{(0)}(\mathbf{r},t) \Delta A_i(\mathbf{r},t)\,, \tag{18}$$

where $\hat{\rho}^{(0)}$ and $\hat{\mathbf{j}}^{(0)}$ are the charge and current density operators, respectively, in the non-perturbed system. The last term in (18) originates from *the non-relativistic nature* of the system and is needed to maintain the charge conservation law.

Evaluating the expectation value using the ground state and substituting (11) and (12) leads to (1) and (2), in which the causes of the responses are the two types of electric fields and their temporal derivatives, defined as

$$\Delta E_j^{(\ell)}(\mathbf{0},t) \equiv \quad \Delta E_j^{(\ell)}(\mathbf{0}) \cos\omega t\,, \quad \Delta E_j^{(t)}(\mathbf{0},t) \equiv \quad \Delta E_j^{(t)}(\mathbf{0}) \cos(\omega t + \xi)\,, \tag{19}$$

$$\Delta \dot{E}_j^{(\ell)}(\mathbf{0},t) \equiv \frac{\partial}{\partial t} \Delta E_j^{(\ell)}(\mathbf{0},t)\,, \qquad \Delta \dot{E}_j^{(t)}(\mathbf{0},t) \equiv \frac{\partial}{\partial t} \Delta E_j^{(t)}(\mathbf{0},t)\,. \tag{20}$$

In the above, no magnetic response appears because it is the higher order in the LWA[16, 19]. Cho derived a Taylor series of the non-local response function[20] under the LWA, and assigned the electric permittivity and magnetic permeability in the MCE as the term of order $\mathcal{O}(ka)^0$ (the leading order) and $\mathcal{O}(ka)^2$, respectively, where $ka \ll 1$, $2\pi/k$ is the light wavelength, and a is the representative size of the material.

Furthermore, he pointed out that the MCE is irrational because the separability of the electric and magnetic responses and the term of order $\mathcal{O}(ka)^1$ appears in a chiral symmetric system, including a NF optical system with a low-symmetric nanostructure. The present work is concerned with another type of irrationality, which appears in the electric response (the leading order from the viewpoint of Cho) in NFO under *a non-resonant condition*.

(ii) Derivation of the expressions for susceptibilities, (3), (6) and (7).

To obtain these formulas using the two-level model, we take the expectation values of (17)

and (18) using the ground state, $\varphi_0(\mathbf{r})$, and insert the projection operator [the left side of the second equation in (21)], assuming that the two orbitals are real functions, and form the normalized orthogonal complete set:

$$\int \mathrm{d}^3 r\, \varphi_m(\mathbf{r})\varphi_n(\mathbf{r}) = \delta_{m\,n}\,, \qquad \sum_m \varphi_m(\mathbf{r})\varphi_m(\mathbf{r}') = \delta^3(\mathbf{r}-\mathbf{r}')\,, \tag{21}$$

where $\varphi_m(\mathbf{r})$ satisfies,

$$\hat{H}^{(0)}\varphi_m(\mathbf{r}) = \hbar\omega_m\,\varphi_m(\mathbf{r})\,, \quad (m=0,1)\,. \tag{22}$$

Having real orbitals infers even temporal parity, such that there is a null magnetic field in the non-perturbed system or null vector potential in the non-perturbed Hamiltonian. Furthermore, we use the well-known linear relationship between the two types of dipole transition matrix elements,

$$\mathcal{C}_i \equiv \int \mathrm{d}^3 r\ (\partial_i\varphi_1(\mathbf{r})\varphi_0(\mathbf{r}) - \varphi_1(\mathbf{r})\partial_i\varphi_0(\mathbf{r})) = \frac{2m}{\hbar^2}\hbar\Delta\omega_1\,\mathcal{D}_i\,. \tag{23}$$

Equation (23) is derived from the matrix element of the Heisenberg equation for dipole charge density:

$$\frac{\partial}{\partial t}\, r_j\hat{\rho}^{(0)}(\mathbf{r},t) = \frac{1}{i\hbar}\left[r_j\hat{\rho}^{(0)}(\mathbf{r},t)\,,\ \hat{H}^{(0)}\right]\,, \tag{24}$$

using $\hat{\rho}^{(0)}(\mathbf{r},t) = e^{-\frac{\hat{H}^{(0)}t}{i\hbar}}\hat{\rho}^{(0)}(\mathbf{r},0)e^{+\frac{\hat{H}^{(0)}t}{i\hbar}}$, the projection operator, (21) and (22).

(iii) Derivation of the spatial average of the susceptibilities, (9) and (10). These following replacements in (3), (6) and (7) lead to (9) and (10):

$$\varphi_0(\mathbf{r})\varphi_1(\mathbf{r}) \quad\longrightarrow\quad \frac{1}{\mathcal{V}}\int \mathrm{d}^3 r\,\varphi_0(\mathbf{r})\varphi_1(\mathbf{r}) = 0\,, \tag{25}$$

$$\partial_i\varphi_1(\mathbf{r})\varphi_0(\mathbf{r}) - \varphi_1(\mathbf{r})\partial_i\varphi_0(\mathbf{r}) \quad\longrightarrow\quad \frac{1}{\mathcal{V}}\int \mathrm{d}^3 r\,\partial_i\varphi_1(\mathbf{r})\varphi_0(\mathbf{r}) - \varphi_1(\mathbf{r})\partial_i\varphi_0(\mathbf{r}) = \frac{1}{\mathcal{V}}\mathcal{C}_i\,, \tag{26}$$

$$\varphi_0(\mathbf{r})\varphi_0(\mathbf{r}) \quad\longrightarrow\quad \frac{1}{\mathcal{V}}\int \mathrm{d}^3 r\,\varphi_0(\mathbf{r})\varphi_0(\mathbf{r}) = \frac{1}{\mathcal{V}}\,. \tag{27}$$

To derive (10), we additionally use the trade-off relationship between the two types of dipole transition matrix elements,

$$\mathcal{D}_i\,\mathcal{C}_j = \delta_{i\,j}. \tag{28}$$

This is effective in the two-level system with well-defined parity and derived from the quantum-mechanical commutation relationship:

$$[r_i\,,\,\frac{\hbar}{i}\partial_j] = i\hbar\,\delta_{ij}\,,\quad \text{i.e.,}\quad r_i\left(\frac{\hbar}{i}\partial_j\cdots\right)+\frac{\hbar}{-i}\partial_j\,(r_i\cdots) = i\hbar\delta_{ij}\cdots\,. \tag{29}$$

Inserting the projection operator between r_i and $\frac{\hbar}{i}\partial_j$, and eliminating the null integrals caused by mismatched parity result in (28). From (23) and (28), $\mathcal{D}_i$ and $\mathcal{C}_i$ are specified as

$$\mathcal{D}_i = \frac{1}{\mathcal{C}_i} = \frac{\hbar}{\sqrt{2m\,\hbar\Delta\omega_1}}\,. \tag{30}$$

(We do not use (30) in this paper.)

Acknowledgments

The authors are grateful Drs. I. Ojima (Research Origin of Dressed Photon (RODreP)), H. Sakuma (RODreP), H. Saigo (Nagahama Insitute of Bio-Science and Technology), K. Okamura (Nagoya Univ.), H. Ando (Chiba Univ.) , and T. Kawazoe (Tokyo Denki Univ.) for useful discussions on the context of dressed photon. One of the authors (I. B.) thanks Professor K. Cho in Osaka Univ. for useful discussions concerning susceptibility. This work is partially supported by JSPS KAKENHI Grant Number JP25610071 during 2013-2015, and Research Foundation for Opto-Science and Technology during 2018-2019.

---

[1] T. Kawazoe, M. A. Mueed, and M. Ohtsu, Appl. Phys. B **104,** 747 (2011).

[2] M. Ohtsu, *Silicon Light-Emitting Diodes and Lasers* (Springer International Publishing, Switsland, 2016).

[3] T. Kawazoe, M. Ohtsu, K. Akahane, and N. Yamamoto, Appl. Phys. B **107,** 659 (2012).

[4] T. Kawazoe, Y. Yamamoto, and M. Ohtsu, Appl. Phys. Lett. **79,** 1184 (2001).

[5] H. Yonemitsu, T. Kawazoe, K. Kobayashi, and M. Ohtsu, J. Photolumin. **122,** 230 (2007).

[6] T. Yatsui, K. Hirata, W. Nomura, Y. Tabata, and M. Ohtsu, Appl. Phys. B **93,** 55 (2008).

[7] T. Kawazoe, H. Fujiwara, K. Kobayashi, and M. Ohtsu, IEEE J. of Selected Topics in Quantum Electronics **15,** 1380 (2009).

[8] H. Fujiwara, T. Kawazoe, and M. Ohtsu, Appl. Phys. B **100,** 85 (2010).

[9] T. Kawazoe, K. Kobayashi, and M. Ohtsu, Appl. Phys. Lett. **86,** 103102-1 (2005).

[10] T. Kawazoe, M. Ohtsu, S. Aso, Y. Sawado, Y. Hosoda, K. Yoshizawa, K. Akahane, N. Yamamoto, and M. Naruse, Appl. Phys. B **103,** 537 (2011).

[11] N. Tate, T. Kawazoe, W. Nomura, and M. Ohtsu, Scientific Reports **5,** 12762-1 (2015) .

[12] N. Tate, T. Kawazoe, S. Nakashima, W. Nomura, M. Ohtsu, *Abstracts of the 22nd International Display Workshops* (Dec. 9-11, 2015, Otsu, Japan, PRJ3-1).

[13] T. Kawazoe, K. Kobayashi, S. Takubo, and M. Ohtsu, J. Chem. Phys. **122,** 024715-1 (2005).

[14] K. Kobayashi, T. Kawazoe, and M. Ohtsu, IEEE Trans. Nanotech. **4,** 517 (2005).

[15] M. Ohtsu, *Dressed Photons: Concepts of Light-Matter Fusion Technology* (Springer-Verlag, Berlin, Heidelberg, 2014).

[16] K. Cho, *Reconstruction of Macroscopic Maxwell Equations* (Springer-Verlag, Berlin, Heidelberg, 2010).

[17] K. Yee, *IEEE Transactions on Antennas and Propagation* **14,** 302 (1966).

[18] O. Keller, *Quantum Theory of Near-Field Electrocynamics* (Springer-Verlag, Berlin, Heidelberg, 2011).

[19] K. Cho, J. Phys. Condens. Matter **20,**175202 (2008).

[20] K. Cho, *Optical Response of Nanostructures* (Springer-Verlag, Berlin, Heidelberg, 2003).

High-Power Infrared Silicon Light-emitting Diodes Fabricated and Operated using Dressed Photons

M. Ohtsu[1] and T. Kawazoe[2]

[1]Research Origin for Dressed Photon,
c/o Nichia Corp., 3-13-19 Moriya-cho, Kanagawa-ku, Yokohama, Kanagawa 221-0022 Japan
[2]Tokyo Denki University,
5 Senju-Asahi-cho, Adachi-ku, Tokyo 120-8551, Japan

Abstract

Mesh-electrode type and flip-chip type silicon light-emitting diodes were fabricated by using dressed photons. Their emission spectral profiles showed several peaks originating from phonons in a dressed-photon–phonon, from which the existence of a photon breeding phenomenon was confirmed. The highest optical output power emitted from these devices was 2 W at a substrate temperature of 77 K. The highest optical power density from the flip-chip type was as high as eight-times that from the mesh-electrode type.

1 Introduction

There is a long-held belief in optical science and technology that crystalline silicon (Si) is not suitable for use in light-emitting devices. The reason for this is that it is an indirect-transition type semiconductor, in which the momentum of an electron at the bottom of the conduction band and that of a hole at the top of the valence band are different from each other. Therefore, for electron–hole recombination, a phonon is required to satisfy the momentum conservation law. However, the probability of the electron–phonon interaction is low, resulting in a low interband transition probability.

In order to realize light-emitting devices using Si, porous Si [1], a super-lattice structure of Si and SiO_2 [2,3], Si nanoprecipitates in SiO_2 [4], Er-doped Si [5], and Si-Ge [6] have been employed. However, in these examples, the optical output powers were very low since the Si still worked as an indirect-transition type semiconductor.

In contrast to these examples, the authors have previously realized novel light-emitting diodes (LEDs), lasers, and related light-emitting and -detecting devices by using Si bulk crystal and dressed photons (DPs) [7]. A DP is a novel quantum field created as a result of the interaction between a photon and an electron–hole pair in a nanometric space. A dressed-photon–phonon (DDP), created as a result of the interaction between the DP and a phonon, has also been used [8]. The DPP was created in an Si crystal,

resulting in efficient light emission by the momentum exchange between a multi-mode coherent phonon in the DPP and an electron in the conduction band of the Si.

In the present study, we improved on a previously fabricated infrared Si-LED (wavelength: 1.3 μm) [9] to achieve higher current injection and more efficient heat dissipation. This paper reports the fabrication method and light-emission characteristics of the improved high-power Si-LEDs.

2 Fabrication

The first part of this section reviews the principles of fabrication based on a novel DPP-assisted annealing method. The second part is devoted to the procedures for fabricating devices of a mesh-electrode type and a flip-chip type for allowing higher current injection and more efficient heat dissipation.

2.1 Principles

To fabricate an LED, as the first step, the surface of an n-type Si crystal is doped with boron (B) atoms to transform it to a p-type layer, thereby forming a pn-homojunction. As the second step, the crystal is annealed using a novel method named DPP-assisted annealing [7]. In this method, by means of current injection, the Si crystal is heated by Joule energy to diffuse the B atoms. During this heating, the Si crystal surface is irradiated with light to create DPPs at the B atoms. The electrons injected into the conduction band exchange momenta with the phonons in the created DPPs, thus recombining with positive holes and emitting light. This emission process is stimulated emission because it is triggered by light irradiation. The emitted light propagates outside the Si crystal, which means that a part of the Joule energy for heating is dissipated out in the form of optical energy. As a result, the diffusion rate of the B atoms decreases locally. By a balance between heating by the Joule energy and cooling by the optical energy dissipation, the spatial distribution of B atoms varies autonomously and reaches a stationary state.

Such a stationary distribution of B atoms can be the optimum distribution for spontaneous emission because its probability is proportional to the probability of the stimulated emission above. From high-resolution analysis of the B atom distribution, it was confirmed that two B atoms formed a pair whose length was three-times the crystal lattice constant of Si. It was also confirmed that the pair was oriented perpendicular to the propagation direction and to the polarization direction of the irradiated light [10].

2.2 Procedures

Sb-doped n-type Si crystal was used. In order to transform its surface to an n-type layer, the Si crystal was doped with B atoms by a two-step ion implantation method, where the doping energies were 700 keV and 10 keV.

2.2.1 Mesh-electrode type LED

Figure 1 shows a photographic profile of the fabricated device: A homogeneously flat film of Cr/Al/Au (thicknesses: 30/200/300 nm) was coated on the n-type surface of the Si crystal described above to serve as a cathode. A mesh film of Cr/Au (thicknesses: 30/300 nm) was coated on the p-type surface to serve as an anode. The crystal was diced to form devices with areal sizes of 1 mm × 1 mm, and these devices were bonded on a PCB substrate made of high-thermal-conductivity AlN. The diameters of eight electric wires were increased from the previously employed 25 μm [9] to 45 μm to avoid damage to the electric wires and electrodes during high current injection.

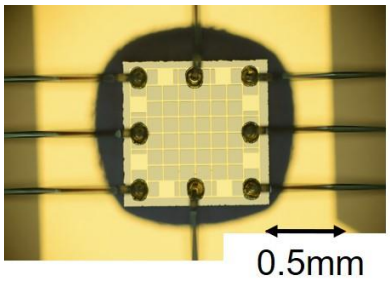

Fig. 1 Photographic profile of the fabricated mesh-electrode type LED.

The conditions for the DPP-assisted annealing were: (1) A substrate temperature, of 285 K; (2) irradiation light with a wavelength of 1342 nm and a power of 2.0 W; (3) injected current having a triangular waveform (50 s period) and a peak current of 1.3 A (current density 1.3 A/mm^2); and (4) an annealing time of 2 hours.

Figure 2 shows the relation between the applied voltage and injected current in the fabricated Si-LED. A drastic decrease in the electrical resistance can be seen after the DPP-assisted annealing, which is evidence of successful annealing.

2.2.2 Flip-chip type LED

To achieve higher injected current density than that of the mesh-electrode type, a flip-chip type LED was fabricated. First, its areal size was decreased. Second, a larger-diameter electric wire was used. Third, the flip-chip structure was employed, in which

the p-type layer was contacted to the PCB substrate for efficient heat dissipation.

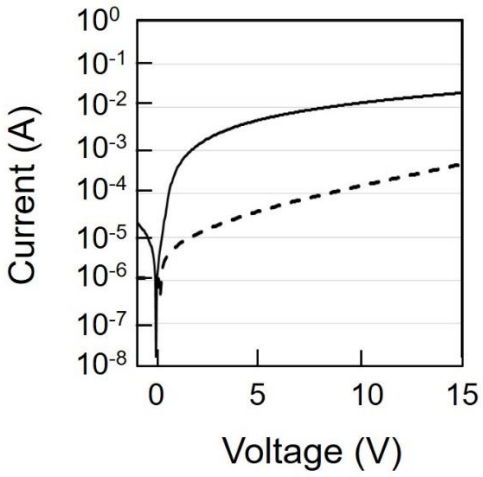

Fig. 2 Relation between the applied voltage and injected current.
Broken and solid curves are the results acquired before and after the DPP-assisted annealing, respectively.

Figure 3 shows a photographic profile of the fabricated device: A homogeneously flat film of Cr/Au/Ti/Pt/Au (thicknesses: 3/300/100/300/500 nm) was coated on the p-type surface of the Si crystal to serve as an anode. A patterned film of Cr/Au (thicknesses: 10/500 nm) was coated on the n-type surface as a cathode. The crystal was diced to form devices with areal sizes of 0.35 mm × 0.35 mm, which was smaller than that of the mesh-electrode type described in Subsection 2.2.1. This is equivalent to the size of commercially available devices made by using a conventional direct-transition type semiconductor. The diced device was bonded on a PCB substrate made of AlN. A single electric wire with a diameter as large as 60 μm was used to realize high-density current injection without any electrical damage.

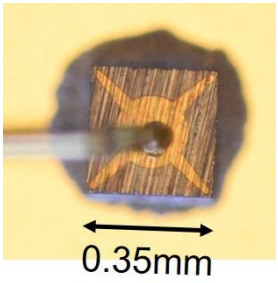

Fig. 3 Photographic profile of the fabricated flip-chip type LED.

The conditions for the DPP-assisted annealing were: (1) A substrate temperature of 289 K; (2) irradiation light with a wavelength of 1342 nm and a power of 0.24 W (areal power density: 1.9 W/mm^2); (3) injected current with a triangular waveform (10 s period)

and a peak current of 0.16 A (current density: 1.3 A/mm^2); and (4) an annealing time of 7.2 hours.

3 Light emission characteristics

With conventional current injection, the fabricated device worked as a Si-LED: The electrons injected into the conduction band exchanged momenta with phonons even though the probability of this exchange was extremely low. As a result, they recombined with a positive hole, resulting in spontaneous light emission. Since this light created DPPs at the B atoms, phonons in the DPP could exchange momenta with other electrons, resulting in further light emission. By repeating this process, the emitted light intensity increased and reached a stationary state to establish steady LED operation.

3.1 Mesh-electrode type LED

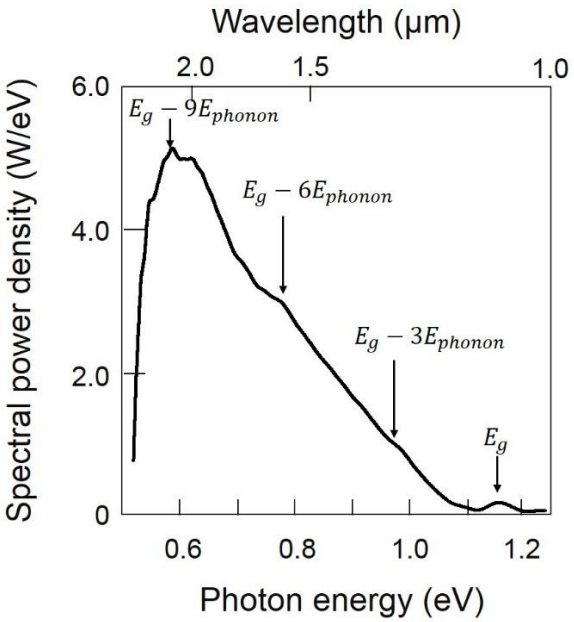

Fig. 4 Spectral profile of the emitted light at substrate temperature of 77 K.

Figure 4 shows the spectral profile of the emitted light, which was acquired by cooling the substrate to 77 K and injecting a current of 2.0 A. In this figure, E_g represents the bandgap energy of the Si crystal at 77 K. This figure shows that the spectral profile has several peaks at $E_g - nE_{phonon}$, where n is an integer and E_{phonon} is the phonon energy.

The spectral peak at $E_g - 3E_{phonon}$ corresponds to the photon energy of the light irradiated during the DPP-assisted annealing [10]. This correspondence has been named photon breeding [11], which originates from the autonomous formation of pairs of B atoms by DPP-assisted annealing, as was described in Subsection 2.1. Three phonons contribute to the light emission at $E_g - 3E_{phonon}$, because the length of the B atom pair is three-times the crystal lattice constant of Si. This figure also shows the higher harmonics of the phonon contributions, i.e., $E_g - 6E_{phonon}$ and $E_g - 9E_{phonon}$.

Figure 5 shows relations between the injected current (I) and the optical output power (P) of the upward-emitted light from the upper surface of the Si-LED, which were acquired at several substrate temperatures. It shows that P is proportional to I^2 in the lower current region, whereas it is proportional to I^4 in the higher current region. The origin of the I^2-relation has been identified as Auger scattering [9]. The I^4-relation originated in amplification by the stimulated emission.

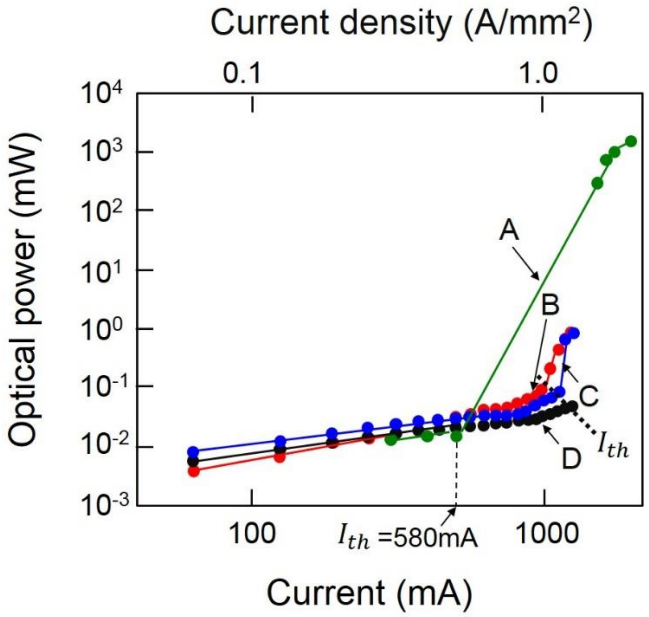

Fig. 5 Relations between the injection current and the optical output power. Substrate temperatures were 77 K (A), 273 K (B), 290 K (C), and 293 K (D).

By defining the current at the boundary between the region of the I^2- and I^4-relations as the threshold I_{th}, it is found that its value was lower at lower substrate temperatures. For example, it was 580 mA at 77 K. This means that the threshold current density was 0.58 A/mm², which is close to the threshold current density (0.20–0.35

A/mm^2) of the Si-laser fabricated by the DPP-assisted annealing [12]. The highest optical output power in Fig. 5 was 2 W with an injection current of 2 A and a substrate temperature of 77 K. This value is as high as 10^3-times that of a commercially available LED*.

The image A in Fig.6 shows the photograph of the light spot emitted from the presently fabricated Si-LED. The image B is from the commercially available LED above*. By comparing these images, a very high optical output power of the present Si-LED can be recognized.

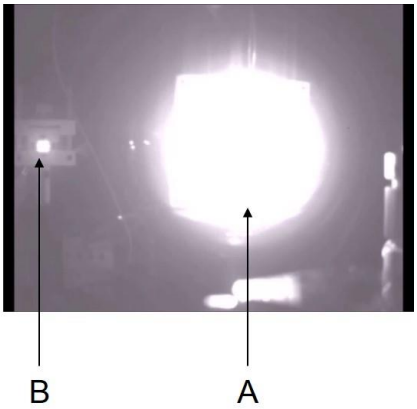

Fig. 6 Photographs of light spots.
A and B are the spots emitted from the Si-LED fabricated in the present study and from a commercially available LED, respectively.

*For example, the optical output power of a Hamamatsu Photonics model L12509-0155K, which is made of a direct-transition type semiconductor (InGaAs), is 2 mW. The peak emission wavelength is 1.55 μm.

3.2 Flip-chip type LED

Figure 7(a) shows the spectral profile of the light emitted from the flip-chip type LED, which was acquired by cooling the substrate to 77 K and by injecting a current of 3.21 A. Figure 7(b) shows the profile at a substrate temperature of 283 K and an injection current of 2.45 A. These figures also clearly demonstrate spectral peaks at $E_g - 3E_{phonon}$, $E_g - 6E_{phonon}$, and $E_g - 9E_{phonon}$, as was the case in Fig. 4.

Figure 8 shows relations between I and P of the upward-emitted light from the upper surface of the Si-LED, which were acquired at several substrate temperatures. The highest optical output power in this figure was as high as 2 W at 3 A-injection current

and at a 77 K-substrate temperature. This demonstrates an extremely high optical output power density was achieved, as high as eight-times that of the mesh-electrode type LED described in Subsection 3.1.

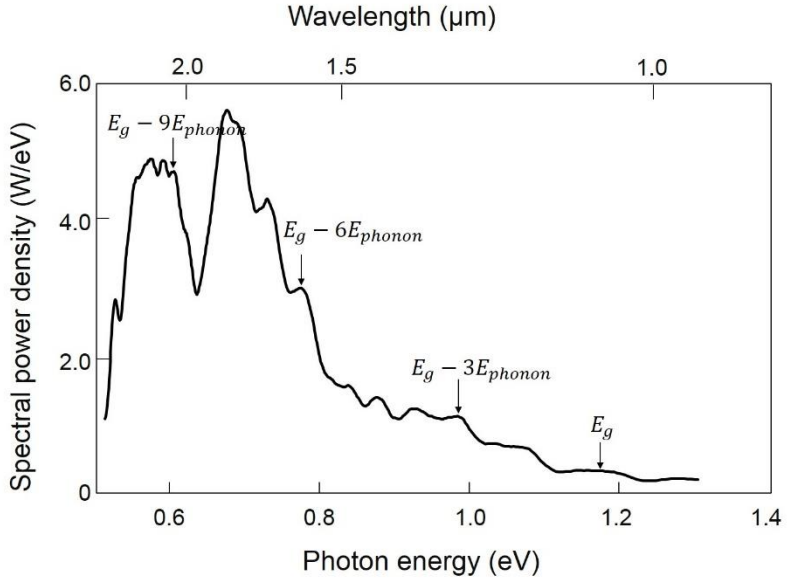

(a)

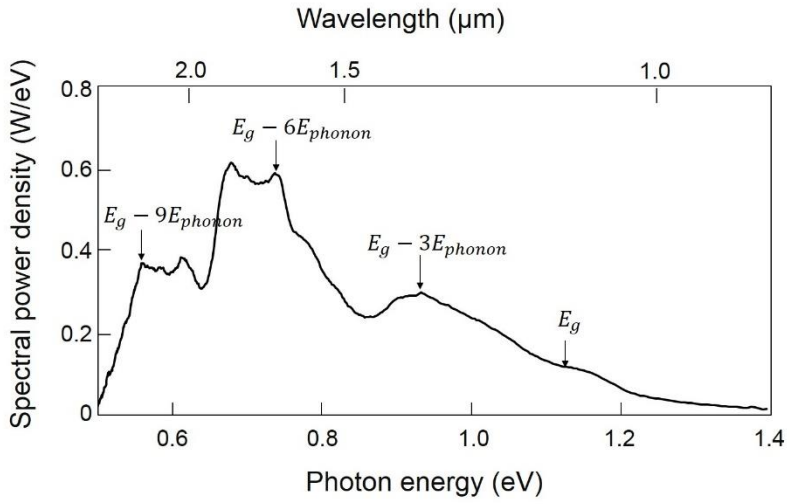

(b)

Fig. 7 Spectral profile of the light emitted from the flip-chip type LED.
(a),(b) The substrate temperatures were 77 K and 283 K, respectively.

It can be seen that the relations between I and P showed more complicated profiles than those in Fig. 5: In the low-current region [a], P increased slowly with increasing I, whereas it increased rapidly in the high-current region [c]. The unique feature is that P decreased with increasing I in the intermediate region [b]. Figures

9(a)-(c) show photographs of the upward-emitted light spots in the regions [a]-[c], respectively. Among them, Fig. 9(b) shows that the light was emitted not only in the upward direction but also in the side direction of the device. This side-emission was attributed to the decrease in the acquired value of P in region [b]. It should be noted that this side-emission was due to stimulated emission, which suggests the possibility of super-luminescent diode and laser operation.

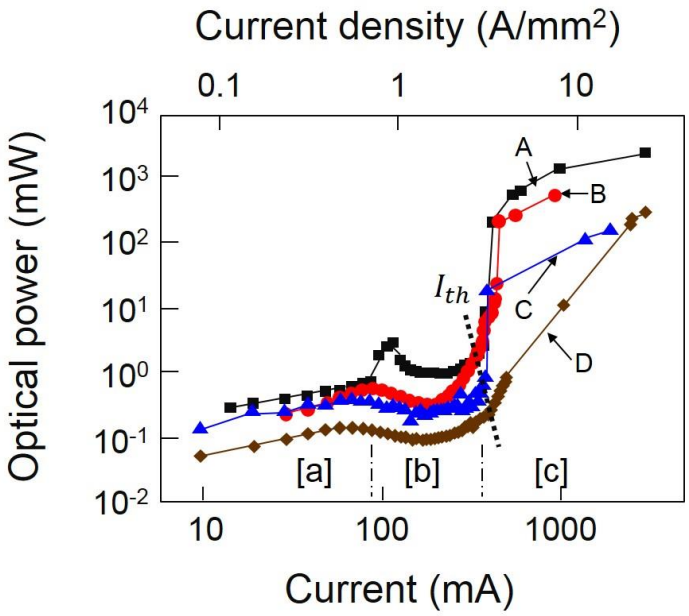

Fig.8 Relations between the injection current and the optical output power of the upward-emitted light from the surface of the Si-LED.

Substrate temperatures were 77 K (A), 195 K (B), 255 K (C), and 283 K (D).

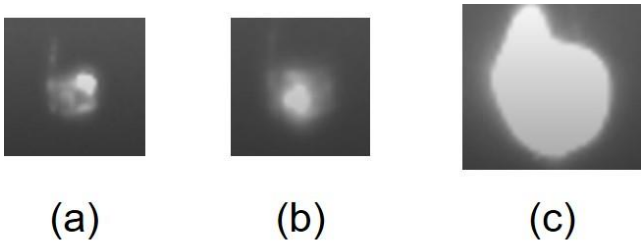

Fig.9 Photographs of the upward-emitted light spots.

(a), (b), (c) are images obtained in regions [a], [b], and [c] in Fig. 8, respectively.

As was the case in Fig. 5, the threshold I_{th} can be defined as the current at the boundary between regions [b] and [c]. Figure 10 shows its dependence on the substrate temperature T. The solid line, fitted to the experimental results of the closed circles, was expressed as $I_{th} = I_0 \exp(T / T_0)$. The characteristic temperature T_0 in this

expression was 63 K, which corresponded to the energy $3E_{phonon}$ of three phonons in the DPP. This means that the electron–hole pair was confined in the potential well formed by three phonons. This value of T_0 was as high as that of a conventional laser fabricated by a direct-transition type semiconductor (InGaAsP), lasing at a wavelength of 1.3 μm [13], which suggests that future progress in the present study can realize highly reliable light-emitting devices using crystalline Si.

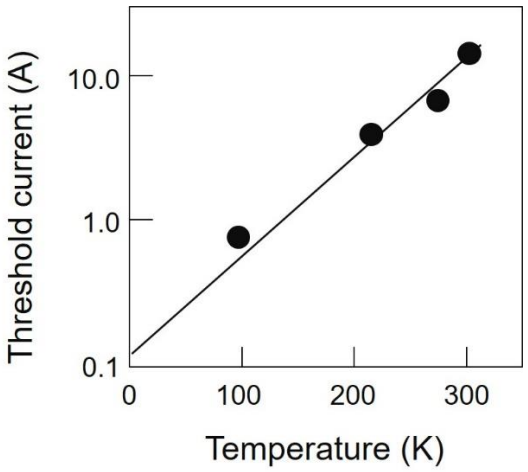

Fig. 10 Relation between the substrate temperature and the threshold current.

4 Summary

Mesh-electrode type and flip-chip type Si-LEDs were fabricated to realize higher-density current injection and more efficient heat dissipation. Their emission spectral profiles showed several peaks that originated from phonons in the DPP, by which a photon breeding phenomenon was confirmed. Their highest optical output powers were 2 W at injection currents of 2 A and 3 A, respectively, and a substrate temperature of 77 K. The highest optical power density from the flip-chip type was as high as eight-times that from the mesh-electrode type. In the case of the flip-chip type, the characteristic temperature of the threshold current for the rapid increase in the optical output power was 65 K, which corresponded to the energy of three phonons in the DPP.

Acknowledgements

The authors acknowledge Dr. B. Thumbthimthong for his collaboration in acquiring the experimental data.

References

[1] K.D. Hirschman, L.Tysbekov, S.P. Duttagupta, P.M. Fauchet, "Silicon-based visible light-emitting devices integrated into microelectronic circuits," Nature, **384** (1996) pp.338-341.

[2] Z.H. Lu, D.J. Lockwood, J.-M. Baribeau, Nature, "Quantum confinement and light emission in SiO_2/Si Superlattices," Nature, **378** (1995) pp.258-260.

[3] L. Dal Negro, R. Li, J. Warga, S.N. Basu, " Electroluminescence from silicon-rich nitride/silicon superlattice structures,"Appl. Phys. Lett., **93**, 151116(2008).

[4] T. Komoda, J. Kelly, E. Cristiano, A. Nejim, P. L. F. Hemment, K. P. Homewood, R. Gwilliam, J. E. Mynard, B. J. Sealy, "Visible photoluminescence at room temperature from micro- crystalline silicon precipitates in SiO_2 formed by ion implantation," Nucl. Instrum. and Methods in Phys. Res. Sect.B, **96**, 387 (1995) pp.387-391.

[5] S. Yerci, R. Li, L. Dal Negro, "Electroluminescence from Er-doped Si-rich silicon nitride light emitting diodes,"Appl. Phys. Lett., **97**, 081109 (2010).

[6] S.K. Ray, S. Das, R.K. Singha, S. Manna, A. Dhar, "Structural and optical properties of germanium nanostructures on Si(100) and embedded in high-k oxides," Nanoscale Res. Lett., **6**, 224 (2011) doi: 10.1186/1556-276X-6-224.

[7] M. Ohtsu, *Silicon Light-Emitting Diodes and Lasers*, (Springer, Heidelberg, 2016), pp.15-138.

[8] M. Ohtsu, *Dressed Photons*, (Springer, Heidelberg, 2014), pp.1-88.

[9] J.H. Kim, T. Kawazoe, and M.Ohtsu, "Dependences of emission intensity of Si light-emitting diodes on dressed-photon—phonon-assisted annealing conditions,"Appl. Phys. A ,**123**,606 (2017).

[10] T. Kawazoe, K. Nishioka, and M. Ohtsu, "Polarization control of an infrared silicon light-emitting diode by dressed photons and analyses of the spatial distribution of doped boron atoms," Appl. Phys.A , **121** (2015) pp. 1409-1415.

[11] M. Ohtsu, *Silicon Light-Emitting Diodes and Lasers*, (Springer, Heidelberg, 2016), pp.8-10.

[12] T. Kawazoe, K. Hashimoto, and S. Sugiura, "High-power current-injection type Silicon laser using nanophotonics," Abstract of the EMN Nanocrystals Meeting, October 17-21, 2016, Xi'an, China, pp.9-11 (paper number 03).

[13] R.Adams, M.Asada, Y.Suematsu, and S.Arai, "The Temperature Dependence of the Efficiency and Threshold Current of $In_{1-x}Ga_xAs_yP_{1-y}$ Lasers Related to Intervalence Band Absorption," Jpn. J. Appl. Phys., **19** (1980) L621.

Embarking on theoretical studies for off-shell science guided by dressed photons

M. Ohtsu

Research Origin for Dressed Photon,
c/o Nichia Corp., 3-13-19 Moriya-cho, Kanagawa-ku, Yokohama, Kanagawa 221-0022 Japan

Abstract

By noting that the dressed photon (DP) is a quantum field whose energy–momentum relation deviates from the mass-shell, novel theoretical studies of so-called off-shell science have been launched. This article reviews recent progress in these studies. After reviewing the characteristics of the DP as an off-shell quantum field, theories having a physical basis are introduced. These theories are an electromagnetic response theory and a theory based on spatio-temporal vortex hydrodynamics. Next, theories having a mathematical basis are introduced, and these can serve as helpful tools for gaining a deep understanding of the concepts of the physics-based theories above. These theories are a quantum probability theory and a quantum walk model. As a further helpful tool, a quantum measurement theory is introduced. A theory based on micro–macro duality is demonstrated, which serves as the foundation to embark on a stuy of off-shell science. Correlations among the theories reviewed here are also shown.

1 Introduction

Studies on dressed photons (DPs) have found that the DP is a quantum field created by light–matter interaction in a nanometric space [1]. Some of its unique characteristics, outline below, have been demonstrated by experimental studies*:

[a] The DP is a field composed of photons and electrons (or excitons). It is created and localized at the boundary or at the singular point of a nanometric material, i.e., on the material surface or at an impurity atom in the material.

[b] The energy and momentum of the DP range widely.

[c] The DP is a quantum field off the mass-shell (“off-shell quantum field” for short).

[d] Electrons and excitons can be excited and de-excited by the DP even under non-resonant condition.

[e] The DP energy is exchanged and transferred between nano-materials when they are

located in the close proximity to each other.

[f] The DP field is disturbed when it is measured by inserting a probe into the field.

[g] The DP is transferred in an autonomous manner between the nano-materials.

[h] The spatial distribution of DPs on a material surface has a hierarchical structure.

Characteristics [a]–[h] above have been applied to the invention of novel optical logic gate devices, nano-fabrication technology, and energy conversion technology [2]. They have also been applied to the invention of novel high-power lasers and light-emitting diodes using crystalline Si, even though Si is an indirect-transition-type semiconductor [3]. These applications demonstrate the advent of a revolutionary generic technology that could never have been realized as long as conventional light (free photons) is used (Fig.1) [4].

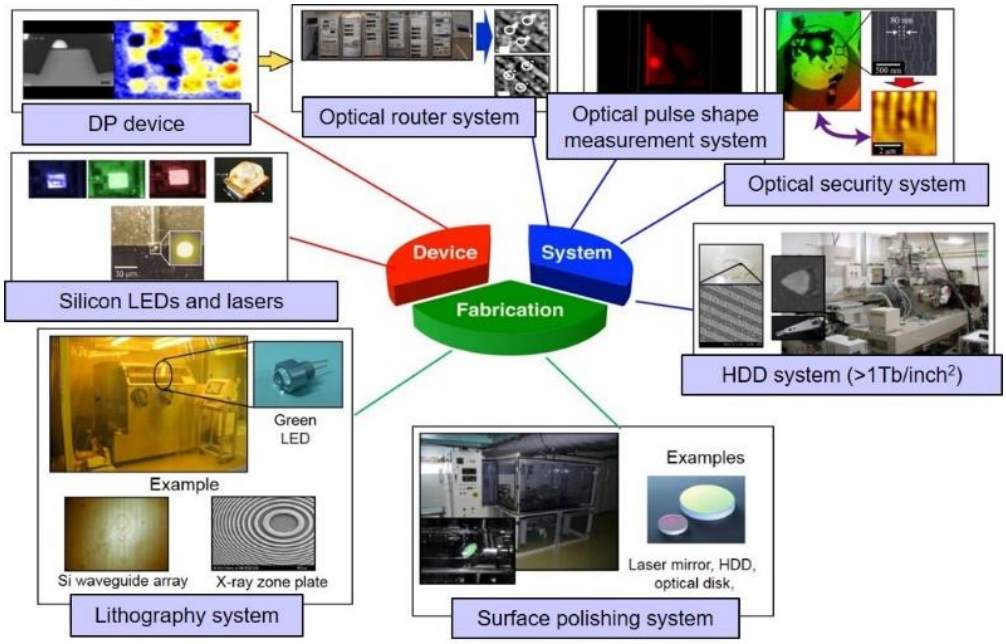

Fig.1 Generic technology that has emerged by applying the unique characteristics of the DP [4].

The advent of this technology suggests that the study of the DP has entered a new era in which the construction of advanced theories will be indispensable for accelerating technological progress.

(*) Characteristic [a] can be considered as the origin of characteristics [b] and [e]. Furthermore, characteristic [b] can be considered as the origin of characteristics [c] and [d], and characteristic [e] that of characteristic [f].

2 The dressed photon as an off-shell quantum field

Characteristics [a]–[h] in Section 1 cannot be described by conventional optical theories. This is because these theories have treated only a photon in vacuum (free photon) and in a macroscopic material, whose dispersion relation is on the mass-shell ("on-shell", for short). It has been popularly known that massless particles with non-zero spin, such as free photons, cannot be localized in space, in the sense that the position operator cannot be well-defined [5, 6]. However, it turns out to be natural to consider localized photons when the effective mass of photons, created by the light–matter interactions, is taken into account. Especially in the case of nano-materials, space–time localization and energy–momentum fluctuation provide brand new aspects of light. A photon in such a context is called a DP [1].

For a theoretical definition of the DP, the "off-shell" nature of the interaction has to be considered. That is, the DP is an off-shell quantum field that conspicuously deviates from the mass-shell in the dispersion relation (Fig. 2). As has been well known, quantum field theories cannot be formulated without off-shell entities. In other words, the traditional particle description has failed to treat the composite system of quantum fields. Hence, DPs must be entities that are very different from Einstein's quanta of light, or free photons.

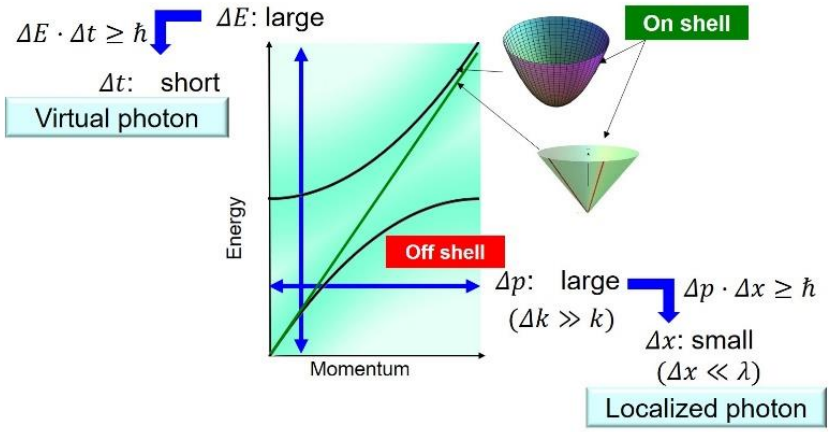

Fig.2 The dispersion relation of the electromagnetic field on-shell or off-shell.

E, t, p, x, k, and λ are energy, time, momentum, position, wave-number, and wavelength, respectively. $\hbar$ is Planck 's constant h divided by 2π.

Here, a fundamental question arises: How can the DP be described as an individual entity? As long as one sticks to the notion of individual entities as irreducible on-shell particles, it is impossible to treat the DP as an individual entity. However, a

more general perspective, advocated by Ojima [7], has shown that macroscopic physical phenomena can emerge out of a condensation of microscopic off-shell entities.

By following this perspective, a basic idea can be proposed: In the interaction between light and a nano-material, certain families of modes of the composite system will behave as individuals. This behavior suggests that the DP is the quantum field of a composite system in which an electromagnetic field and an electron (or an exciton) interact in a nanometric space. Furthermore, it is a virtual field localized in a nanometric space within a short time duration. Thus, the DP is a quantum field whose nature is incompatible with that of an on-shell photon. This means that conventional optical theories are incapable of giving a systematic description of characteristics [a]–[h] above. Fortunately, however, as will be reviewed in Sections 3 and 4, novel theoretical studies have been commenced in order to draw a precise theoretical picture of the DP to provide a systematic description of these characteristics.

Several hints have been found to construct such novel theories by noting that the virtual photon plays an essential role in the electromagnetic Coulomb interactions. They are:

[A] The longitudinal mode of an electromagnetic field (the longitudinal wave) contributes to the Coulomb interaction [8].

[B] The field interaction accompanies the 4-momentum [9].

[C] The spacelike field is not spatially localized because it behaves as a stable wave. However, it becomes unstable and can localize if it interacts with a timelike field [10].

By referring to these hints, novel theoretical studies relying on physical as well as mathematical bases have commenced [11].

3 Theories having a physical basis

This section reviews two examples of novel theories constructed on a physical basis. One is a response theory based on classical electromagnetics. The other is a theory based on spatio-temporal vortex hydrodynamics, supported by relativity theory.

3.1 Electromagnetic response theory

A novel response theory was constructed using an electromagnetic response function. As shown by Fig. 3, a nano-particle 1 (NP1) serves as a light source. It corresponds to a fiber probe that creates a DP on its tip. A nano-particle 2 (NP2) is illuminated by the light emitted from NP1. Since NP2 is placed in close proximity to NP1 in the case of

Fig. 3(a) ($d \ll \lambda$: d is the separation between NP1 and NP2, and λ is the wavelength of the light), the electron in NP2 responds not only to the transverse electric field ($\boldsymbol{E}^{(trans)}$) of the light but also to its longitudinal electric field ($\boldsymbol{E}^{(lon)}$).

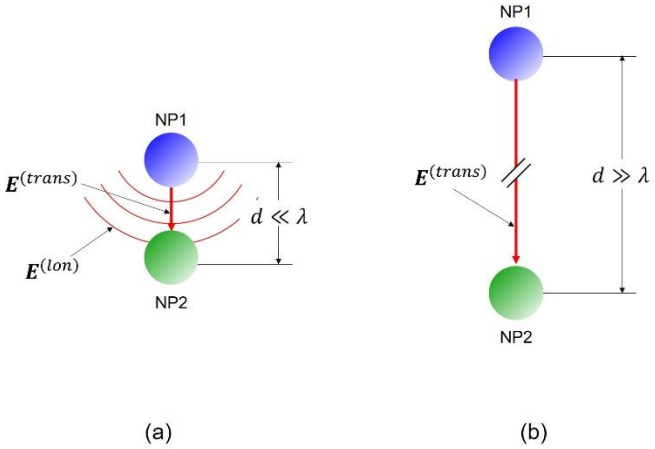

Fig.3 Schematic explanation of the theoretical model.
(a) Near-field condition. (b) Far-field condition.

The field $\boldsymbol{E}^{(trans)}$ is created by a transverse current in NP1. It is a radiative field that follows the Ampère-Maxwell law. It has been popularly known that conventional optical phenomena occur and are observed by this field even under far-field condition ($d \gg \lambda$: Fig.3(b)). On the other hand, $\boldsymbol{E}^{(lon)}$ is a non-radiative field, which is created by an electric charge in NP1 and follows Coulomb's law. It causes unique optical phenomena to occur only under the near-field condition ($d \ll \lambda$: (Fig.3(a)).

The Schrödinger equation was used to describe the electronic state in NP2 under light illumination, for which both the scalar (ϕ) and vector ($\boldsymbol{A}$) potentials, originated respectively from $\boldsymbol{E}^{(lon)}$ and $\boldsymbol{E}^{(trans)}$, were adopted to represent the light–matter interaction. The potentials ϕ and $\boldsymbol{A}$ appeared with the linear and quadratic forms, respectively, in the relevant equations. The difference in their forms originated from the non-relativistic nature of the system under study.

For describing the phenomena that originated from the DP, the present theory treats ϕ equivalently with $\boldsymbol{A}$. It should be noted here that the conventional response theories have eliminated ϕ by transforming it to the two-body Coulomb interaction potential. Being different from them, the present theory treats not only $\boldsymbol{A}$ but also ϕ as the "cause" of the response. For this treatment, a semiclassical response theory was constructed to derive the electric charge density and the electric current density, induced as the "response" of the electron in NP2. For representing the response, the single susceptibility was calculated by a method based on density functional theory.

From the time-integral of the commutator in the expressions for the electric charge and current densities in the NP2 (eqs. (6.17) and (6.18) in ref. [12], respectively), variables representing the energies appeared in the denominators of the derived fractions. These fractions denote the resonance phenomena because they diverge to infinity by tuning the photon energy. However, eq. (6.18) in ref. [12] also has non-resonant fractions that originated from the non-relativistic nature of the system. Since ϕ and $\boldsymbol{A}$ are respectively represented by $\boldsymbol{E}^{(lon)}$ and $\boldsymbol{E}^{(trans)}$, the susceptibility can be derived from the proportional constants between the induced electric charge density (current density) and $\boldsymbol{E}^{(lon)}$ ($\boldsymbol{E}^{(trans)}$).

In the case of the electric dipole-allowed transition between the two-energy levels of the electron, the cause of the response can be attributed to the total electric field $\boldsymbol{E}^{(total)}(=\boldsymbol{E}^{(lon)}+\boldsymbol{E}^{(trans)})$ when the system is under the far-field and resonant conditions. That is, the cause can be represented by $\boldsymbol{E}^{(total)}$ and the electric permittivity. However, in the case of phenomena that originated from the DP, especially the one that occurred under the non-resonant condition, it should be noted that $\boldsymbol{E}^{(total)}$ cannot serve as the cause of the response. This means that neither the constitutive equation using electric permittivity and magnetic permeability nor numerical simulation using the finite-domain and time-domain (FDTD) method are valid.

In the case of the electric dipole-forbidden transition, on the other hand, only the non-resonant term contributes. It was confirmed that this term led to an equation that is equivalent to the London constitutive equation for the Meissner effect. Thus, in this case, $\boldsymbol{A}$ serves as the cause of the response.

NP2 was assumed to be a nonmetallic material in the present theoretical study, and this has also been employed in a series of experimental studies on the DP [2,3]. A metallic material was not employed here because it is unsuitable for creating the DP. This is because the temporal coherence of the incident electromagnetic field is lost within a very short time due to the very short transverse relaxation time of an electron in the metal.

The constructed theory successfully described the excitation and de-excitation of electrons or excitons, the contribution of phonons, and the magnetic interactions found in experimental studies of the DP under the non-resonant condition of light–matter interaction. The main derived result is that: $\boldsymbol{E}^{(lon)}$ caused a large electronic response. Furthermore, the non-resonant term of the electric susceptibility was much larger than the resonant term [12], which explains characteristics [d] and [e].

As is understood from the discussions above, $\boldsymbol{E}^{(total)}$ failed to describe the response of NP2 in the case where the conditions of non-resonance and near-field

illumination/measurement are simultaneously met. This failure was never found in previous studies on the DP because only $\boldsymbol{A}$ was employed as the cause. The present theory succeeded in specifying that ϕ is indispensable for describing the bound state of the electron for which the quantum many-electron effect (i.e., an exchange/correlation interaction) was taken into account.

In future studies, more advanced response theories are expected to systematically explain characteristic [e].

3.2 Theory based on spatio-temporal vortex hydrodynamics

Characteristic [b] suggests that the inequality $E < cp$ holds (E, c, and p are the energy, speed, and momentum of an electromagnetic field, respectively), which means that the field can exist in the spacelike domain of the Minkowski space. In addition, [B] in Section 2 suggests that a timelike-support and spacelike-support of the 4-momenta are required to describe the interacting fields. By referring to these suggestions and also to [C] in Section 2, it can be conjectured that the DP can be created by the interaction between the fields in the timelike and the spacelike domains.

Prompted by this conjecture, a novel theory has been constructed by focusing on the similarity in formulation between vortex hydrodynamics and electromagnetics [13]. For this construction, it was also noted that the contribution of the spacelike momenta was indispensable for the interaction between the quantum fields to occur [9].

Conventional classical theories have claimed that the Coulomb mode played a principal role in the electromagnetic interaction and that the longitudinal wave was a physically existing mode [8, 14-16] (refer also to [A] in Section 2)[*]. In contrast, conventional theories of quantum electrodynamics have excluded the longitudinal wave as a "non-physical mode" even though it had a close relation with the Coulomb mode. Instead, they have introduced the exchange of virtual photons into the theoretical model for describing the electromagnetic interaction. This contrast suggests that a rift exists between the classical and quantum explanations above. This problem should be solved to draw a consistent physical picture of the DP that exists in an intermediate area between the classical and quantum worlds.

(*) This claim is consistent with the discussions in Section 3.1, where it was pointed out that the longitudinal electric field $\boldsymbol{E}^{(lon)}$ (and also ϕ) plays an essential role in the phenomena that originated from the DP.

It should be pointed out that the theory of micro-macro duality (Subsection 4.2 (2)) has already explained how to connect the classical and quantum worlds, by which a clue to solve the problem above can be found. The principal advantage of this theory is the capability of analyzing versatile structures of quantum fields with infinite degrees of freedom. This theory has demonstrated that the two worlds above coexist in the sense that the classical–quantum correspondence is mathematically guaranteed. The main purpose of the present subsection is to describe the electromagnetic interaction by adopting the micro–macro duality theory. It is expected that this description can systematically demonstrate the contributions of the longitudinal wave and the spacelike 4-momenta for drawing a physical picture of the DP.

For this demonstration, a novel mathematical expression, called the Clebsch representation, is adopted for the 4-vector potential of the electromagnetic field. The Clebsch representation is a method involving the use of Clebsch variables for representing the velocity vector field v_μ that is introduced to analyze the Hamiltonian of a barotropic fluid. It should be noted here that the mathematical structure (eq. (1a)) of the 4-vector potential $\boldsymbol{A}$ of the skew-symmetric electromagnetic field is similar to that of the equation of motion (eq. 1(b)) for a barotropic fluid based on relativity theory:

$$F_{\mu\nu}\partial^\nu\phi = 0, \tag{1a}$$

$$\omega_{\mu\nu}v^\nu = 0, \tag{1b}$$

where $F_{\mu\nu}$ denotes the skew-symmetric transverse electromagnetic field, and $\omega_{\mu\nu}$ is the skew-symmetric vorticity defined by the rotation of the velocity field v^ν. This similarity is due to the fact that the scalar field $\phi\left(=\partial_\nu A^\nu\right)$ satisfies the wave equation and its gradient vector $\partial_\nu\phi$ is parallel to the propagation direction of the wave (normal to the electric and magnetic fields).

Next, using the two-variable (λ and ϕ) Clebsch representation ($U_\mu = \lambda\partial_\mu\phi$), the v^ν in eq. (1b) is regarded as the vector potential of the electromagnetic field. Here, U_μ denotes the Clebsch parameterized 4-vector potential that is parallel to the 4-Poynting vector. Since $\omega_{\mu\nu}$ in eq. (1b) can also be regarded as denoting the

electromagnetic field, it is represented by the skew-symmetric field

$$S_{\mu\nu} = \partial_\mu U_\nu - \partial_\nu U_\mu . \tag{2}$$

Furthermore, the following two equations are derived, whose mathematical structure is similar to that of the Maxwell equation:

$$\partial^\nu \partial_\nu \lambda^\mu - \kappa^2 \lambda^\mu = 0 , \tag{3a}$$

$$\partial^\nu \lambda \partial_\nu \phi = 0 . \tag{3b}$$

Here, eqs. 3(a) and (b) indicate that λ follows a spatial Klein-Gordon (KG) equation, and that the two vectors ($\partial^\nu \lambda$ and $\partial_\nu \phi$) are normal to each other, respectively. Using the vector U_ν, these equations can be rewritten as

$$\partial^\nu \partial_\nu U^\mu - \kappa^2 U^\mu = 0 . \tag{4}$$

The field, represented by U_μ, can be called the Clebsch dual (CD) field by comparison with A^μ that satisfies the Proca equation

$$\partial^\nu \partial_\nu A^\mu + \kappa^2 A^\mu = 0 . \tag{5}$$

The energy-momentum tensor T_μ^ν for $S^{\mu\nu}$ is expressed as

$$T_\mu^\nu = -S_{\mu\sigma} S^{\nu\sigma} = \rho C_\mu C^\nu , \tag{6}$$

where $\rho \equiv -\partial^\mu \lambda \partial_\mu \lambda$ denotes a spacelike vector, being proportional to the spacelike momentum. $C_\mu \equiv \partial_\mu \phi$ represents a longitudinal wave. The middle part of eq. (6) has the same form as that of the conventional electromagnetic field. The right-hand side is given by the product of ρ and $C_\mu C^\nu$, which shows that the Clebsch representation succeeded in including two essential elements (the spacelike momentum and the longitudinal wave) in the equations.

Although U_μ was a null vector in the discussion above, it can be extended to

the spacelike domain so that T_{μ}^{ν} can be represented by

$$T_{\mu}^{\nu} = -S_{\mu\sigma}S^{\nu\sigma} + S_{\alpha\beta}S^{\alpha\beta}g_{\mu}^{\nu}. \tag{7}$$

The mathematical form of the right-hand side is equivalent to the curvature term in the Einstein equation. It should be pointed out that this equivalency was derived by breaking the U(1) gauge symmetry for extending the CD field to the spacelike domain. Equation (7) is acceptable because the CD field plays the role of the basic mode to represent the spacelike 4-momenta of the interacting fields and because the inherent feature of the relativistic field is represented by its space-time structure.

In order to apply the concept of the CD field above to draw the physical picture of the DP, several points should be noted: The spatially homogeneous spacelike momentum field becomes unstable if it interacts with the timelike momentum field, as was shown in [C] of Section 2. By such an interaction, the timelike and spacelike momentum fields can be transformed between each other, and, as a result, the spatial structures of the fields are significantly deformed. Although such a transformation occurs throughout the whole of the interacting area, it occurs more conspicuously at a singular point of the material, such as at the surface of the material or at the impurity atoms in the material (characteristic [a]).

Several discussions were made to describe this transformation: When the timelike momentum vector satisfies the timelike KG equation, its solution takes the form of a homogeneous wave. Such a homogeneous wavy solution can be also derived from the spacelike KG equation satisfied by the spacelike momentum vector. Since the constants in the KG equation represent the physical quantities of the material under study, the transformation between the timelike and spacelike vectors can be expressed by reversing the signs of these constants.

The information derived by these discussions is:

1) The complex-conjugate amplitudes

$$S_{0r}^{\dagger} = \frac{\omega}{c}R'\exp\left[\frac{\omega}{c}x^0\right], \quad S_{0r} = -\frac{\omega}{c}R'\exp\left[-\frac{\omega}{c}x^0\right] \tag{8}$$

of the derived CD field correspond to the creation ($\hat{a}^{\dagger}$) and annihilation ($\hat{a}$) operators of the quantum harmonic oscillator, respectively. Here, ω is the angular frequency. R' is the radial component of the solution of the KG equation. This correspondence enabled the definition of the normal mode of the electromagnetic field in a sub-wavelength-sized field, which had been impossible with the previous theory [17].

2) The CD field represents a longitudinal wave (the complex-conjugate amplitudes C_μ and C_μ^*) that is accompanied by the components ($L_\mu (= \partial_\mu \lambda)$ and L_μ^*) satisfying the KG equation in the spacelike domain (Fig. 4).

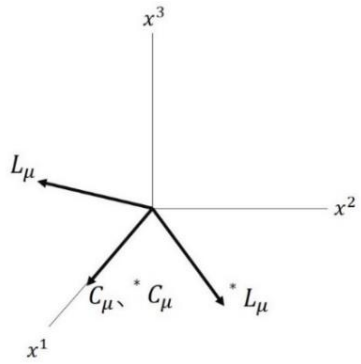

Fig.4 Directions of the amplitudes of the longitudinal wave (C_μ and C_μ^*) and those of the accompanying components (L_μ and L_μ^*).

x^1 represents the propagation direction of the electromagnetic wave.

3) The components (L_μ and L_μ^*) become temporally unstable due to the interaction with the field in the timelike domain. As a result, they are created or annihilated within a very short duration, which means that the CD field corresponds to a virtual photon.

4) The transverse wave of the CD field is converted to a longitudinal wave at the material surface. This means that the material surface serves as the source of a longitudinal wave, thus successfully describing characteristic [a].

5) The spatial profile of the field is described by a Yukawa-type function, which can be understood by replacing x^0 in S_{0r} of eq.(8) by x^1, x^2, or x^3. As a result, characteristic [a] was also described. This means that the DP is a localized quantum field, created as a result of the transformation of the spacelike momentum field to the timelike field at a singular point of the material.

6) The DP can be represented by the superposition of the longitudinal waves of the CD field. This representation is possible because these waves behave as normal modes. It

should be pointed out that the virtual photon behavior of the components (L_μ and L_μ^*), accompanying this longitudinal wave, is nothing less than the origin of this successful representation.

These findings 1) – 6) were derived by adopting the longitudinal wave in the present theory as a physical mode. Future progress is expected to explain characteristics [g] and [h], and also to establish the theory of the fully quantum optical version.

4 Theories having a mathematical basis

It is expected that mathematics-based theories will serve as invaluable guides for gaining a deep understanding of the concepts of the physics-based theories for the phenomena that originate from the DP. Examples of these theories are the quantum probability theory and the quantum measurement theory, which are reviewed in this section. Also demonstrated is a theory based on micro–macro duality, which serves as a foundation for embarking on theoretical studies of off-shell science.

4.1 Quantum probability theory

Quantum probability theory has been constructed by noting characteristic [b] above [18]. This theory focuses on the families of the higher and lower energy–momentum modes for investigating phenomena that cannot be analyzed by conventional on-shell theories. The family of higher modes of the composite system is created as a result of light–matter interaction and behaves like an individual entity. This entity can be defined as the DP. The family of lower modes serves as a kind of heat-bath.

Since no a priori strict boundary between the higher and lower modes exists, it is required to investigate the asymptotic behavior of modes where the energy–momentum becomes large. In other words, the core of a mathematical theory for the DP is nothing but a kind of quantum-classical correspondence for describing an asymptotic state that appears as its quantum number increases to infinity. Hence, some general frameworks are required for both quantum/micro and classical/macro systems. Fortunately, a mathematical theory that meets this requirement has been constructed, that is, the quantum probability theory. The intermediate realm, appearing between the micro- and the macro-systems, has been successfully described by this theory.

As has been popularly known, a quantum harmonic oscillator with a large quantum number behaves very much like a classical harmonic oscillator. The composite

system created by light–matter interaction is considered to be a typical example of such a quantum harmonic oscillator. This consideration and the definition of the DP above lead to the fact that the time averaged distribution of the position of the DP can be governed by an arcsine law. Note that each mode of the DP gains an effective mass by the interaction between the light and nano-material, and thus, it is not paradoxical to consider the position of the DP. Moreover, since the size of the nano-material is much less than the wavelength of light, the variance of the distribution will be determined by this size. The stronger the interaction, the higher the energy at a suitable boundary between the family of the higher mode (DP) and that of the lower mode (heat bath). Hence, it is expected that the arcsine law will represent a sufficiently accurate distribution of the DP when the interaction is sufficiently strong.

Since the arcsine function has a twin-peaked profile, the probability of finding the DP will be the highest at the singular point, which is the reason why localization of the DP occurs at the boundary. This localization feature is quite consistent with the experimental results acquired so far [19].

Here, let us take as the most fundamental example the localization of the DP in a fiber probe [20]. The three-dimensional density of the DP can be expressed by an arcsine function

$$f(x) = C\frac{1}{S(x)\sqrt{2-x^2}}, \tag{9}$$

where C and $S(x)$ respectively denote the normalization constant and the cross-sectional area of the fiber probe on which the DP is created. The localization of the DP at the tip of the fiber probe, and furthermore, at the position of the impurity atoms in the material were successfully described based on the twin-peaked spatial feature (peaks at $x = \pm\sqrt{2}$ in eq. (9)) [18].

In conjunction with the quantum probability theory above, a quantum walk model was used to mathematically describe characteristics [a], [g], and [h]. It was also used to analyze the dynamic behavior of the composite system created as a result of the interaction between multiple quantum fields. Furthermore, it was aimed at exploring the master equation for describing the dynamics of the DP by noting that their behaviors are similar to those of the quantum walk. It has been experimentally confirmed that these behaviors exhibited inherent characteristics that corresponded to those of the quantum walk [21]: The temporal behavior of the DP energy transfer between the two NPs in Fig.

3(a) was least-squares fitted to an exponentially decaying function $\exp(-t/\tau)$, where t and τ represent time and the time constant of the phenomena, respectively. This exponential decay corresponds to the quantum walk dynamics*.

(*) The temporal behavior of the random walk is represented by $\exp\left(-\sqrt{t/\tau}\right)$, which exhibits slower decay than that of the quantum walk.

By referring to the arcsine law derived by the quantum probability theory, numerical simulations were carried out to analyze the creation of the DP and its energy transfer in a fiber probe-to-fiber probe system. As is schematically explained by Fig. 5(a), two fiber probes served as a sender and a receiver of the DP energy under collective excitation by conventional propagating light.

Two assumptions were made for this analysis. They were: (a1) The sender fiber probe was coherently excited by the incident light. (a2) The created DP hopped from one atom to an adjacent atom in a coherent manner, which corresponded to the quantum walk process. The analysis described three energy dissipation phenomena caused by the energy conversion from the DP to the conventional propagating light: (d1) The conversion to a conventional electromagnetic field to be guided backward to the main body of the sender fiber probe. (d2) The conversion to a conventional electromagnetic field to be guided forward to the main body of the receiver fiber probe. (d3) The conversion to a conventional electromagnetic field that propagates out from the tapered part of the fiber probe to the outer free space. As a result, it was confirmed that, among all of the created DPs, the one created by the pair of anti-parallel electric dipoles was localized at the tip of the fiber probe without being dissipated through phenomena (d1) – (d3).

Figures 5(b) and (c) show the calculated results for the single-tapered and double-tapered fiber probes, respectively [22]. They demonstrate that the double-tapered fiber probe concentrated the DP energy at its tip more efficiently than that at the single-tapered one. This suggests that the double-tapered fiber probe is more advantageous for creating/measuring the DP with higher efficiency, which is consistent with the experimental results [23].

Future developments in this study are expected to explain also characteristics [a], [g], and [h].

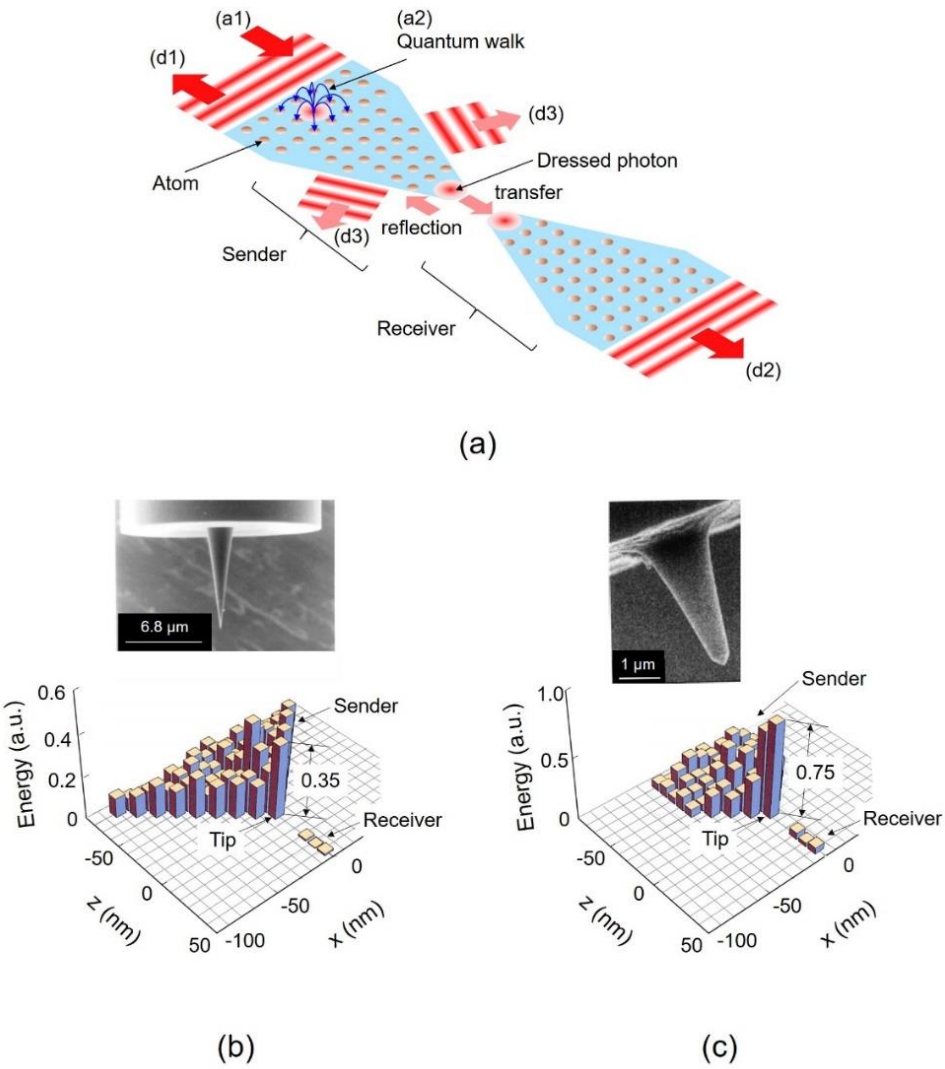

Fig.5 Simulation by a quantum walk model.

(a) The fiber probe-to-fiber probe system. (a1) and (a2) represent the two assumptions. (d1)-(d3) are the energy dissipation phenomena. (b) and (c) represent the calculated results for single-tapered and double-tapered fiber probes, respectively. The photos show scanning electron microscopic images of these fiber probes.

4.2 Other basic theories having a mathematical basis

(1) Quantum measurement theory: A theoretical description of characteristic [f] is essential for understanding the process of measuring the DP. Here, the problem is how to describe the dynamics of the DP energy transfer that occurs during the measurement. To solve this problem, quantum measurement theory, a branch of algebraic quantum theory, is under construction based on the theory of operator algebra, especially, C^*-

algebra. C^*-algebraic quantum theory is advantageous because it can explicitly describe macroscopic classical levels of quantum systems.

Mathematical issues for constructing the algebraic quantum measurement theory for the DP have been surveyed [24, 25]. They are:

1) Two methods are possible. Their mathematical issues are: [For the top-down method] After the mathematical model is built based on the universal gauge principle of quantum electrodynamics, several approximations should be made depending on the scale of the system or the properties of the material fields. [For the bottom-up method] This method is advantageous to build a mathematical model for describing the properties of the energy–momentum and the properties of localization of the DP. This model should be built by considering the ability to extend and scale it.

2) Mathematical modeling should start from the space-time area $\mathcal{O}$ in which nano-materials are provided. Here, a sub-space of the real space can work as the area $\mathcal{O}$. Next, an algebra $\mathcal{A}(\mathcal{O})$, composed of physical quantities in the area $\mathcal{O}$, is considered. Then, the temporal evolution $\alpha_t{}^{\circ} \cap \mathcal{A}(\mathcal{O})$ is considered for each area $\mathcal{O}$. Microscopic physical quantities, representing the boundary conditions (the lattice defects, as an example), can be included in $\alpha_t{}^{\circ}$. For this consideration, the measurement process can be represented by the inclusion relation $\mathcal{O} \subset \mathcal{O}_2$, where $\mathcal{O}_2$ represents the space-time domain under study. Finally, the measurement theory is expected to be established by the algebra $\mathcal{A}(\mathcal{O}_2)$.

(2) Theory based on micro–macro duality: Based on an algebraic quantum field theory, micro–macro duality theory has been constructed as a powerful mathematical guide for analyzing the nature of the DP [26]: Symmetry breaking in the algebra in a microscopic area can produce multiple sector spaces. Some physical quantities in these sector spaces satisfy the commutativity requirement, and the quantity named the center can be used to classify the sector spaces. That is, a commutative observable classical system and a non-commutative quantum system can coexist in each sector space, and this provides the basic structure for quantum-classical correspondence.

The sector space can be interpreted also as a mathematically symmetric space. It has been found through this interpretation that the automorphic form plays an essential role. Several discussions were made by taking a fiber probe as a test system: In order to construct a consistent theory for describing the DP, it will be a crucial breakthrough to faithfully reproduce its proper dynamic functions. This reproduction forms the micro–macro boundary level described by a symmetric space arising from a broken symmetry,

which is possible by projecting the *s*-channel structure at the invisible micro-level to the spacelike *t*-channel. If suitable automorphic forms defined on this symmetric space are successfully identified, it will become possible to describe any of non-trivial dynamic phenomena caused by the DP. In particular, the automorphic factor appearing in the definition of an automorphic form will play an important role as a cocycle carrying the dynamic properties of the invisible micro-level. In the context of the DP, this will perhaps justify an analogy with the dynamic behavior played by the Regge trajectories, which carry spacelike momenta in the hadronic scattering processes originating from the dual resonance structure.

As is shown by Fig. 6, the theory based on micro–macro duality serves as a foundation of the theories reviewed in this article. This figure also summarizes the principal characteristics of the DP, the developed theories, their physical and/or mathematical methods, and information derived by these theories. The red double-pointed arrows indicate the topics commonly described by the multiple theories. By noting these arrows, correlations between the theoretical studies can be clearly recognized. Successful construction of off-shell science, guided by systematic studies on the DP, is expected by analyzing these correlations. It is also expected that the micro–macro duality theory will serve as a guide to this development.

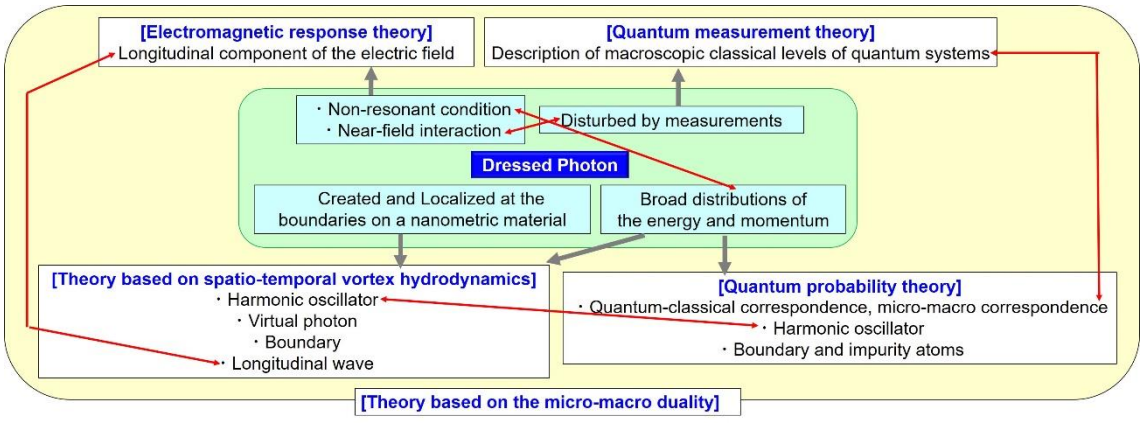

Fig.6 The principal characteristics of the DP, developed theories, their physical and/or mathematical methods, and information from the theoretical studies described in Sections 3 and 4.

Red double-pointed arrows indicate the topics common to the adjacent theories.

5. Summary

This article reviewed recent progress in the theoretical studies toward the development of off-shell science. First, it was pointed out that the DP is a quantum field whose

energy–momentum relation deviates from the mass-shell. Second, the characteristics of the DP, as an off-shell quantum field, were reviewed. Third, theories having a physical basis were demonstrated. They were the electromagnetic response theory and a theory based on spatio-temporal vortex hydrodynamics. Fourth, theories having a mathematical basis were introduced, which can serve as invaluable guides for gaining a deep understanding of the concepts of the physics-based theories above. These theoreies were quantum probability theory and quantum measurement theory. Finally, a micro–macro duality theory was demonstrated, which serves as a foundation for embarking on the study of off-shell science.

Acknowledgements

A part of this work was supported by Research Foundation for Opto-Science and Technology. The author thanks Dr. I. Ojima(RODreP), Dr. H. Sakuma (RODreP), Dr. H. Saigo (Nagahama Inst. Bio-Sci. and Technol.), Dr. K. Okamura (Nagoya Univ.), Dr. I. Banno (Yamanashi Univ.), and Dr. K. Ando (Chiba Univ.) for their collaborations in theoretical research on the dressed photons and off-shell science.

References

[1] M. Ohtsu: *Dressed Photons*, Springer, Heidelberg （2014）pp.1-136.

[2] M. Ohtsu: *Dressed Photons*, Springer, Heidelberg （2014）pp.137-246.

[3] M. Ohtsu: *Silicon Light-Emitting Diodes and lasers*, Springer, Heidelberg (2016) pp.1-138.

[4]M. Ohtsu, “Historical Review of Dressed Photons: Experimental Progress and Required Theories,” *Progress in Nanophotonics* 5, (ed.) T. Yatsui, Springer, Heidelberg (2018) pp.1-51.

[5] T.D. Newton and E. P. Wigner, “Localized States for Elementary Systems,” Rev. Mod. Phys, **21** (1949) pp.400 - 406.

[6] A. S. Wightman, “On the Localizability of Quantum Mechanical Systems,” Rev. Mod. Phys., **34** (1962) pp.845 - 872.

[7] I. Ojima, “Micro-macro duality in quantum physics, “ in *Stochastic Analysis:Classical and Quantum Perspectives of White Noise Theory*, (ed.) T. Hida, World Scientific, Singapore (2005) pp. 143–161.

[8] I. Ojima,"Nakanishi-Lautrup B field, crossed product and duality," in R*esearch on Quantum Field Theory*, RIMS Workshop, Kyoto, 2006, pp.29-37.

[9] R. Jost, "The General Theory of Quantized Fields," in *Lectures in Applied Mathematics*, Volume IV, XV + 157 S. Providence, Rhode Island, 1965, American Mathematical Society.

[10] Y. Aharanov, A. Komar, L. Susskind, "Superluminal Behavior, Causality, and Instability," Phys. Rev., **182** (1969) pp.1400-1403.

[11] T. Yatsui (ed.): *Progress in Nanophotonics* 5, Springer, Heidelberg (2018) pp.1-210.

[12] I. Banno, "Response Theory Supporting Dressed Photons," *Progress in Nanophotonics 5*, (ed.) T. Yatsui, Springer, Heidelberg (2018) pp.169-200.

[13] H. Sakuma, "Virtual Photon Model by Spatio-Temporal Vortex Dynamics," *Progress in Nanophotonics* 5, (ed.) T. Yatsui, Springer, Heidelberg (2018) pp.53-77.

[14] H. Sakuma, I. Ojima, and M. Ohtsu, "Gauge symmetry breaking and emergence of Clebsch-dual electromagnetic field as a model of dressed photons," Appl. Phys.A (2017) 123:750.

[15] H. Sakuma, I. Ojima and M. Ohtsu, "Dressed photons in a new paradigm of off-shell quantum fields," Progress in Quantum Electronics, **55** (2017) pp.74-87.

[16] L. Cicchitelli, H. Hora, and R. Postle, "Longitudinal field components for laser beams in vacuum," Phys. Rev. A **41** (1990) pp.3727-3732.

[17] M. Ohtsu, *Dressed Photons*, Springer, Heidelberg (2014) pp.11-36.

[18] H. Saigo, "Quantum Probability for Dressed Photons: The Arcsine Law in Nanophotonics," *Progress in Nanophotonics* 5, (ed.) T. Yatsui, Springer, Heidelberg (2018) pp.79-106.

[19] M. Ohtsu, *Dressed Photons*, Springer, Heidelberg (2014) pp.89-246.

[20] M. Ohtsu (ed.), *Near-Field Nano/Atom Optics and Technology*, Springer, Tokyo (1988) pp.15-100.

[21] M. Ohtsu, T. Kawazoe, and H. Saigo, "Spatial and Temporal Evolutions of Dressed Photon Energy Transfer," Offshell: 1710R,001.v1 (2017).

[22] S. Sangu, H. Saigo, M. Ohtsu, “Simulation of Dressed Photon Energy Transfer based on Quantum-Walk Model,” “An approach from measurement theory to dressed photon,” Abstracts of the 79th Jpn. Soc. Appl. Phys. Autumn Meeting, September 2018, Nagoya, Japan, paper number 19a-437-7.

[23] M. Ohtsu (ed.), *Near-Field Nano/Atom Optics and Technology*, Springer, Tokyo (1988) pp.71-87.

[24] K. Okamura, “An Approach from Measurement Theory to Dressed Photon,” *Progress in Nanophotonics 5*, (ed.) T. Yatsui, Springer, Heidelberg (2018) pp.137-167.

[25] K. Okamura, “An approach from measurement theory to dressed photon,” Abstracts of the 79th Jpn. Soc. Appl. Phys. Autumn Meeting, September 2018, Nagoya, Japan, paper number 19a-437-4.

[26] I. Ojima, “Control over Off-Shell QFT via Induction and Imprimitivity,” *Progress in Nanophotonics 5*, (ed.) T. Yatsui, Springer, Heidelberg (2018) pp.107-135.

Gigantic Ferromagnetic Magneto-Optical Effect in a SiC Light-emitting Diode Fabricated by Dressed-Photon–Phonon-Assisted Annealing

M. Ohtsu[1] and T. Kawazoe[2]

[1]Research Origin for Dressed Photon,
c/o Nichia Corp., 3-13-19 Moriya-cho, Kanagawa-ku, Yokohama, Kanagawa 221-0022 Japan
[2]Tokyo Denki University,
5 Senju-Asahi-cho, Adachi-ku, Tokyo 120-8551, Japan

Abstract

This paper investigates the gigantic magneto-optical effect in a SiC light-emitting diode fabricated by dressed-photon–phonon (DPP)-assisted annealing. Very large values of the Verdet constant and the Faraday rotation angle were obtained, namely, 660 deg/A and 2480 deg/cm, respectively, at a wavelength of 405 nm. The remanent magnetization was 0.36 mT. The magnetization curve, acquired at 27 °C, exhibited a clear hysteresis characteristic. This behavior of the SiC crystal, equivalent to that of a ferromagnet, was attributed to Al atom pairs autonomously formed as a result of the DPP-assisted annealing.

1 Introduction

Although crystalline silicon (Si) has been popularly used for electronic devices, there is a long-held belief that Si is not suitable for use in light-emitting devices because it is an indirect-transition-type semiconductor, and thus, its emission efficiency is very low. However, dressed-photon–phonon (DPP)-assisted annealing [1] has drastically increased the emission efficiency, resulting in the realization of novel light sources, including light-emitting diodes (LEDs) and lasers [2]. A novel photo-detector with optical gain [3] has also been realized by using crystalline Si. These devices can be advantageously applied to future photonic technology because crystalline Si is a nontoxic, abundant material, and furthermore, these devices can be integrated with electronic devices. Crystalline SiC, another indirect-transition-type semiconductor, has also been used to fabricate LEDs having light emission in the short-wavelength region

with the DPP-assisted annealing [4,5]. In addition to these optical functional devices, an optical polarization rotator using crystalline SiC has been invented [6,7], which can be used as an optical signal modulator. The advent of such novel devices means that conventionally used direct-transition-type composite semiconductors can be replaced by indirect-transition-type semiconductors in the fabrication of the basic devices needed for future optical signal processing and transmission systems.

The present paper investigates the fabrication and operation of an optical polarization rotator using crystalline SiC. The unique phenomenon involved here is that the crystalline SiC exhibits a gigantic magneto-optical effect and also a ferromagnetic characteristic.

2 Device structure

This section briefly describes the SiC device structure for the optical polarization rotator. A detailed description has been given in refs. [4,5]. An n-type 4H-SiC crystal with a resistivity of 25m Ωcm and (0001) surface orientation was used. A 500 nm-thick n-type buffer layer was deposited on this crystal, after which a 10 μm-thick n-type epitaxial layer (n-type dopant (N atoms) density 1×10^{16} cm^{-3}) was deposited. The surface of the 4H-SiC crystal was then implanted with an p-type dopant (Al atoms) by ion implantation. To activate the Al ions for forming a p-n homojunction, thermal annealing was performed for 5 min. at 1800 °C. After this, a second thermal annealing was performed under the same conditions as above.

Although the structure was almost the same as that of the SiC-LED described in refs. [4,5], it was inverted, resulting in the SiC substrate being the top layer. Furthermore, an H-shaped electrode formed of a Cr/Pt/Au (100 nm/150 nm/200 nm thick) stripe film was deposited on the top surface, as shown in Fig. 1(b). A homogeneous electrode formed of Cr/Ni/Au (100 nm/150 nm/200 nm thick) was deposited on the bottom surface. After this, the 4H-SiC crystal was diced to form a device with an area of $500\ \mu m \times 500\ \mu m$. Figures 1(a) and (b) show the cross-sectional structure of a fabricated device and a photograph of the device taken from above, respectively.

A forward bias voltage of 12 V (current density 45 A/cm^2) was applied to the device to bring about annealing due to Joule-heat, which caused the Al atoms to diffuse. During this process, the device was irradiated from the top surface with laser light (optical power 20 mW) having a wavelength of 405 nm. This induced the DPP-assisted

annealing process, which modified the Al diffusion, leading to the autonomous formation of a spatial distribution of Al atoms. As a result, the device worked as an LED by momentum exchange between the electrons in the conduction band and the multimode coherent phonons in the DPP. The light emission principle, device fabrication, and operating characteristics of this LED were described in refs. [4, 5].

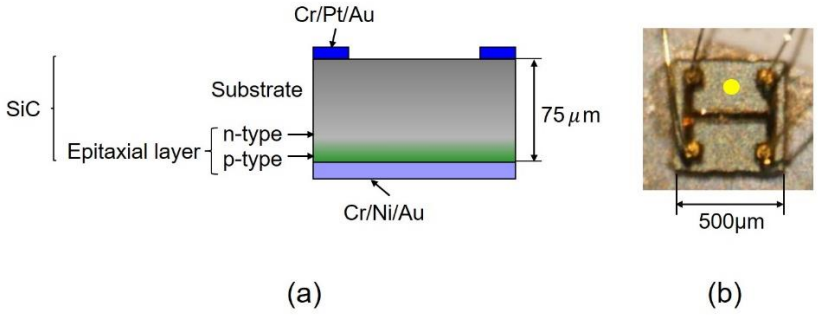

Fig. 1 Cross-sectional profile (a) and photograph (b) of a polarization rotator using a 4H-SiC crystal. The yellow circle represents the cross-sectional position of the incident light beam.

3 Performance of optical polarization rotator

To operate the device as an optical polarization rotator, a current was injected to the H-shaped electrode to inject electrons and to generate a magnetic field, simultaneously. The spatial distribution of the magnetic flux density $\boldsymbol{B}_{\perp}$ normal to the top surface (the upward green arrow in Fig. 2(a)) was estimated by numerical simulation. Figure 2(b) shows the result, where the injection current I was 30 mA. (Since the p-n homojunction was only 75 μm below the top surface, the value of $\boldsymbol{B}_{\perp}$ in this figure can be considered to be equal to that at the p-n homojunction.)

In order to measure the polarization rotation angle θ_{rot}, linearly polarized 405 nm-wavelength light was made normally incident on the top surface of this device, as schematically illustrated in Fig. 3(a). The yellow circles in Figs. 1(b) and 2(b) represent the cross-section of the incident light beam. The value of $\boldsymbol{B}_{\perp}$ at this spot was evaluated to be 1.8 mT from Fig. 2(b). That is, the relation

$$\frac{dB_{\perp}}{dI} = 0.06 \text{ (T/A)} \qquad (1)$$

holds.

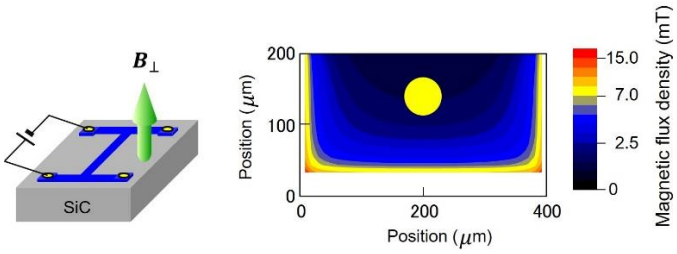

(a) (b)

Fig. 2 Magnetic flux density generated by the current injected into the H-shaped electrode. (a) Schematic illustration of the profile of the H-shaped electrode formed of a Cr/Pt/Au stripe film on the top surface. The upward green arrow represents the normal component $\boldsymbol{B}_\perp$ of the generated magnetic flux density. (b) Calculated spatial distribution of $\boldsymbol{B}_\perp$, where the injected current was 30 mA. The yellow circle represents the cross-sectional position of the incident light beam (Fig. 3(a)).

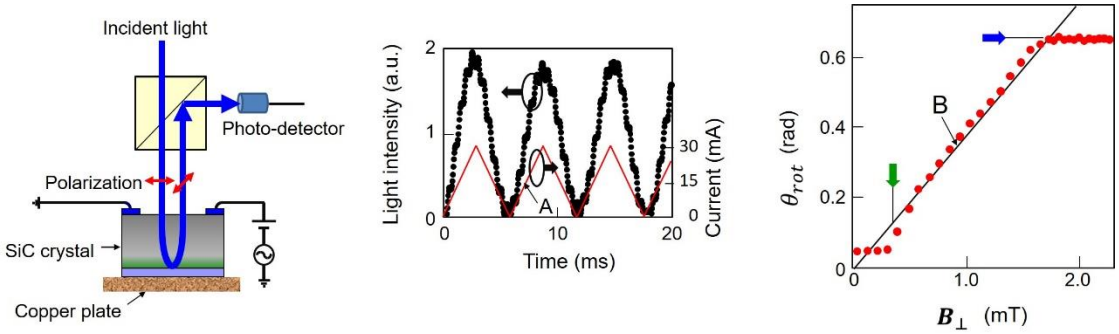

(a) (b) (c)

Fig. 3 Measured temporal variation of the light intensity and the estimated values of the polarization rotation angle θ_{rot}. (a) Experimental setup to measure the value of θ_{rot}. (b) Closed circles represent the measured light intensity transmitted through the Glan-Thompson prism. The red line A is the waveform of the triangular current injected into the device. Its frequency and amplitude were 166 Hz and 30 mA, respectively. (c) The relation between $\boldsymbol{B}_\perp$ and θ_{rot}. (The unit (π rad) written along the vertical axis of Fig. 2 in ref.[6], and also that of Fig. 8.18(b) in ref. [7], is wrong. The correct unit (rad) is written on the vertical axis of (b) above.)

The light reflected from the Cr/Ni/Au film on the rear surface propagated back to the top surface and was transmitted through a Glan-Thompson prism, after which the transmitted light intensity was measured. Closed circles in Fig. 3(b) represent the measured values of the transmitted light intensity. As shown by a red line A, the frequency and the amplitude of the triangular current injected into the H-shaped

electrode were 166 Hz and 30 mA, respectively. The measured relation between $\boldsymbol{B}_{\perp}$ and θ_{rot} was derived from this figure and is represented by the red circles in Fig. 3(c). The solid line B was fitted to these circles. From the slope of the line B, the relation

$$\frac{d\theta_{rot}}{dB_{\perp}} = 2.2 \times 10^{3} (\text{deg/T}) \qquad (2)$$

is derived.

From eqs. (1) and (2), the relation

$$\frac{d\theta_{rot}}{dI} = \frac{dB_{\perp}}{dI} \times \frac{d\theta_{rot}}{dB_{\perp}} \times \frac{1}{2} = 660 (\text{deg/A}) \qquad (3)$$

is derived, where the value (1/2) was inserted in the left-hand side in order to evaluate the value for the one-way propagation of the light through the SiC crystal. This value corresponds to the Verdet constant, which was 10^5-10^6 times higher those of conventional paramagnetic materials that are transparent in the visible region [8]. This means that the present SiC crystal exhibited a gigantic magneto-optical effect.

The right-pointing blue arrow in Fig. 3(c) indicates that θ_{rot} saturated as $\boldsymbol{B}_{\perp}$ increased, as has been widely observed in conventional ferromagnetic materials. The saturated value was 0.65 rad (=37 deg). The total optical path length of the incident light propagating through the SiC crystal was 150 μm because the crystal thickness was 75 μm, as shown in Fig. 1(a). Thus, the saturated value, normalized to the unit optical path length, corresponding to the Faraday rotation angle [8], was as large as 2480 deg/cm. Furthermore, the downward green arrow indicates the threshold value of $\boldsymbol{B}_{\perp}$, which was 0.36 mT. This value corresponds to the remanent magnetization in conventional ferromagnetic materials, and was as large as those values. The two arrows suggest that the presently used SiC crystal acquired novel properties, equivalent to those of ferromagnetic materials.

In order to find the origin of such novel ferromagnetic properties, a magnetization curve was acquired uisng a SQUID [6]. The results are given in Fig. 4. Here, the applied magnetic field $\boldsymbol{H}$ (Oe) was proportional to the current injected to the H-shaped electrode. The black squares represent the measured values of the magnetization $\boldsymbol{M}$ (emu/cm^3) per unit volume of the SiC crystal. The solid curves were fitted to the black squares. These results clearly exhibit a hysteresis characteristic, which is inherent to ferromagnetic materials. Since these results were acquired at 27 °C, it was confirmed that the Curie temperature was estimated to be higher than 27 °C. Red open circles in this figure are the measured values before the DPP-assisted annealing was carried out, where the values of $\boldsymbol{M}$ are much smaller those of the black squares, and no hysteresis characteristic is seen.

By comparing the black squares and red open circles, it was confirmed that the semiconductor SiC crystal was made to behave as a ferromagnet as a result of the DPP-assisted annealing. This behavior originated from the formation of Al atom pairs, autonomously formed as a result of the DPP-assisted annealing. (For reference, this autonomous formation has also been confirmed in the case of B atoms in a Si-LED [2].) This origin can be understood by referring to the following two research findings:

(1) It has been found that the triplet state of the electron orbital in an Al atom pair is more stable than the singlet state [9].

(2) Two electrons with parallel spins in the triplet state induce the ferromagnetic characteristic [10].

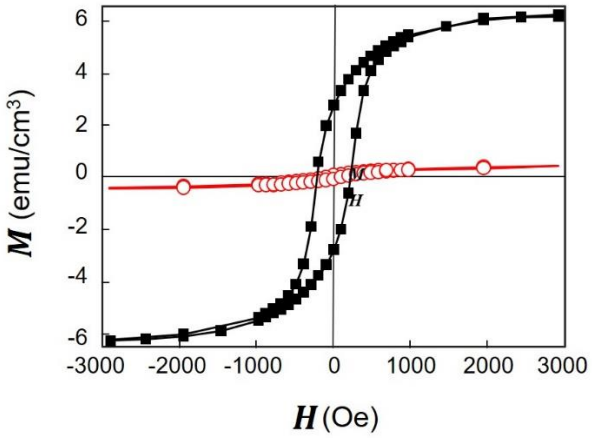

Fig. 4 Magnetization curve, measured at 27 °C. Black squares and red open circles are for the 4H-SiC crystals after and before the DPP-assisted annealing, respectively.

4 Summary

This paper investigated the gigantic magneto-optical effect in a SiC-LED fabricated by DPP-assisted annealing. This device rotated the polarization angle of linearly polarized incident light. Very large values of the Verdet constant and the Faraday rotation angle were obtained, namely, 660 deg/A and 2480 deg/cm, respectively, at a wavelength of 405 nm.

The magnetization curve, acquired at 27 °C, exhibited a clear hysteresis characteristic, by which it was confirmed that the SiC crystal behaved as a ferromagnet. This characteristic was attributed to Al atom pairs, autonomously formed as a result of the DPP-assisted annealing.

References

[1] M. Ohtsu, *Silicon Light-Emitting Diodes and Lasers*, Springer, Heidelberg (2016) pp.16-19.

[2] M. Ohtsu, *Silicon Light-Emitting Diodes and Lasers*, Springer, Heidelberg (2016) pp.15-102.

[3] M. Ohtsu, *Silicon Light-Emitting Diodes and Lasers*, Springer, Heidelberg (2016) pp.126-131.

[4] T. Kawazoe and M. Ohtsu, Appl. Phys. A, **115** (2014) pp.127-133.

[5] M. Ohtsu, *Silicon Light-Emitting Diodes and Lasers*, Springer, Heidelberg (2016) pp.83-101.

[6] T. Kawazoe, N. Tate, and M. Ohtsu, "SiC magneto-optical current-transformer applicable to a polarization rotator using dressed photons," Abstract of the 22nd International Display Workshops, Dec. 9-11, 2015, Otsu, Japan, PRJ3-5L.

[7] M. Ohtsu, *Silicon Light-Emitting Diodes and Lasers*, Springer, Heidelberg (2016) pp.132-138.

[8] *Chronological Scientific Tables*, the 77th edition, (ed)National Astronomical Observatory of Japan, Maruzen Co., Tokyo, Japan (2004) p.449

[9] T.H. Upton, "Low-lying valence electronic states of the aluminum dimer," J. Phys. Chem., **90** (1986) pp.754-759.

[10] A. Rajca, "Organic Diradicals and Polyradicals: From Spin Coupling to Magnetism?, " Chem. Rev., **94** (1994) pp.871-893.

Principles and Practices of Si Light Emitting Diodes using Dressed Photons

M. Ohtsu[1] and T. Kawazoe[2]

[1]Research Origin for Dressed Photon,
c/o Nichia Corp., 3-13-19 Moriya-cho, Kanagawa-ku, Yokohama, Kanagawa 221-0022 Japan
[2]Tokyo Denki University,
5 Senju-Asahi-cho, Adachi-ku, Tokyo 120-8551, Japan

Abstract

This paper reviews basic research and technical developments on silicon (Si) light-emitting diodes (Si-LEDs) fabricated by using a novel dressed-photon–phonon (DPP) annealing method. These devices exhibit unique light emission spectral profiles in the wavelength range 900–2500 nm, including novel photon breeding features. The highest optical output power demonstrated was as high as 2.0 W. It is pointed out that boron (B) atoms, serving as p-type dopants, formed pairs whose length was three-times the lattice constant of the host Si crystal. These B atom pairs are the origin of the photon breeding. A phenomenological two-level two-state (TLTS) model is presented, revealing that the external electric and optical fields, applied during the DPP-assisted annealing, drastically decrease the height of the potential barrier between the two states. This decrease is the reason why the spatial distribution of B atoms is efficiently modified by the DPP-assisted annealing even at low temperature. The TLTS model and a stochastic model confirm that the optimum DPP-assisted annealing is realized by setting the ratio of the electron injection rate and the photon irradiation rate to 1:1. A phase diagram is presented as an aid for developing a novel theory for realizing more efficient and higher-power Si-LEDs.

1 Introduction

Crystalline silicon (Si) has long been a key material supporting the development of electronics engineering for more than half a century. However, because Si is an indirect-transition type semiconductor, it has been considered to be unsuitable for light-emitting devices. Because the bottom of the conduction band and the top of the valence band in Si are at different positions in reciprocal lattice space, the momentum conservation law requires an interaction between an electron–hole pair and phonons for radiative recombination; however, the probability of this interaction is low.

Nevertheless, Si has been the subject of extensive research on the fabrication of Si light-emitting devices. These include, for example, research using porous Si [1], a

super-lattice structure of Si and SiO_2 [2], and Si nanoprecipitates in SiO_2 [3]. However, the devices fabricated in these research studies have some limitations, such as low efficiency, the need to operate at low temperature, complicated fabrication processes, and the difficulty of current injection.

To solve these problems, a novel method that exploits the dressed photon (DP) has been invented [4,5]. The DP is a quantum field created when a photon couples with an electron–hole pair in a nanometric space. Theoretical studies have shown that a DP could excite multi-mode coherent phonons and couple with them to create a novel state called a dressed-photon–phonon (DPP) [4,6]. To realize a light-emitting diode (LED) by using crystalline Si, DPPs are used two times: first for device fabrication, and second for device operation.

In the present paper, first, the fabrication and operation of a Si-LED are described in Sections 2 and 3, respectively. Second, Sections 4 and 5 review a technique for controlling the spatial distribution of boron (B) atoms by using a novel DPP-assisted annealing method. Finally, the optimum condition for this annealing is presented in Section 6. A summary is given in Section 7. Note that this paper discusses the principle and method of realizing infrared Si-LEDs. Refer to ref. [7] for details of visible light Si-LEDs, Si-lasers, and LEDs fabricated using other indirect-transition-type semiconductors (SiC and GaP), and related devices, which have been developed by using DPP-assisted annealing.

2 Fabrication

For device fabrication, first, the surface of an n-type Si crystal is doped with B atoms to transform it to a p-type material for forming a p–n homojunction structure. Second, the Si crystal is annealed via Joule heat generated by current injection. During the annealing, the Si crystal surface is irradiated with light to create DPPs at the B atoms. This novel annealing has been called DPP-assisted annealing [7].

In early work on fabrication, an n-type Si crystal with low arsenic (As) concentration was used [5]. Recently, however, As atoms have been replaced by antimony (Sb) atoms (density, 1×10^{15} /cm^3) because Sb atoms, which are heavier than As and Si atoms, are more advantageous for localizing the created phonons, which can couple with a DP for creating a DPP more efficiently. The thickness and the electrical

resistivity of the n-type Si crystal were 625 μm and 5.0 Ωcm, respectively.

Two-step ion implantation was carried out to dope the Si with B atoms:
(1) First step: B atoms were implanted with an energy of 700 keV at a dose of $2.7\times10^{14}/cm^2$. The peak concentration of B atoms was $1\times10^{19}/cm^3$ at a depth of 1400 nm from the Si crystal surface.
(2) Second step: B atoms were implanted with an energy of 10 keV at a dose of $5.3\times10^{14}/cm^2$. The peak concentration of B atoms was $1\times10^{20}/cm^3$ at a depth of 45 nm from the Si crystal surface. This second doping step was advantageous for decreasing the resistivity at the crystal surface.

Mesh-electrode type and flip-chip type devices were fabricated to achieve higher current injection and efficient heat dissipation. These devices are described in the following subsections.

2.1 Mesh-electrode type LED

Figure 1 shows a photographic profile of the fabricated mesh-electrode type device [8,9]. A homogeneous flat film composed of Cr/Al/Au layers (thicknesses: 30/200/300 nm) was coated on the n-type surface of the Si crystal described above to serve as a cathode. A mesh film of Cr/Au (thicknesses: 30/300 nm) was coated on the p-type surface to serve as an anode. The crystal was diced to form devices with areal sizes of 1 mm × 1 mm, and these devices were bonded on a PCB substrate made of high-thermal-conductivity AlN. The diameters of the electric wires bonded to the devices were increased from the previously employed 25 μm [10] to 45 μm to avoid damage to the wires and electrodes during high current injection.

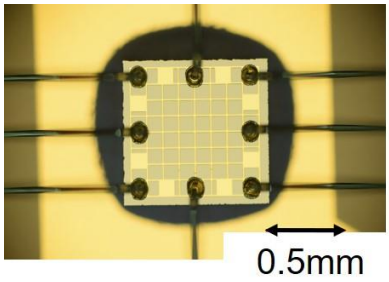

Fig. 1 Photographic profile of the fabricated mesh-electrode type LED.

The conditions for the DPP-assisted annealing were: (1) A substrate temperature of 285 K; (2) irradiation light with a wavelength of 1342 nm (photon energy $h\nu_{anneal}$ =

0.925 eV) and a power of 2.0 W; (3) injected current having a triangular waveform (50 s period) and a peak current of 1.3 A (current density 1.3 A/mm^2); and (4) an annealing time of 2 hours.

Since $h\nu_{anneal}$ is lower than the bandgap energy E_g of the Si crystal, the irradiated light is not absorbed by the Si crystal. Therefore, in the regions where DPPs are hardly created, B atoms diffuse simply due to the Joule heat generated by the applied electrical energy. However, in the regions where DPPs are easily created, the thermal diffusion rate of the B atoms becomes smaller via the following processes:

(1) Since the energy of the electrons driven by the forward-bias voltage is higher than E_g, the energy difference $E_{Fc} - E_{Fv}$ between the quasi Fermi energies in the conduction band E_{Fc} and the valence band E_{Fv} is larger than E_g. Therefore, the Benard–Duraffourg inversion condition is satisfied. Furthermore, since $h\nu_{anneal} < E_g$, the irradiated light propagates through the Si crystal without absorption and reaches the p–n homojunction. As a result, it creates DPPs efficiently at the B atoms. Since stimulated emission takes place via DPPs, the electrons create photons and are de-excited from the conduction band to the valence band via the phonon energy level.

(2) The annealing rate decreases because a part of the electrical energy for generating the Joule heat is spent for the stimulated emission of photons. As a result, at the regions where the DPPs are easily created, the B atoms become more difficult to diffuse.

(3) Spontaneous emission occurs efficiently at the regions in which the DPPs are easily created because the probability of spontaneous emission is proportional to that of stimulated emission. Furthermore, with the temporal evolution of process (2), the light from stimulated and spontaneous emission spreads through the whole Si crystal, and as a result, process (2) takes place autonomously throughout the entire volume of the Si crystal.

It is expected that this DPP-assisted annealing will form the optimum spatial distribution of the B atoms for efficient creation of DPPs, resulting in efficient LED operation. In a previous experimental study, temporal evolution of the temperature of the Si crystal surface was measured as annealing progressed [5]. After the temperature rapidly rose to 427 K, it fell and asymptotically approached a constant value (413 K) after 6 min, at which time the temperature inside the Si crystal was estimated to be about 573 K. The features of this temporal evolution are consistent with those of the principle

of the DPP-assisted annealing under light irradiation described above: The temperature rises due to the Joule heat generated by the applied electrical energy. However, the temperature gradually falls because stimulated emission is induced by the DPPs created at the B atoms. Finally, the system reaches the stationary state. This temporal decrease in the device temperature, and the temporal increase in the emitted light intensity, have been theoretically reproduced by a stochastic model of the spatial distribution of B atoms, which was controlled by DPPs [11].

2.2 Flip-chip type LED

To achieve higher injected current density than that of the mesh-electrode type device, a flip-chip type LED was fabricated [8,9]. First, its areal size was decreased. Second, larger-diameter electric wire was used. Third, a flip-chip structure was employed, in which the p-type layer was contacted to a PCB substrate for efficient heat dissipation.

Figure 2 shows a photographic profile of the fabricated device: A homogeneous flat film formed of Cr/Au/Ti/Pt/Au layers (thicknesses: 3/300/100/300/500 nm) was coated on the p-type surface of the Si crystal to serve as an anode. A patterned film of Cr/Au (thicknesses: 10/500 nm) was coated on the n-type surface as a cathode. The crystal was diced to form devices with areal sizes of 0.35 mm × 0.35 mm, which was smaller than that of the mesh-electrode type described in Subsection 2.1. This is equivalent to the size of commercially available devices made by using a conventional direct-transition type semiconductor. The diced device was bonded on a PCB substrate made of AlN. A single electric wire with a diameter as large as 60 μm was used to realize high-density current injection without any electrical damage.

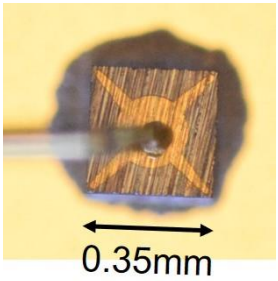

Fig. 2 Photographic profile of the fabricated flip-chip type LED.

The conditions for the DPP-assisted annealing were: (1) A substrate temperature of 289 K; (2) irradiation light with a wavelength of 1342 nm (photon energy $h\nu_{anneal}$ =

0.925 eV) and a power of 0.24 W (areal power density: 1.9 W/mm^2); (3) injected current with a triangular waveform (10 s period) and a peak current of 0.16 A (current density: 1.3 A/mm^2); and (4) an annealing time of 7.2 hours.

3 Operation

The operating principle of the fabricated Si-LED involves electron–hole pairs receiving enough momentum from coupled coherent phonons if the spatial distribution of B atoms in the p–n homojunction can be optimized for creating DPPs. Therefore, the light emission efficiency would be drastically increased by obeying the momentum conservation law.

For this operation, the light irradiation is no longer required; it is used only during the DPP-assisted annealing. Only forward current is injected, as in the case of conventional LED operation. This forward current causes an electron to be injected into the conduction band at the p–n homojunction, creating a photon by spontaneous emission even though its probability is very low. However, once this photon is created, it subsequently creates a DPP at the B atom in the p–n homojunction, and this DPP interacts with another electron in the conduction band to exchange momentum so that a secondary photon is created. By repeating these momentum exchange and photon creation processes, the emitted light intensity is amplified and reaches a stationary value within a short duration, so that sufficiently high-power light is emitted from the p–n homojunction.

It should be noted that photon breeding occurs during device operation [12]: The photon energy of the emitted light is equal to the photon energy $h\nu_{anneal}$ of the light irradiated during the annealing. (This is in contrast to a conventional device, where the photon energy of the emitted light is determined by E_g.) This is because the difference between $h\nu_{anneal}$ and E_g is compensated for by the energy of the created phonons. This compensation is possible because the spatial distribution of the B atoms has been controlled by the light irradiated during the DPP-assisted annealing, enabling the most efficient emission of photons with identical photon energy. In other words, the light irradiated during the DPP-assisted annealing serves as a “breeder” that creates photons with an energy equivalent to $h\nu_{anneal}$. This is the reason why this novel phenomenon is named photon breeding with respect to photon energy.

Photon breeding has been observed not only for the photon energy but also for

photon spin [13]. For example, linearly polarized light is emitted from the LED if it was fabricated by irradiating the LED with linearly polarized light during the annealing step. (Remember that the light emitted from a conventional LED is not polarized.)

The relationship between the forward-bias voltage (V) applied to the Si-LED and the injection current (I) indicated negative resistance [14]. This was due to the spatially inhomogeneous current density and the generation of filament currents. In other words, the B distribution had a domain boundary, and the current was concentrated in this boundary region. A center of localization where the electrical charge is easily bound was formed in this current concentration region, and a DPP was easily created there. That is, the negative resistance is consistent with the principle of the device fabrication described in Section 2.

3.1 Mesh-electrode type LED

Figure 3 shows the relations between the injected current (I) and the optical output power (P) of the upward-emitted light from the upper surface of the Si-LED, acquired at several substrate temperatures [8,9]. The figure shows that P is proportional to I^2 in the lower current region, whereas it is proportional to I^4 in the higher current region. The origin of this I^2-dependence has been attributed to the momentum transfer between localized phonons and electrons caused by electron–electron scattering [10]: In the case of a conventional LED fabricated with a direct-transition-type semiconductor, electron–electron scattering decreases the light emission efficiency. However, in the present Si-LED, this scattering process plays a different role. As will be explained in Section 4, the B atom pairs in the p–n homojunction are apt to stretch in a plane perpendicular to the [001] orientation of the Si crystal, i.e., perpendicular to the propagation direction of the light irradiated during the DPP-assisted annealing. Here, not only phonons but also electrons can be captured by these B atom pairs because they serve as cavity resonators for creating localized phonons. In other words, electrons can appear due to DPP-assisted annealing even in the area of the energy band structure where electrons cannot exist originally. Thus, two electrons could couple with localized phonons, leading to light emission by electron–electron scattering and the observed I^2-dependence of the emitted light power P.

The I^4-dependence originated in amplification by stimulated emission. By

defining the current at the boundary between the region of the I^2 - and I^4 -dependences as the threshold I_{th} , it is found that its value was lower at lower substrate temperatures. For example, it was 580 mA at 77 K. This means that the threshold current density was 0.58 A/mm^2, which is close to the threshold current density (0.20–0.35 A/mm^2) of a Si-laser fabricated by the DPP-assisted annealing [15]. The highest optical output power in Fig. 3 was 2.0 W with an injection current of 2.0 A and a substrate temperature of 77 K. This value is as high as 10^3-times that of a commercially available LED*.

*For example, the optical output power of a Hamamatsu Photonics device L12509-0155K, which is made of a direct-transition type semiconductor (InGaAs), is 2 mW. The peak emission wavelength is 1.55 μm.

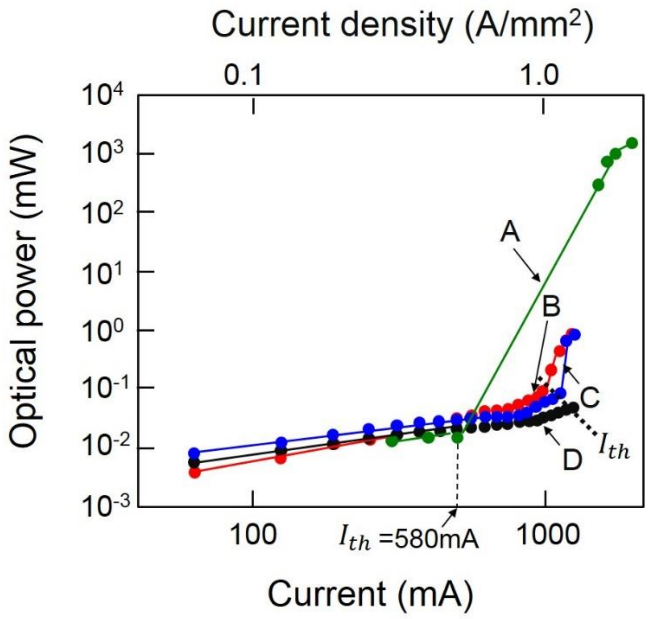

Fig. 3 Relations between the injection current and the optical output power.
Substrate temperatures were 77 K (A), 273 K (B), 290 K (C), and 293 K (D).

Figure 4 shows the spectral profile of the emitted light, which was acquired by cooling the substrate to 77 K and injecting a current of 2.0 A. In this figure, E_g represents the bandgap energy of the Si crystal at 77 K. This figure shows that the spectral profile has several peaks at $E_g - nE_{phonon}$, where n is an integer and E_{phonon}

is the phonon energy. The spectral peak at $E_g - 3E_{phonon}$ corresponds to the photon energy $h\nu_{anneal}$ of the light irradiated during the DPP-assisted annealing [13]. This correspondence is the photon breeding described in Subsection 2.1 [12]. Three phonons contribute to the light emission at $E_g - 3E_{phonon}$, because the length of the B atom pair is three-times the crystal lattice constant of Si. This figure also shows the higher harmonics of the phonon contributions, i.e., $E_g - 6E_{phonon}$ and $E_g - 9E_{phonon}$.

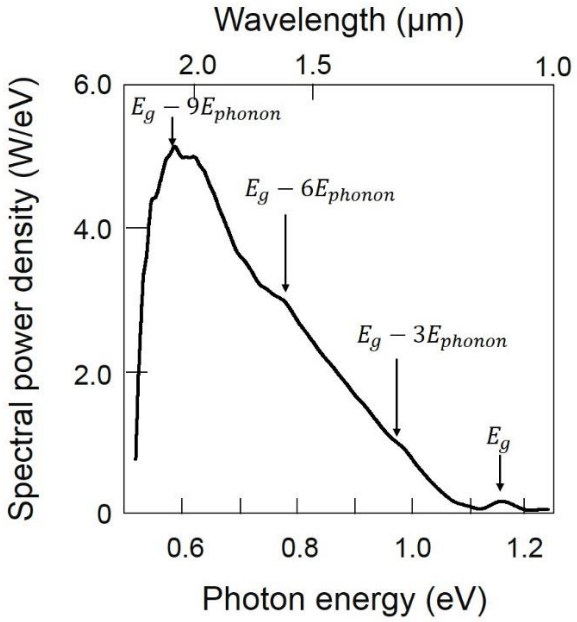

Fig. 4 Spectral profile of the emitted light at substrate temperature of 77 K.

3.2 Flip-chip type LED

Figure 5 shows the relations between I and P of the upward-emitted light from the upper surface of the Si-LED, acquired at several substrate temperatures. The highest optical output power in this figure was as high as 2.0 W at an injection current of 3.0 A and a substrate temperature of 77 K. This demonstrates that an extremely high optical output power density was achieved, as high as eight-times that of the mesh-electrode type LED described in Subsection 3.1.

The relations between I and P exhibited more complicated profiles than those in Fig. 3: In the low-current region [a], P increased slowly with increasing I,

whereas it increased rapidly in the high-current region [c]. The unique feature is that P decreased with increasing I in the intermediate region [b]. Figures 6(a)-(c) show photographs of the upward-emitted light spots in the regions [a]-[c], respectively. Among them, Fig. 6(b) shows that the light was emitted not only in the upward direction but also toward the side of the device. This side emission was attributed to the decrease in the observed value of P in region [b]. It should be noted that this side emission was due to stimulated emission, which suggests the possibility of super-luminescence or lasing operation.

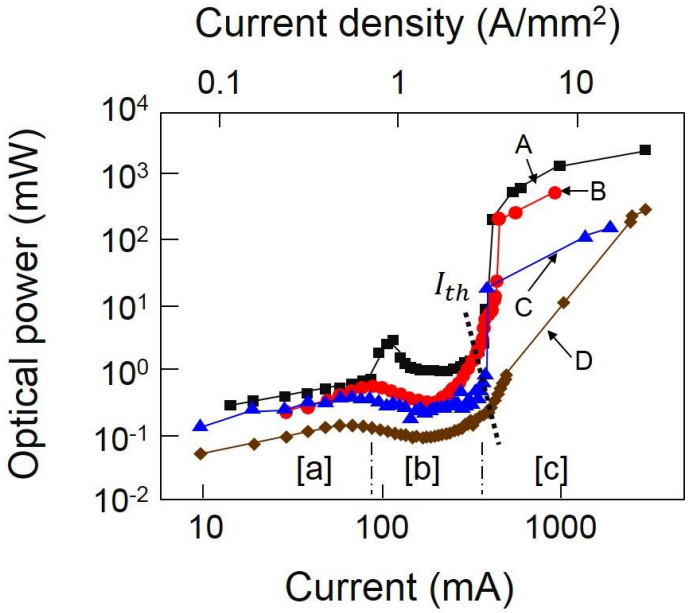

Fig.5 Relations between the injection current and the optical output power of the upward-emitted light from the surface of the Si-LED.

Substrate temperatures were 77 K (A), 195 K (B), 255 K (C), and 283 K (D).

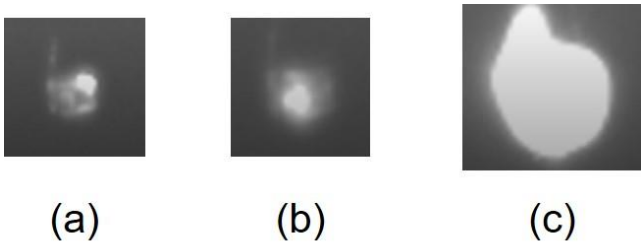

Fig.6 Photographs of the upward-emitted light spots.

(a), (b), (c) are images obtained in regions [a], [b], and [c] in Fig. 5, respectively.

As was the case in Fig. 3, the threshold I_{th} can be defined as the current at

the boundary between regions [b] and [c]. Figure 7 shows its dependence on the substrate temperature T. The solid line, fitted to the experimental results indicated by the closed circles, was expressed as $I_{th} = I_0 \exp(T / T_0)$. The characteristic temperature T_0 in this expression was 63 K, which corresponded to the energy of three phonons, $3E_{phonon}$, in the DPP. This means that the electron–hole pair was confined in the potential well formed by three phonons. This value of T_0 was as high as that of a conventional laser fabricated by a direct-transition type semiconductor (InGaAsP), lasing at a wavelength of 1.3 μm [16], which suggests that future progress in this work will realize highly reliable light-emitting devices using crystalline Si.

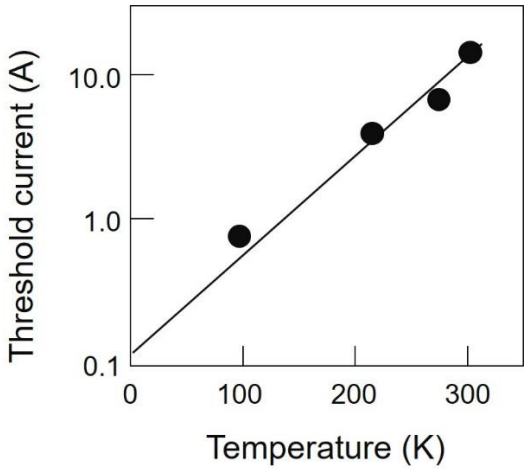

Fig. 7 Relation between the substrate temperature and the threshold current.

Figure 8(a) shows the spectral profile of the light emitted from the flip-chip type LED, which was acquired by cooling the substrate to 77 K and injecting a current of 3.21 A. Figure 8(b) shows the profile at a substrate temperature of 283 K and an injection current of 2.45 A. These figures also clearly demonstrate spectral peaks at $E_g - 3E_{phonon}$, $E_g - 6E_{phonon}$, and $E_g - 9E_{phonon}$, as was the case in Fig. 4.

4 Spatial distribution of boron

This section reviews the three-dimensional spatial distribution profile of the doped B

atoms formed as a result of the DPP-assisted annealing [13]. Atom probe field ion microscopy was used to acquire this distribution with sub-nanometer resolution [17]. It should be noted that the Si crystal is composed of multiple cubic lattices with a lattice constant a of 0.54 nm [18], and its top surface lies in the *xy*-plane (Fig. 9). The light irradiated during the DPP-assisted annealing is normally incident on this plane; i.e., the light propagation direction is parallel to the z-axis.

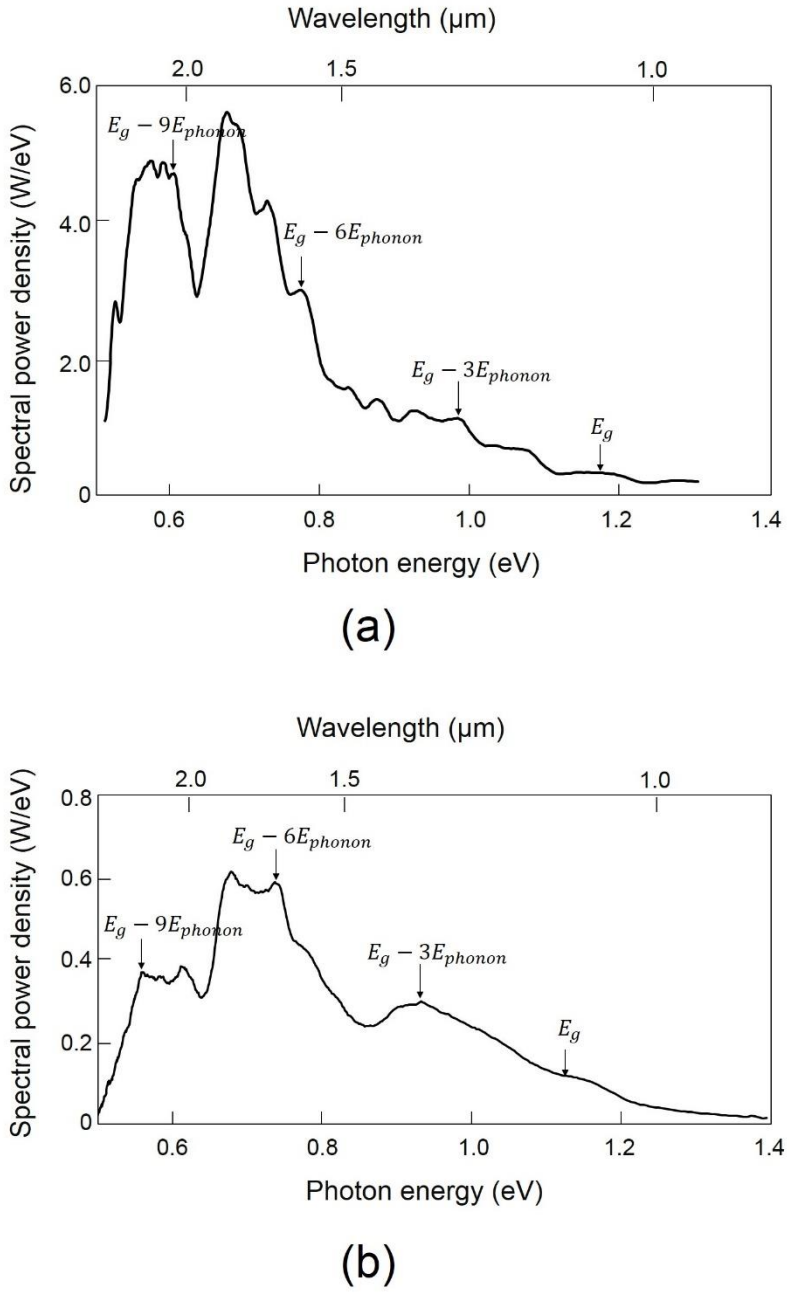

Fig. 8 Spectral profiles of the light emitted from the flip-chip type LED at substrate temperatures of 77 K (a) and 283 K (b).

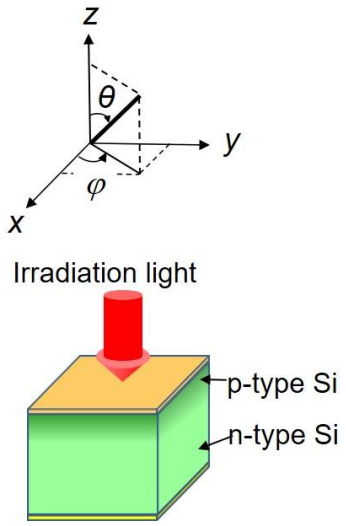

Fig. 9 Profile of the Si-LED under irradiation for the DPP-assisted annealing.

Some of the regularly arranged Si atoms are replaced by the doped B atoms in the DPP-assisted annealing. It has been pointed out that phonons can be localized at the B atoms for creating DPPs under light irradiation because the B atoms are lighter than the Si atoms. However, for this localization, it has also been pointed out that two or more adjacent B atoms (in other words, two or more unit cells containing B atoms) are required [19]. Since the doped B atom concentration is sufficiently low, making it difficult for more than three B atoms to aggregate, the following discussion considers two closely located adjacent B atoms (a B atom pair), at which a phonon is localized for creating a DPP. That is, the pair of unit cells containing the B atoms serves as a phonon localization center.

Figures 10(a) and (b) show the numbers of B atom pairs plotted as a function of the separation, d, between the B atoms in the pair, which were derived from the measurement results. Since the distribution of the number of B atom pairs is nearly random, it can be least-squares fitted by the Weibull distribution function (the solid curve in these figures). In the un-annealed Si crystal (Fig. 10(a)), the measured number of B atom pairs deviates from the solid curve in the range $d > 4.5$ nm. The deviation depends on the characteristics of the ion implantation.

In contrast, in the Si crystal after the DPP-assisted annealing (Fig. 10(b)), the deviation is much less than that in Fig. 10(a), which means that the DPP-assisted annealing modified the spatial distribution and decreased the deviation induced by the ion implantation, making the distribution more random. However, at specific values of

d ($=na$, where $n=3$, 4, 5, 6; refer to the four downward arrows in this figure), the number of B atom pairs still deviates from the solid curve and is larger than that of the solid curve. This is explained as follows: The B atom pair with the shortest d (i.e., equal to the lattice constant a) can orient in a direction parallel to the [100], [010], or [001] orientation because the Si crystal is composed of multiple cubic lattices. As a result, the momentum of the localized phonon points in this direction, which corresponds to the $\Gamma - X$ direction in reciprocal space. Thus, a photon is efficiently created because this $\Gamma - X$ direction is the same as the direction of the momentum of the phonon required for recombination between an electron at the bottom of the conduction band at the X-point and a hole at the top of the valence band at the Γ-point. Here, it should be noted that the absolute value of the momentum of the phonon has to be h/a for this electron–hole recombination to take place. Furthermore, it should also be noted that, among the phonons localized at the B atom pair with separation d ($=na$), the absolute value of the momentum of the lowest mode is h/na. By comparing these two absolute values, it is found that the DPP at this B atom pair has to create n phonons for recombination. Thus, it can be concluded that the four downward arrows in Fig. 10(b) indicate selective increases in the number of B atom pairs with separation $d = na$ due to the DPP-assisted annealing, and these pairs serve as localization centers for the phonons.

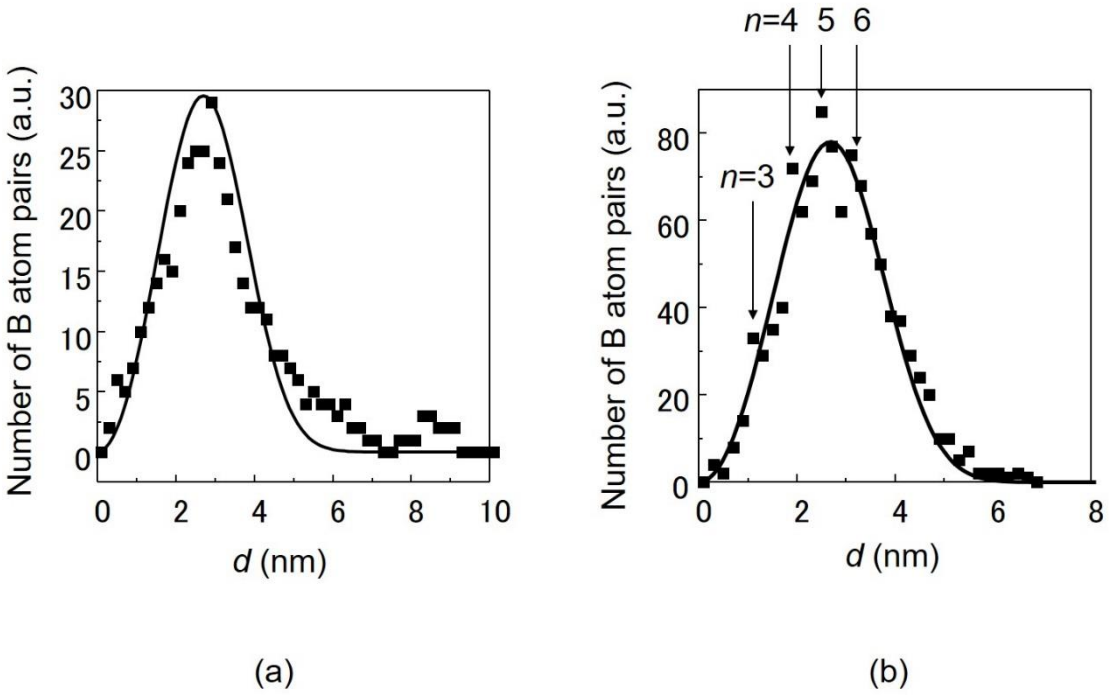

Fig. 10 Number of B atom pairs plotted as a function of the separation d between the B atoms in the pair. (a) The un-annealed Si crystal. (b) The Si crystal subjected to DPP-assisted annealing.

Figure 11(a) shows the spatial distribution of B atom pairs after the DPP-assisted annealing, which was recently acquired by improving the accuracy of atom probe ion microscopy [20]. The thick downward arrow in this figure clearly demonstrates that the deviation takes the maximum value at n=3, which means that B atom pairs most efficiently create three phonons for light emission, as is schematically shown in Fig. 11(b). As a result, the emitted photon energy $h\nu_{em}$ is expressed as $h\nu_{em} = E_g - 3E_{phonon}$. By substituting the values of E_g (= 1.12 eV) and the relevant optical mode phonon energy E_{phonon} (=65 meV [21]) into this equation, the value of $h\nu_{em}$ is derived to be 0.925 eV, which is identical to the photon energy $h\nu_{anneal}$ irradiated during the DPP-assisted annealing. This numerical relation is consistent with the experimental results in Figs. 4 and 8, which confirms that photon breeding with respect to photon energy occurs. The two thin downward arrows in Fig. 11(a) represent the values at $n=6$ and $n=9$, which correspond to $E_g - 6E_{phonon}$ and $E_g - 9E_{phonon}$, respectively, in Figs. 4 and 8.

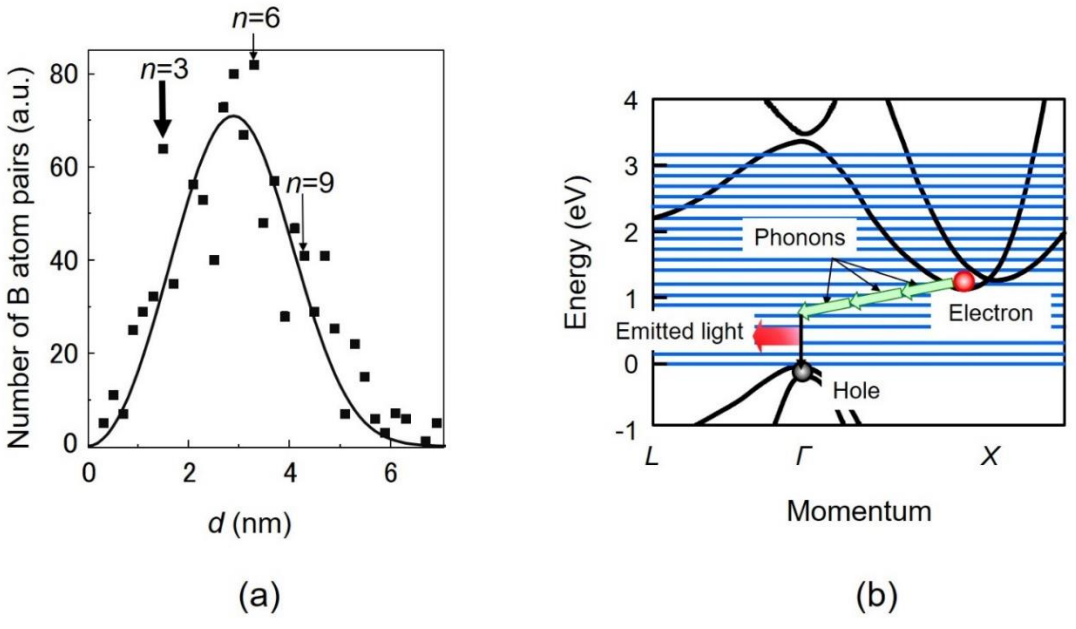

Fig. 11 (a) Number of B atom pairs, acquired by improving the measurement accuracy, and (b) the energy band structure of Si for schematically explaining light emission.

Figures 10(b) and 11(a) indicate selective increases in the number of B atom pairs with separation $d = na$. This means that, since n is an integer, B atom pairs are apt to orient along a plane perpendicular or parallel to the top surface of the Si crystal (zenith angle $\theta = 0°$ or $90°$). Orientation along other directions in which n is not an integer ($\theta \neq 0°, 90°$) hardly occurs. Figure 12 shows the relation between the zenith angle θ and the number of B atom pairs. It can be seen that this number takes the maximum value at $\theta = 90°$, which means that the B atom pairs in the p–n homojunction are apt to stretch in the *xy*-plane, which is perpendicular to the [001] orientation of the Si crystal, i.e., perpendicular to the propagation direction (*z*-axis) of the light irradiated during the DPP-assisted annealing. On the other hand, the number of B atom pairs takes the minimum value at $\theta = 0°$, which means that the B atom pairs hardly orient along the propagation direction (*z*-axis) of the light irradiated during the DPP-assisted annealing. This is because the phonons are hardly localized along this direction since their momenta are parallel to $\theta = 90°$ [22].

It is expected that photon breeding takes place not only with respect to photon energy, as described in Section 3, but also with respect to photon spin. That is, the light emitted from the LED can be polarized if the LED is fabricated by irradiating the Si crystal with polarized light during the DPP-assisted annealing. The fabrication method is the same as that described in Section 2, except that the irradiated light is linearly polarized along the x-axis. The diffusion of the B atoms was controlled by the linearly polarized light irradiated during the DPP-assisted annealing, with the result that the B atom pairs oriented along the y-axis . It has been experimentally confirmed that the degree of linear polarization increased with increasing DPP-assisted annealing time [13].

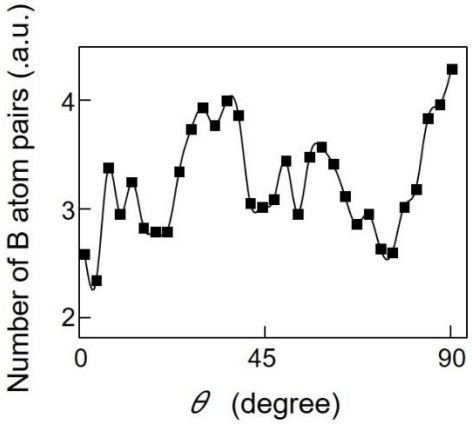

Fig. 12 Relation between the zenith angle θ and the number of B atom pairs.

Recent experimental work has confirmed that B atom pairs tend to form a chain-

like configuration [20]: Figures 13(a) and (b) show these configurations before and after the DPP-assisted annealing, respectively, which were acquired by the atom probe field ion microscopy. The short black arrows in these figures represent B atom pairs. The probability of one B atom pair existing in close proximity to the other pair in Fig. 13(a) was 0.743. In contrast, the probability in Fig. 13(b) increased to 0.788. The increase indicates that the B atom pairs tend to form a chain-like configuration. The red curves in these figures represent such a configuration.

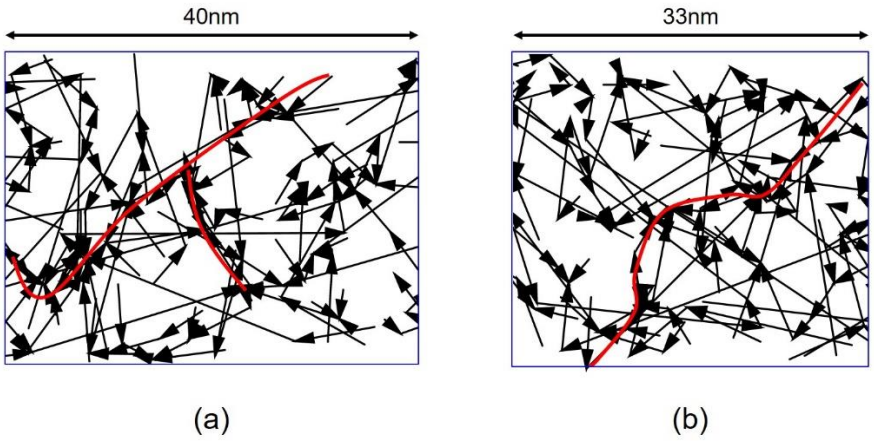

Fig. 13 Measured spatial distribution of B atom pairs, acquired before (a) and after (b) the DPP-assisted annealing.
The arrow in these figures represents the B atom pair. Red curves represent the chain-like configurations of the B atom pairs.

5 Effectiveness of the low-temperature DPP-assisted annealing

This section examines the reason why the spatial distribution of B atoms was effectively controlled by the DPP-assisted annealing at a temperature as low as 573 K, as presented in Subsection 2.1. For this examination, a two-level two-state (TLTS) model is used. This model has been adopted for accurately describing the spatial distribution of Zn atoms doped in a GaP-LED [23]. It enables evaluation of the potential barrier height of the electron, which is decreased by applying an external field. For reference, the details of the TLTS model have been reviewed in refs. [24,25].

Figure 14 shows the energy level diagram of the two-level system model [25]. The horizontal axis does not represent any specific physical quantity, whereas the vertical axis is the electron energy. The states A and B represent the electron states before

and after the DPP-assisted annealing, respectively. They are composed of two energy levels, i.e., the ground state ($\left|E_{gA}\right\rangle$,$\left|E_{gB}\right\rangle$) and the excited state ($\left|E_{exA}\right\rangle$,$\left|E_{exB}\right\rangle$), which respectively correspond to the valence and conduction bands in a semiconductor. The DPP-assisted annealing forces a forward transition from state A to state B. (The possibility of a backward transition from state B to state A is reviewed in Section 6.) The initial and final states of this forward transition are $\left|E_{gA}\right\rangle$ and $\left|E_{gB}\right\rangle$, respectively. Since the potential barrier V_g in the ground state is generally high, the transition takes place through the lower potential barrier V_{ex} in the excited state after excitation from $\left|E_{gA}\right\rangle$ to $\left|E_{exA}\right\rangle$. De-excitation from $\left|E_{exB}\right\rangle$ to the final state $\left|E_{gB}\right\rangle$ takes place after this transition.

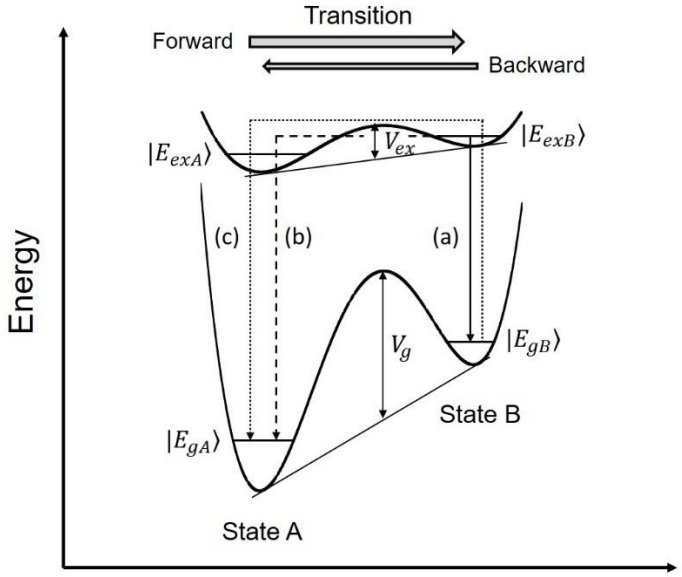

Fig. 14 The energy level diagram of the two-level two-state model.

The TLTS model can describe the DPP-assisted annealing rate, depending on which state the electron is in:

State A: State A corresponds to the region in the Si crystal where the spatial distribution of B atoms is not suitable for generating DPPs. Therefore, the electron in $\left|E_{exA}\right\rangle$

generates Joule heat. On the other hand, the electron in $|E_{gA}\rangle$ is excited by absorbing the irradiated light, and, as a result, Joule heat is also generated. Because of the Joule heat generated in these cases, the annealing rate is higher in state A.

State B: State B corresponds to the region in the Si crystal where the spatial distribution of B atoms is suitable for generating DPPs. Since electron–hole pairs can radiatively recombine in this case, the light irradiated during the DPP-assisted annealing triggers stimulated emission. As a result, the annealing rate is lower in state B because the stimulated emission optical energy dissipates from inside the Si crystal to the outside.

Due to the difference in the annealing rates in states A and B, the spatial distribution of B atoms changes autonomously. When it reaches that of state B, the DPP-assisted annealing is completed, and the Si-LED is thus fabricated. It has been experimentally confirmed for a GaP-LED that the external electric and optical fields applied during the DPP-assisted annealing drastically decreased the value of $V_{ex}{}^{*}$.

This decrease is the reason why the spatial distribution of B atoms was efficiently modified by the DPP-assisted annealing even at low temperature, as described in Subsection 2.1 (573 K). In other words, the outstanding technical advantage of the DPP-assisted annealing is that it does not require any high-temperature electric furnaces, which have been needed for conventional thermal annealing.

---

* In the absence of an external field, the value of V_{ex} that electrons in the doped Zn atoms must exceed to make a transition inside the GaP crystal was 0.61 eV. The value obtained when Ga sites were substituted via the kick-out mechanism was 1.64 eV [26]. However, with the external fields, it was estimated to be as low as 0.48 eV [23].

---

6. Optimum condition for DPP-assisted annealing

This section presents the optimum condition for DPP-assisted annealing, i.e., the optimum ratio between the electron injection rate and the photon irradiation rate for DPP-assisted annealing [23]. First, the electron is assumed to be in the excited or ground state of state B ($|E_{exB}\rangle$ or $|E_{gB}\rangle$) in Fig. 14 as a result of DPP-assisted annealing, i.e.,

as a result of the forward transition from state A to state B. Next, the solid, broken and dotted arrows (a)–(c) in Fig. 14 represent the possible paths of the electron for de-excitation, excitation, and backward transition via photon emission and absorption, which may subsequently occur by continuing the DPP-assisted annealing.

Path (a): The electron in $|E_{exB}\rangle$ can emit a photon via spontaneous or stimulated emission. Thus, it de-excites to $|E_{gB}\rangle$ without a transition back to state A.

Path (b): If the electron in $|E_{exB}\rangle$ does not emit a photon, it transitions back to $|E_{exA}\rangle$ in state A, and subsequently de-excites to $|E_{gA}\rangle$ via nonradiative relaxation.

Path (c): The electron in $|E_{gB}\rangle$ is excited to $|E_{exB}\rangle$ by absorbing a photon. It subsequently transitions back to $|E_{exA}\rangle$ in state A and de-excites to $|E_{gA}\rangle$ via nonradiative relaxation, as in path (b).

In the case of path (a), the spatial distribution of B atoms remains unchanged even though DPP-assisted annealing proceeds, because both the initial and final states ($|E_{exB}\rangle$ and $|E_{gB}\rangle$) are in state B. However, in the case of paths (b) and (c), the final state $|E_{gA}\rangle$ is in state A, and this spatial distribution easily changes as DPP-assisted annealing proceeds. Thus, to confine the electrons in state B, paths (b) and (c) must be blocked to prevent the backward transition.

Noting that a photon causes an electron to emit another photon via stimulated emission, a promising method for blocking the paths is to set the ratio of the electron injection rate and the photon irradiation rate to 1:1, which corresponds to the optimum condition for the DPP-assisted annealing. If the electron injection rate is higher than the photon irradiation rate, the excess electrons do not emit photons via stimulated emission but escape through path (b). On the other hand, if the photon irradiation rate is higher than the electron injection rate, the excess photons do not cause electrons to emit photons via stimulated emission but allow the electrons to escape through path (c).

Experiments have been carried out to confirm this optimum condition by using a GaP-LED as a specimen [23]. The experimental results showed that the rate of increase in the emitted light intensity due to the DPP-assisted annealing took the maximum value

when the ratio between the photon number and the electron number was 1.3:1, which is approximately 1:1. This clearly shows the optimum condition claimed above. This optimum condition has been theoretically reproduced by a stochastic model of the spatial distribution of B atoms, which was controlled by the DPPs [11].

This optimum condition suggests that conventional thermal annealing, i.e., by heating the sample in an electric furnace, is not compatible with fabricating novel devices having photon breeding features even if the furnace temperature can be increased to much higher than the value given in Subsection 2.2 (573 K). DPP-assisted annealing is the only suitable fabrication method.

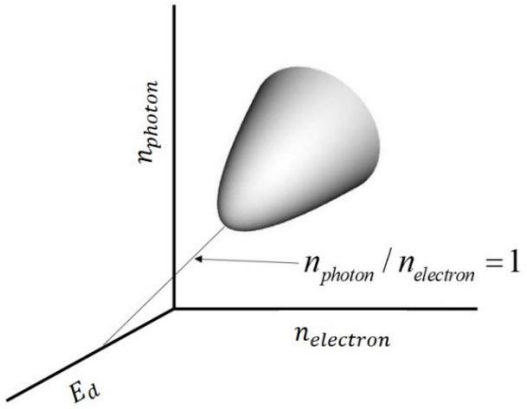

Fig. 15 Phase diagram for representing the area in which the rate of increase in the emitted light intensity due to the DPP-assisted annealing is high.

The gray cone in the phase diagram of Fig. 15 represents the area in which the rate of increase in the emitted light intensity due to the DPP-assisted annealing is high, which was empirically illustrated through experiments and the discussion on the optimum condition above. Here, $n_{electron}$ and n_{photon} are the electron injection rate and the photon irradiation rate, respectively. It should be pointed out that the rate of increase is the largest when $n_{photon} / n_{electron} = 1$, as was discussed above. In this figure, E_d is the magnitude of the dissipated optical energy. It is the magnitude of the energy of the stimulated emission, which is emitted from the electron that jumped into the DPP field.

Since this light propagates out from the Si crystal, the diffusion rate of the B atoms locally decreases around this DPP field, by which the spatial distribution of the B atom pairs is autonomously controlled to promote the DPP-assisted annealing.

A novel theory is required since one of the major requests from experimentalists is to find the optimum condition for realizing the highest efficiency of creation and measurement of DPs. It is expected that Fig. 15 will serve as a reference to find such an optimum condition.

7 Summary

After reviewing fabrication of Si-LEDs using a novel DPP-assisted annealing method, their unique light emission spectral profiles were presented in the wavelength range 900–2500 nm, including novel photon breeding features. The highest optical output power demonstrated was as high as 2.0 W, which was 10^3-times that of a conventional LED.

It was experimentally found that the B atoms formed pairs as a result of the DPP-assisted annealing, and the length of these pairs was three-times the lattice constant of the Si crystal. The pairs extended in a plane perpendicular to the propagation direction of the light irradiated during the DPP-assisted annealing. These B atom pairs were confirmed to be the origin of the photon breeding. It was also found that photon breeding took place with respect to photon spin. Recent measurements confirmed that the B atom pairs tend to form a chain-like configuration.

A phenomenological two-level two-state (TLTS) model confirmed that the external electric and optical fields applied during the DPP-assisted annealing drastically decreased the height of the potential barrier between the two states. This decrease was the reason why the spatial distribution of B atoms was efficiently modified by the DPP-assisted annealing even at low temperature. The TLTS model and a stochastic model confirmed that the optimum DPP-assisted annealing was realized by setting the ratio of the electron injection rate and the photon irradiation rate to 1:1, which was also confirmed experimentally.

A phase diagram was presented as an aid for developing a novel theory for finding the optimum condition for the highest efficiency of creation/measurement of DPs and for realizing more efficient and higher-power Si-LEDs.

References

[1] K.D. Hirschman, L.Tysbekov, S.P. Duttagupta, and P.M. Fauchet, “Silicon-based visible light-emitting devices integrated into microelectronic circuits,” Nature, **384** (1996) pp.338-341.

[2] Z.H. Lu, D.J. Lockwood, and J.-M. Baribeau, Nature, “Quantum confinement and light emission in SiO_2/Si Superlattices,” Nature, **378** (1995) pp.258-260.

[3] T. Komoda, J. Kelly, E. Cristiano, A. Nejim, P. L. F. Hemment, K. P. Homewood, R. Gwilliam, J. E. Mynard, and B. J. Sealy, “Visible photoluminescence at room temperature from micro- crystalline silicon precipitates in SiO_2 formed by ion implantation,” Nucl. Instrum. and Methods in Phys. Res. Sect.B, **96** (1995) pp.387-391.

[4] M. Ohtsu, “Dressed photon technology,” Nanophotonics **1**, (2012) pp.83-97.

[5] T. Kawazoe, M. Mueed, and M. Ohtsu, “Highly efficient and broadband Si homojunction structured near-infrared light emitting diodes based on the phonon-assisted optical near-field process,” Appl. Phys. B **104**, (2011) pp.747-754.

[6] Y. Tanaka and K. Kobayashi, “Optical near field dressed by localized and coherent phonons,” J. Microscopy **229** (2008) pp.228-232.

[7] M. Ohtsu, *Silicon Light-Emitting Diodes and Lasers* (Springer, (Springer, Heidelberg 2006), pp. 1-138.

[8] T. Kawazoe and M. Ohtsu, “Operation with 1W-optical output of Si-LED and current dependence,” Abstracts of the 65th Jpn. Soc. Appl. Phys. Spring Meeting, March 2018, Tokyo, Japan, paper number 19p-F310-13.

[9] M. Ohtsu and T. Kawazoe, “High-Power Infrared Silicon Light-emitting Diodes Fabricated and Operated using Dressed Photons,” Off-shell Archive, Offshell:1804O.001.v1.

[10] J.H. Kim, T. Kawazoe, and M.Ohtsu, "Dependences of emission intensity of Si light-emitting diodes on dressed-photon—phonon-assisted annealing conditions,”Appl. Phys. A , **123**,606 (2017).

[11] M. Katori and H. Kobayashi, “Nonequillibrium Statistical Mechanical Models for Photon Breeding

Processed Assisted by Dressed-Photon—Phonons," *Prog. In Nanophotonics* 4 (ed. By M. Ohtsu and T. Yatsui) (Springer, Heidelberg, 2017) pp.19-55.

[12] M. Ohtsu, *Silicon Light-Emitting Diodes and Lasers*, (Springer, Heidelberg, 2016), pp.8-10.

[13] T. Kawazoe, K. Nishioka, and M. Ohtsu, "Polarization control of an infrared silicon light-emitting diode by dressed photons and analyses of the spatial distribution of doped boron atoms," Appl. Phys.A , **121** (2015) pp. 1409-1415.

[14] E.Shl, *Nonequilibrium Phase Transitions in Semiconductors* (Springer, Heidelberg 1987), pp. 5-6.

[15] T. Kawazoe, K. Hashimoto, and S. Sugiura, "High-power current-injection type Silicon laser using nanophotonics," Abstract of the EMN Nanocrystals Meeting, October 17-21, 2016, Xi'an, China, pp.9-11 (paper number 03).

[16] R.Adams, M.Asada, Y.Suematsu, and S.Arai, "The Temperature Dependence of the Efficiency and Threshold Current of $In_{1-x}Ga_xAs_yP_{1-y}$ Lasers Related to Intervalence Band Absorption," Jpn. J. Appl. Phys., **19** (1980) pp.L621-L624.

[17] K. Hono, "Nanoscale microstructural analysis of metallic materials by atom probe field ion microscopy, " Prog. Mater. Sci. **47** (2002) pp.621–729.

[18] K. Godwod, R. Kowalczyk, and Z. Szmid, "Application of a precise double X-ray spectrometer for accurate lattice parameter determination," Phys. Stat. Sol. (a), **21** (1974) pp.227-234.

[19] M. Ohtsu, *Dressed Photons* (Springer, Heidelberg, 2014), pp. 62-67.

[20] T. Kawazoe, J.H. Kim, and M. Ohtsu, "Regularity of Boron dopant distribution in a Si-crystal annealed by the dressed photon-phonon assisted annealing," *Abstract of the 77th Japan. Soc. Appl. Phys. Autumn Meeting*, (Niigata, Japan, 2016), 16a-B12-4.

[21] E. Anastassakis, A. Pinczuk, E. Burstein, F.H. Pollak, and M. Cardona, "Effect of static uniaxial stress on the Raman spectrum of silicon," Solid State Commun. **8** (1970) pp.133-138.

[22] Y. Shinohara, T. Otobe, J. Iwata, K. Yanaba, "First-Principles Calculation to Explore Mechanisms of Coherent Phonon Generation," J. Phys. Soc. Jpn. **67** (2012) pp.685-689.

[23] J. H. Kim, T. Kawazoe, and M. Ohtsu, "Optimization of dressed-photon—phonon-assisted annealing for fabricating GaP light-emitting diodes," Appl. Phys. A **121** (2015) pp.1395-1401.

[24] R. Jankowiak, R. Richert, and H. Bässler, "Nonexponential hole burning kinetics in organic glasses," J. Phys. Chem. **89** (1985) pp 4569-4574.

[25] W. Köhler, J. Meiler, and J. Friedrich, "Tunneling dynamics of doped organic low-temperature glasses as probed by a photophysical hole-burning system," Phys. Rev. B **35** (1987) pp.4031-4037.

[26] A. Höglund, C. Castleton, and S. Mirbt, “Diffusion mechanism of Zn in InP and GaP from first principles,”Phys. Rev.B **77** (2008) 113201.

Experimental estimation of the maximum size of a dressed photon

M. Ohtsu[1,2] and T. Kawazoe[3]

[1] Institute of Engineering Innovation, Graduate School of Engineering,
The University of Tokyo, 2-11-16 Yayoi, Bunkyo-ku, Tokyo, 113-8656, Japan
[2] Research Origin for Dressed Photon,
c/o The University of Tokyo, 2-11-16 Yayoi, Bunkyo-ku, Tokyo, 113-8656, Japan
[3] Tokyo Denki University,
Tokyo Senju Campus, Bldg.4-9F 906A, Senju-Asahi-cho, Adachi-ku, Tokyo 120-8551, Japan

Abstract: This article describes experimental estimation of the maximum size of a dressed photon (DP) by a photochemical vapor deposition method that has been used for forming a metallic zinc nanoparticle (Zn-NP) on a sapphire substrate. Because of the localized feature of the DP and of a unique non-resonant DP–molecule interaction, this method succeeded in excluding the contribution of the propagating light in the Zn-NP formation. The size of the deposited Zn-NP increased with increasing deposition time. Finally, the size saturated to a value that was independent of the radius of curvature of the fiber probe tip and the wavelength of the light used for irradiating the end of the fiber probe. From these results, it was concluded that the experimentally estimated maximum size was 50–70 nm.

1. Introduction

A dressed photon (DP) is a quasi-particle representing the coupled state of a photon and an electron–hole pair in a nanometer-sized material (nanoparticle: NP) [1]. It has been confirmed that the size a_{DP} of a DP is equivalent to the size a_{NP} of the NP on which the created DP is localized [2]. This size is much smaller than the wavelength λ of conventional propagating light.

Because of the unique localization feature mentioned above and

because $a_{DP} < \lambda$, a variety of application technologies developed so far [3] have realized an ultrahigh spatial resolution beyond the diffraction limit of conventional optical technologies. To realize further developments in these technologies, it is essential to estimate the minimum and maximum sizes of the DP ($a_{DP,Min}$ and $a_{DP,Max}$, respectively). A reasonable estimate is to assume that the minimum size $a_{DP,Min}$ is equivalent to the size of an atom a_{atom}. This is because a fundamental interaction takes place between a photon and an electron in an atom for creating the DP*.

On the other hand, the maximum size $a_{DP,Max}$ has never been estimated. The advent of a novel theory is expected to make this estimation possible. To this end, this article describes experimental estimations of the maximum size $a_{DP,Max}$ by using the localized features of the DP mentioned above and also a unique feature, called non-resonant DP–molecule interaction.

(*)

Experiments on DPs have been carried out by using ultraviolet light, visible light, or infrared light as a light source for creating the DP. Some infrared wavelengths can excite molecular vibrations, which can be treated by a theoretical model known as the dressed-photon–phonon model [4]. Microwaves have also been used to realize a spatial resolution as high as $\lambda / 4000$, where the wavelength λ was 12 cm [5]. Here, it should be noted that microwaves do not interact with the electron in the atom even though it can excite a molecular rotation. Thus, the experiments using microwaves are not compatible with the present study described here.

---

2. Methods for experimental estimation

Photochemical vapor deposition (PCVD) based on DP-molecule interaction was adopted as the most appropriate method to experimentally estimate the maximum size $a_{DP,Max}$. This is because the size, conformation, and position of the DP were transcribed to those of an NP formed on a substrate as a result

of deposition. As shown in Figs. 1(a) and (b), this method involved molecular dissociation by the DP and subsequent deposition of the dissociated atoms on the substrate [6,7].

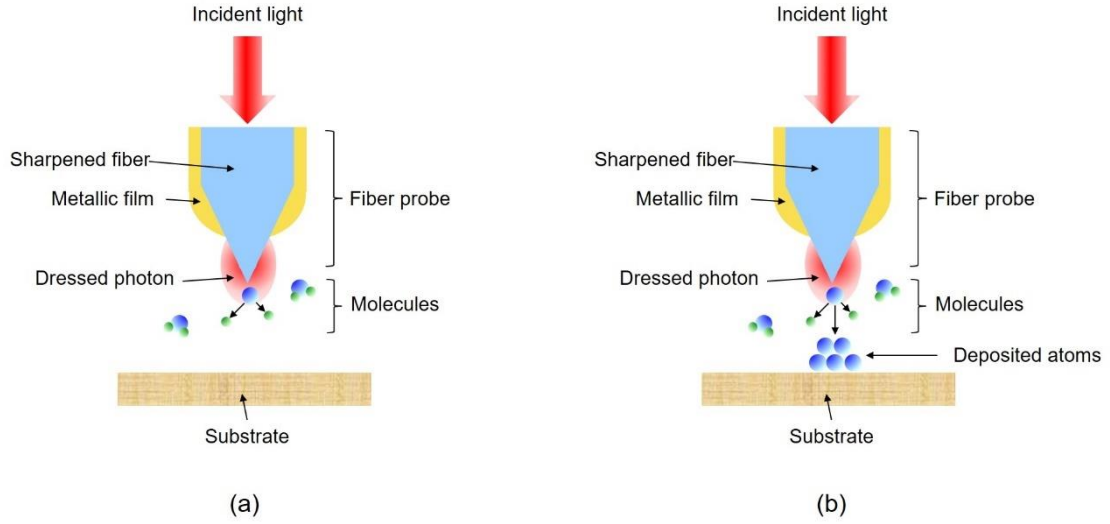

Fig. 1 Photochemical vapor deposition based on DP–molecule interaction.
(a) Dissociation of molecules. (b) Deposition of the dissociated atoms.

First, $Zn(C_2H_5)_2$ (DEZn for short) was adopted as a specimen molecule. Gaseous DEZn molecules were filled into the vacuum chamber. A fiber probe and a substrate were also installed in the chamber. A DP was created on the tip of the fiber probe by irradiating the end of the fiber probe with propagating light. The DEZn molecules were dissociated when these freely flying molecules jumped into the field of the DP. The dissociated Zn atom subsequently landed on the substrate. After a very short migration on the substrate, the atom was adsorbed on the substrate. By repeating these processes, the number of adsorbed Zn atoms increased, resulting in the deposition of Zn atoms and the formation of a nanometer-sized metallic zinc nanoparticle (Zn-NP) on the substrate. Since the DEZn molecules were dissociated in the field of the DP, the size, conformation, and position of the formed Zn-NP were equivalent to those of the DP.

In the case of dissociating the DEZn molecules by conventional propagating light instead of by a DP, the wavelength of this light had to be shorter than 270 nm (photon energy 4.59 eV) for exciting an electron in the

DEZn molecule. To estimate $a_{DP,Max}$, the DEZn molecules must be dissociated only by the DP on the tip of the fiber probe (Fig. 1(a)), for which the contribution of the propagating light used for creating the DP must be excluded. To achieve this, three ingenious tricks were employed:

(1) The first was a photochemical trick: The wavelength of the propagating light for creating the DP was set longer than 270 nm. As a result, it was expected that the DEZn molecules would not be dissociated even if irradiated with propagating light, which scattered out from the tip of the fiber probe. Instead, it was expected that the DP on the tip would dissociate the DEZn molecules due to the non-resonant DP–molecule interaction. It has been confirmed that this novel dissociation originated from the multi-step excitation of the electron via molecular vibration energy levels, triggered by the DP [6,7].

(2) The second was an instrumentational trick: A primitive bare fiber probe was employed on which no metallic films were formed. As shown in Fig. 2(a), a conventionally used fiber probe was fabricated by sharpening a fiber with an advanced selective chemical etching method [8], resulting in high-precision control of the nanometer-sized tip diameter, cone angle, and throughput of the DP creation. This high precision was essential to control the size, conformation, and position of the created DP on the tip for estimating $a_{DP,Max}$. The tapered part of the sharpened fiber was subsequently coated with an opaque metallic film in order to prevent the scattered propagating light from leaking out from the fiber probe. In contrast, the fiber probe used here was fabricated by a very primitive method. That is, the fiber was heated and mechanically pulled to sharpen it. As a result, high-precision control of the size, cone angle, and throughput were not expected. In addition, the probe was not coated with a metallic film (Fig. 2(b)), allowing the scattered propagating light to leak from the taper and tip of the fiber probe. Even when using such an unreliable fiber probe, the contribution of the propagating light was expected to be excluded because of its long wavelength, as discussed in (1) above.

(3) The third was again a photochemical trick: For further insurance, the DEZn molecules were replaced by zinc-bis(acetylacetonate) ($Zn(acac)_2$ for short) molecules [9,10]. $Zn(acac)_2$ is known to be an optically inactive molecule,

and thus, it has never been dissociated by propagating light. However, it was expected here that it could be dissociated by the DP via excitation of a molecular vibration for depositing the dissociated Zn atoms on the substrate. This is also the application of a non-resonant DP–molecule interaction.

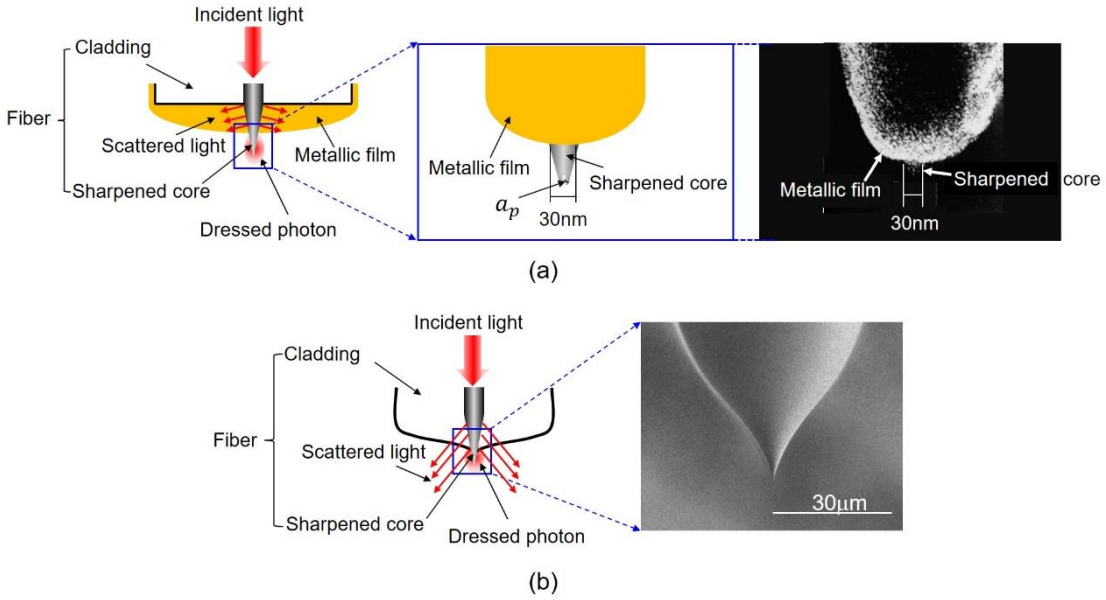

Fig. 2 Structures and scanning electron microscopic images of fiber probes. (a) A high-precision fiber probe, which has been popularly used for high-spatial-resolution microscopy and spectroscopy. a_p is the radius of curvature of the tip. (b) A primitive fiber probe, which was used for the present experiments.

3. Estimated results and discussion

Figures 3(a)-(c) show images of a three-dimensional Zn-NP formed on a sapphire substrate by dissociating DEZn molecules; these images were acquired by using an atomic force microscope (AFM) [7]. The wavelengths λ of the propagating light for creating the DP were 325, 488, and 684 nm, respectively. In the case of Fig. 3(a), this wavelength was close to the value of 270 nm given in Section 2. Thus, the contribution from the conventional propagating light might not have been sufficiently excluded. Tails represented by white broken curves in this figure were attributed to this contribution.

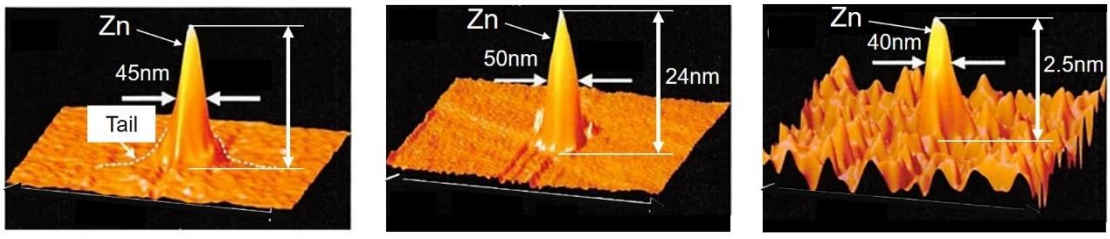

Fig. 3 AFM images of three-dimensional Zn-NPs formed on a sapphire substrate. The DEZn molecules were dissociated by the DP. The wavelengths of the propagating light for creating the DP were (a) 325 nm, (b) 488 nm, and (c) 684 nm.

In contrast to Fig. 3(a), the wavelengths of the propagating light in Figs. 3(b) and (c) were sufficiently longer than 270 nm, which means that the contribution from the propagating light was sufficiently excluded due to tricks (1) and (2) described in Section 2. That is, the DEZn molecules were dissociated only by the non-resonant DP–molecule interaction, resulting in AFM tail-free images of the Zn-NPs. The full width at the half-maximum (FWHM) of the AFM images were 45, 50, and 40 nm*, respectively, in Figs. 3 (a)-(c), which were independent of the wavelength λ of the propagating light. Thus, it was confirmed that these values corresponded to the size of the DP used for the present PCVD.

(*)

It should be noted that these values contained a systematic error originating from the spatial resolution of the AFM, which corresponded to the tip size of several nanometers of the AFM probe. Thus, the corrected values of the FWHM, obtained by subtracting this error, were slightly smaller than 45, 50 , and 40 nm.

Figure 4 shows images of the three-dimensional Zn-NPs formed on a sapphire substrate, where DEZn molecules were replaced by $Zn(acac)_2$ molecules based on tricks (2) and (3) in Section 2 [9,10]. The wavelength λ of the propagating light for creating the DP was 457 nm. In the case of Fig. 4(a), low-power (65 μW) propagating light entered the fiber in order to form a small Zn-NP on the substrate by maintaining the deposition rate sufficiently low. Because high-precision control of the deposition time was ensured by this low deposition rate, an FWHM for the Zn-NP as narrow as 5–

10 nm was realized, which was the smallest value realized by the present PCVD method. The height was as low as 0.3 nm, which corresponded to the thickness of two layers of Zn atoms, demonstrating the high precision of deposition.

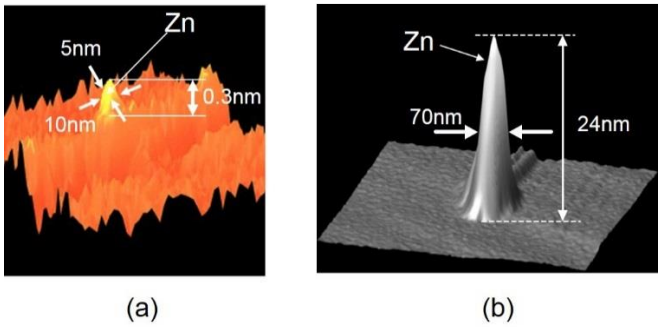

Fig. 4 AFM images of three-dimensional Zn-NPs formed on a sapphire substrate. The $Zn(acac)_2$ molecules were dissociated by the DP. The wavelength of the propagating light for creating the DP was 457 nm. (a) The power of the propagating light incident on the fiber probe was 65 μW. The irradiation time was 30 s. (b) The power of the propagating light incident on the fiber probe was 1 mW. The irradiation time was 15 s.

By increasing the incident propagating light power (1 mW), a larger Zn-NP was formed, from which the maximum size $a_{DP,Max}$ of the DP was accurately estimated. Figure 4(b) shows the result. The value of the FWHM was 70 nm, which was close to the values in Fig. 3.

Figure 5 shows the dependence of the rate R of depositing Zn atoms on the FWHM of the formed Zn-NP. Here, the value of the FWHM increased with increasing deposition time [11]. The DEZn molecules were dissociated by irradiating the end of the fiber probe with 325 nm-wavelength propagating light. This figure shows that the rate R took the maximum when the FWHM was equal to the tip diameter $2a_p$ (a_p=4.4 nm: tip radius of the fiber probe tip). This was due to the size-dependent resonance of the DP energy transfer between the tip of the fiber probe and the formed Zn-DP [12]. Further increases in the deposition time decreased R while the size of the Zn-NP increased. Finally, the size and conformation of the Zn-NP became stable, independently of the value of a_p. As a result, the value of the FWHM

saturated. Figures 3 and 4(b) show the profiles acquired after this stabilization.

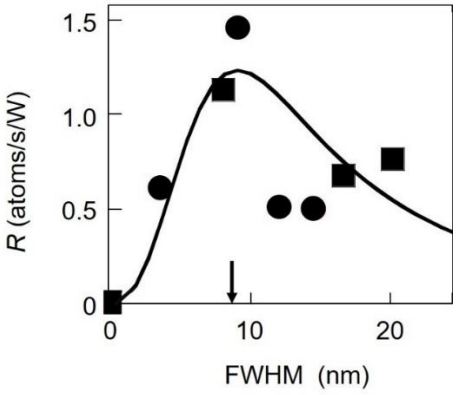

Fig. 5 Dependence of the deposition rate R on the FWHM of the Zn-NP.
The wavelength of the propagating light for creating the DP was 325 nm. Closed circles and squares represent the measured values when the powers of the light incident on the fiber probe were 5 μW and 10 μW, respectively. The downward arrow represents the value of $2a_p$.

The FWHM values in Figs. 3 and 4(b) were 50–70 nm, including systematic errors due to the spatial resolution of the AFM. They were independent of a_p and the wavelength λ of the light used for irradiating the end of the fiber probe. A larger FWHM was not realized even by increasing the deposition time. From these unique results, it was concluded that the experimentally estimated maximum size $a_{DP,Max}$ of the DP was 50–70 nm.

4. Summary

In order to stimulate the advent of a novel theory for describing the maximum size $a_{DP,Max}$ of a DP, this article described experimental estimation of $a_{DP,Max}$ by PCVD for dissociating DEZn molecules and $Zn(acac)_2$ molecules in order to form a Zn-NP on a sapphire substrate.

The experimental methods and results are summarized as follows:
(1) The present PCVD method excluded the contribution of the propagating

light even though this light leaked out from the fiber probe. This exclusion was ensured by using a non-resonant DP–molecule interaction.

(2) The size of the Zn-NP increased with increasing deposition time, and finally, the size and conformation of the Zn-NP became stable. As a result, the value of the FWHM saturated.

(3) The saturated value of the FWHM was independent of the tip radius a_p of the fiber probe and the wavelength λ of the propagating light used for creating the DP.

From the results above, it was concluded that the experimentally estimated maximum size $a_{DP,Max}$ of the DP was 50–70 nm.

References

[1] M. Ohtsu, *Dressed Photons* (Springer, Heidelberg, 2014) pp.11-33.

[2] K. Kobayashi and M. Ohtsu, Quantum theoretical approach to a near-field optical system, J. Microscopy, **194** (1999) pp.249-254.

[3] M. Ohtsu, *Dressed Photons* (Springer, Heidelberg, 2014) pp.89-246.

[4] M. Ohtsu, *Dressed Photons* (Springer, Heidelberg, 2014) pp.59-88.

[5] M. Fee, S. Chu, and T. W. Hänsch, *Scanning electromagnetic transmission line microscope with sub-wavelength resolution*, Opt. Commun., Vol.69 (3,4) , January 1, 1989, pp.219-224.

[6] T. Kawazoe, Y. Yamamoto, and M. Ohtsu, *Fabrication of a nanometric Zn dot by nonresonant near-field optical chemical-vapor deposition*, Appl. Phys. Lett., **79** (2001) pp.1184-1186.

[7] T. Kawazoe, K. Kobayashi, S. Takubo, and M. Ohtsu, *Nonadiabatic photodissociation process using an optical near field*, J. Chem. Phys. **122**, 024715 (2005).

[8] M. Ohtsu, *Near-Field Nano/Atom Optics and Technology* (Springer, Tokyo, 1998) pp.31-100.

[9] T. Kawazoe and M. Ohtsu, *Adiabatic and nonadiabatic nanofabrication by localized optical near fields*, in *Photon Processing in Microelectronics and Photonics III*, ed. by P.R.Heman, J. Fieret, A. Pique, T. Okada, F.G. Bachmann, W. Hoving, K. Washio, X. Xu, J.J. Dubouwki, D.B. Geohegan, F. Trager, Prof. SPIE Vol.5339 (SPIE, Bellingham, WA, 2004) pp.619-97.

[10] T. Kawazoe, K. Kobayashi, and M. Ohtsu, *Near-field optical chemical vapor deposition using Zn(acac)₂ with a non-adiabatic photochemical process*, Appl. Phys. B, 84 (2006) pp.247-251.

[11] J. Lim, T. Yatsui, and M. Ohtsu, *Observation of Size-Dependent Resonance of Near-Field*

Coupling between a Deposited Zn Dot and the Probe Apex during Near-Field Optical Chemical Vapor deposition, IEICE Trans. Electron., E88-C (2005) pp.1832-1834.
[12] M. Ohtsu, *Dressed Photons* (Springer, Heidelberg, 2014) pp.33-36.

Logical Fallacy of using the Electric Field in Non-resonant Near-field Optics

Itsuki Banno*

Graduate Faculty of Interdisciplinary Research

Faculty of Engineering, University of Yamanashi,

*4-3-11 Takeda, Kofu, Yamanashi, 400-8511, Japan**

Motoichi Ohtsu

Research Origin for Dressed Photon,

c/o Yokohama Technology Center, NICHIA Corporation,

3-13-19 Moriya-cho Kanagawa-ku, Yokohama-shi, 221-0022, Japan

(Dated: July 31, 2018)

Abstract

We find that the electric field is not a suitable physical quantity to describe the response of *a non-metallic material* in the study of *non-resonant* near-field optics. In practice, we show the spin-less one-electron two-level system responds differently to longitudinal and transverse electric fields under the non-resonant condition. This difference originates from *the non-relativistic nature* of the system, and should exist in actual many-electron systems. For this type of system, it is a logical fallacy to use the constitutive equation in terms of the total electric field and the associated permittivity. Recognizing this fallacy, both experimental and theoretical progress is needed in the field of non-resonant near-field optics of non-metallic materials.

PACS numbers: 78.67.-n, 78.20.Bh, 41.20.-q, 42.25.Ja

Keywords: non-resonant condition, non-metallic material, optical near field, response function

*Electronic address: banno@yamanashi.ac.jp

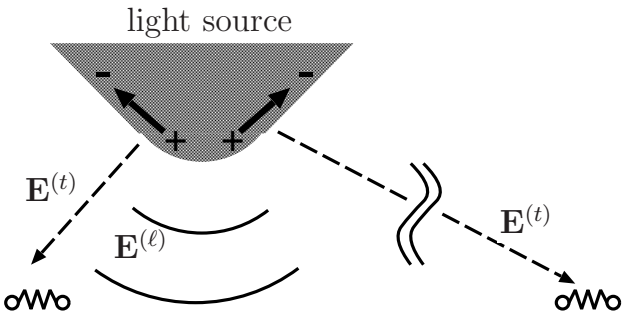

FIG. 1: Target materials under near- and far-field incidences: the former is exposed to the incident longitudinal and transverse electric fields simultaneously (the left side), whereas the latter is exposed to only the transverse field (the right side).

Under *non-resonant conditions* in the optical near field, *non-metallic materials* cause various phenomena not observed in conventional optics, such as highly efficient light emission from indirect-transition-type semiconductors (LED[1, 2] and Laser[2, 3]), chemical reaction with insufficient photon energy (chemical vapor deposition[4], optical near-field lithography[5], optical near-field etching[6]), frequency up-conversion[7, 8], non-adiabatic effect beyond forbidden transition (local energy concentration[9], nano-photonic gate device[10]), and gigantic magneto-optical rotation of the LED[2, 11, 12]. Theoretically, *dressed photons*, namely, the localized electromagnetic field easily coupled with phonons, were introduced to allow non-adiabatic transitions[13–15].

This Rapid communication focuses on another fundamental role of the non-resonant condition in near-field optics (NFO) with non-metallic materials. We examine the one-electron two-level system close to both the light source and the observation point under long wavelength approximation (LWA), and find it a logical fallacy to regard *the total electric field* as causing the response under the non-resonant condition. In contrast, under the resonant condition or the far-field observation condition, the electric field works as expected. These findings originate from *the non-relativistic nature* of the system and should be applicable in actual optical systems with non-metallic materials. For the readability, calculation details are given in the last part of this paper.

Suppose a small-scale material is placed in the vicinity of a nanostructure, which functions as a light source (Fig.1). In such a system, under the NF incidence condition, the target material is exposed to longitudinal and transverse electric fields simultaneously, whereas

in a system under the far-field incidence condition, the target material is exposed only to the transverse field, which survives far from the light source. Therefore, the coexistence of longitudinal and transverse electric fields distinguishes such a system under the NF incidence condition from that under the far-field incidence condition.

Here, the longitudinal electric field originates from the charge density on the nanostructure, obeys Coulomb's law, and has a non-radiative nature to localize around the nanostructure. On the other hand, the transverse electric field originates from the transverse current density on the nanostructure, obeys the Ampere-Maxwell law and Faraday's law, and has a radiative nature allowing it to propagate far from the light source, accompanied by the magnetic field. (The longitudinal current density is determined via the charge conservation law, once the charge density is known, and is not an independent source.) Therefore, the two incidences coexisting in an NF optical system have distinct properties.

Furthermore, owing to *the non-relativistic nature* of the system, the scalar and vector potentials appear in a different manner in the Hamiltonian, which governs the electron response, for example, (13) of *Calculation details* (i) in the last part of this paper. Considering that the scalar and vector potentials under the Coulomb gauge represent the longitudinal and transverse electric fields, respectively, one may confirm that the two types of incidences in NFO cause different responses. Now our question is the following: under what condition can we observe these differences?

Before proceeding with the analysis, let us first classify the optical systems. The two systems under near- and far-field incidence conditions in Fig.1 are subdivided into two classes depending on the near- or far-field observation condition. These four classes are listed in Table I, together with a summary of the results mentioned below. In particular, the systems of (I′) and (II′) are the limiting cases of null longitudinal incidence of the systems (I) and (II), respectively. Thus, in the systems (I′) and (II′), the longitudinal response vanishes and the difference in response may not be observed. In the following, therefore, we focus mainly on systems (I) and (II), in which longitudinal incidence exists.

Microscopic responses to longitudinal and transverse electric fields. Applying the linear response theory and the LWA to the electron system of the target material on a small scale, the induced charge and current densities (*as a result of the response*), $\Delta\rho(\mathbf{r},t)$ and $\Delta\mathbf{j}(\mathbf{r},t)$, are described as the total derivative with respect to the longitudinal and transverse electric fields (*as the cause of the response*), $\Delta\mathbf{E}^{(\ell)}(\mathbf{0},t)$ and $\Delta\mathbf{E}^{(t)}(\mathbf{0},t)$, where $\mathbf{0}$ is the

TABLE I: Classification of optical systems by distance from the target material to the light source and distance from that to the observation point, together with a summary of the results; the validity of the electric field as the cause of the response.

	Near-field observation Source:$\Delta\rho$ and $\Delta\mathbf{j}$	**Far-field observation** Source: $\overline{\Delta\mathbf{j}}$
Near-field incidence : $\Delta\mathbf{E}^{(\ell)} + \Delta\mathbf{E}^{(t)}$	**(I) NF optical system** non-resonant / resonant	**(II) NF optical system** non-resonant / resonant
Validity of the electric field	NG / OK	OK / OK
Far-field incidence : $\Delta\mathbf{E}^{(t)}$	**(I′) NF optical system** non-resonant / resonant	**(II′) conventional optical system** non-resonant / resonant
Validity of the electric field	OK / OK	OK / OK

representative position in the electron system under the LWA:

$$\Delta\rho(\mathbf{r},t) = \chi_j^{\rho\leftarrow(\ell)}(\mathbf{r},\omega)\,\Delta E_j^{(\ell)}(\mathbf{0},t) + \chi_j^{\rho\leftarrow(t)}(\mathbf{r},\omega)\,\Delta E_j^{(t)}(\mathbf{0},t)\,, \tag{1}$$

$$\Delta j_i(\mathbf{r},t) = \chi_{ij}^{\mathbf{j}\leftarrow(\ell)}(\mathbf{r},\omega)\,\Delta \dot{E}_j^{(\ell)}(\mathbf{0},t) + \chi_{ij}^{\mathbf{j}\leftarrow(t)}(\mathbf{r},\omega)\,\Delta \dot{E}_j^{(t)}(\mathbf{0},t)\,, \tag{2}$$

where the partial derivative coefficients, $\chi_{\cdots}^{\cdots}(\mathbf{r},\omega)$'s are susceptibilities (response functions), and Einstein's rule is used for the summation over the vector indices, for example, $\chi_j^{\rho\leftarrow(\ell)}(\mathbf{r},\omega)\,\Delta E_j^{(\ell)}(\mathbf{0},t) = \sum_{j=1}^{3} \chi_j^{\rho\leftarrow(\ell)}(\mathbf{r},\omega)\,\Delta E_j^{(\ell)}(\mathbf{0},t)$. In (2), the time derivatives of the two types of electric fields, namely, $\Delta\dot{E}_j^{(\ell)}(\mathbf{0},t)$ and $\Delta\dot{E}_j^{(t)}(\mathbf{0},t)$, are regarded as the causes, instead of the two types of electric fields themselves. The magnetic response vanishes in the leading order under the LWA ; see Ref.[16]. The derivation of (1) and (2) is given in *Calculation details* (i).

For simple evaluation of the susceptibilities in (1) and (2), suppose we have a spinless one-electron system with two levels, the ground and excited states in the non-perturbed system with eigenenergies, $\hbar\omega_0$ and $\hbar\omega_1$, and orbitals, $\varphi_0(\mathbf{r})$ and $\varphi_1(\mathbf{r})$, respectively. Those orbitals are assumed to be bound states expressed by real functions, carry well-defined and distinct spatial parities (even and odd parities), and form the normalized orthogonal complete set. The excitation energy is $\hbar\Delta\omega_1 \equiv \hbar\omega_1 - \hbar\omega_0 > 0$; this finite excitation energy means that the target is a non-metallic material, such as a molecule, nano-structured semiconductor

and insulator.

The susceptibilities in (1) and (2) are derived in *Calculation details* (ii), and those leading to the induced charge density result in the following:

$$\chi_j^{\rho\leftarrow(\ell)}(\mathbf{r},\omega) = \chi_j^{\rho\leftarrow(t)}(\mathbf{r},\omega) = 2q^2\,\frac{\eta}{\eta^2-1}\,\frac{1}{\hbar\omega}\,\mathcal{D}_j\,\varphi_0(\mathbf{r})\varphi_1(\mathbf{r})\,, \tag{3}$$

$$\text{where} \qquad \eta \equiv \frac{\hbar\Delta\omega_1}{\hbar\omega} = \frac{\text{excitation energy}}{\text{photon energy}}\,, \text{ and} \tag{4}$$

$$\mathcal{D}_i \equiv \int \mathrm{d}^3 r\ \varphi_1(\mathbf{r})\, r_i\, \varphi_0(\mathbf{r})\,. \tag{5}$$

This means that the responses to the longitudinal and transverse electric fields are common, such that the induced charge density has a linear relationship with *the total electric field*, namely, $\Delta\rho(\mathbf{r},t) = \chi_j^{\rho\leftarrow(\ell)\text{ or }(t)}(\mathbf{r},\omega)\left(\Delta E_j^{(\ell)}(\mathbf{0},t) + \Delta E_j^{(t)}(\mathbf{0},t)\right)$.

The susceptibilities leading to the induced current density are not so simple and result in the following:

$$\chi_{ij}^{\mathbf{j}\leftarrow(\ell)}(\mathbf{r},\omega) = \frac{q^2\hbar^2}{m}\,\frac{1}{\eta^2-1}\,\frac{1}{(\hbar\omega)^2}\,\mathcal{D}_j\,\left(\partial_i\varphi_1(\mathbf{r})\varphi_0(\mathbf{r}) - \varphi_1(\mathbf{r})\partial_i\varphi_0(\mathbf{r})\right)\,, \tag{6}$$

$$\chi_{ij}^{\mathbf{j}\leftarrow(t)}(\mathbf{r},\omega) = \eta^2\,\chi_{ij}^{\mathbf{j}\leftarrow(\ell)}(\mathbf{r},\omega) - \frac{q^2\hbar^2}{m}\,\frac{1}{(\hbar\omega)^2}\,\varphi_0(\mathbf{r})\varphi_0(\mathbf{r})\,. \tag{7}$$

The susceptibility to the transverse electric field, (7), is composed of two terms. The first term, namely, the resonant term, includes the energy denominator enhanced under the resonant condition, $\eta \simeq 1$, as in the susceptibility to the longitudinal electric field, (6). The second term, namely, the non-resonant term, does not include such a resonance factor.

Equal responses under the resonant condition. Under the condition $\eta \simeq 1$ in all cases in Table I, (7) is dominated by the resonant term (the first term) over the non-resonant term (the second term) and asymptotically equals (6).

$$\chi_{ij}^{\mathbf{j}\leftarrow(t)}(\mathbf{r},\omega) \simeq \chi_{ij}^{\mathbf{j}\leftarrow(\ell)}(\mathbf{r},\omega)\,. \tag{8}$$

Equation (8) together with (3) reveal the equivalency of the responses to the longitudinal and transverse electric fields, so that the total electric field is regarded as the cause of the response in *any* optical system under the resonant condition listed in Table I .

Equal responses under the far-field observation condition. In the system (II) and (II′) in Table I, the far field to be observed is insensitive to the details of the source but is determined by the spatial average of the source. Under the LWA, such an average can be

achieved by the spatial average of the susceptibilities. Detailed calculations are shown in *Calculation details* (iii); the results are as follows.

$$\overline{\chi_j^{\rho\leftarrow(\ell)}(\mathbf{r},\omega)} = \quad \overline{\chi_j^{\rho\leftarrow(t)}(\mathbf{r},\omega)} = 0\,, \tag{9}$$

$$\overline{\chi_{ij}^{\mathbf{j}\leftarrow(\ell)}(\mathbf{r},\omega)} = \overline{\chi_{ij}^{\mathbf{j}\leftarrow(t)}(\mathbf{r},\omega)} = \delta_{i\,j}\frac{q^2\hbar^2}{m\,\mathcal{V}}\frac{1}{(\hbar\Delta\omega_1)^{\,2}-(\hbar\omega)^2}\,, \tag{10}$$

where the overline represents the spatial average and $\mathcal{V}$ is the volume of the target material. From (9) and (10), one may not observe different responses to the two types of incidences under the far-field observation condition. The null response represented in (9) is reasonable because the induced charge density yields the longitudinal electric field, which has a non-radiative nature and vanishes in the far-field regime.

Unequal responses under the non-resonant, NF incidence, and NF observation conditions. The different responses claimed in the beginning of this Rapid communication may be detected only in the system (I) in Table I under the non-resonant condition, which is just the compliment to the popular optical systems under the resonant condition and/or the far-field observation condition. In the NF optical system (I) with a non-metallic material under the non-resonant condition, *the total electric field* is not the cause of the response; therefore, the response may not be described by the macroscopic constitutive equation (MCE), namely, the linear relationship between the polarization and "electric field" via permittivity, and the microscopic susceptibilities are essential to treat separately the longitudinal and transverse incidences.

In NFO, the response to the longitudinal electric field is discussed in Chap. 5 in Ref.[16] and Chap. 9 in Ref.[18]. The present work is a further comparison of the two responses, considering *the non-resonant condition*.

The present model is very simple and the responses may be modified in a many-electron system or a low-symmetry system. However, the difference in the responses to the two types of electric fields originates in *the non-relativistic nature* of the system (as stated in the beginning of this Rapid communication), and should survive in actual NF optical systems with non-metallic materials (the materials with finite excitation energy). Actually, there is no reason for equating the two responses in the many-electron and low-symmetry systems. Therefore, one may infer a guiding principle to highlight NF optical phenomena: under the non-resonant condition and simultaneous NF-incident and NF-observation conditions, non-metallic materials bring about NF-specific optical phenomena that may not be described

by the MCE in terms of the electric field and the permittivity. Some of the experiments mentioned in the beginning of this paper were performed under such conditions; thus, we will analyze them in detail in future investigation.

A remark on applying the finite differential time domain (FDTD) method to an NF optical system. The MCE in terms of the permittivity has been widely employed to calculate the optical near field in the FDTD method[17]. One may notice that the permittivity in the FDTD method carries a simple spatial dependence and leads to some quantitative error. Actually, the microscopic susceptibilities, for example, (3), (6), and (7), have rippling spatial distributions originating from the orbitals.

In the case of the NF optical system (I) in Table I with a non-metallic material under the non-resonant condition, the situation is more serious because the concept *electric field* is not available, such that it is a logical fallacy to use the MCE. Thus, a novel simulation method is necessary.

NFO and many-electron problem. Why has the comparison of responses to the two types of electric fields not been addressed in NF optical theory? First, in the long history of optics, the NF optical system (I) in Table I under a non-resonant condition has been out of focus. Such a system could not be resolved until the technical difficulty of NF observation was overcome. Additionally, resonance phenomena continue to attract attention. Furthermore, even in NFO, there has been less emphasis on non-metallic materials, as opposed to metallic materials, which are essential for plasmonics.

The second reason is that the ordinary Hamiltonian for a many-electron system does not include the longitudinal electric field, which is rewritten to the two-body Coulomb interaction and eliminated. With this Hamiltonian, the response to the longitudinal electric field incidence accompanies the Coulomb interaction, and is difficult to analyze. Therefore, NFO is inevitably related to the many-electron problem; however, this has not been well recognized for a long time. This study considered a one-electron system, avoiding the many-electron problem. In future studies, the present scenario will be extended to a many-electron system and nonlinear response, overcoming the many-electron problem, and applying the findings to various phenomena mentioned in the beginning of this Rapid communication.

To the best of our knowledge, the present near-field optical system with non-metallic material under the non-resonant condition is the third example that cannot be described in terms of electric field and/or magnetic field, after the superconductor system with the

Meissner effect and the electron system with the Aharonov-Bohm effect. The diversity of non-metallic materials including semiconductors, dielectrics, and magnetic materials has been utilized in conventional optics. We believe that focusing on non-metallic materials in NFO promotes further development both conceptually and technically.

Calculation details. Here we provide the calculation details, including the derivation of the unfamiliar relationship (28) between two types of dipole transition matrix elements.

(i) Derivation of the microscopic constitutive equations, (1) and (2). The incident scalar and vector potentials, $\Delta\phi(\mathbf{r},t)$ and $\Delta A_i(\mathbf{r},t)$, are assumed to be monochromatic with the angular momentum ω, and are expressed using the Coulomb gauge and LWA, as follows:

$$\Delta\phi(\mathbf{r},t) = \Delta\phi(\mathbf{r})\cos\omega t = \left(\Delta\phi(\mathbf{0}) - \Delta\mathbf{E}^{(\ell)}(\mathbf{0})\cdot\mathbf{r}\right)\cos\omega t\,, \tag{11}$$

$$\Delta\mathbf{A}(\mathbf{r},t) = \Delta\mathbf{A}(\mathbf{r})\sin(\omega t+\xi) = -\frac{1}{\omega}\Delta\mathbf{E}^{(t)}(\mathbf{0})\sin(\omega t+\xi)\,, \tag{12}$$

where and ξ is the phase difference between the two incident potentials. The nanostructure is assumed to be a robust light source, which is not affected by the target material, and the electromagnetic field is assumed to be a classical field.

Using a spinless one-electron system, let us evaluate the induced charge and current densities caused by the coexisting incidences of the scalar and vector potentials. The total Hamiltonian is as follows:

$$\hat{H} = \frac{1}{2m}\left(\frac{\hbar}{i}\frac{\partial}{\partial x_i(t)} - qA_i(\mathbf{x}(t),t)\right)\left(\frac{\hbar}{i}\frac{\partial}{\partial x_i(t)} - qA_i(\mathbf{x}(t),t)\right) + q\phi(\mathbf{x}(t),t)\,, \tag{13}$$

where t is time, $\mathbf{x}(t)$ is the position of the electron, and $q(=-e), m$ are the electron charge and mass, respectively. The perturbation Hamiltonian is given by

$$\int \mathrm{d}^3r\,\left(\hat{\rho}(\mathbf{r},t)\Delta\phi(\mathbf{r},t) - \hat{j}_i(\mathbf{r},t)\Delta A_i(\mathbf{r},t)\right), \tag{14}$$

where $\hat{\rho}(\mathbf{r},t), \hat{j}_i(\mathbf{r},t)$ are the Heisenberg operators of the charge and current densities defined as

$$\hat{\rho}(\mathbf{r},t) = q\delta^3(\mathbf{r}-\mathbf{x}(t))\,, \tag{15}$$

$$\hat{j}_i(\mathbf{r},t) = \frac{q}{2m}\left\{\left(\frac{\hbar}{i}\frac{\partial}{\partial x_i(t)} - qA_i(\mathbf{x}(t),t)\right)\delta^3(\mathbf{r}-\mathbf{x}(t)) + \delta^3(\mathbf{r}-\mathbf{x}(t))\left(\frac{\hbar}{i}\frac{\partial}{\partial x_i(t)} - qA_i(\mathbf{x}(t),t)\right)\right\}. \tag{16}$$

The linear response theory leads to the operators of the induced charge and current densities, as follows:

$$\Delta\hat{\rho}(\mathbf{r},t) = \int_{-\infty}^{t} \mathrm{d}t_1 \int \mathrm{d}^3 r_1 \left\{ \frac{1}{i\hbar} \left[\hat{\rho}^{(0)}(\mathbf{r},t)\,,\, \hat{\rho}^{(0)}(\mathbf{r}_1,t_1) \right] \Delta\phi(\mathbf{r}_1,t_1) \right. \\ \left. - \frac{1}{i\hbar} \left[\hat{\rho}^{(0)}(\mathbf{r},t)\,,\, \hat{j}_{i_1}^{(0)}(\mathbf{r}_1,t_1) \right] \Delta A_{i_1}(\mathbf{r}_1,t_1) \right\}, \tag{17}$$

$$\Delta\hat{j}_i(\mathbf{r},t) = \int_{-\infty}^{t} \mathrm{d}t_1 \int \mathrm{d}^3 r_1 \left\{ \frac{1}{i\hbar} \left[\hat{j}_i^{(0)}(\mathbf{r},t)\,,\, \hat{\rho}^{(0)}(\mathbf{r}_1,t_1) \right] \Delta\phi(\mathbf{r}_1,t_1) \right. \\ \left. - \frac{1}{i\hbar} \left[\hat{j}_i^{(0)}(\mathbf{r},t)\,,\, \hat{j}_{i_1}^{(0)}(\mathbf{r}_1,t_1) \right] \Delta A_{i_1}(\mathbf{r}_1,t_1) \right\} - \frac{q}{m} \hat{\rho}^{(0)}(\mathbf{r},t) \Delta A_i(\mathbf{r},t)\,, \tag{18}$$

where $\hat{\rho}^{(0)}$ and $\hat{\mathbf{j}}^{(0)}$ are the charge and current density operators, respectively, in the non-perturbed system. The last term in (18) originates from *the non-relativistic nature* of the system and is needed to maintain the charge conservation law.

Evaluating the expectation value using the ground state and substituting (11) and (12) leads to (1) and (2), in which the causes of the responses are the two types of electric fields and their temporal derivatives, defined as

$$\Delta E_j^{(\ell)}(\mathbf{0},t) \equiv \quad \Delta E_j^{(\ell)}(\mathbf{0}) \cos\omega t\,, \quad \Delta E_j^{(t)}(\mathbf{0},t) \equiv \quad \Delta E_j^{(t)}(\mathbf{0}) \cos(\omega t + \xi)\,, \tag{19}$$

$$\Delta \dot{E}_j^{(\ell)}(\mathbf{0},t) \equiv \frac{\partial}{\partial t} \Delta E_j^{(\ell)}(\mathbf{0},t)\,, \qquad \Delta \dot{E}_j^{(t)}(\mathbf{0},t) \equiv \frac{\partial}{\partial t} \Delta E_j^{(t)}(\mathbf{0},t)\,. \tag{20}$$

In the above, no magnetic response appears because it is the higher order in the LWA[16, 19]. Cho derived a Taylor series of the non-local response function[20] under the LWA, and assigned the electric permittivity and magnetic permeability in the MCE as the term of order $\mathcal{O}(ka)^0$ (the leading order) and $\mathcal{O}(ka)^2$, respectively, where $ka \ll 1$, $2\pi/k$ is the light wavelength, and a is the representative size of the material.

Furthermore, he pointed out that the MCE is irrational because the separability of the electric and magnetic responses and the term of order $\mathcal{O}(ka)^1$ appears in a chiral symmetric system, including a NF optical system with a low-symmetric nanostructure. The present work is concerned with another type of irrationality, which appears in the electric response (the leading order from the viewpoint of Cho) in NFO under *a non-resonant condition*.

(ii) Derivation of the expressions for susceptibilities, (3), (6) and (7).

To obtain these formulas using the two-level model, we take the expectation values of (17)

and (18) using the ground state, $\varphi_0(\mathbf{r})$, and insert the projection operator [the left side of the second equation in (21)], assuming that the two orbitals are real functions, and form the normalized orthogonal complete set:

$$\int \mathrm{d}^3 r\, \varphi_m(\mathbf{r})\varphi_n(\mathbf{r}) = \delta_{m\,n}\,, \qquad \sum_m \varphi_m(\mathbf{r})\varphi_m(\mathbf{r}') = \delta^3(\mathbf{r}-\mathbf{r}')\,, \tag{21}$$

where $\varphi_m(\mathbf{r})$ satisfies,

$$\hat{H}^{(0)}\varphi_m(\mathbf{r}) = \hbar\omega_m\,\varphi_m(\mathbf{r})\,, \quad (m=0,1)\,. \tag{22}$$

Having real orbitals infers even temporal parity, such that there is a null magnetic field in the non-perturbed system or null vector potential in the non-perturbed Hamiltonian. Furthermore, we use the well-known linear relationship between the two types of dipole transition matrix elements,

$$\mathcal{C}_i \equiv \int \mathrm{d}^3 r\ (\partial_i\varphi_1(\mathbf{r})\varphi_0(\mathbf{r}) - \varphi_1(\mathbf{r})\partial_i\varphi_0(\mathbf{r})) = \frac{2m}{\hbar^2}\hbar\Delta\omega_1\,\mathcal{D}_i\,. \tag{23}$$

Equation (23) is derived from the matrix element of the Heisenberg equation for dipole charge density:

$$\frac{\partial}{\partial t}\, r_j\hat{\rho}^{(0)}(\mathbf{r},t) = \frac{1}{i\hbar}\left[r_j\hat{\rho}^{(0)}(\mathbf{r},t)\,,\ \hat{H}^{(0)}\right]\,, \tag{24}$$

using $\hat{\rho}^{(0)}(\mathbf{r},t) = e^{-\frac{\hat{H}^{(0)}t}{i\hbar}}\hat{\rho}^{(0)}(\mathbf{r},0)e^{+\frac{\hat{H}^{(0)}t}{i\hbar}}$, the projection operator, (21) and (22).

(iii) Derivation of the spatial average of the susceptibilities, (9) and (10). These following replacements in (3), (6) and (7) lead to (9) and (10):

$$\varphi_0(\mathbf{r})\varphi_1(\mathbf{r}) \quad \longrightarrow \quad \frac{1}{\mathcal{V}}\int \mathrm{d}^3 r\,\varphi_0(\mathbf{r})\varphi_1(\mathbf{r}) = 0\,, \tag{25}$$

$$\partial_i\varphi_1(\mathbf{r})\varphi_0(\mathbf{r}) - \varphi_1(\mathbf{r})\partial_i\varphi_0(\mathbf{r}) \quad \longrightarrow \quad \frac{1}{\mathcal{V}}\int \mathrm{d}^3 r\,\partial_i\varphi_1(\mathbf{r})\varphi_0(\mathbf{r}) - \varphi_1(\mathbf{r})\partial_i\varphi_0(\mathbf{r}) = \frac{1}{\mathcal{V}}\mathcal{C}_i\,, \tag{26}$$

$$\varphi_0(\mathbf{r})\varphi_0(\mathbf{r}) \quad \longrightarrow \quad \frac{1}{\mathcal{V}}\int \mathrm{d}^3 r\,\varphi_0(\mathbf{r})\varphi_0(\mathbf{r}) = \frac{1}{\mathcal{V}}\,. \tag{27}$$

To derive (10), we additionally use the trade-off relationship between the two types of dipole transition matrix elements,

$$\mathcal{D}_i\,\mathcal{C}_j = \delta_{i\,j}. \tag{28}$$

This is effective in the two-level system with well-defined parity and derived from the quantum-mechanical commutation relationship:

$$[r_i\,,\,\frac{\hbar}{i}\partial_j] = i\hbar\,\delta_{ij}\,,\quad \text{i.e.,}\quad r_i\left(\frac{\hbar}{i}\partial_j\cdots\right)+\frac{\hbar}{-i}\partial_j\,(r_i\cdots) = i\hbar\delta_{ij}\cdots\,. \tag{29}$$

Inserting the projection operator between r_i and $\frac{\hbar}{i}\partial_j$, and eliminating the null integrals caused by mismatched parity result in (28). From (23) and (28), $\mathcal{D}_i$ and $\mathcal{C}_i$ are specified as

$$\mathcal{D}_i = \frac{1}{\mathcal{C}_i} = \frac{\hbar}{\sqrt{2m\,\hbar\Delta\omega_1}}\,. \tag{30}$$

(We do not use (30) in this paper.)

Acknowledgments

The authors are grateful Drs. I. Ojima (Research Origin of Dressed Photon (RODreP)), H. Sakuma (RODreP), H. Saigo (Nagahama Insitute of Bio-Science and Technology), K. Okamura (Nagoya Univ.), H. Ando (Chiba Univ.) , and T. Kawazoe (Tokyo Denki Univ.) for useful discussions on the context of dressed photon. One of the authors (I. B.) thanks Professor K. Cho in Osaka Univ. for useful discussions concerning susceptibility. This work is partially supported by JSPS KAKENHI Grant Number JP25610071 during 2013-2015, and Research Foundation for Opto-Science and Technology during 2018-2019.

---

[1] T. Kawazoe, M. A. Mueed, and M. Ohtsu, Appl. Phys. B **104,** 747 (2011).

[2] M. Ohtsu, *Silicon Light-Emitting Diodes and Lasers* (Springer International Publishing, Switsland, 2016).

[3] T. Kawazoe, M. Ohtsu, K. Akahane, and N. Yamamoto, Appl. Phys. B **107,** 659 (2012).

[4] T. Kawazoe, Y. Yamamoto, and M. Ohtsu, Appl. Phys. Lett. **79,** 1184 (2001).

[5] H. Yonemitsu, T. Kawazoe, K. Kobayashi, and M. Ohtsu, J. Photolumin. **122,** 230 (2007).

[6] T. Yatsui, K. Hirata, W. Nomura, Y. Tabata, and M. Ohtsu, Appl. Phys. B **93,** 55 (2008).

[7] T. Kawazoe, H. Fujiwara, K. Kobayashi, and M. Ohtsu, IEEE J. of Selected Topics in Quantum Electronics **15,** 1380 (2009).

[8] H. Fujiwara, T. Kawazoe, and M. Ohtsu, Appl. Phys. B **100,** 85 (2010).

[9] T. Kawazoe, K. Kobayashi, and M. Ohtsu, Appl. Phys. Lett. **86,** 103102-1 (2005).

[10] T. Kawazoe, M. Ohtsu, S. Aso, Y. Sawado, Y. Hosoda, K. Yoshizawa, K. Akahane, N. Yamamoto, and M. Naruse, Appl. Phys. B **103,** 537 (2011).

[11] N. Tate, T. Kawazoe, W. Nomura, and M. Ohtsu, Scientific Reports **5,** 12762-1 (2015) .

[12] N. Tate, T. Kawazoe, S. Nakashima, W. Nomura, M. Ohtsu, *Abstracts of the 22nd International Display Workshops* (Dec. 9-11, 2015, Otsu, Japan, PRJ3-1).

[13] T. Kawazoe, K. Kobayashi, S. Takubo, and M. Ohtsu, J. Chem. Phys. **122,** 024715-1 (2005).

[14] K. Kobayashi, T. Kawazoe, and M. Ohtsu, IEEE Trans. Nanotech. **4,** 517 (2005).

[15] M. Ohtsu, *Dressed Photons: Concepts of Light-Matter Fusion Technology* (Springer-Verlag, Berlin, Heidelberg, 2014).

[16] K. Cho, *Reconstruction of Macroscopic Maxwell Equations* (Springer-Verlag, Berlin, Heidelberg, 2010).

[17] K. Yee, *IEEE Transactions on Antennas and Propagation* **14,** 302 (1966).

[18] O. Keller, *Quantum Theory of Near-Field Electrocynamics* (Springer-Verlag, Berlin, Heidelberg, 2011).

[19] K. Cho, J. Phys. Condens. Matter **20,**175202 (2008).

[20] K. Cho, *Optical Response of Nanostructures* (Springer-Verlag, Berlin, Heidelberg, 2003).

[V] PUBLISHED BOOKS

Progress in Nanophotonics 5

Table of contents (6 chapters)

Chapter 1
Historical Review of Dressed Photons: Experimental Progress and Required Theories

Motoichi Ohtsu

Abstract First, this article reviews the experimental and theoretical studies of dressed photons (DPs), carried out in the last three decades. It is pointed out that future theoretical studies can be developed by following three steps. Second, it is proposed how to proceed in the first and second steps by describing a unique DP energy transfer process. As an application of this transfer process, novel functional devices are demonstrated. The DP energy transfer in these devices is shown to exhibit an autonomous spatial evolution feature. A temporal evolution feature is also revealed. Another application is a highly efficient optical energy conversion film that gives a drastically increased electrical power generation efficiency of a silicon solar battery. Lastly, in order to identify the requirements for future theoretical studies, this article reviews how to proceed in the third step by employing a fiber probe. Among these requirements, an essential requirement is to describe the autonomy mentioned above and also the hierarchy observed in DP measurements. To meet the requirements, novel theoretical approaches are reviewed for developing a new field known as off-shell science. These approaches are based on Clebsch dual field theory, the quadrality scheme in category theory, and a novel measurement theory.

1.1 Introduction

The dressed photon (DP), a novel form of photon created in a nanometer-sized space, has been referred to as an optical near field, and the science for dealing with this type of photon has been called near field optics. The history of near field optics is long and can be classified into older and modern times, based on the great differences in the concepts, principles, and methods of studying the DP. The older time started

M. Ohtsu (✉)
Research Origin for Dressed Photon, c/o Nichia Corp., 3-13-19 Moriya-cho, Kanagawa-ku, Yokohama, Kanagawa 221-0022, Japan
e-mail: ohtsu@rodrep.or.jp

T. Yatsui (ed.), *Progress in Nanophotonics 5*, Nano-Optics and Nanophotonics,
https://doi.org/10.1007/978-3-319-98267-0_1

[VI] PRESENTATIONS

IN DOMESTIC CONFERENCES

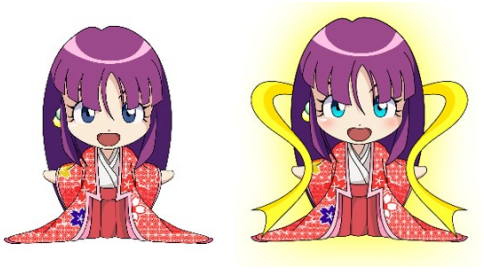

ドレスト光子系での電場の概念の破綻

A Logical Fallacy of Electric Field in the Dressed-Photon Systems

○ 坂野　斎[1]、大津元一[2](1. 山梨大院、2. ドレスト光子研究起点)

○Itsuki Banno[1], Motoichi Ohtsu[2] (1.Univ. of Yamanashi, 2.Research Origin of Dressed Photon)

E-mail: banno@yamanashi.ac.jp

川添，大津と共同研究者らは 2000 年代以降，非金属を使った非共鳴条件下での近接場光学特有の現象を発見，実用に供してきた．例えば間接半導体での高効率の発光 [1] をはじめ，不十分な光子エネルギーによる光化学反応，周波数上方変換，禁制・非断熱遷移，巨大磁気光学効果などである．これらの原因は電子系の励起，格子系の励起と結合した電磁場＝ドレスト光子 (DP；Dressed Photon) と考えられる [2]．これら DP 系における非共鳴条件の役割を理解するため，非金属物質の電子系をスピンレス１電子２準位系にモデル化し，光源（light source）からの遠近，観測点（light sink）からの遠近，共鳴か非共鳴かに従って光学系を８つに分類した．このうち，近接場入射条件かつ近接場観測条件かつ非共鳴条件の下でのみ，応答関数の非共鳴応答項によって縦電場と横電場に対する応答の違いが顕れる．これは，前の発表 [3] の詳細化であり，全電場が応答の原因みなせないこと，誘電率と電場を用いる構成方程式の記述が破綻することを意味する．電場という概念の破綻の起源は非相対論の性質，すなわち，ハミルトニアンの中でベクトルポテンシャル（クーロンゲージの下で横電磁場自由度）とスカラーポテンシャル（同じく縦電場自由度）の依存性が異なることであり多電子系についても正しいはずである．

今まで電場を応答の原因として扱えない光学系の存在を認識できなかった理由は次である：(1) この破綻が露わになるのは近接場入射かつ近接場観測かつ非共鳴条件下の場合だけで，通常の光学で関心がある遠隔場入射または遠隔場観測または共鳴条件下の系の補償の系であること．(2) 近接場光学に限ってもプラズモニクスが対象とする金属を用いる系ではなく非金属（有限の励起エネルギーをもつ物質）を用いる系であること．(3) 多電子系のハミルトニアンでは縦電場の効果を電荷間のクーロン相互作用に書き換えるため縦・横電場への応答の違いを理論的に見極めにくいこと．

DP 系の現象を説明するには電場という概念の破綻，非共鳴応答の考慮が重要と考えられる．

参考文献

[1] 川添 忠，橋本 和信，杉浦 聡，”高出力ホモ接合シリコンレーザー”，応物講演会 (2018 春 19p-F310-14); 川添 忠, 杉浦聡, 大津 元一，”高出力ホモ接合シリコンレーザーの作製 ”, 応物講演会 (2017 春 15a-F202-9); T. Kawazoe and M. Ohtsu，”Bulk crystal SiC blue LED with p-n homojunction structure fabricated by dressed-photon-phonon-assisted annealing ”, Appl. Phys. A, **115**, 127-133, (2014); M. A. Tran, T. Kawazoe, M. Ohtsu, ”Fabrication of a bulk silicon p-n homojunction-structured light-emitting diode showing visible electroluminescence at room temperature ”, Appl Phys A **115**,105-111(2014).

[2] 実験，理論のレビューとして: M. Ohtsu, ”Progress in Dressed Photon Technology and the Future ”, in *Progress in Nanophotonics* **4** eds. by M. Ohtsu and T. Yatsui (Springer, 2017) Chap. 1; M. Ohtsu, ”Dressed photon technology ”, Nanophotonics **1**, 83-97 (2012).

[3] 坂野　斎，”近接場光学における非共鳴効果の理論 I”，応物講演会（2017 春 15a-F202-12）.

謝辞

ドレスト光子研究起点 (RODreP) での数理物理的，実験的な議論に参加して下さった以下の方々に感謝いたします：小嶋泉博士 (RODreP)，佐久間弘文博士 (RODreP)，西郷甲矢人博士 (長浜バイオ大学)，岡村和弥博士 (名古屋大学)，安藤浩志博士 (千葉大学)，川添忠博士 (東京電機大学)．この研究の一部は光科学技術研究振興財団からの援助（2018-2019）を受けています.

ドレスト光子系の反磁性電流

Diamagnetic Current in the Dressed-Photon Systems

○坂野　斎[1]、川添　忠[2,3]、大津元一[3](1. 山梨大院、2. 東京電機大、3. ドレスト光子研究起点)

○Itsuki Banno[1], Tadashi Kawazoe[2,3], Motoichi Ohtsu[3]

(1.Univ. of Yamanashi, 2. Tokyo Denki Univ., 3.Research Origin of Dressed Photon)

E-mail: banno@yamanashi.ac.jp

川添・大津らが行った非金属を用いた近接場光学系の非共鳴条件下での一連の実験は，通常の光学系で見られない様々な現象をもたらし，その原因はドレスト光子（DP）と考えられる．１件前の発表で 近接場入射条件かつ近接場観測条件かつ非共鳴条件下で電場の概念，及び，電場と誘電率を用いた構成方程式が破綻することを述べたが，川添・大津の DP 系はこの条件下にある．

電場を応答の原因とみなせないので，私どもが開発した電磁ポテンシャルを原因として扱う単一感受率 [1] による記述が適する．この理論ではスカラーポテンシャル（SP）を２体のクーロン相互作用に書き換えず，ベクトルポテンシャル（VP）と対等に応答の原因として扱う．また，Heisenberg 演算子としての線型・非線型応答関数を作用積分の SP・VP による汎関数微分で導出し，電荷保存則とゲージ不変性を保証する．線型応答関数の Heisenberg 演算子として次を得る：

$$\hat{\chi}^{\mu}{}_{\mu_1}(x,x_1) = \frac{-q}{mc^2}\,\tilde{\delta}^{\mu}{}_{\mu_1}\delta^4(x-x_1)\,\hat{j}^{(in0)\,0}(x) + \frac{1}{i\hbar c^2}\theta(ct-ct_1)\left[\hat{j}^{(in0)\,\mu}(x),\,\hat{j}^{(in0)}_{\mu_1}(x_1)\right],$$

第１項が非共鳴項であり，VP のみを応答の原因とし，縦・横電場の応答の違い＝電場の概念の破綻の原因である．交換子を含む第２項は時間積分によりエネルギー分母が現れ共鳴条件下で主要となる．川添・大津らの非共鳴条件下の実験は第１項を強調する．特に双極子禁制条件下での量子ドット系 [2][3] やフランク=コンドンの原理による非断熱遷移禁制条件下での光化学反応系 [4] と間接遷移半導体の LED・レーザー系 [5] では共鳴項は 0 となり非共鳴項だけが応答に寄与する．

この非共鳴項の性質を調べるにあたり，電場の概念が破綻する先例としての超伝導体系と対応づけることが有効に思われる．非共鳴項は超伝導の文脈では London の構成方程式であり，反磁性電流を生み Meissner 効果をもたらす．実際，印加される静磁場（クーロンゲージ下での時間に依存しない VP）は BCS 状態からの２電子状態励起（超伝導ギャップ）エネルギーに対して，究極の非共鳴条件をみたし，さらに静磁場の波長は無限大ゆえ，究極の近接場入射条件，近接場観測条件をも満たす．この類似をたよりに反磁性電流と DP の関係を調べていきたい．

参考文献

[1] 坂野　斎，”非放射場と放射場を対等に扱う 単一感受率による光学の理論 V”，応物講演会（2016 春 19a-S622-13）など．

[2] T. Kawazoe, K. Kobayashi, M. Ohtsu, ”Optical nanofountain: A biomimetic device that concentrates optical energy in a nanometric region” Appl. Phys. Lett. **86**, 103102-1–3 (2005).

[3] T. Kawazoe, M. Ohtsu, S. Aso, Y. Sawado, Y. Hosoda, K. Yoshizawa, K. Akahane, N. Yamamoto, M. Naruse, ”Two-dimensional array of room-temperature nanophotonic logic gates using InAs quantum dots in mesa structures” Appl. Phys. B **103**, 537-546 (2011).

[4] T. Kawazoe, Y. Yamamoto, M. Ohtsu, ”Fabrication of a nanometric Zn dot by nonresonant near-field optical chemical-vapor deposition” Appl. Phys. Lett. **79**, 1184-1186 (2001).

[5] １件前のアブスラクトの [1]．及びレビューとして：Ohtsu, M. *Silicon Light-Emitting Diodes and Lasers* (Springer International Publishing, Switsland, 2016).

謝辞

ドレスト光子研究起点 (RODreP) での数理物理的な議論について次の方々に感謝いたします：小嶋泉博士 (RODreP)，佐久間弘文博士 (RODreP)，西郷甲矢人博士 (長浜バイオ大学)，岡村和弥博士 (名古屋大学)，安藤浩志博士 (千葉大学)．この研究の一部は光科学技術研究振興財団からの援助（2018-2019）を受けています．

Timelike と Spacelike な場の合成による停留状態のドレスト光子の数学的表現

A mathematical expression of stationary dressed photon as a composite of timelike and spacelike fields

○佐久間弘文[1]、小嶋泉[1]、大津元一[1]

○Hirofumi Sakuma[1], Izumi Ojima[1], and Motoichi Ohtsu[1]

1:ドレスト光子研究起点

E-mail: sakuma@rodrep.ro.jp

ドレスト光子（DP）を光子と対比した場合の決定的な違いは、前者は①極度に局在化した停留状態として現れ、②それは光と物質場の相互作用の結果生じる“合成”場であるという点にある。また、量子場の基礎理論 [1] によれば、相互作用する場の記述には、4-momentum p_μ の時間的並びに空間的 support の両者が必要である事が示される。上記の二つの特性と量子場理論の帰結として、著者らは、これまで扱われる事の無かった空間的 support に対する具体的表現としての Clebsch dual (CD) [2,3] 場という概念を導入し、通常の電磁場を空間的領域へと拡張し、その特性を調べた。相互作用下にない CD 場それ自体は拡張された電磁場の基本モードとして振る舞う為、相互作用により生じる複雑な場は、その基本モードの重ね合わせに似たもので表現できるであろうと期待される [3]。今回の報告では、問題を簡素化する為に、図 1 に示すような一つのナノ粒子の周りに生じる DP 場を考察の対象として、timelike な場と spacelike な場が局所的に相互作用を行う

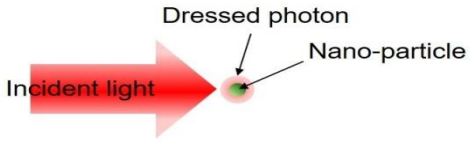

図 1 ：ナノ粒子の周りに生じる DP 場

物理過程の特徴を捉えた“簡易素過程”なるものを Clebsch parametreiztion で表現したものを考えて、それによって DP の特徴が如何にして再現されうるのかという事を示す。DP は通常の光子のような自由場の基本モードとして表現できない為に、その量子論的な記述は未解決な問題として残っているが、今回の発表では、古典場としての Clebsch モデルの表現が、量子化された調和振動子モデルで重要となる生成・消滅演算子を用いた Hamiltonian の表現に如何なる意味において“相似”的な形となり、その中で、基本モードとしての CD 場が重要となる事を説明する。

謝辞：本研究の一部は、（公財）光科学技術研究振興財団の研究助成による。

[1] R.F. Streater, A.S. Wightman, PCT, Spin and Statistics, and All that, Princeton Univ. Press, 2000

[2] H.Sakuma, I. Ojima and M. Ohtsu, Appl. Phys. A (2017) 123:750. https://doi.org/10.1007/s00339-017-1364-9

[3] H. sakuma, I. Ojima, M. Ohtsu, Dressed photons in a new paradigm of off-shell quantum fields. Prog. Quantum Electron. **55**, 74-87 (2017)

量子ウォークモデルを用いた ドレスト光子エネルギー移動シミュレーション

Simulation of Dressed Photon Energy Transfer based on Quantum-Walk Model

㈱リコー[1]，長浜バイオ大[2]，東大院工[3]，ドレスト光子研究起点[4]

○三宮 俊[1]，西郷 甲矢人[2]，大津 元一[3,4]

Ricoh Co. Ltd.[1], Nagahama Inst. Bio-Sci. Tech.[2], Univ. of Tokyo[3], Res. Origin Dressed Photon[4]

○Suguru Sangu[1], Hayato Saigo[2], Motoichi Ohtsu[3,4]

E-mail: suguru.sangu@jp.ricoh.com

近年、ナノスケール領域において生じる特異な光学現象が注目されている。例えば、間接遷移型半導体であるシリコンの発光現象[1]、近接場光エッチングによる原子レベル超平滑化[2]、巨大磁気光学効果の発現[3]などの報告がある。これらの光学現象は従来光学理論において常識的に扱われてきた光と物質のエネルギー保存則、運動量保存則を破る「ドレスト光子」描像、すなわち環境影響により質量をもった仮想光子を仲介した現象として解釈されている。

ドレスト光子の理論構築が数年来進められてきたが[4]、少数粒子のような理想物質と光の相互作用を表現するに留まっており、ミクロ系からマクロ系までを一貫して扱う解析手法の提案が望まれている。このような状況において我々は、量子ウォーク研究[5]とドレスト光子の振る舞い(局在現象)との類似性に注目し、ドレスト光子のエネルギー移動を離散量子ウォークとして記述する試みを行った。本試行はナノフォトニクス研究で多用される Maxwell 方程式に基づく電磁界シミュレーションとは異なり、ドレスト光子の存在を予め仮定した際に現れるダイナミクスから支配方程式を探るアプローチである。

以降では、量子ウォークとしてのモデル化と、数値解析事例について概説する。解析対象はミクロ系とマクロ系が連続的に繋がるプローブープローブ構造とした。Fig.1 に示すように、プローブ構造をドレスト光子が占有する格子点で近似し、格子点間のホッピング伝導によりエネルギー移動を表現した。本モデルでは、外界またはプローブ自身に存在する（自由）光子場とドレスト光子の結合および散逸(すなわちリザーバ) が重要であり、取り扱う系に依存したリザーバを導入する必要がある。本系では、プローブープローブ構造が光の波長に対して十分に小さいという仮定の下、系全体の集団的な励起と光子場が相互作用するとした。Fig. 2 はドレスト光子の格子点位置に対するポピュレーション時間平均値を表わしており、空間を隔てたプローブ構造の先端にドレスト光子の局在が確認できる。(ただし、物理状況把握のため、コヒーレントな励起およびプローブ端からのエネルギー散逸は、本計算では無視している。) 巨視的なモードが散逸する一方で、長寿命（電気双極子禁制）のドレスト光子成分のみがプローブ構造先端に停留すると解釈できる。

講演では、プローブ形状の最適化や従来 Maxwell 方程式による描像との対応についても議論したい。

[1] 川添・他, 光学 43 巻 8 号 (2014) 366.
[2] 八井, OPTRONICS 35(413) (2016) 204.
[3] N. Tate, et.al., Sci. Rep. 5 (2015) 12762.
[4] 例えば、大津, 「ドレスト光子」(朝倉書店, 2013).
[5] 今野,「量子ウォーク」 (森北出版, 2014).

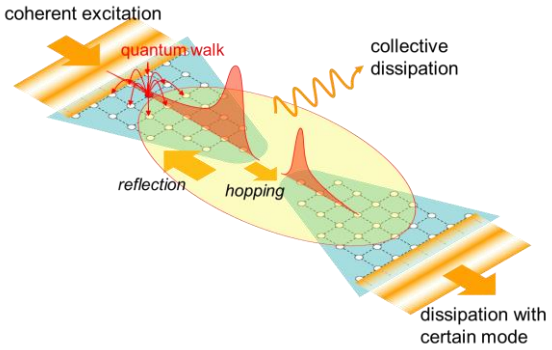

Fig. 1: プローブープローブ構造のモデル

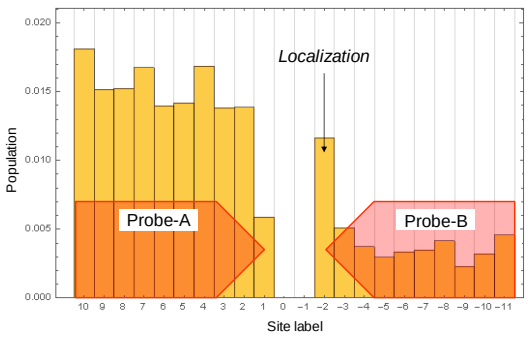

Fig. 2: ポピュレーションの局在現象

シュテファンボルツマン則による Si-LED の注入電流依存性の考察

Consideration of injection current dependence of Si-LED using Stefan-Boltzmann law

電機大 [1], 東大院工 [2], ドレスト光子研究起点 [3], ○川添 忠[1]、大津元一 [3,4]
TDU[1], Univ. of Tokyo[2], Res. Origin Dressed Photon[3], ○T. Kawazoe[1], M.Ohtsu[2,3]
E-mail: kawazoe@mail.dendai.ac.jp

我々は間接遷移型半導体であるシリコン(Si)を用いた LED，レーザーなど発光素子の開発を行っている[1-4]。その発光原理は通常の直接遷移過程半導体を用いた素子とは異なりドレスト光子フォノンと呼ばれる中間状態を経る。

Si-LED は DPP アニールという方法を用いて作製される。この方法では順方向に印加する電流が起こすジュール発熱によるドーパントの拡散促進とそれを抑制する発光（誘導放出）のバランスによって特定のドーパント配列ができる事を利用している。ドーパントは数 nm～数十 nm といった非常に近い距離に隣接するためこの過程によってドーパントの規則的な配置が完成するためには局所的に大きな温度差が生じる必要がある。

Figure1 にアニール途中の Si-pn 接合素子の EL スペクトルを示す。図中の発光スペクトルには大き分けて 2 成分が存在し、極めて注入電流依存性の大きい成分とそうでない成分が混在して見られ、通常の分光計測でこれらを分離観測する事は不可能であった。注入電流依存性の大きい成分は Si のバンド間遷移に起因する成分であり、このシフト量から 400℃以上温度変化があると予想される。一方、注入電流によるシフト量の小さい成分は 50℃以下の温度変化に相当するピークシフトしか示さなかった。これらの違いはまさに局所的な温度(差)が存在することを意味している。

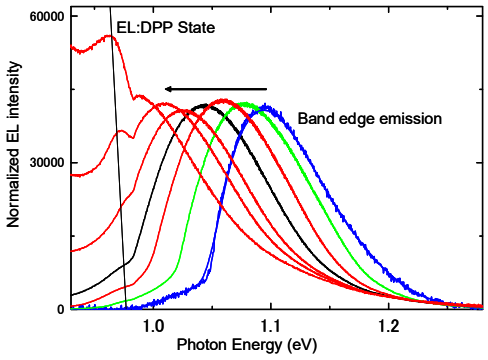

Fig.1

次に DPP アニールされた Si-LED の注入電流依存性を Fig.2,3 示す。閾値後に発光強度は急速に強くなり、その注入電流依存性はほぼ 4 乗に比例する事が分かった(図中破線)。

また、その電流領域での EL 発光スペクトル形状は Fig.3 に示すようにほとんど変わらない。注入電流と素子発熱量はほぼ比例するので素子温度は注入電流に比例すると考えられる。すなわち立ち上がり以後の発光強度は素子温度のおよそ 4 乗に比例すると考えられる。これは黒体放射におけるシュテファンボルツマン則で理解すると分かりやすいが、EL 発光スペクトル形状がほとんど変わっていない。

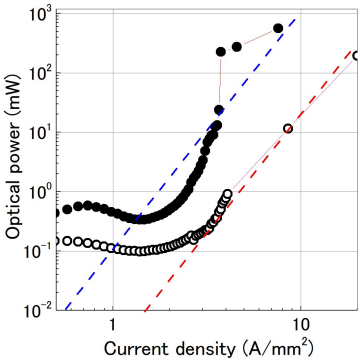

Fig.2

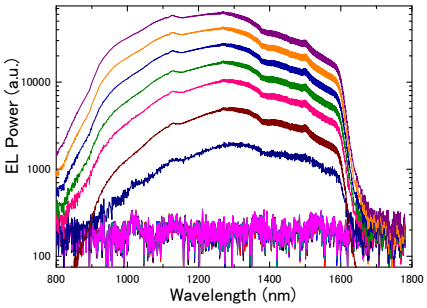

Fig.3

この理由を以下のように考えている。DPP を介した発光においても波数保存則を満たすためのフォノン放射が必要である。そしてフォノン(光子エネルギー<100meV)は赤外線として放射される。この放射率は発光部の局所的な温度決定され、温度の 4 乗すなわち、注入電流の 4 乗に比例する。フォノン放率と電子正孔の対消滅による発光確率は比例するので EL 強度は注入電流の 4 乗に比例する。

発表では上記の過程のより詳細な検討を行う。

[1] T. Kawazoe & M. Ohtsu, Appl. Phys. A, **115**, 127-133, (2014).
[2] T. Kawazoe, et al., Appl. Phys. B-Lasers and Optics, **98**, 5-11 (2010). also **107**, 659-663 (2012).
[3] H. Tanaka, et al., Appl. Phys. B-Lasers and Optics, **108**, 51-56 (2012).
[4] 川添忠、橋本和信、杉浦聡、大津 元一、2017 年第 78 回秋季応用物理学会、福岡 講演番号 7a-A405-5.

ドレスト光子定数の存在可能性とその意味するもの

On the existence of dressed photon constant and its implication

○佐久間弘文[1]、小嶋泉[1]、大津元一[1,2]

○Hirofumi Sakuma[1], Izumi Ojima[1], and Motoichi Ohtsu[1,2]

1:ドレスト光子研究起点、2:東京大学大学院工学系研究科総合研究機構

E-mail: sakuma@rodrep.ro.jp

本発表は、前回（2017 年秋季大会）報告した spacelike Clebsch dual field （SCDF）[1,2,3]による新たなドレスト光子（DP）モデルの構築に関する研究の続報であり、今回の主テーマは、「DP の帰結する物理定数の存在」である。SCDF の基本式は spacelike Klein Gordon (SKG) であるが、超光速「粒子」タキオン解は不安定 [4] である事が知られており、SKG に現れる長さの次元を持つ定数は、timelike な KG に対応する様な局在化した個別粒子の質量に対応するものではなく、ドレスト光子の出現する状況全てに関わる普遍性を有することが期待される。SCDF の基本式から、Clebsch photon は Regge poles として現れる共鳴ハドロンの寄与するポテンシャル項の特性を持ち、その“基底状態”は spacelike な性質より加速膨張を引き起こす宇宙項（反重力）と類似した機能を担うため、この文脈での DP 研究は広い分野に影響を及ぼす可能性がある。今回の報告では、図 1 に示す非共鳴光を光源とし、金属膜非塗布ファイバープローブの先端の DP を用いた光化学気相堆積法によるナノパターン形成実験[5]で得られた DP の半値全幅を「DP 定数」と見てスケール解析を実行すると，宇宙論における宇宙項にオーダー的に近い効果が再現されること、更に，“基底状態”ではない一般の場合の DP dynamics の本質を理解する上で重要な役割を演ずる数理的視点を提示する。

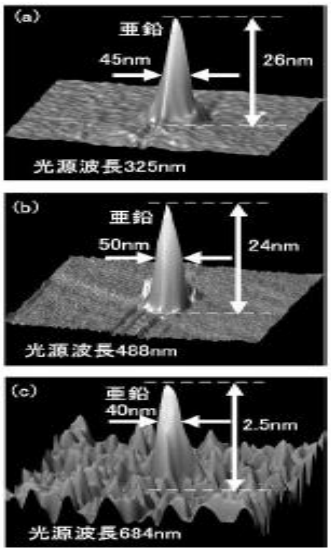

図 1 ：堆積された Zn のナノパターン。光源波長は各々 325nm(a), 488nm(b), 684nm(c)

[1] 佐久間弘文、小嶋泉、大津元一、第 78 回応用物理学会秋季学術講演会(2017 年 9 月、福岡) 7a-A405-10.

[2] H.Sakuma, I. Ojima and M. Ohtus, Appl. Phys. A (2017) 123:750. https://doi.org/10.1007/s00339-017-1364-9

[3] 小嶋泉、量子場とミクロ・マクロ双対性、平成 25 年、丸善出版

[4] Y. Aharonov, A. Komar, and L. Susskind, Phys. Rev. **182**, 1400-1403 (1969)

[5] T. Kawazoe, K. Kobayashi, S. Takubo, and M. Ohtsu, J. Chem. Phys. **122**, 024715 (2005)

Si 発光ダイオードの光出力 1W 動作と電流依存性

Operation with 1W-optical output of Si-LED and current dependence

東電大[1]，東大[2] ○川添 忠[1]，大津元一[2]
TDU[1], University of Tokyo[2] ○Tadashi Kawazoe[1], Motoichi Ohtsu[2]
E-mail: kawazoe@mail.dendai.ac.jp

我々が開発した Si を用いたホモ接合 LED はフォノンを含む準粒子であるドレスト光子の状態を介して発光する[1,2]。これまでの電流注入による発光計測では素子冷却が不十分であったため最大 200mW が限界であった[3,4]。今回、素子の電極を改良し、動作時の素子温度が液体窒素温度まで耐えるように改良を加え光出力パワー>1W を達成する事に成功した。また光出力パワーの注入電流依存性が明瞭な閾値を持ち、閾値以上の電流では光パワーが電流の 4 乗に比例する事が分かったのでその機構について報告する。

Si-LED はアンチモン(Sb)がドープされた基板にボロン(B)をイオン打ち込み法によって注入する事によって得られる。B の打ち込みエネルギーは 700KeV と 10eV である。このようにしてして得られた基板に Cr/Au(30/300nm) のメッシュ電極および Cr/Al/Au(30/200/300nm)のべた電極を作製し 1mm ×1mm の寸法に切り出した。切り出した Si チップを PCB 基板にボンディングして 1 素子とし、室温にて DPP アニーリング(光源:アニール波長 1342nm,パワー 2W，電流:1.3A)を行った[1,2]。

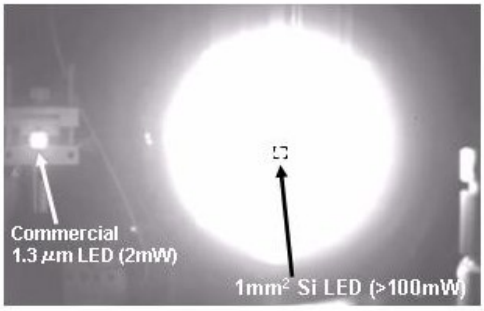

Fig.1

この DPP アニールの工程による Si ダイオードは非常に光出力パワーの大きな LED として機能するようになる。Fig.1 に作製した Si-LED を 100mW 程度で動作させた時の赤外写真を示す。Si-LED の隣には 2mW の市販赤外 LED を最大定格で動作させ比較として撮影してある。

この時の EL スペクトルを Fig.2 に示す。発光スペクトル帯域は 1000nm～2400nm 程度まで広がっているが、DPP アニールして作製した素子は特有の構造を持つ。素子の動作温度は液体窒素温度温度であったため、1342nm のアニール光による発光帯(E_{BG}-3phonon)は温度依存性により短波長側にシフトし 1270nm 付近に現れている。またその整数倍である E_{BG}-6phonon の位置および E_{BG}-9phonon の位置に発光帯が確認された。

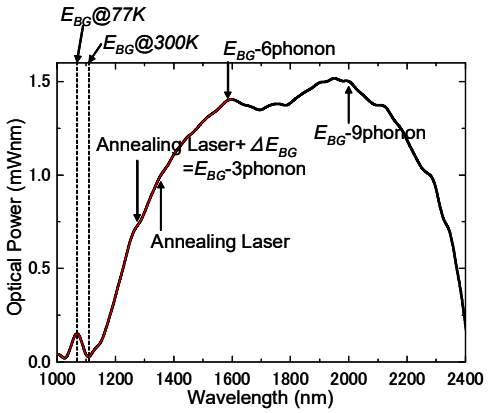

Fig.2

次に異なる温度にて計測した光出力パワーの電流依存性を Fig.3 に示す。素子温度が低いほど明瞭にかつ低電流位置に閾値が現れ、光出力パワーは閾値以下では電流の 2 乗に、閾値以上では電流の 4 乗に比例する結果を得た。電流の 2 乗に比例する領域はオージェ散乱過程の寄与であることを既に報告した[3]。4 乗に比例する領域のはじまる閾値の電流密度は 5.8A/cm^2 であり、同様の基板構造持つ Si レーザー閾値に近い値であった。これは誘導放出過程が関与している事を示すものである。

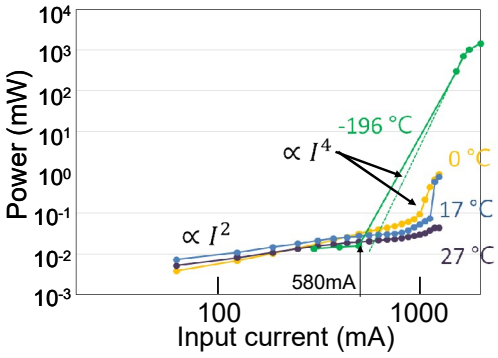

Fig.3

東京大学 B. Thubthimthong 氏には実験面でご協力を頂いたので感謝の意を表します。

[1] M. Ohtsu, Silicon Light-Emitting Diodes and Lasers (Springer, 2016).
[2] T. Kawazoe, M. A. Mueed, and M. Ohtsu. Applied Physics B: Lasers and Optics 104.4 (2011): 747-754.
[3] J. H. Kim, T. Kawazoe, and M. Ohtsu. Applied Physics A, 123.9 (2017): 606.
[4] B. Thubthimthong, T. Kawazoe, and M. Ohtsu, 第 78 回応用物理学会秋季学術講演会(2017，福岡) 7a-405-4.

近接場光学における非共鳴効果の理論 III: 非線形応答理論によるドレスト光子の基礎づけの試み，ゲージ条件の検討

Theory of Non-resonant Effect in Near-filed Optics III: Approach to a Base of Dressed Photon employing Non-linear Response Theory under a Preferable Gauge Condition

○ 坂野　斎[1]，大津元一[2,3]
(1. 山梨大院，2. 東大院工，3. ドレスト光子研究起点)

○I. Banno[1]，M. Ohtsu[2,3]
(1. Univ. of Yamanashi, 2. Univ. of Tokyo, 3. Research Origin of Dressed Photon)
E-mail: banno@yamanashi.ac.jp

川添・大津らは非共鳴条件下での様々な実験 [3,4] によりドレスト光子が原因と目される近接場光学（NFO）特有の現象を発見，実用に供してきた．理論的には多フォノンが関わるモデルで説明され [5]，近頃，光学フォノンが関わる実験的証拠が得られている [6].

ドレスト光子は光の波長程度以下のサイズ (a) の空間での電磁場の一般的存在形態として，詳細なモデルに依らずに理解できる．このような「光」を観測できたら，それには $\hbar/a$ 程度の運動量の不確定さが伴う．この「光」は，真空中の光やバルク物質中の光＝オンシェルの光の分散関係から外れたオフシェルの光＝ドレスト光子であり，その存在は環境との相互作用に支えられている．川添・大津の実験はフォノンを含む環境の自由度と相互作用しているオフシェルの光＝ドレスト光子を積極的に利用するために非共鳴条件を使っていると解釈できる．

本理論は，非共鳴条件下での電子と電磁場環境との相互作用を明らかにしてドレスト光子を第１原理から基礎付けることを目的としている．そのために私たちは光源であるナノ構造近傍の多電子系という NFO 系を記述するのに相応しい線形・非線形応答関数を第１原理から定式化してきた [1]．その応答関数は，NFO 系に共存するスカラー・ベクトルポテンシャル（SP ϕ・VP $\mathbf{A}$）を応答の原因として対等に扱い，結果である誘導電荷・電流密度と関係づける．n 次の非線形応答関数は作用積分の ϕ・$\mathbf{A}$ による $(n+1)$ 階の汎関数微分として Heisenberg 演算子の形式で得られ，電荷保存則とゲージ不変性を保証する．

この方法により非共鳴条件下の NFO 系には，線形・非線形応答関数に $\mathbf{A}$ により強調される寄与があり，誘電率による記述が破綻することを示し，また，前回は非線形感受率演算子の漸化式を検討し，電磁ポテンシャルと感受率演算子を再定義して非共鳴条件に相応しい描像を導いた [2]. この再定義はもともとの SPϕ に，非相対論下でスカラーとなる VP の２乗 $\mathbf{A}^2$ に比例した項が付加する非線形変換である．これにより光学フォノンに伴う電磁場や局所磁場など環境に存在する VP が SP と同じ資格で応答に関われ，NFO 系で顕現するドレスト光子の記述として相応しく思える．この SP・VP の非線形変換では特定のゲージが理論上好ましいものとして選択される可能性があり，本講演ではこの点を議論する．

通常の光学系では ϕ（縦電場）を荷電粒子間のクーロン相互作用に転化して応答の原因として扱わないところ本理論では NFO 系の応答の原因として考慮することにより以上の議論が可能になる．実は NFO は SPϕ を介して多電子問題と不可分である．クーロン相互作用こそは物質の多様な存在形態の原因であり，NFO 系の非共鳴条件下ではその変調により，ドレスト光子＝オフシェルの光が活躍する新しいパラダイムがあると私たちは考えている．

謝辞: 本研究の一部は（公財）光科学技術研究振興財団の研究助成を受けています.

[1] 坂野　斎, ”ナノ構造と非放射場の理論, ”応物講演会 (2013 秋 **17p-D2-2**); ”非放射場と放射場を対等に扱う単一感受率による光学の理論 I ,II, III,IV,V”, 応物講演会 (2013 秋 **18p-C13-1**,2014 春 **17p-F6-5**, 秋 **18p-C1-1**,2015 春 **12a-A12-1**,2016 春 **19a-S622-13**).
[2] 坂野　斎,”近接場光学における非共鳴効果の理論 I,II”応物講演会 (2017 春 **15a-F202-12**, 秋 **7a-A405-9**); I. Banno.,”Response Theory in Near-field Optics: Two Distinct Dipole Transitions”,14th International Conference on Near-field Optics, Nanophotonics, and Related Technics,(浜松市, 2016 **We-10A-5**); 坂野　斎,”近接場光学における 2 種の双極子遷移”, Optics and Photonics Japan 2016(2016 秋 **1PC3**).
[3] 川添 忠, 杉浦聡, 大津 元一, ”高出力ホモ接合シリコンレーザーの作製 (1),(2)”, 応物講演会 (2017 春 **15a-F202-9**, 秋 **7a-A405-5**); T. Kawazoe and M. Ohtsu,”Bulk crystal SiC blue LED with p-n homojunction structure fabricated by dressed-photon-phonon-assisted annealing”, Appl. Phys. A, **115**, 127-133, (2014); M. A. Tran, T. Kawazoe, M. Ohtsu, ”Fabrication of a bulk silicon p-n homojunction-structured light-emitting diode showing visible electroluminescence at room temperature”, Appl Phys A **115**,105-111(2014).
[4] For review articles: M. Ohtsu, ”Progress in Dressed Photon Technology and the Future”, *in Progress in Nanophotonics 4* eds. by M. Ohtsu and T. Yatsui (Springer, 2017) Chap. 1; M. Ohtsu, ”Dressed photon technology”, Nanophotonics **1** 83-97 (2012).
[5] T. Kawazoe, K. Kobayashi, S. Takubo, and M. Ohtsu, ”Nonadiabatic photodissociation process using an optical near field”, J. Chem. Phys. **122**, 024715 (2005); K. Kobayashi, T. Kawazoe, and M. Ohtsu, ”Importance of Multiple-Phonon Interactions in Molecular Dissociation and Nanofabrication Using Optical Near Fields”, IEEE Trans. Nanotech. **4(5)** 517-522 (2005).
[6] T. Kawazoe, K. Nishioka, and M. Ohtsu, ”Polarization control of an infrared silicon light-emitting diode by dressed photons and analyses of the spatial distribution of doped boron atoms”, Appl. Phys. A **121**, 1409-1415 (2015); M. Yamaguchi, T. Kawazoe, and M. Ohtsu, ”Evaluating the coupling strength of electron-hole pairs and phonons in a 0.9 μ m-wavelength silicon light emitting diode using dressed-photon-phonons”, Appl Phys A **115**, 119-125 (2014); N. Wada, M. A. Tran, T. Kawazoe, and Motoichi Ohtsu, ”Measurement of multimode coherent phonons in nanometric spaces in a homojunction-structured silicon light emitting diode”, Appl. Phys. A **115**, 113-118 (2014).

[VII] AWARDS

IAAM
Advancement of Materials to Global Excellence

Certificate

This certifies that

Dr. Motoichi Ohtsu, Research Origin for Dressed Photon, Japan has given Keynote talk presentation entitled *"High-power Silicon Light-emitting Diodes and Lasers by Dressed Photons"* in the **European Advanced Materials Congress** from 20th – 23rd August 2018 at the Conference Centre, M/S Mariella, Stockholm, Sweden.

20th AWARD ASSEMBLY

Dr. Ashutosh Tiwari
Secretary General
International Association of Advanced Materials

www.iaamonline.org

[VIII] APPENDIX

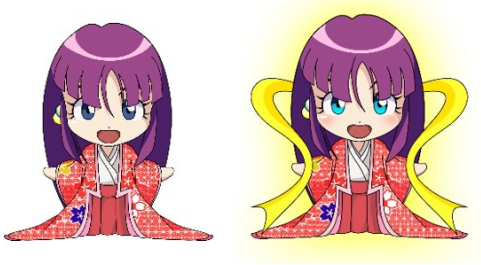

The 18th Workshop "NONCOMMUTATIVE PROBABILITY, OPERATOR ALGEBLA, RANDOM MATRICES AND RELATED TOPICS, WITH APPLICATIONS", July 15-21, Bedlewo, Poland

Micro-Macro duality for Inductions/ Reductions

Izumi OJIMA

Research Origin for Dressed Photon
c/o Nichia Corp., 3-13-19 Moriya-cho, Kanagawa-ku, Yokohama, Kanagawa 221-0022
Japan
Phone:+81-90-1603-0562
E-mail:• u6jic7qh@za.ztv.ne.jp
URL: http://rodrep.or.jp/

Abstract:
Paradoxical appearance of negative metrics in the processes of emergences will be analyzed from the viewpoint of Morse theory, induced representations and of imprimitivity systems.

Micro-Macro Duality for Inductions/ Reductions

Izumi Ojima

Research Origin for Dressed Photon

c/o Nichia Corp., 3-13-19 Moriya-cho, Kanagawa-ku,
Yokohama, Kanagawa 221-0022 Japan

Abstract

Paradoxical appearance of negative metrics in the processes of emergences will be analyzed from the viewpoint of Morse theory, induced representations and of imprimitivity systems.

1 How to control inclusion relations

The essence of the present notes is to discuss the following issues which have been triggered by the requirement for a theoretical framework to treat Dressed Photons:

how to fill the gap between Macroscopic Phenomena & Microscopic Theory,

on the basis of Micro-Macro Duality in Quadrality Scheme,

comined with Saddle-Point Instability,

Through the following examples, Lorentz symmetry/ Regge structure/ Dressed photons/ Coulomb modes/ Tomita-Takesaki modular theory for statistical mechnaics, controlling mechanism will be explained on the basis of induced representations.

Existence of quantum modes with "**indefinite metric**" breaks the consistency of theory at Micro level, as is well known by the difficulties caused by **longitudinal photons**. Therefore, one always tries to avoid longitudinal photons in QED.

However, this is in contradiction to the existence of Coulomb modes in Macro world!!

To understand such contradictory situations, we need first re-examine the concept and phenomena of symmetry breaking.

2 Symmetry Breaking creates Symmetric Space

When symmetry of the system described by a group G is broken up to unbroken subgroup H, a homogeneous space G/H emerges in *sector classifying space*. In this situation, G/H is shown to be a **symmetric space** with many nice properties [Hel], according to the following criterion for *symmetry breaking*.

For this reason, **induced representation** Ind_H^G [Mackey] to describe the broken symmetry G on the sector classifying space G/H as a symmetric space has a strong connection with *automorphic forms* and *zeta functions* playing important roles in number theory.

The mutual relation between the quadrality scheme and the groups to describe symmetries can be depicted as follows:

	Spec= classifying space	$=$	G/H	: Visible Macro
Emergence $\nearrow$	$\uparrow\downarrow$		$\uparrow$	
(Family of) States	$\leftrightarrows$ ***Algebra***	$\curvearrowleft$	G	: Micro-Macro boundaries : t-**ch**
	$\uparrow\downarrow$ $\nearrow$		$\uparrow$	
	Dynamics	$\curvearrowleft$	H	: Invisible Micro: s-**ch**

2.1 Symmetry Breaking

General definition of symmetry breaking [IO03]:

Definition (*Symmetry Breaking*): Let $\mathcal{X}$ be a C*-algebra describing quantum fields with an automorphic action τ:$\mathcal{X} \underset{\tau}{\curvearrowleft} G$ of a Lie group G on $\mathcal{X}$ and $(\pi, \mathfrak{H})$ be a representation of $\mathcal{X}$. If the spectrum $Spec(\mathfrak{Z}_\pi(\mathcal{X}))$ of its center $\mathfrak{Z}_\pi(\mathcal{X}) = \mathfrak{Z}(\pi(\mathcal{X})'')$ is pointwise G-invariant (almost everywhere w.r.t. the central measure), the symmetry (G, τ) on $\mathcal{X}$ is said to be ***unbroken*** in $(\pi, \mathfrak{H})$ and ***broken*** otherwise.

The reason for complicated situations concerning symmetry breaking in QFT is due to such a contrast between quantum systems with *finite* vs. *infinite* degrees of freedom: while the use of a unitary representation U of G leads automatically to the ***unbroken*** symmetry (which is always the case for systems with *finite* degrees of freedom), the very non-existence of U realizable only in those with *infinite* degrees of freedom characterizes the ***broken*** symmetry. This is the reason why we need G-actions both in C*- and W*-versions in the above criterion for symmetry breaking.

2.2 Induced Representation from Unbroken to Broken

To streamline the discussion, we define "***augmented algebra***" [IO03] by a (C*-)crossed product $\mathcal{X} \rtimes \widehat{(H\backslash G)} =: \widehat{\mathcal{X}}$ of $\mathcal{X}$ with the dual $\widehat{(H\backslash G)}$ of (G/H), which allows unitary implementation of broken G at the expense of non-trivial center $\mathfrak{Z}_\pi(\widehat{\mathcal{X}})$ with

$Spec(\mathfrak{Z}_\pi(\widehat{\mathcal{X}})) = G/H$ in the representation of $\widehat{\mathcal{X}}$. Thus the corresponding von Neumann algebra $\pi(\mathcal{X})''$ can be taken as $(\pi \rtimes U_\tau)(\widehat{\mathcal{X}})''$ in the above definition. The existence of a central spectrum as $Spec(\mathfrak{Z}_\pi(\widehat{\mathcal{X}})) = G/H$ suggests relevance of ***induced representations*** and ***imprimitivity*** [Mackey] involving the following ***exact sequences***:

$$\mathrm{Rep}(G/H) \hookrightarrow \mathrm{Rep}(G) \overset{Ind_H^G}{\leftrightarrows} \mathrm{Rep}(H),$$

$$H \underset{(Ind_H^G)^*}{\rightleftarrows} G \twoheadrightarrow G/H.$$

The bigger group G can be viewed as a principal H-bundle over base space $G/H = Spec(\mathfrak{Z}_\pi(\widehat{\mathcal{X}}))$ as sector classifying space, and dual map $(Ind_H^G)^*$ of Ind_H^G (sometimes called "Wigner rotation") plays the role of ***gauge connection***.

2.3 Physical Meaning of Central Spectrum

Note here that the starting point of our present discussion is just a C*-dynamical system $\mathcal{X} \underset{\tau}{\curvearrowleft} G$ given by C*-algebra $\mathcal{X}$ of quantum fields acted upon by a Lie group G of the symmetry of the system. In a sense, however, spacetime background.of the dynamical system $\mathcal{X} \underset{\tau}{\curvearrowleft} G$ without being mentioned at the beginning, has emerged automatically in the form of G/H as a result of the symmetry breaking from G to H. In this sense, the essence of symmetry breaking is crucial and universal for general understanding of the meaning of the above quadrality scheme for Micro-Macro duality.

For this purpose, we remark first such a crucial point that the center of represented algebra $\pi(\widehat{\mathcal{X}})''$ consisting of Macro variables of the system as low energy modes has such a spectrum as $Spec(\mathfrak{Z}_\pi(\widehat{\mathcal{X}})) = G/H$. Its non-trivial motion is driven by the action of G to exhibit the essence of symmetry breaking as the "infrared instability". Arbitrary representations of $\widehat{\mathcal{X}}$ are decomposed into the direct sum of G-*unbroken* factor representations and G-centrally ergodic non-factor representations (the latter ones corresponding to symmetry breaking). according to which a "phase diagram" can be drawn on the central spectrum.

2.4 Symmetry Breaking and Symmetric Spaces

Symmetry Breaking of Lie group G with Lie algebra $\mathfrak{g}$ creates an interesting Micro-Macro interface between Micro level invariant under unbroken Lie subgroup H with Lie algebra $\mathfrak{h}$ and visible Macro level of sector classifying space $M = G/H$.

M: formed in the emergence of condensed order parameters which parametrize the so-called "degenerate vacua" arising from symmetry breaking.

According to the criterion for symmetry breaking, $M = G/H$ becomes a ***symmetric space*** (É. Cartan) [Hel] whose Lie structure $\mathfrak{m} = \mathfrak{g}/\mathfrak{h}$ is characterized locally by the relation $[\mathfrak{m}, \mathfrak{m}] \subset \mathfrak{h}$ [RIMS2014].

Here commutator $[\mathfrak{m},\mathfrak{m}]$ of tangent vectors in M describes **holonomy effect** of the curvature of M in loop motions on M. Since a trajectory forming a loop returns to its starting point on sector classifying space M, net effect of the loop reduces to such components of transformation group as fixing the sector unchanged, being contained in unbroken symmetry corresponding to $\mathfrak{h}$, which can be expressed as Macro loops $[\mathfrak{m},\mathfrak{m}]$ penetrated by Micro arrows in $\mathfrak{h}$.

2.5 Examples of Symmetric Spaces: Chiral symmetry, Lorentz boosts & Second Law of Thermodynamics

1) Typical example of symmetry breaking yielding symmetric space structure can be found in chiral symmetry of current algebra:

$$[V,V]=V,[V,A]=A,[A,A]=V,$$
$$(V\in\mathfrak{h}\text{: vector currents, } A\in\mathfrak{m}\text{: axial currents}).$$

2) For Lorentz group $L_+^{\uparrow}$ as G with rotation group $SO(3)$ as unbroken H, we can find a symmetric space $M=G/H\cong\mathbb{R}^3$ given by the space of all Lorentz frames connected by Lorentz boosts. In fact, relations $[\mathfrak{h},\mathfrak{h}]=\mathfrak{h}$, $[\mathfrak{h},\mathfrak{m}]=\mathfrak{m}$, $[\mathfrak{m},\mathfrak{m}]\subset\mathfrak{h}$ with $\mathfrak{h}:=\{M_{ij};i,j=1,2,3,i<j\}$, $\mathfrak{m}:=\{M_{0i};i=1,2,3\}$ can be extracted from the Lorentz Lie algebra:

$$[iM_{\mu\nu},iM_{\rho_\sigma}]=-(\eta_{\nu\rho}iM_{\mu\sigma}-\eta_{\nu\sigma}iM_{\mu\rho}-\eta_{\mu\rho}iM_{\nu\sigma}+\eta_{\mu\sigma}iM_{\nu\rho}).$$

3) The essence of characterization of symmetric spaces by "Macro loops $[\mathfrak{m},\mathfrak{m}]$ penetrated by Micro arrows in $\mathfrak{h}$" can be exhibited directly in Macro world in the form of ***second law of thermodynamics***. Its mathematical essense can be seen in the following exact sequence[1]

$$\Delta'Q\overset{q}{\hookrightarrow}\Delta E=\Delta'Q+\Delta'W\overset{p}{\twoheadrightarrow}\Delta'W,$$

$$\text{i.e., }\mathrm{Im}(q)=\ker(p),$$

This is the same as the relation $\mathfrak{h}\hookrightarrow\mathfrak{g}\twoheadrightarrow\mathfrak{m}=\mathfrak{g}/\mathfrak{h}$ to characterize Lie structure of homogeneous space $M=G/H$.

The cyclic processes of a heat engine correspond to loops on the thermodynamic phase space M described by thermodynamic variables and holonomy $[\mathfrak{m},\mathfrak{m}]$ associated with such cycles describes the incoming & outgoing heat between the heat engine & the external world in combination with the relations $[\mathfrak{m},\mathfrak{m}]\subset\mathfrak{h}$ and $\Delta E=\Delta'Q+\Delta'W=0$: $-\Delta'W=-[\mathfrak{m},\mathfrak{m}]=\Delta'Q>0$, in which the characterization of M as a symmetric space $[\mathfrak{m},\mathfrak{m}]\subset\mathfrak{h}$ corresponds to the ***second law of thermodynamics*** in ***Kelvin's version!***

[1]Equality $\mathrm{Im}(q)=\ker(p)$ menas that the vanishing energy balance ($\ker(p)$) taken as the visible work is equivalent to the input-output of the heat ($\mathrm{Im}(q)$).

3 Sector Bundle & Holonomy

In the case of symmetry breaking of G up to its unbroken compact subgroup H, the sector structure should be understood in two levels, one with the totality $\widehat{H}$ of irreducible rep.'s of unbroken subgroup H of G, and the other with G/H as the broken part of G. To unify these two levels, it is convenient to introduce the concept of a sector bundle:

$$\widehat{H} \hookrightarrow G \underset{H}{\times} \hat{H} \twoheadrightarrow G/H.$$

In this context we can see the physical origin of space-time concept in its ***physical emergence process*** [IO10].

For simplicity, we assume here that a group G of broken internal symmetry be extended by a group $\mathcal{R}$ of space-time symmetry (typically translations) into a larger group $\Gamma = \mathcal{R} \dot{\times} G$ defined by a semi-direct product of $\mathcal{R}$ & G with $\Gamma/G = \mathcal{R}$.

In this case, the sector bundles have a double fibration structure:

$$\begin{array}{ccccc} \widehat{H} & \hookrightarrow & G \underset{H}{\times} \hat{H} & \hookrightarrow & \Gamma \underset{G}{\times} (G \underset{H}{\times} \hat{H}) = \Gamma \underset{H}{\times} \hat{H} \\ & & \downarrow & & \downarrow \\ & & G/H & & \Gamma/G = \mathcal{R} \end{array} .$$

3.1 Holonomy along Goldstone condensates

Thus, we see that Spec= sector-classifying space has three different axes on different levels:

i) sectors $\widehat{H}$ of ***unbroken*** symmetry H,

ii) degenerate vacua $G/H = M$ due to ***broken internal*** symmetry [IO03, IO04],

iii) $\Gamma/G = \mathcal{R}$ as emergent ***space-time*** [IO10] in broken external symmetry.

These axes appear geometrically as a series of structure group contractions $H \leftarrow G \leftarrow \Gamma$ of principal bundles $P_H \hookrightarrow P_G \hookrightarrow P_\Gamma$ over $\mathcal{R}$, specified by ***solderings*** as bundle sections, $\mathcal{R} \overset{\rho}{\hookrightarrow} P_G/H = P_H \underset{H}{\times} (G/H)$, $\mathcal{R} \overset{\tau}{\hookrightarrow} P_\Gamma/G = P_G \underset{G}{\times} (\Gamma/G) = P_G \underset{G}{\times} \mathcal{R}$, which correspond physically to ***Goldstone modes***.

3.2 Helgason duality with Hecke algebra

We see the duality between ***Helgason duality*** [HRad] $K\backslash G \leftrightarrow G/H$ in $\begin{array}{ccc} & K\backslash G/H & \\ \nearrow & & \nwarrow \\ K\backslash G & \leftrightarrow & G/H \\ \nwarrow & & \nearrow \\ & G & \end{array}$

with Radon transform & ***Hecke algebra*** $K\backslash G/H$

and the algebraic structure of "***augmented algebras***" [IO03] for symmetry breaking as "stereo-graphic" extension of planar diagrams:

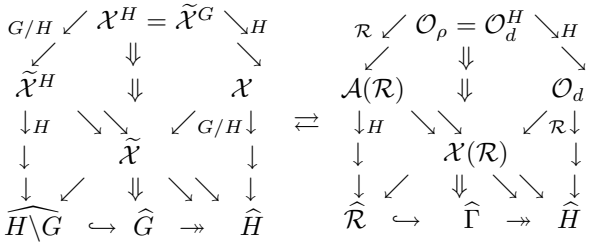

[same kinds of lines constitute exact sequences]

Similar push-out diagram appears also in Doplicher-Roberts reconstruction [DR90] for field algebra $\mathcal{X}(\mathcal{R})$ with unbroken symmetry

3.3 Symmetric space structure = Maxwell-type equation due to symmetry breaking

Symmetric space structures of $G/H = M$ & $\Gamma/G = \mathcal{R}$ arising from symmetry breaking are characterized by the equation $[\mathfrak{m}, \mathfrak{m}] \subset \mathfrak{h}$ to ***connect holonomy*** $[\mathfrak{m}, \mathfrak{m}]$ (in terms of curvature) ***with unbroken generators*** in $\mathfrak{h}$.

It is really interesting to note that ***this feature is shared in common by Maxwell & Einstein equations*** of electromagnetism and of gravity, respectively:

LHS: (curvature $F_{\mu\nu}$ or $R_{\mu\nu}$) = (source current J_μ or $T_{\mu\nu}$) : RHS,

which can be seen by noting that all the quantities $[\mathfrak{m}, \mathfrak{m}]$, $F_{\mu\nu}$ and $R_{\mu\nu}$ on LHS represent holonomy terms and that those on RHS are associated with generators $\mathfrak{h}$ of unbroken subgroups.

In the usual context (related to the 2nd Noether thm), Maxwell equation is understood as an identity following from the gauge invariance of "action integral" under local gauge transformations. In contrast we have *no such classical quantities as action integrals nor Lagrangian densities* defined in our algebraic & categorical formulation of quantum fields.

3.4 Possibility for Dressed Photon equations?

Without such quantities as "action integrals", symmetry breaking criterion with $[\mathfrak{m}, \mathfrak{m}] \subset \mathfrak{h}$ tells us that Maxwell-type equation with curvature term $[\mathfrak{m}, \mathfrak{m}]$ on the left-hand side and the internal symmetry term $\mathfrak{h}$ on the right-hand side is just a consequence of symmetry breaking of local gauge invariance into spacetime and internal symmetries. Putting the Clebsch-dual electromagnetic field $S_{\mu\nu}$ due to Sakuma [SOO] in the place of $[\mathfrak{m}, \mathfrak{m}]$, therefore we can learn that $S_{\mu\nu}$ represents the condensation effect of dressed photons.

3.5 Galois Functor in Doplicher-Roberts reconstruction of symmetry

We recall here how Doplicher & Roberts (DR) [DR90] recovers internal symmetry group from *DR category* $\mathcal{T}$ of local excitations as *group-invariant* data.

Objects of $\mathcal{T}$: local endomorphisms $\rho \in End(\mathcal{A})$ of observable algebra $\mathcal{A}$, selected by DHR localization criterion [DHR] $\pi_0 \circ \rho \restriction_{\mathcal{A}(\mathcal{O}')} \cong \pi_0 \restriction_{\mathcal{A}(\mathcal{O}')}$, and
Morphisms of $\mathcal{T}$: $T \in \mathcal{T}(\rho \to \sigma) \subset \mathcal{A}$ intertwining $\rho, \sigma \in \mathcal{T}$: $T\rho(A) = \sigma(A)T$.

The group H of unbroken internal symmetry arises as the group $H = End_{\otimes}(V)$ of unitary tensorial (=monoidal) natural transformations $u : V \to V$ with the representation functor $V : \mathcal{T} \hookrightarrow Hilb$ to embed $\mathcal{T}$ into the Hilbert-space category $Hilb$ with morphisms as bounded linear maps.

3.6 Galois Functor in Category & local gauge invariance

Recall that a natural transformation $u : V \to V$ is characterized by the commutativity diagrams: $\begin{array}{ccc} V(\rho) & \stackrel{u_\rho}{\to} & V(\rho) \\ V(T)\downarrow & \circlearrowleft & \downarrow V(T) \\ V(\sigma) & \underset{u_\sigma}{\to} & V(\sigma) \end{array}$, namely, $V(T)u_\rho = u_\sigma V(T)$ for $T \in \mathcal{T}(\rho \to \sigma)$.

Our simple proposal here is to define a local gauge transformation $\tau_u(V)$ of functor V by $\tau_u(V)(T) := u_\sigma V(T) u_\rho^{-1}$ corresponding to a natural transformation $u \in H = End_{\otimes}(V)$ [RIMS2013, RIMS2014].

Then, the above equality, $V(T)u_\rho = u_\sigma V(T)$, can be reinterpreted as *local gauge invariance* $\tau_u(V) = V$ of functor V under *local gauge transformation* $V \to \tau_u(V)$ induced by a natural transformation $u \in H = End_{\otimes}(V)$, as has been visualized in the context of lattice gauge theory.

4 *Trinity relation of Saddle point, Indefinte metric & Non-compact group*

For the purpose of theorteical description of dressed photons, crucial step will be to recognize proper dynamic functions in close relation with "tapering" cone structure formed by condensed dressed photons. To implement ideas in this direction, it is important to install the *Clebsch-dual variables* due to Sakuma [SOO] which carry *spacelike momenta* and constitute the characteristic *off-shell structure* of electromagnetic field.

To see the general meaning of off-shell structures, a ***trinity connection*** is to be focused, among ***saddle-point instability***, presence of ***indefinite metric*** (in some Hessians of *Morse functions*) and the action of a ***non-compact group*** on the saddle point.

In wider contexts including thermodynamics, statistical mechanics, gauge theories and induced representations of groups, most important common aspects are the trinity connection between ***saddle points*** & ***indefinite metric***, due to the co-existence of ***stable & unstable*** directions corresponding to compact subgroup H and to ***non-compact*** G/H part of the bigger group G, respectively.

4.1 Saddle points and Morse theory

When this mechanism for determining geometric invariants is applied to sector classifying space, non-trivial relations between quantum Micro dynamics & geometric Macro structure of classifying space can be envisaged and described in terms of ***unstable modes*** and indefinite metric corresponding to saddle point structures. In *Morse theory* contexts [Morse] of deriving homologies and/or cohomologies as geometric invariants, they are determined by negative-metric components of ***Hessians*** defined as the second derivatives of ***Morse functions*** whose dimensionality is called "***Morse index***".

In concrete systematic descriptions of dynamical processes from this viewpoint, the actual meaning of treating "stability" aspects would be restricted to examining which "branches" would satisfy the (conditional) stability and which conditions can support the classifying space *Spec* describing the multi-sector structure serves as the setting up for such discussions.

4.2 Stability vs. instability

Thus it becomes possible for us to envisage the problems of whether stable or unstable naturally in wider perspectives. Moreover, this kind of contexts would require us to pursue such processes as the formation of classifying spaces *Spec* through emergences triggered by the instability at saddle points as the bifurcation points between stability & instability.

Through this kind of changes, big transitions would perhaps be implemented to enable us to be faithful to such natural recognition that ***dynamical motions are absolute and fundamental*** and ***stable states are conditional***.

Are the basic points for this direction hidden in "indefinite metric" which has been disliked so far?: answer to this question is really affirmative when we combine the following points, i) ***indefinite metric at the saddle point***, ii) ***symmetry breaking aspects inherent in Maxwell equation***, and iii) ***spacelike supports of dressed photon momenta described by Clebsch-dual field***.

4.3 Roles Separated into Micro vs. Macro with geometric invariants

Now we consider the problems along the above line.

For this purpose, we consider first 1) induced representation of groups, and 2) guage theories.

1) As is well known,

Lie group G: compact $\Longleftrightarrow$ Killing form θ of its Lie algebra $\mathfrak{g}$ is negative definite,

G: non-compact $\Longleftrightarrow$ Killing form θ of $\mathfrak{g}$ is indefinite

While irreducible representation (σ, W) of maximally compact subgroup H is realized in a (finite-dimensional) positive definite Hilbert space W, the irreducible finite-dimensional representation of ***non-compact semisimple*** G is possible only in a vector space ***with indefinite metric***.

5 Induced representation Ind_H^G

In this situation, the induced representation $Ind_H^G(\sigma)$ [Mackey] of G induced from a representation (σ, W) of H can be realized in an *infinite-dimensional* positive definite Hilbert space $L^2_\sigma(G \to W) = L^2(G) \underset{H}{\otimes} W$ which is defined as the subspace of W-valued functions $\xi : G \longrightarrow W$ on G satisfying the condition of H-equivariance:

$$\xi(gh) = \sigma(h)\xi(g) \quad \text{for } g \in G \quad \text{and } h \in H.$$

According to the equivariance condition, the representation (σ, W) of H is recovered (by the left translation) at the origin $e \in G$:

$$[l_{h^{-1}}\xi](e) = \xi(he) = \xi(eh) = \sigma(h)\xi(e).$$

In this way the appearance of ***indefinite metric*** in the representation space due to non-compactness of G is ***absorbed into*** the ***infinite dimensionality*** of the representation space.

5.1 Micro-unphysical can become Macro-physical

2) In the case of (abelian) gauge theory with a gauge potential A_μ, its Lorentz covariant formulation is possible only in a state vector space with an indefinite metric. In the total space with indefinite metric, we can introduce the concept of a physical subspace $\mathcal{V}_{phys}$ consisting of gauge-invariant physical modes, by imposing such a "subsidiary condition" [KO] as $\Phi \in \mathcal{V}_{phys} \Longleftrightarrow (\partial_\mu A^\mu)^{(+)}\Phi = 0$. In this physical subspace $\mathcal{V}_{phys}$ longitudinal modes causing the difficulties of indefinite metric are shown to be absent, according to which consistency of the probabilistic interpretation is guaranteed within $\mathcal{V}_{phys}$ at the Micro level.

Existence of quantum modes with indefinite metric spoils the consistency of the theory at Micro levels, as is seen in the difficulties caused by longitudinal photons in probabilistic interpretation. For this reason, one tries to exclude longitudinal photons from QED and it is common wisdom that such unphysical modes can be systematically expelled from physical subspace of physical modes selected by imposing a suitable "subsidiary condition".

5.2 Coulomb mode as Micro-unphysical & Macro-physical

As a plain fact in real Macro world, Coulomb modes exist and mediate interactions between electric charges. According to the *standard* "quantum-classical correspondence", mutual relations between Micro & Macro, between quantum & classical, can be understood in such a way that quantum observables non-commutative in Micro scales become mutually commutative classical observables in the "classical limit" with $\hbar \to 0$ and that classical observables can be "quantized" through imposing the canonical commutation relations as a result of which quantum theory equipped with non-commutative quantum observables can be realized.

In non-trivial emergence processes to Macro, however, this simple-minded picture between quantum & classical observables fails to hold by such **paradoxical situations** that some physical variables invisible (or driven away as unphysical modes) at Micro level may become **visible in Macro world**, as is exemplified by longitudinal Coulomb modes. In such cases, how is the fate of risky "indefinite metric"??

5.3 How Induced Representations avoid Indefinite Metric?

In emergence to Macro, indefinite metric in Micro disappears to be substituted by geometric non-triviality. This phenomenon takes place also in the construction of representations of non-compact groups induced from its compact subgroup.

Typical example found in ∞-dimensional unitary rep. of (inhomogeneous) Lorentz group $(\mathbb{R}^4 \rtimes) SL(2,\mathbb{C})$, first established by a physicist E. Wigner in 1939 [Wig39] in use of the method of induced representations. In spite of non-compactness of $SL(2,\mathbb{C})$, we do not encounter infefinite metric in this situation.

Mechanism of induced representations to suppress infefinite metric can be seen in such a form that non-compact group $SL(2,\mathbb{C})$ possibly inducing infefinite metric is treated here as base space $M := G/H = SL(2,\mathbb{C})/SU(2)$ of $SU(2)$-bundle:

$$H := SU(2) \hookrightarrow G = SL(2,\mathbb{C}) \twoheadrightarrow M = SL(2,\mathbb{C})/SU(2).$$

5.4 Alternation between indefinite metric in Micro & geometric non-triviality in Macro

At each point of base space $M = SL(2,\mathbb{C})/SU(2)$ (as a part of sector classifying space), we have a fixed Lorentz frame acted upon by rotation group $SU(2)$ as the structure group of each Lorentz frame and the actions of Lorentz boosts $SL(2,\mathbb{C})$ are just to move from one Lorentz frame to another, which do not exhibit infefinite metric related with $SL(2,\mathbb{C})$ like the case of its matrix representation.

On this geometric setting up, the representation $Ind_{SU(2)}^{SL(2,\mathbb{C})}(\sigma) \in \mathrm{Rep}(SL(2,\mathbb{C}))$ induced from a representation $\sigma \in \mathrm{Rep}(SU(2))$ is defined on the Hilbert space $L^2_\sigma(SL(2,\mathbb{C}) \to W)$ as given above, which is isomorphic to $L^2(M) \otimes W$ in the present situation where the base space $M = SL(2,\mathbb{C})/SU(2)$ is a symmetric space.

5.5 "Wigner rotation" as Dual of Ind_H^G

Owing to the duality,

$$[Ind_H^G(\sigma)](g) = \langle g|Ind_H^G(\sigma)\rangle = \langle (Ind_H^G)^*(g)|\sigma\rangle = \sigma((Ind_H^G)^*(g)),$$

each group element $g \in G$ belonging to non-compact $G = SL(2,\mathbb{C})$ is transferred to $(Ind_H^G)^*(g)$ belonging to compact subgroup $H := SU(2)$:

$$\mathrm{Rep}(SU(2)) \ni \sigma \longmapsto Ind_H^G(\sigma) \in \mathrm{Rep}(SL(2,\mathbb{C})),$$

$$SU(2) \ni (Ind_H^G)^*(g) \leftarrow g \in SL(2,\mathbb{C}).$$

This mapping $(Ind_H^G)^*$ is called (in physics) "Wigner rotation", since each of its image $(Ind_H^G)^*(g) \in SU(2)$ is a rotation.

5.6 "Wigner rotation" as Gauge Connection

According to exact sequence $H \hookrightarrow G \twoheadrightarrow M = G/H$, group G can be interpreted as an H-principal bundle with structure group H over base space $M = G/H$. In this context, the sequences $\mathrm{Rep}(G/H) \hookrightarrow \mathrm{Rep}(G) \twoheadrightarrow \mathrm{Rep}(H)$ and $H \hookrightarrow G \twoheadrightarrow G/H$ are *split* exact sequences, owing to the induced representation $Ind_H^G : \mathrm{Rep}(H) \longrightarrow \mathrm{Rep}(G)$ and to the "Wigner rotation" as its dual $(Ind_H^G)^* : G \ni g \longmapsto (Ind_H^G)^*(g) \in H$, resepectively:

$$\mathrm{Rep}(G/H) \hookrightarrow \mathrm{Rep}(G) \underset{}{\overset{Ind_H^G}{\leftrightarrows}} \mathrm{Rep}(H),$$

$$H \underset{(Ind_H^G)^*}{\rightleftarrows} G \twoheadrightarrow G/H.$$

I.e. vector bundle $\mathrm{Rep}(G)$ on base space $\mathrm{Rep}(H)$ with standard fiber $\mathrm{Rep}(G/H)$ has Ind_H^G as a horizontal lift.
Principal H-bundle G over G/H has a H-valued connection given by $(Ind_H^G)^*$.

$\Longrightarrow$ Induced representation gives a basis for structural analogy with gauge theory, in terms of gauge connection $(Ind_H^G)^*$ as a splitting of exact sequence.

5.7 No Problem for Macro Coulomb Mode

In the case of 2) with the Coulomb mode, we need not worry about the appearance of indefinite metric because the longitudinal Coulomb mode of classical gauge fields is already described in terms of the commutative variables. Instead, what can be non-trivial now is the possibility for condensed modes of particles due to Coulomb attractive force, according to which such non-trivial effects as superconductivity phenomena can be realized.

6 Spacelike momenta shared by statistical mechanics, Regge poles, dressed photons & Coulomb force

After the case studies of 1) induced representations and 2) gauge theories with Coulomb mode, what to be analyzed for the purpose of understanding common features among various composite systems with inclusion relations can be found as follows:

3) statistical mechanics and thermodynamics
4) Regge trajectories appearing in hadron scattering processes,
5) mechanism of dressed photons.

Because of the big difference in the appearance among these five cases, however, it may be unclear where we can find any coherent common features. Just skipping the detailed account along individual specific features, the common essence shared by all these cases can be found in the existence of the following three levels as well as their mutual relationship:

6.1 Exact Sequence consisting of Broken/ Unbroken Symmetry groups

a) a compact Lie group H to describe inivisible Micro dynamics associated with some flows,

b) the level of "*horizontal duality*" formed by the algebra $\mathcal{X}$ of observables to visualize H and the state space $E_{\mathcal{X}}(\subset \mathcal{X}^*)$ of $\mathcal{X}$ which is controlled by a Lie group G containing H as a subgroup, and,

c) the sector classifying space $Spec(\supset G/H)$ emerging from the states $E_{\mathcal{X}}$ of $\mathcal{X}$,

What is most important is such a situation that the group $G(\supset H)$ controlling the level b) of "*horizontal duality*" is a non-compact Lie group with a Killing form with indefinite signature, arising from the extention of the group H of Micro dynamics, characterized by the exact sequences:

$$H \hookrightarrow G \twoheadrightarrow G/H,$$

$$\mathrm{Rep}(G/H) \hookrightarrow \mathrm{Rep}(G) \twoheadrightarrow \mathrm{Rep}(H).$$

6.2 Examples of Broken/ Unbroken Sequences

For instance, in the case of dressed photons, the region with ***spacelike momenta*** is created by introducing the ***Clebsch-dual variables*** and in the case of Regge trajectory in hadron physics, the t and ***u-channels*** formed via the duality transformations $s \rightleftarrows t$ & $s \rightleftarrows u$ interchanging s, t & ***u-channels*** provide the stages of ***Regge trajectories*** consisting of the series of ***Regge poles with complex angular momenta.*** While well-known Gibbs formula $\langle A \rangle = Tr(Ae^{-\beta H})/Tr(e^{-\beta H})$ in statistical mechanics shows no remarkable structural features, it can be applied only to small finite systems with

discrete energy spectrum, In contrast, ***Tomita-Takesaki modular theory*** required for the treatment of general systems with infinite degrees of freedom is equipped with such a double structure as consisting of the von Neumann algebra $\mathcal{M}$ of physical variables in the system and its modular dual $\mathcal{M}' = J\mathcal{M}J$ whose composite system $\mathcal{M} \vee J\mathcal{M}J$ is controlled by the Hamiltonian $H_\beta = -JH_\beta J$ with "indefinite metric", whose physical interpretation can be reduced to the concept of heat bath.

6.3 Induced Representations & Automorphic Forms

The induced representation $Ind_H^G(\sigma)$ of the Lorentz group $G = SL(2,\mathbb{C})$ determined by a unitary representation σ of the rotation group $H = SU(2)$ in a finite-dimensional vector space W is given in an infinite-dimensional Hilbert space V defined by

$$V := \{\varphi : G \longrightarrow W; \varphi(gh) = \sigma(h^{-1})\varphi(g) \text{ for } g \in G, h \in H\}$$

according to the defining equation $[Ind_H^G(\sigma)(g)\varphi](g_1) := \varphi(g^{-1}g_1)$, which reproduces $\sigma(h)$ for $h \in H$ at $g = e \in G$:

$$[Ind_H^G(\sigma)(h)\varphi](e) = \sigma(h)[\varphi(e)].$$

6.4 Automorphic Forms arising from Induced Representation

By means of the horizontal lift $G/H \longrightarrow G$ of $G/H = SL(2,\mathbb{C})/SU(2)$ associated with the "Wigner rotation" $(Ind_H^G)^*$, the domain of $Ind_H^G(\sigma)$ can be shifted from G to G/H. Therefore, if we express the elements $g \in G$ in the form of fractional linear transformation, the above definition of V can be rewritten with as

$$V = \{\varphi : G/H \to W; \varphi(gz) = \sigma(cz+d)^{-1}\varphi(\frac{az+b}{cz+d}),$$

$$g = \begin{matrix} a & b \\ c & d \end{matrix} \in G, z \in G/H\},$$

which shows that the module V consists of automorphic forms φ. Since automorphic forms are transformed into ζ functions by Mellin transform, the pair (G, H) with G/H a symmetric space is related to the number-theoretical contexts.

6.5 Fractional Linear Transformaions

While the use of *fractional linear transformation:* $gz := \frac{az+b}{cz+d}$ for $g = \begin{matrix} a & b \\ c & d \end{matrix} \in G$ may look accidental owing to the (2×2)-matricial form of $SL(2,\mathbb{C})$, this is not the case because this speciality can be easily lost by such identification of the Lorentz group as $G \simeq SO(1,3) \hookrightarrow M(4,\mathbb{R})$. Actually, what is essential is not such a special form of matrices but the decomposition of representation vector space $\mathfrak{V}$ of G into unbroken $\mathfrak{V}_1$

and broken subspaces $\mathfrak{V}_2$, $\mathfrak{V} = \mathfrak{V}_1 \oplus \mathfrak{V}_2$, according to which G has such a decomposition as $\begin{array}{c} \\ \mathfrak{V}_1 \\ \mathfrak{V}_2 \end{array} \begin{array}{cc} \mathfrak{V}_1 & \mathfrak{V}_2 \\ A & B \\ C & D \end{array}$ in a certain neighbourhood of the identity element of G.

6.6 Flag manifold as Generalization of Fractional Linearity

Moreover, if we want to extend the above bipolar contrast between unbroken vs broken into some scale-dependent multi-polar gradations of symmetry breakings along many steps, we can consider such a flag manifold structure as related with a multi-component decomposition $\mathfrak{V} = \mathfrak{V}_1 \oplus \mathfrak{V}_2 \oplus \cdots \oplus \mathfrak{V}_r$ of the representation space $\mathfrak{V}$:

$$\begin{aligned} G &= U(p_1 + p_2 + \cdots \ + p_r) \\ &\curvearrowright G/H = U(p_1 + p_2 + \cdots \ + p_r)/[U(p_1) \times U(p_2) \times \cdots \ \times U(p_r)], \end{aligned}$$

which may be related with the continued fractions. In this context, we can see the intrinsic relation between fractional linearity and Grassmann manifold in the case of $r = 2$.

7 "Indefinite Metric" inherent in Modular Structure of Thermal Equilibrium

Here we want to touch on a blind spot in the "common sense" in physics which can interpret the "stability" of a state only in such a restricted form as the poisitivity of the energy in the form of spectral condition.

While, in inifinite system with the operator $e^{-\beta H}$ out of trace class, it is impossible to separate sharply the physical system and its heat bath, the mutual relation between them can be mathematically understood [HHW, BR] by the relation:

$$H_\beta = -JH_\beta J. \tag{1}$$

If the component H of H_β acting on the system $\mathcal{X}_\omega$ can safely be extracted and be separated from that on the commutant $\mathcal{X}'_\omega$, then the essential contents of this equation could be seen in such a form as

$$H_\beta = H - JHJ,$$

7.1 Negative Metric in Modular Theory and Heat Bath

In infinite systems, however, meaning of the above H is only formal. Apart from this subtlety, the above formal equation explains that anti-unitary operator J interchanges the system & its heat bath. Since total system consisting of the system & heat bath has Hamiltonian H_β whose spectrum is positive/ negative symmetric as in (1), negative

energy component may be interpreted as energy going from the system to the heat bath. Interestingly enough, concept of "heat bath" which is mysterious but important in thermodynamics has once been expelled by Gibbs formula $\langle A\rangle = Tr(Ae^{-\beta H})/Tr(e^{-\beta H})$ (applicable only for the system with *discrete spectrum*), but, has survived.in the abstract form in algebraic general formulation of statistical mechanics based upon the Kubo-Martin-Schwinger condition [KMS, HHW, BR]:

$$\omega_\beta(AB(t)) = \omega_\beta(B(t - i\beta)A),$$

which is free from such a restriction of discrete energy spectrum.

Similarly to longitudinal photons with "***negagive metric***" Hamiltonian H_β of the total system contains negative component (formally $-JHJ$), which means the **existence of a saddle point instability** associated with thermal equilibrium states. Without unstable modes and their condensations, existence of Macro heat bath may have been impossible.

8 Frobenius Reciprocity

Two opposite directions are involved in induced representations, to expand $\sigma \in Rep_H$ of smaller H into that $Ind_H^G(\sigma) \in Rep_G$ of bigger G, and to identify a given $\gamma \in Rep_G$ of G as $\gamma = Ind_H^G(\sigma)$ induced from $\sigma \in Rep_H$ of H. This latter process is controlled by the **imprimitivity**. Mutual relation between two processes is controlled by **Frobenius reciprocity**:

$$Rep_H(\gamma \restriction_H \longrightarrow \sigma) \leftrightarrows Rep_G(\gamma \longrightarrow Ind_H^G(\sigma))$$

or

$$Rep_G(Ind_H^G(\sigma) \longrightarrow \gamma) \leftrightarrows Rep_H(\sigma \longrightarrow \gamma \restriction_H),$$

where $Rep_G(\gamma_1 \longrightarrow \gamma_2)$ means the set of intertwiners $T : \gamma_1 \longrightarrow \gamma_2$ from γ_1 to γ_2 satisfying the intertwining relation $\forall g \in G\ T\gamma_1(g) = \gamma_2(g)T$, namely,

$$T \in Rep_G(\gamma_1 \longrightarrow \gamma_2) \Longleftrightarrow \forall g \in G : T\gamma_1(g) = \gamma_2(g)T$$

$$\begin{array}{ccc} V_{\gamma_1} & \stackrel{T}{\longrightarrow} & V_{\gamma_2} \\ \gamma_1(g)\downarrow & \circlearrowleft & \downarrow\gamma_2(g) \\ V_{\gamma_1} & \underset{T}{\longrightarrow} & V_{\gamma_2} \end{array}$$

9 Towards Theory of Dressed Photons

In order to construct a consistent theory for describing dressed photons, it will become a crucial breakthrough to reproduce faithfully its proper dynamic functions by grasping properly the "tapering" cone structure formed by the condensed dressed photons. To

implement the ideas in this direction, it is important to install the ***Clebsch-dual electromagnetic field*** [SOO] discovered by Sakuma carrying spacelike momenta which constitute the characteristic off-shell structure of electromagnetic field. which forms the Micro-Macro boundary level described by a symmetric space $G/H = Spec$ arising from a broken symmetry by visualizing the s-channel strictire at the invisible Micro level into spacelike t-channel.

Acknowledgment

In July the author presented a talk based on these notes at Bedlewo in Poland. The trip to go there was supported financially by RODreP (Resarch Origin for Dressed Photon). The author would like to express his sincere thanks to Prof. M. Ohtsu for these financial supports.

A Brief Summary of Micro-Macro Duality in Quadrality Scheme

Integrating [dynamical aspects of the system in question] with [geometric description of the relevant structure in terms of invariants generated by dynamical processes which implement classification of the processes and structures]

$\Longrightarrow$ category-theoretical framework of "Micro-Macro duality+quadrality scheme" ([IO03]; I.O., "Quantum Fields and Micro-Macro Duality" [IO13] [2013, in Japanese] and also see [IOOk13]) by incorporating categorically natural *duality between dynamical processes & classifying spaces*.

By analyzing closely in this framework dynamical processes and classifying scheme based on geometric invariants generated by the former processes, we can understand that both of invisible Micro domain corresponding to dynamical processes and of visible Macro structure to the classifying structure in terms of geometric invariants constitute duality structure, to be called "***Micro-Macro duality***" [IO06].

A.1 Quadrality Scheme

Duality between on-shell $\leftrightarrows$ off-shell means that on-shell corresponds to the particle-like Macro and the off-shell to the existence of quantum fields in virtual invisible modes.

Micro processes of motions can be described by a group(oid) structure acting on the algebras of physical quantities, Macro classifying structure emerging from dynamical processes can be extracted from the structure of state space as the dual of algebra of physical quantities and a geometric space emerges consisting of classifying indices extracted from states which functions as the dual of the Micro dynamical system. Putting altogether these four ingredients of dynamics, algebras, states and classifying space, they constitute a "***quadrality scheme***" describing "***Micro-Macro duality***" [IO06]:

$\nearrow$	***Classifying Space*** ***= Spec***	
(***Family of***) ***States***	$\leftrightarrows$ $\uparrow$ (***Representations***) $\downarrow$ $\leftrightarrows$	***Algebra***
	Dynamics	$\nearrow$

.

A.2 Emergence of sector classifying space

In this mathematical framework for describing emergence process, crucial roles are played by the concept of a "sector".

What is a ***sector***: for the mathematical description of a quantum system, we need a ***non-commutative*** (***C****-)***algebra*** $\mathcal{X}$ (: ***Algebra***) of physical variables to characterize the system and a certain family of ***states*** $\omega \in E_{\mathcal{X}}$ to quantify measured values $\omega(A)$ of physical variables $A \in \mathcal{X}$. According to GNS theorem [BR], a representation $(\pi_\omega, \mathfrak{H}_\omega, \Omega_\omega)$ (called GNS representation) of $\mathcal{X}$ is so constructed from ω that physical variables $A \in \mathcal{X}$ are represented as linear operators $\pi_\omega(A)$ acting on a Hilbert space $\mathfrak{H}_\omega$, the totality of which determines a very important concept of representation von Neumann algebra $\pi_\omega(\mathcal{X})'' =: \mathcal{X}_\omega$. Elements $C \in \mathfrak{Z}_\omega(\mathcal{X})$ of the center $\mathfrak{Z}_\omega(\mathcal{X})$ of $\mathcal{X}_\omega$ defined by

$$\mathfrak{Z}_\omega(\mathcal{X}) := \pi_\omega(\mathcal{X})'' \cap \pi_\omega(\mathcal{X})' = \mathcal{X}_\omega \cap \mathcal{X}'_\omega,$$

are commuting with all elements X in $\mathcal{X}_\omega$: $[C, X] = 0$ for $\forall X \in \mathcal{X}_\omega$
and play the role of "order parameters" as commutative Macro observables.

A.3 Sectors = Factor States

Commutativity of center allows simultaneous diagonalization of $\mathfrak{Z}_\omega(\mathcal{X})$ yields spectral decomposition of a commutative algebra $\mathfrak{Z}_\omega(\mathcal{X}) = L^\infty(Spec)$ with spectrum of $\mathfrak{Z}_\omega(\mathcal{X})$ denoted by $Spec := Sp(\mathfrak{Z}_\omega(\mathcal{X}))$. The diagonalized situation with all the order parameters specified corresponds physically to a ***pure phase***, or mathematically corresponding to a quasi-equvalence class of a ***factor state*** γ with a trivial cener: $\mathfrak{Z}_\gamma(\mathcal{X}) = \mathcal{X}_\gamma{}'' \cap \mathcal{X}_\gamma{}' = \mathbb{C}1$ which is called a ***sector***. Here ***quasi-equvalence*** [Dix] means ***unitary equivalence up to multiplicity*** and a factor state corresponds to a minimal unit of states or representations in the sense that its center cannot be decomposed any more.

A.4 Sectors and Disjointness

To understand properly the concept of sectors, it is crucial to note the following points about the mutual relations between different sectors. Namely, the relation betwen two ***different sectors*** π_1, π_2 is expressed by the concept of disjointness as follows:

$$T\pi_1(A) = \pi_2(A)T \quad (\forall A \in \mathcal{X}) \quad \Longrightarrow \quad T = 0,$$

which is stronger than unitary inequivalence and has deep implications as seen later. Macro quantities characterized by their commutativity appear as the center $\mathfrak{Z}_\omega(\mathcal{X})$ of a mixed phase algebra $\pi_\omega(\mathcal{X})'' = \mathcal{X}_\omega$ containing many different sectors as pure phases, and its spectrum $Spec = Sp(\mathfrak{Z}_\omega(\mathcal{X}))$ as realized values $\chi \in Spec$ of order parameters $C \in \mathfrak{Z}_\omega(\mathcal{X})$ discriminates the pure phases contained in the mixed phase state ω, The sectors as pure phases play the roles as the Mico-Macro boundary between quantum Micro system & classical Macro system as the environment, and they unify, at the same time, both these into a Micro-Macro composite system as a mixed phase.

A.5 Relations among Sectors

According to this story, the duality between intra-sectorial domains vs. inter-sectorial relations holds as follows:

$\longleftarrow$ ***Visible***	***Macro*** consisting of ***sectors***		$\longrightarrow$	***inter-sectorial*** relations
$\cdots \quad \gamma_N$	***sectors*** γ	γ_2	γ_1	$Spec$
$\vdots$	$\vdots$	$\vdots$	$\vdots$	$\uparrow$ ***intra-sectorial***
$\cdots \pi_{\gamma_N}$ $\vdots$	π_γ $\vdots$	π_{γ_2} $\vdots$	π_{γ_1} $\vdots$	$\parallel$
$\vdots$	$\vdots$	$\vdots$	$\vdots$	$\downarrow$ ***invisible Micro***

The concept of sectors defined in this way as Micro-Macro boundaries between invisible Micro & visible Macro realizes the theoretical framework of quadrality scheme which provides the precise formulation of "quantum-classical correspondence".

A.6 Disjointness vs. Quasi-equivalence

Along this line, we clarify the homotopical basis of Tomita theorem of central decomposition of states and representations [BR].

In the C*-category $Rep_\mathcal{X}$ of representations of a C*-algebra $\mathcal{X}$, there exists the *universal representation* $\pi_u = (\pi_u, \mathfrak{H}_u) \in Rep_\mathcal{X}$ containing $\forall \pi = (\pi, \mathfrak{H}_\pi) \in Rep_\mathcal{X}$ as its subrepresentation: $\pi_u \succeq \pi = (\pi, \mathfrak{H}_\pi) \in Rep_\mathcal{X}$.

Such π_u can be concretely realized as the direct sum $(\pi_u, \mathfrak{H}_u) := \underset{\omega \in E_\mathcal{X}}{\oplus} (\pi_\omega, \mathfrak{H}_\omega)$ of all the GNS representations, with the action of universal enveloping von Neumann algebra

$$\mathcal{X}'' \cong \mathcal{X}^{**} \cong \pi_u(\mathcal{X})'' \curvearrowright \mathfrak{H}_u.$$

For a representation $\pi \in Rep_\mathcal{X}$ its "disjoint complement" $\pi^{\overset{|}{\circ}}$ is defined [IO04a] as maximal representation disjoint from π:

$$\pi^{\overset{|}{\circ}} := \sup\{\rho \in Rep_\mathcal{X}; \rho \overset{|}{\circ} \pi\},$$

where $\rho \overset{\cdot}{\circ} \pi \Longleftrightarrow Rep_{\mathcal{X}}(\rho \to \pi) = \{0\}$: i.e., no non-zero intertwiners.

A.7 Disjoint Complements & Quasi-equivalence

Then, we observe the following four points, i) – v) [IO04a]:

i) $P(\pi^{\overset{\cdot}{\circ}}) = c(\pi)^{\perp}$,
$P(\pi^{\overset{\cdot}{\circ}\overset{\cdot}{\circ}}) = c(\pi)^{\perp\perp} = c(\pi) := \underset{u \in \mathcal{U}(\pi(\mathcal{X})')}{\vee} u P_{\pi} u^* \in \mathcal{P}(\mathfrak{Z}(W^*(\mathcal{X})))$,
where $P(\pi) \in W^*(\mathcal{X})'$ is defined as the projection corresponding to $(\pi, \mathfrak{H}_{\pi})$ in $\mathfrak{H}_u$ and $c(\pi)$ is the central support of $P(\pi)$ defined by the minimal central projection majorizing $P(\pi)$ in the center $\mathfrak{Z}(W^*(\mathcal{X})) := W^*(\mathcal{X}) \cap W^*(\mathcal{X})'$ of $W^*(\mathcal{X})$.

ii) $\pi_1^{\overset{\cdot}{\circ}\overset{\cdot}{\circ}} = \pi_2^{\overset{\cdot}{\circ}\overset{\cdot}{\circ}} \Longleftrightarrow \pi_1 \approx \pi_2$ (: quasi-equivalence= unitary equivalence up to multiplicity $\Longleftrightarrow \pi_1(\mathcal{X})'' \simeq \pi_2(\mathcal{X})'' \Longleftrightarrow c(\pi_1) = c(\pi_2) \Longleftrightarrow W^*(\pi_1)_* = W^*(\pi_2)_*$)

A.8 Quasi-equivalence & Modular Structure

iii) Representation $(\pi^{\overset{\cdot}{\circ}\overset{\cdot}{\circ}}, c(\pi)\mathfrak{H}_u)$ of the von Neumann algebra $W^*(\pi) \simeq \pi^{\overset{\cdot}{\circ}\overset{\cdot}{\circ}}(\mathcal{X})''$ in $c(\pi)\mathfrak{H}_u = P(\pi^{\overset{\cdot}{\circ}\overset{\cdot}{\circ}})\mathfrak{H}_u$ gives the ***standard form*** of $W^*(\pi)$ equipped with a normal faithful semifinite weight φ and the associated Tomita-Takesaki modular structure $(J_{\varphi}, \Delta_{\varphi})$ [BR], whose universality is characterized by the adjunction,

$$Std(\pi^{\overset{\cdot}{\circ}\overset{\cdot}{\circ}} \to \sigma) \simeq Rep_{\mathcal{X}}(\pi \to \sigma).$$

Namely, any intertwiner $T \in Rep_{\mathcal{X}}(\pi \to \sigma)$ to a standard form representation $(\sigma, \mathfrak{H}_{\sigma})$ of $W^*(\sigma)$ is uniquely factored $T = T^{\overset{\cdot}{\circ}\overset{\cdot}{\circ}} \circ \eta_{\pi}$ through the canonical homotopy $\eta_{\pi} \in Rep_{\mathcal{X}}(\pi \to \pi^{\overset{\cdot}{\circ}\overset{\cdot}{\circ}})$ with $\exists! T^{\overset{\cdot}{\circ}\overset{\cdot}{\circ}} \in Rep_{\mathcal{X}}(\pi^{\overset{\cdot}{\circ}\overset{\cdot}{\circ}} \to \sigma)$.

A.9 Symmetry and Fixed-point subalgebra

Let a physical system be described by the algebra $\mathcal{X}$ of its physical variables. Under action $\alpha = (\alpha_g)_{g \in G}$ of a Lie group G via automorphisms α_g on $\mathcal{X}$, the observable algebra $\mathcal{A}$ is defined as G-invariant subalgebra of $\mathcal{X}$ by

$$\mathcal{A} = \mathcal{X}^G := \{A; \alpha_g(A) = A \text{ for } \forall g \in G\}.$$

Under suitable assumptions, an exact sequence

$$\mathcal{A} \hookrightarrow \mathcal{X} \twoheadrightarrow \mathcal{X}/\mathcal{A} \cong \widehat{G}$$

arises in this situation, from which total algebra $\mathcal{X}$ can be recovered from the observable algebra $\mathcal{A}$ [DR89, DR90] by means of the crossed product of $\widehat{G}$ in the context of the categorical adjunction:

$$\mathcal{A} = \mathcal{X}^G \leftrightarrows \mathcal{X} = \mathcal{A} \lhd \widehat{G}.$$

When we combine the inclusion relation of groups controlled by the exact sequence $H \hookrightarrow G \twoheadrightarrow G/H$ with the group actions on the algebras of physical variables, we encounter the situation of symmetry breakings which involves the mutual relations among various subalgebras $\mathcal{X}^G \hookrightarrow \mathcal{X}^H \hookrightarrow \mathcal{X}$.

B Group & Representations in Categorical Context

In view of the definition for a group representation $\gamma \in Rep_G$ given by the group homomorphism properties $\gamma(g_1 g_2) = \gamma(g_1)\gamma(g_2), \gamma(e) = id_{V_\gamma}$, $\gamma(g^{-1}) = \gamma(g)^{-1}$, a G-representation γ can be viewed as a ***functor*** from the group G as a one-object category $G = \mathcal{C}_G$ consisting of an object $*$ and of group elements $g \in G$ as morphisms $* \xrightarrow{g} * \in G = Mor(\mathcal{C}_G))$ to another category $Hom(V_\gamma)$ consisting of continuous linear operators in the Hilbert space V_γ. From this categorical viewpoint, the intertwiner $T \in Rep_G(\gamma_1 \longrightarrow \gamma_2)$ from γ_1 to γ_2 is to be interpreted as a ***natural transformation*** from a functor γ_1 to another one γ_2 characterized by the commutativity diagram. In this way, the totality Rep_G of G-representations can be viewed as a category $Hilb^G$ of functors from the group G as a category $\mathcal{C}_G = G$ to the category $Hilb$ of Hilbert spaces with morphisms given by G-intertwiners as natural transformatrions. In this context, the group induction Ind_H^G from the functor category Rep_H of H-representations to that Rep_G of G-representations can be viewed as a natural transformation $Ind_H^G : Rep_H \longrightarrow Rep_G$ (preserving the tensor product structures of Rep_H and Rep_G: $Ind_H^G(\sigma_1 \otimes \sigma_2) = Ind_H^G(\sigma_1) \otimes Ind_H^G(\sigma_2)$ for $\sigma_1, \sigma_2 \in Rep_H$).

B.1 Kan Extensions as Categorical Inductions

Given a funcor $K : \mathcal{B} \to \mathcal{A}$ from a category $\mathcal{B}$ to $\mathcal{A}$ we consider the problem of extending a given functor $S : \mathcal{B} \to \mathcal{M}$ from $\mathcal{B}$ to $\mathcal{M}$ into one $T : \mathcal{A} \to \mathcal{M}$ from $\mathcal{A}$ to $\mathcal{M}$ so as to satisfy the relation $T \circ K = S$:

$$\begin{array}{ccc} & T? & \\ \mathcal{A} & \dashrightarrow & \mathcal{M} \\ K \uparrow & \circlearrowleft \nearrow S & \\ \mathcal{B} & & \end{array} \quad .$$

In this situation, the functor T is called a Kan extension [MacL] of functor S along functor K.

B.2 From Kan Extension to Induced Representation

For instance, if we identify $K : \mathcal{B} \to \mathcal{A}$ as the inclusion $\iota : H \hookrightarrow G$ of a subgroup H into the total group G and $S : \mathcal{B} \to \mathcal{M}$ as a representation $\sigma : H \to \mathcal{M} = Hilb$ of H with

$Hilb$ identified with the category of Hilbert spaces, then $T : \mathcal{A} \to \mathcal{M}$ corresponds to an extension of H-representation σ to G-representation γ:

$$\begin{array}{ccc} & \gamma? & \\ G & \dashrightarrow & \mathcal{M} \\ \iota\uparrow & \circlearrowleft \nearrow \sigma & \\ H & & \end{array} ,$$

since the commutativity $\sigma = \gamma \circ \iota$ of the diagram means $\sigma = \gamma \restriction_H$. In this sense, the Kan extension can be viewed as a categorical version of the induced representations of groups.

B.3 Kan Extension and Yoneda Lemma

In view of the important roles played by natural transformations in mediating adjoint functors, we need to distinguish between the right & left Kan extensions as follows:

$$Nat_{\mathcal{M}^{\mathcal{B}}}(T \circ K \longrightarrow S) \leftrightarrows Nat_{\mathcal{M}^{\mathcal{A}}}(T \longrightarrow Ran_K(S))$$

$$Nat_{\mathcal{M}^{\mathcal{A}}}(Lan_K(S) \longrightarrow T) \leftrightarrows Nat_{\mathcal{M}^{\mathcal{B}}}(S \longrightarrow T \circ K)$$

The concept of *Yoneda embedding* [MacL]:

$$\mathbf{y}_c(-) = \mathcal{C}((-) \longrightarrow c) \in Sets^{\mathcal{C}^{op}} : \mathcal{C} \ni d \longmapsto \mathcal{C}(c \longleftarrow d) \in Sets$$

gives an embedding of a category $\mathcal{C}$ into the category $Sets^{\mathcal{C}^{op}}$ of pre-sheaves on $\mathcal{C}$ (as a categorical generalization of the concept of functions), and hence, it would be quite useful to consider the Kan extensions $Ran_{\mathbf{y}_c}$ or $Lan_{\mathbf{y}_c}$ along $K = \mathbf{y}_c$. However, systematic investigation on this topic should be done on the next occasions.

References

[1] Helgason, S., *Differential Geometry, Lie Groups, and symmetric spaces.* Academic Press New York, 1978.

[2] Mackey, G.W., *Induced Representations of Groups and Quantum Mechanics,* W.A.Benjamin, Inc., 1968.

[3] Ojima, I., A unified scheme for generalized sectors based on selection criteria – Order parameters of symmetries and of thermal situations and physical meanings of classifying categorical adjunctions–, Open Sys. Info. Dyn. **10**, 235-279 (2003).

[4] Ojima, I., Dynamical relativity in family of dynamics, RIMS Kôkyûroku **1921**, 73-83 (2014); Local gauge invariance and Maxwell equation in categorical QFT, RIMS Kôkyûroku **1961**, 81-92 (2015).

[5] Ojima, I., Local Gauge Invariance, Maxwell Equation and Symmetry, talk at NWW2015; Algebraic QFT and local gauge invariance, RIMS Kôkyûroku **2010**, 78-88 (2016).

[6] Ojima, I., Space(-time) emergence as symmetry breaking effect, Quantum Bio-Informatics IV, 279 - 289 (2011) (arXiv:math-ph/1102.0838 (2011)); Micro-Macro Duality and space-time emergence, Proc. Intern. Conf. "Advances in Quantum Theory", 197 – 206 (2011).

[7] Ojima, I., Temperature as order parameter of broken scale invariance, Publ. RIMS (Kyoto Univ.) **40**, 731-756 (2004) (math-ph0311025).

[8] Helgason, S., *The Radon Transform*, Birkhäuser, 1980.

[9] Doplicher, S. and Roberts, J.E., Endomorphism of C*-algebras, cross products and duality for compact groups, Ann. Math. **130**, 75-119 (1989); A new duality theory for compact groups, Inventiones Math. **98**, 157-218 (1989).

[10] Doplicher, S. and Roberts, J.E., Why there is a field algebra with a compact gauge group describing the superselection structure in particle physics, Comm. Math. Phys. **131**, 51-107 (1990).

[11] Milnor, J., *Morse theory*, Princeton Univ. Press (1963).

[12] Doplicher, S., Haag, R. and Roberts, J. E., Fields, observables and gauge transformations I & II, Comm. Math. Phys. **13**, 1-23 (1969); **15,** 173-200 (1969); Local observables and particle statistics, I & II, **23**, 199-230 (1971) & **35**, 49-85 (1974).

[13] Kugo. T. and Ojima, I., *Local Covariant Operator Formalism of Non-Abelian Gauge Theories and Quark Confinement Problem,* Suppl. Prog. Theor. Phys. No. 66 (1979); Nakanishi, N. and Ojima, I., *Covariant Operator Formalism of Gauge Theories and Quantum Gravity*, World Scientific Lecture Notes in Physics Vol.27, World Scientific Publishing Company, Singapore-New Jersey-London-Hong Kong (1990).

[14] Wigner, E. P., On unitary representations of the inhomogeneous Lorentz group, Ann. Math. **40**, 149–204 (1939).

[15] Haag, R., Hugenholtz, N.M. & Winnink, M., On the equilibrium states in quantum statistical mechanics, Comm. Math. Phys. **5**, 215-236 (1967).

[16] Bratteli, O. & Robinson, D.W., *Operator Algebras and Quantum Statistical Mechanics*, Vols.1 & 2, Springer-Verlag (1979, 1981).

[17] Kubo, R., J. Phys. Soc. Japan **12**, 570-586 (1957); Martin, P.C. & Schwinger, J., Theory of many particle systems I, Phys. Rev. **115**, 1342-1373 (1959).

Theory of Single Susceptibility for Near-field Optics Equally Associated with Scalar and Vector Potentials

Itsuki Banno*

Interdisciplinary Graduate School of Medicine and Engineering,

University of Yamanashi, 4-3-11 Takeda,

Kofu, Yamanashi 400-8511, Japan

(Dated: September 28, 2018)

Abstract

A nonlocal response theory was developed to describe a many-electron system within the neighborhood of a nanostructure radiating the longitudinal and transverse electric fields, which are fundamentally reduced to the scalar and vector potentials (SP and VP). The coexistence of the SP and VP incidences distinguishes such a near-field optical system from the ordinary optical system, in which only the VP (under the Coulomb gauge) incidence survives far from the light source. This fact is the motivation for equal treatment of the SP and VP as the cause of the response in the near-field optical system. In the semiclassical treatment, the linear and nonlinear single susceptibilities are derived in the form of Heisenberg operators by the functional derivatives of the action integral of the matter with respect to the SP and VP. These single susceptibilities relate the SP and VP (as the cause) to the induced charge and current densities (as the result), and guarantee charge conservation and gauge invariance; this theory is free from gauge-fixing. It is necessary to consider the quantum many-electron effect (exchange-correlation effect) to make the ground state bounded in the non-perturbed system. This is done by employing the fundamental idea of density functional theory, instead of the ordinary unequal treatment of the SP and VP, that is, remaking the SP into a Coulomb interaction between electron charges. Applying the present linear response theory to the non-metallic material in a limited near-field optical system reveals that the electric field with the associated permittivity is not suitable quantity to describe the response, instead, the SP and VP with associate single susceptibility are essential.

PACS numbers: 78.67.-n, 78.20.Bh, 41.20.-q, 42.25.Ja

Keywords: single susceptibility, non-resonant effect, optical near field, response function, electromagnetic potential

*Electronic address: banno@yamanashi.ac.jp

I. INTRODUCTION

This paper develops a nonlocal response theory adequate for near-field optics (NFO) in the semiclassical treatment. The linear and nonlinear single susceptibilities are derived systematically by the functional derivatives of the action integral of the matter with respect to the scalar and vector potentials (SP and VP). These linear and nonlinear single susceptibilities relate the SP and VP (as the cause) to the induced charge and current densities (as the result), and guarantee charge conservation and gauge invariance. The present single susceptibilities and associated induced charge and current densities are given in the form of Heisenberg operators.

In Ref.[1], the present author discussed the linear single susceptibility, its application to an one-electron optical system, and a naive idea of employing the density functional theory. This paper is its generalization including systematic derivation of linear and nonlinear single susceptibilities in the form of Heisenberg operator, a simple proof of charge conservation and gauge invariance guaranteed by such the susceptibilities, and application to a many-electron system with detailed discussion on the density functional theory.

The introduction below contains the followings: §I A reveals the necessity of the single susceptibility, instead of the electric permittivity and magnetic permeability. §I B points out the preference to equal treatment of the SP and VP as the cause of response in NFO, instead of the unequal treatment in ordinary optics under the Coulomb gauge. §I C explains the difficulty of constructing the response theory in NFO, which inevitably connected to a many-electron problem via the SP. §I D represents the purpose of this paper .

A. The necessity of the single susceptibility

As the cause of response, it is natural and essential to use the SP and VP, which represent for the electromagnetic (EM) field in the Hamiltonian for quantum electrodynamics. Three reasons are given below for the *inapplicability of the electric and magnetic fields* as the cause of response. First, there exist such systems that cannot be described in terms of the electric and/or magnetic fields, namely, the superconductor system with the Meissner effect[2] and the coherent electron system with the Aharanov-Bohm effect[3]. A limited NF optical system is another example, as shown in the one-electron system in Ref.[1] (and will be shown in a

many-electron system in §VI of this paper).

Second, the constitutive equations with the electric permittivity and magnetic permeability give relationships between redundant degrees of freedom. Actually, the essential source of the EM field is the three components of charge density and the transverse current density. The longitudinal current density is excluded because it can be determined through charge conservation law, once the charge density is known. However, the polarization and magnetization as the source of the EM field have totally six components, which include the redundancy. So that the associated constitutive equations using the two susceptibilities include the constraint condition for the redundancy, of which the physical meaning is not declared. This situation is physically unreasonable and should be fixed by the constitutive equation using a single susceptibility associated with the proper degrees of freedom.

Third, as first claimed by Cho[4, 5] for the low-symmetry systems with chirality (such as the NF optical system with a skewed nanostructure), the ordinary two constitutive equations are not available because the electric and magnetic responses become indistinguishable. He also revealed that this error cannot be fixed by the Drude-Born-Fedorov fomulas[6], which extends the two constitutive equations adding the cross terms of the electric-field-induced magnetization and the magnetic-field-induced polarization.

Therefore, from a general view point, it is essential to employ a single susceptibility with the SP and VP, instead of the electric permittivity and magnetic permeability with the electric and magnetic fields.

B. The preference to equal treatment of the SP and VP in a NF optical system

Suppose a small-scale material is placed in the vicinity of a nanostructure, which functions as a light source (FIG.1). In such a system, under the NF incidence condition, the target material is exposed to the longitudinal and transverse electric fields simultaneously, whereas in a system under the far-field incidence condition, the target material is exposed only to the transverse field, which survives far from the light source. Therefore, the coexistence of longitudinal and transverse electric fields distinguishes such a system under the NF incidence condition from that under the far-field incidence condition.

Here, the longitudinal electric field originates from the charge density on the nanostructure, obeys Coulomb's law, and has a non-radiative nature to localize around the nanos-

tructure. On the other hand, the transverse electric field originates from the transverse current density on the nanostructure, obeys Ampere-Maxwell law and Faraday's law, and has a radiative nature allowing it to propagate far from the light source, accompanied by the magnetic field. (The longitudinal current density is determined via the charge conservation law, once the charge density is known, and is not an independent source.) Therefore, the two incidences coexisting in an NF optical system have distinct properties.

Furthermore, owing to *the non-relativistic nature* of the system, the SP and VP appear in a different manner in the Hamiltonian, (for example, Eq.(30) in §IV,) which governs the electron response. Considering that the SP and VP under the Coulomb gauge represent the longitudinal and transverse electric fields, respectively, one may confirm that the two types of incidences in NFO cause different responses ; see §VI for an explicite demonstration.

Therefore, it is reasonable to treat SP and VP equally as the cause of response in the NF optical system. Up to now, there has been no such theoretical framework for equally treating the SP and VP. The reason for this lies in the the many-electron problem inevitably related to NFO via the SP (the longitudinal electric field), as is mentioned in the next subsection.

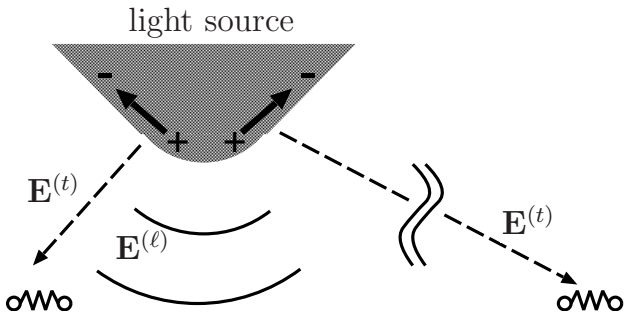

FIG. 1: Optical systems under near- and far-field incidences (the left and right side figures, respectively) . The former system is exposed simultaneously to the incident longitudinal and transverse electric fields (fundamentally represented by the scalar and vector potentials, respectively, under the Coulomb gauge), whereas the latter system is exposed to only the transverse field (the vector potential under the Coulomb gauge).

C. A many-electron problem inevitably related with NFO

The relationship between NFO and many-electron problem has not been well recognized, although the problem of how to consider the Coulomb interaction in response function has remained for a long time[7]. In the usual Hamiltonian for a many-electron system under the Coulomb gauge, the SP is rewritten as the interaction between the electron charge density operators, and only the VP is considered as the cause of the response. This unequal treatment of the SP and VP is needed to consider the quantum many-electron effect (the so-called exchange-correlation effect) to construct the ground and excited states as the proper bound states in a many-electron system. This usual procedure to treat the non-relativistic many-electron system is compatible with ordinary optics, where the electron system of interest is far from the light source, and the SP incidence is negligible. By contrast, in an NF optical system, the usual approach results in a difficulty of understanding the response to the SP incidence, because both the SP incidence (radiated by the nanostructure) and the inherent SP (originating from the particle charge) are built into the two-body Coulomb interaction, and the two contributions are indistinguishable. To make matters worse, the Coulomb interaction in itself is so difficult to treat that it is often ignored, without considering it includes the effect of the SP incidence.

For the NF optical system, there are two existing approaches based on certain single susceptibilities (the nonlocal response functions). Cho formulated a single susceptibility that relates the transverse VP (as the cause) to the current density (as the result), and applied it to various optical systems[8]. Additionally, a modification that considers the longitudinal electric field incidence in NF optical systems has been proposed in Chap. 5 of Ref.[5]. Keller formulated the linear single susceptibility, which relates the transverse electric field and the incident part of the longitudinal electric field (as the cause) to the current density (as the result) [9].

In the above two existing formulations, the SP under the Coulomb gauge (or the longitudinal electric field), except the linear-dependence of the incidence, is rewritten as the two-body Coulomb interaction in the usual manner. Therefore, the response to the SP, in principle, can be rigorously considered via the Coulomb interaction if the many-electron problem is properly solved, whereas the response to the VP incidence under the Coulomb gauge (or the transverse electric field incidence) is treated in the perturbative manner. In

this type of approach, it is essential to solve the many-electron problem, in particular, for the nonlinear process related with the SP. Even if the Coulomb interaction is properly considered, the unequal treatment may make it difficult to regulate the perturbation order of the responses and to understand the role of the SP incidence.

As a result, the response theory in NFO is inevitably relates to the many-electron problem, which causes difficulty.

D. The purpose of this paper

§I A-§I C lead to the logical fallacy to use the ordinary two susceptibilities with the electric and magnetic fields, and the preference to use the single susceptibility equally associated with the SP and VP, considering properly the many-electron effect in NF optical systems, although the ordinary two susceptibilities have been widely used both in ordinary optics and NFO. To best understand the fundamental physics in NFO, it is essential to develop an adequate response theory. For this purpose, the present paper defines and characterizes a single susceptibility equally associated with the SP and VP based on the action integral from scratch.

The contents of this paper are as follows: §II defines the linear and nonlinear single susceptibilities equally associated with the SP and VP, starting from the action integral. §III shows that the present susceptibility respects both charge conservation and gauge invariance in a general manner. §IV derives the linear and nonlinear single susceptibilities in the form of the Heisenberg operators. §V shows that the many-electron effect in the present response theory may be supported by the density functional theory to prepare the non-perturbed ground state as well as a complete set of many-electron states. §VI applies the present linear response theory to a simplified many-electron system, and show that the electric field with the associated permittivity is not suitable to describe the response of a limited NF optical system with a non-metallic material, so that the SP and VP with the single susceptibility is essential. §VII provides a summary of this work. Two appendices are included: §A and §B provides calculation details of §II and §VI, respectively.

II. DEFINITION OF NEW SINGLE SUSCEPTIBILITY

Based on the Lagrangian formulation of non-relativistic quantum electrodynamics, we define the single susceptibility, which relates the SP and VP (as the cause) to the induced charge and current densities (as the result). Furthermore, it is shown that this susceptibility guarantees that charge conservation and gauge invariance hold; see the next section. The action integral for non-relativistic quantum electrodynamics is:

$$\mathcal{I}[\hat{\psi}^\dagger_\alpha, \hat{\psi}_\alpha, \phi, \mathbf{A}] \equiv \mathcal{I}_{\rm mat}[\hat{\psi}^\dagger_\alpha, \hat{\psi}_\alpha, \phi, \mathbf{A}] + \mathcal{I}_{\rm EM}[\phi, \mathbf{A}], \tag{1}$$

$$\begin{aligned}\mathcal{I}_{\rm mat}[\hat{\psi}^\dagger_\alpha, \hat{\psi}_\alpha, \phi, \mathbf{A}] \equiv \frac{1}{c}\int {\rm d}^4x \, \Big\{ & \hat{\psi}^\dagger_\alpha(x)(i\hbar\partial_t - q\phi(x))\hat{\psi}_\alpha(x) \\ & - \frac{1}{2m}\left(\frac{\hbar}{-i}\partial_i - qA_i(x)\right)\hat{\psi}^\dagger_\alpha(x)\cdot\left(\frac{\hbar}{i}\partial_i - qA_i(x)\right)\hat{\psi}_\alpha(x) \\ & - \phi(x)\rho^{\rm (EXT)}(x) + A_i(x)j^{\rm (EXT)}_i(x) - \hat{\psi}^\dagger_\alpha(x)v^{\rm (AUX)}(x)\hat{\psi}_\alpha(x)\Big\}\end{aligned} \tag{2}$$

$$\begin{aligned}\mathcal{I}_{\rm EM}[\phi, \mathbf{A}] \equiv \frac{1}{c}\int {\rm d}^4x \, \Big\{ & \frac{\epsilon_0}{2}\left(\partial_t A_i(x) + \partial_i\phi(x)\right)\left(\partial_t A_i(x) + \partial_i\phi(x)\right) \\ & - \frac{\epsilon_0 c^2}{2}\epsilon_{ijk}\partial_j A_k(x)\epsilon_{ilm}\partial_l A_m(x)\Big\},\end{aligned} \tag{3}$$

where m and $q(=-e)$ are the electron mass and charge, c is the speed of light, $\phi, \mathbf{A}$ are the SP and VP, which are assumed to be classical field in the semiclassical treatment, $\hat{\psi}^\dagger_\alpha, \hat{\psi}_\alpha$ are the electron field operators with the spin state α (one of the two spin states; so called "up" and "down" states), and $\rho^{\rm (EXT)}, \mathbf{j}^{\rm (EXT)}$ are the nuclear charge and the current densities, respectively, which possibly generate inherent EM field. A static auxiliary potential $v^{\rm (AUX)}(x)$ is null for now, but is introduced here for the discussion in §V concerning the density functional theory to consider the quantum many-electron effect (the exchange-correlation effect), ϵ_{ijk} is an antisymmetric tensor, and the Einstein rule is used for indices of vector and Grassmann fields, that is, summation should be executed over repeated indices. At this first stage of investigation, the interaction between spin polarization and the EM field is ignored. The soundness of the above action integral is confirmed by its Euler equations, which will soon be derived.

The electron field operators are considered as quantized Grassmann fields. The Grassmann field satisfies $[\hat{\psi}_\alpha(\mathbf{r}, t), \hat{\psi}^\dagger_\beta(\mathbf{r}', t')]_+ = 0$ [10], and corresponds to the "classical" field of the electron. These operators become the creation and annihilation operators of the electron in quantum theory (the quantized Grassmann fields), introducing the anti-commutation

relationship: $[\hat{\psi}_\alpha(\mathbf{r},t),\hat{\psi}^\dagger_\beta(\mathbf{r}',t)]_+ = \delta^3(\mathbf{r}-\mathbf{r}')\delta_{\alpha\beta}$.

The action integral is composed of two parts: one is the action integral of the matter (including the interaction between the matter and EM field), $\mathcal{I}_{\rm mat}[\hat{\psi}^\dagger_\alpha,\hat{\psi}_\alpha,\phi,\mathbf{A}]$, and the other is the action integral of the EM field, $\mathcal{I}_{\rm EM}[\phi,\mathbf{A}]$. Applying the extremal (optimizing) conditions with respect to $\hat{\psi}_\alpha(x)\,,\hat{\psi}^\dagger_\alpha(x)$ leads to Heisenberg's equation, and optimizing with respect to $\phi(x)$, $\mathbf{A}(x)$ leads to Maxwell's wave equations:

$$\begin{aligned}
0 &= c\,\delta\hat{\psi}^\dagger_\alpha(x)\backslash\delta\mathcal{I} = c\,\delta\hat{\psi}^\dagger_\alpha(x)\backslash\delta\mathcal{I}_{\rm mat} \\
&= \left(i\hbar\partial_t - q\phi(x) - \frac{1}{2m}\left(\frac{\hbar}{i}\partial_i - qA_i(x)\right)\cdot\left(\frac{\hbar}{i}\partial_i - qA_i(x)\right) - v^{(\rm AUX)}(x)\right)\hat{\psi}_\alpha(x), \qquad (4)\\
0 &= c\,\delta\mathcal{I}/\delta\hat{\psi}_\alpha(x) = c\,\delta\mathcal{I}_{\rm mat}/\delta\hat{\psi}_\alpha(x) \\
&= \left(-i\hbar\partial_t - q\phi(x) - \frac{1}{2m}\left(\frac{\hbar}{-i}\partial_i - qA_i(x)\right)\cdot\left(\frac{\hbar}{-i}\partial_i - qA_i(x)\right) - v^{(\rm AUX)}(x)\right)\hat{\psi}^\dagger_\alpha(x), \qquad (5)\\
0 &= c\,\frac{\delta\mathcal{I}}{\delta A_i(x)} = \epsilon_0 c^2\left(-\epsilon_{ijk}\partial_j\epsilon_{klm}\partial_l A_m(x) - \frac{1}{c^2}\partial_t^2 A_i(x) - \frac{1}{c^2}\partial_t\partial_i\phi(x) + \frac{1}{\epsilon_0 c^2}(\hat{j}_i(x) + j_i^{(\rm EXT)}(x))\right), \qquad (6)\\
0 &= c\,\frac{\delta\mathcal{I}}{\delta\phi(x)} = \epsilon_0\left(-\partial_i\partial_i\phi(x) - \partial_t\partial_i A_i(x) - \frac{1}{\epsilon_0}(\hat{\rho}(x) + \rho^{(\rm EXT)}(x))\right). \qquad (7)
\end{aligned}$$

In Eqs.(4) and (5), the left- and right-hand functional derivatives with respect to the Grassmann field are executed, respectively. In Eqs.(6) and (7), the following definitions are introduced for the electron charge and current densities, respectively:

$$\begin{aligned}
\hat{\rho}(x) &\equiv -c\frac{\delta}{\delta\phi(x)}\mathcal{I}_{\rm mat} = q\hat{\psi}^\dagger_\alpha(x)\hat{\psi}_\alpha(x), \qquad (8)\\
\hat{j}_i(x) &\equiv +c\frac{\delta}{\delta A_i(x)}\mathcal{I}_{\rm mat} = \frac{q}{2m}\hat{\psi}^\dagger_\alpha(x)\left(\frac{\hbar}{i}\partial_i - qA_i(x)\right)\hat{\psi}_\alpha(x) + \text{h.c.}\,. \qquad (9)
\end{aligned}$$

The charge conservation law below holds, and is checked through explicit calculation:

$$\partial_t\hat{\rho}(x) + \partial_i\hat{j}_i(x) = 0. \qquad (10)$$

In the four-element representation, Eqs.(6) and (7) become:

$$\begin{aligned}
&(\delta^\mu{}_\nu\Box - \partial^\mu\partial_\nu)\,A^\nu(x) = \frac{1}{\epsilon_0 c}(\hat{j}^\mu(x) + j^{(\rm EXT)\mu}(x)), \qquad (11)\\
&\text{where}\quad \hat{j}^\mu = (c\hat{\rho},\hat{\mathbf{j}}),\ \hat{j}_\mu = (c\hat{\rho},-\hat{\mathbf{j}}),\\
&\qquad A^\mu = (\phi,c\mathbf{A}),\ A_\mu = (\phi,-c\mathbf{A}),\\
&\qquad \partial^\mu = (1/c\,\partial_t,-\nabla),\ \partial_\mu = (1/c\,\partial_t,\nabla),\\
&\qquad \Box = \partial^\mu\partial_\mu = 1/c^2\,\partial_t^2 - \Delta\ \text{, etc.} \qquad (12)
\end{aligned}$$

Although Lorentz invariance is not maintained in the non-relativistic theory, we use the four-element notation to simply represent charge conservation and gauge invariance. For example, Eqs.(8)-(10) become:

$$\hat{j}^{\mu}(x) = -c^2 \frac{\delta}{\delta A_{\mu}(x)} \mathcal{I}_{\rm mat}, \tag{13}$$

$$\partial_{\mu}\, \hat{j}^{\mu}(x) = 0. \tag{14}$$

The action integral, Eq.(1) is invariant under the following gauge transformation:

$$\begin{aligned} A^{\mu}(x) \;&\rightarrow\; A^{\mu}(x) - c\,\partial^{\mu}\eta(x), \\ \hat{\psi}_{\alpha}(x) \;&\rightarrow\; e^{\frac{i}{\hbar}q\eta(x)}\hat{\psi}_{\alpha}(x), \quad \hat{\psi}^{\dagger}_{\alpha}(x) \rightarrow \hat{\psi}^{\dagger}_{\alpha}(x) e^{\frac{-i}{\hbar}q\eta(x)}\,, \end{aligned} \tag{15}$$

where $\eta(x)$ is the gauge function. From the point of view of Noether's theorem[11], the gauge invariance of the action integral is the cause of the charge conservation law, Eq.(10) or Eq.(14).

Let us separate the EM field into two parts:

$$A^{\mu}(x) = A^{(0)\mu}(x) + \Delta A^{\mu}(x), \tag{16}$$

where $A^{(0)\mu}$ is the static, non-perturbative EM potential satisfying Eqs.(6) and (7), and $\Delta A^{\mu}(x)$ is the perturbative EM potential. Under this variation of the EM field, let us re-optimize the action integral of the matter, $\mathcal{I}_{\rm mat}[\hat{\psi}^{\dagger}_{\alpha}, \hat{\psi}_{\alpha}, A^{\mu}]$. That is, we re-optimize the electron field operator satisfying Eqs.(4) and (5) under $A^{(0)\mu} + \Delta A^{\mu}(x)$. In the above procedure, the variation of the action integral of the matter is expressed by the total functional derivative with respect to $A^{\mu}(x)$:

$$\begin{aligned} & \frac{\delta}{\delta A_{\mu}(x)} \mathcal{I}_{\rm mat}[\hat{\psi}^{\dagger}_{\alpha}[A^{\nu}]\,, \hat{\psi}_{\alpha}[A^{\nu}]\,, A^{\nu}]\Big|_{A^{\nu}=A^{(0)\nu}} \\ = \; & \left[\frac{\delta}{\delta A_{\mu}(x)}\Big|_{\rm explicit} \mathcal{I}_{\rm mat} + \int {\rm d}^4x' \frac{\delta \hat{\psi}^{\dagger}_{\alpha}(x')}{\delta A_{\mu}(x)} \delta\hat{\psi}^{\dagger}_{\alpha}(x') \backslash \delta \mathcal{I}_{\rm mat} \right. \\ & \qquad \left. + \int {\rm d}^4x'\, \delta\mathcal{I}_{\rm mat}/\delta\hat{\psi}_{\alpha}(x') \frac{\delta\hat{\psi}_{\alpha}(x')}{\delta A_{\mu}(x)} \right]_{A^{\nu}=A^{(0)\nu}} \\ = \; & \frac{-1}{c^2}\hat{j}^{\mu}(x; [A^{(0)\nu}])\,, \end{aligned} \tag{17}$$

where the first term in the second expression is the variation explicitly caused by the perturbative EM field, and the second and third terms are the implicit variations, created through

re-optimization of the field operator to satisfy Eqs.(4) and (5) under the existence of the perturbative EM field. The last expression is derived using Eq.(13), Eqs.(4) and (5). The above equation reveals that the first order total functional derivative of the action integral of the matter is simply the current density in the non-perturbed system. Furthermore, the second order total functional derivative is calculated as follows:

$$
\begin{aligned}
&\frac{\delta}{\delta A^{\mu_1}(x_1)}\frac{\delta}{\delta A_\mu(x)}\mathcal{I}_{\rm mat}[\hat{\psi}^\dagger_\alpha[A^\nu]\,,\hat{\psi}_\alpha[A^\nu]\,,A^\nu]\Big|_{A^\nu=A^{(0)\nu}} \\
&= \left[\frac{\delta}{\delta A^{\mu_1}(x_1)}\left(\frac{\delta}{\delta A_\mu(x)}\Big|_{\rm explicit}\mathcal{I}_{\rm mat}\right)+\int {\rm d}^4x'\frac{\delta}{\delta A^{\mu_1}(x_1)}\left(\frac{\delta\hat{\psi}^\dagger_\alpha(x')}{\delta A_\mu(x)}\delta\hat{\psi}^\dagger_\alpha(x')\backslash\delta\mathcal{I}_{\rm mat}\right)\right. \\
&\qquad\left.+\int {\rm d}^4x'\frac{\delta}{\delta A^{\mu_1}(x_1)}\left(\delta\mathcal{I}_{\rm mat}/\delta\hat{\psi}_\alpha(x')\frac{\delta\hat{\psi}_\alpha(x')}{\delta A_\mu(x)}\right)\right]_{A^\nu=A^{(0)\nu}} \\
&= \frac{-1}{c^2}\left.\frac{\delta\hat{j}^\mu(x;[A^\nu])}{\delta A^{\mu_1}(x_1)}\right|_{A^\nu=A^{(0)\nu}}, \qquad (18)
\end{aligned}
$$

where the second and third terms in the second expression are null. Actually, the integrand of the second term is:

$$
\left[\left(\frac{\delta}{\delta A^{\mu_1}(x_1)}\frac{\delta\hat{\psi}^\dagger_\alpha(x')}{\delta A_\mu(x)}\right)\delta\hat{\psi}^\dagger_\alpha(x')\backslash\delta\mathcal{I}_{\rm mat}+\frac{\delta\hat{\psi}^\dagger_\alpha(x')}{\delta A_\mu(x)}\left(\frac{\delta}{\delta A^{\mu_1}(x_1)}\delta\hat{\psi}^\dagger_\alpha(x')\backslash\delta\mathcal{I}_{\rm mat}\right)\right]_{A^\nu=A^{(0)\nu}},
$$

The first term in this equation is null because of Eq.(4), and the second term is also null because of Eq.(A2) in Appendix A. In the same manner as for higher order total functional derivatives of the action integral of the matter, the following extension of Eq.(18) holds, owing to Eqs.(A1) and (A2) in Appendix A,

$$
\left.\frac{\delta^{n+1}\mathcal{I}_{\rm mat}[\hat{\psi}^\dagger_\alpha[A^\nu]\,,\hat{\psi}_\alpha[A^\nu]\,,A^\nu]}{\delta A^{\mu_n}(x_n)\cdots\delta A^{\mu_1}(x_1)\delta A_\mu(x)}\right|_{A^\nu=A^{(0)\nu}}=\frac{-1}{c^2}\left.\frac{\delta^n\hat{j}^\mu(x;[A^\nu])}{\delta A^{\mu_n}(x_n)\cdots\delta A^{\mu_1}(x_1)}\right|_{A^\nu=A^{(0)\nu}}. \qquad (19)
$$

To define the single susceptibility, suppose the system under the non-perturbative EM field $A^{(0)\mu}(x)$ is exposed to the perturbative EM field $\Delta A^\mu(x)$. The non-perturbative EM field $A^{(0)\mu}$ is a solution of the coupled equations Eqs.(4)-(7), namely, Heisenberg's equation and Maxwell's wave equations, and is assumed to be a static solution existing in the ground state. On the other hand, the total EM field $A^{(0)\mu}+\Delta A^\mu$ is not necessarily a solution of Maxwell's wave equations, Eqs.(6) and (7), that is, ΔA^μ is introduced as a virtual variation. The induced current density is the variation from the current density in the non-perturbative

system:

$$
\begin{aligned}
&\hat{j}^{\mu}(x;[A^{(0)\nu}+\Delta A^{\nu}])-\hat{j}^{\mu}(x;[A^{(0)\nu}]) \\
=\quad & \int \mathrm{d}^4x_1\ \frac{\delta\hat{j}^{\mu}(x;[A^{\nu}]))}{\delta A^{\mu_1}(x_1)}\bigg|_{A^{\nu}=A^{(0)\nu}} \Delta A^{\mu_1}(x_1) \\
+\ & \frac{1}{2!}\int \mathrm{d}^4x_1 \int \mathrm{d}^4x_2\ \frac{\delta^2\hat{j}^{\mu}(x;[A^{\nu}])}{\delta A^{\mu_1}(x_1)\delta A^{\mu_2}(x_2)}\bigg|_{A^{\nu}=A^{(0)\nu}} \Delta A^{\mu_1}(x_1)\Delta A^{\mu_2}(x_2) \\
+\ & \frac{1}{3!}\int \mathrm{d}^4x_1 \int \mathrm{d}^4x_2 \int \mathrm{d}^4x_3\ \frac{\delta^3\hat{j}^{\mu}(x;[A^{\nu}])}{\delta A^{\mu_1}(x_1)\delta A^{\mu_2}(x_2)\delta A^{\mu_3}(x_3)}\bigg|_{A^{\nu}=A^{(0)\nu}} \Delta A^{\mu_1}(x_1)\Delta A^{\mu_2}(x_2)\Delta A^{\mu_3}(x_3) \\
+\ & \cdots . \qquad (20)
\end{aligned}
$$

From Eqs.(19) and (20), the linear and nonlinear single susceptibility operators are defined as:

$$
\begin{aligned}
\hat{\chi}^{\mu}{}_{\mu_1}(x,x_1) &\equiv \frac{\delta\hat{j}^{\mu}(x;[A^{\nu}])}{\delta A^{\mu_1}(x_1)}\bigg|_{A^{\nu}=A^{(0)\nu}} \\
&= -c^2\frac{\delta^2\mathcal{I}_{\mathrm{mat}}}{\delta A_{\mu}(x)\delta A^{\mu_1}(x_1)}\bigg|_{A^{\nu}=A^{(0)\nu}}\ , \qquad (21) \\
\hat{\chi}^{\mu}{}_{\mu_1\,\mu_2}(x,x_1,x_2) &\equiv \frac{1}{2!}\,\frac{\delta^2\hat{j}^{\mu}(x;[A^{\nu}])}{\delta A^{\mu_1}(x_1)\delta A^{\mu_2}(x_2)}\bigg|_{A^{\nu}=A^{(0)\nu}}\ , \\
&= \frac{-c^2}{2!}\,\frac{\delta^3\mathcal{I}_{\mathrm{mat}}}{\delta A_{\mu}(x)\delta A^{\mu_1}(x_1)\delta A^{\mu_2}(x_2)}\bigg|_{A^{\nu}=A^{(0)\nu}} \qquad (22) \\
\hat{\chi}^{\mu}{}_{\mu_1\cdots\mu_n}(x,x_1,\cdots,x_n) &\equiv \frac{1}{n!}\,\frac{\delta^n\hat{j}^{\mu}(x;[A^{\nu}])}{\delta A^{\mu_1}(x_1)\cdots\delta A^{\mu_n}(x_n)}\bigg|_{A^{\nu}=A^{(0)\nu}} \\
&= \frac{-c^2}{n!}\,\frac{\delta^{n+1}\mathcal{I}_{\mathrm{mat}}}{\delta A_{\mu}(x)\delta A^{\mu_1}(x_1)\cdots\delta A^{\mu_n}(x_n)}\bigg|_{A^{\nu}=A^{(0)\nu}}\ , \qquad (23)
\end{aligned}
$$

The susceptibility is defined using a small amount of variation, ΔA^{μ}. That is, the EM field does not in general satisfy its Euler equation, Eq.(11), while the electron field operators satisfy Eqs.(4) and (5). To evaluate the real EM field, ΔA^{μ} must be determined and a further procedure is required to solve the coupled equations, with the constitutive equations in terms of the susceptibility and Maxwell's wave equations Eqs.(6) and (7). This procedure is provided in a self-consistent manner, as performed by K.Cho[8] using his single susceptibility.

III. CHARGE CONSERVATION LAW AND GAUGE INVARIANCE OF THE SINGLE SUSCEPTIBILITY

In the last expressions in Eqs.(21)-(23) the coordinates $x_1, x_2, \cdots$ for the cause (the perturbative EM field) and the coordinates x for the result (the induced current density) are symmetric. Charge conservation for the induced charge density holds to each order of the perturbation because of Eq.(10) or Eq.(14) and Eqs.(20)-(23); this is described by the derivative of the coordinate for the result, x:

$$\partial_\mu \hat{\chi}^{\mu}{}_{\mu_1\cdots}(x, x_1, \cdots) = 0\,. \tag{24}$$

The symmetry of the coordinates between the result and the cause leads to the following equation concerning the derivative of any coordinate for the cause, e.g., x_1 :

$$\partial^{\mu_1} \hat{\chi}^{\mu}{}_{\mu_1\cdots}(x, x_1, \cdots) = 0. \tag{25}$$

Equation (25) means that the susceptibility guarantees that gauge invariance is respected. That is, the resultant charge and current densities are independent of the chosen gauge. To confirm this fact, consider the convolution integral of the single susceptibility with the perturbative EM field, in a certain gauge, e.g.,

$$\int \mathrm{d}^4 x_1 \;\; \hat{\chi}^{\mu}{}_{\mu_1\cdots}(x, x_1, \cdots) \Delta A^{\mu_1}(x_1). \tag{26}$$

A gauge transformation of ΔA to $\Delta A'$ in another gauge is expressed as :

$$\Delta A^{\mu_1}(x_1) = \Delta A'^{\mu_1}(x_1) - c\,\partial^{\mu_1}\eta(x_1), \tag{27}$$

where η is the gauge function. Equation (26) leads to:

$$\begin{aligned} & \int \mathrm{d}^4 x_1 \;\; \hat{\chi}^{\mu}{}_{\mu_1\cdots}(x, x_1, \cdots) \Delta A^{\mu_1}(x_1) \\ = & \int \mathrm{d}^4 x_1 \;\; \hat{\chi}^{\mu}{}_{\mu_1\cdots}(x, x_1, \cdots) \Delta A'^{\mu_1}(x_1) + c \int \mathrm{d}^4 x_1 \;\; \partial^{\mu_1} \hat{\chi}^{\mu}{}_{\mu_1\cdots}(x, x_1, \cdots) \eta(x_1) \\ = & \int \mathrm{d}^4 x_1 \;\; \hat{\chi}^{\mu}{}_{\mu_1\cdots}(x, x_1, \cdots) \Delta A'^{\mu_1}(x_1). \end{aligned} \tag{28}$$

The contribution of the gauge function vanishes in the convolution integral. Thus, the gauge of the perturbative EM field may be freely selected. This means that the susceptibility is independent of the chosen gauge and, in practice, one may select a gauge that is most convenient for calculation.

IV. SINGLE SUSCEPTIBILITY IN THE FORM OF HEISENBERG OPERATOR

In this section, the linear and nonlinear single susceptibilities in the form of Heisenberg operators are derived using an expansion of the retarded product in Hamiltonian formulation[12]. The Heisenberg operator of four-element current density, i.e., $\hat{j}^{\mu}(x) = (c\hat{\rho}(x), \hat{\mathbf{j}}(x))$ is:

$$\hat{j}^{\mu}(x) \;=\; \begin{cases} cq\hat{\psi}^{\dagger}_{\alpha}(x)\hat{\psi}_{\alpha}(x) & \text{for} \quad \mu = 0, \\ \hat{\psi}^{\dagger}_{\alpha}(x)\dfrac{q}{2m}\left(\dfrac{\hbar}{i}(-\partial^{\mu}) - \dfrac{q}{c}A^{\mu}(x)\right)\hat{\psi}_{\alpha}(x) + \text{h.c.} & \text{for} \quad \mu = 1,2,3\,. \end{cases} \tag{29}$$

In Eq.(2), if the factor $i\hbar\hat{\psi}^{\dagger}_{\alpha}(x)$ of the first term is regarded as the canonical momentum of $\hat{\psi}_{\alpha}(x)$, then the Hamiltonian density may be determined as the Legendre transformation from the Lagrangian density, that is:

$$\hat{H} \quad \equiv \int \mathrm{d}^3x \;\frac{1}{2m}\left(\frac{\hbar}{-i}\partial_i - qA_i(x)\right)\hat{\psi}^{\dagger}_{\alpha}(x)\;\left(\frac{\hbar}{i}\partial_i - qA_i(x)\right)\hat{\psi}_{\alpha}(x) + q\phi(x)\;\hat{\psi}^{\dagger}_{\alpha}(x)\hat{\psi}_{\alpha}(x). \tag{30}$$

This Hamiltonian governs the motion of electron field operators. Assuming that the non-perturbative EM field $\phi^{(0)}, \mathbf{A}^{(0)}$ is the static EM field existing in the ground state of a many-electron system, the Hamiltonian, $\hat{H}$ may be separated into a non-perturbative part, $\hat{H}^{(0)}$ and a perturbative part, $\hat{V}$ as follows:

$$\begin{aligned} \hat{H}^{(0)} \equiv & \int \mathrm{d}^3x \;\frac{1}{2m}\left(\frac{\hbar}{-i}\partial_i - qA^{(0)}_i(x)\right)\hat{\psi}^{\dagger}_{\alpha}(x)\cdot\left(\frac{\hbar}{i}\partial_i - qA^{(0)}_i(x)\right)\hat{\psi}_{\alpha}(x) + q\phi^{(0)}(x)\;\hat{\psi}^{\dagger}_{\alpha}(x)\hat{\psi}_{\alpha}(x) \\ & + v^{(\mathrm{AUX})}(x)\;\hat{\psi}^{\dagger}_{\alpha}(x)\hat{\psi}_{\alpha}(x), \end{aligned} \tag{31}$$

$$\begin{aligned} \hat{V}(t) \equiv \hat{H} - \hat{H}^{(0)} &= \int \mathrm{d}^3x\;\hat{v}(x), \\ &= \int \mathrm{d}^3x\;\left\{\Delta\phi(x)\;q\hat{\psi}^{\dagger}_{\alpha}(x)\hat{\psi}_{\alpha}(x) - \Delta A_i(x)\;\frac{q}{2m}\left(\hat{\psi}^{\dagger}_{\alpha}(x)\;\left(\frac{\hbar}{i}\partial_i - qA^{(0)}_i(x)\right)\hat{\psi}_{\alpha}(x) + \text{h.c.}\right)\right. \\ &\qquad \left. + \frac{q}{2m}\Delta A_i(x)\Delta A_i(x)\;q\hat{\psi}^{\dagger}_{\alpha}(x)\hat{\psi}_{\alpha}(x)\right\} \\ &= \int \mathrm{d}^3x\;\left\{\frac{1}{c}\Delta A^{\mu}(x)\;\hat{j}_{\mu}(x)\Big|_{A=A^{(0)}} - \frac{q}{2mc^3}\;\tilde{\delta}^{\mu'}_{\mu}\Delta A^{\mu}(x)\Delta A_{\mu'}(x)\hat{j}_0(x)\right\}, \end{aligned} \tag{32}$$

$$\text{where } \tilde{\delta}^{\mu'}_{\mu} = \begin{cases} 1 & \text{for } \mu = \mu' = 1,2,3\,, \\ 0 & \text{otherwise}\,. \end{cases} \tag{33}$$

The auxiliary potential, $v^{(\mathrm{AUX})}(x)$ effectively represents for the quantum many-electron effect (the exchange-correlation effect); this fact will be explained in the next section. The factor

$\hat{j}_\mu(x)\Big|_{A=A^{(0)}}$ in Eq.(32) is the current density Eq.(29), with the explicitly-appeared VP being replaced by that in the non-perturbed system. The tensor Eq.(33) represents the non-relativistic effect. Actually, this tensor is the analogue of the four-element Kronecker delta, but brings inequality of the temporal and spatial coordinates.

Here, the field operators in the interaction picture (the asymptotic field operators) $\hat{\psi}^{(in)\dagger}_\alpha, \hat{\psi}^{(in)}_\alpha$ are governed by the non-perturbative Hamiltonian $\hat{H}^{(0)}$ and coincide with the field operators in the Heisenberg picture, $\hat{\psi}^\dagger_\alpha, \hat{\psi}_\alpha$ at the infinite past time, $t \to -\infty$, assuming the adiabatic switch-on. The unitary operator $\hat{U}(t,-\infty)$ is the time-evolution operator of the states in the interaction picture, and relates the operators between the Heisenberg and interaction pictures as follows:

$$\begin{aligned}
\hat{\psi}_\alpha(x) &= \hat{U}^{-1}(t,-\infty)\hat{\psi}^{(in)}_\alpha(x)\hat{U}(t,-\infty), \qquad (34)\\
\hat{\psi}^\dagger_\alpha(x) &= \hat{U}^{-1}(t,-\infty)\hat{\psi}^{(in)\dagger}_\alpha(x)\hat{U}(t,-\infty),\\
\text{where} \quad & \hat{U}(t,-\infty) = \lim_{t_0\to-\infty}\hat{U}(t,t_0) = \lim_{t_0\to-\infty}\hat{T}e^{\frac{1}{i\hbar}\int_{t_0}^t \mathrm{d}t'\hat{V}^{(in)}(t')},\\
& \hat{V}^{(in)}(t') \equiv \hat{V}([\hat{\psi}^{(in)\,\dagger}_\alpha, \hat{\psi}^{(in)}_\alpha]; t')
\end{aligned}$$

Combining Eq.(34) and Eq.(29), the four-element current density operator in the interaction picture may be defined as: $\hat{j}^{(in)\,\mu}(x) = (c\hat{\rho}^{(in)}(x), \hat{\mathbf{j}}^{(in)}(x))$. These charge and current densities do not satisfy the charge conservation law, except for $A = A^{(0)}$, and are merely convenient tools used for obtaining the expansion of the retarded product of the Heisenberg operators.

$$\hat{j}^\mu(x) = \hat{U}^{-1}(t,-\infty)\hat{j}^{(in)\,\mu}(x)\hat{U}(t,-\infty), \qquad (35)$$

$$\hat{j}^{(in)\,\mu}(x) = \begin{cases} c\,q\hat{\psi}^{(in)\dagger}_\alpha(x)\,\hat{\psi}^{(in)}_\alpha(x) & \text{for} \quad \mu = 0, \\ \hat{\psi}^{(in)\dagger}_\alpha(x)\dfrac{q}{2m}\left(\dfrac{\hbar}{i}(-\partial^\mu) - \dfrac{q}{c}A^\mu(x)\right)\hat{\psi}^{(in)}_\alpha(x) + \text{h.c.} & \text{for} \quad \mu = 1,2,3\,. \end{cases} \qquad (36)$$

To obtain the perturbative expansion (the retarded product series) of the Heisenberg operators, let us introduce an operator in the intermediate picture, where $\hat{U}(t,t_0)$ will be used instead of $\hat{U}(t,-\infty)$:

$$\begin{aligned}
\hat{\rho}^\bullet(x;t_0) &= \hat{U}^{-1}(t,t_0)\,q\,\hat{\psi}^{(in)\dagger}_\alpha(x)\,\hat{\psi}^{(in)}_\alpha(x)\hat{U}(t,t_0),\\
\hat{j}^\bullet_i(x;t_0) &= \hat{U}^{-1}(t,t_0)\frac{q}{2m}\hat{\psi}^{(in)\dagger}_\alpha(x)\left(\frac{\hbar}{i}\partial_i - qA_i(x)\right)\hat{\psi}^{(in)}_\alpha(x)\hat{U}(t,t_0) + \text{h.c.}.
\end{aligned}$$

The corresponding four-element current density is

$$\hat{j}^{\bullet\,\mu}(x;t_0) = (c\hat{\rho}^\bullet(x;t_0), \hat{\mathbf{j}}^\bullet(x;t_0))$$

As $t_0 \to -\infty$, these operators coincide with those of the Heisenberg picture, while at $t_0 = t$, they coincide with those of the interaction picture:

$$\hat{j}^{\bullet\,\mu}(x;-\infty) \;=\; \hat{j}^{\mu}(x), \tag{37}$$

$$\hat{j}^{\bullet\,\mu}(x;t) \;=\; \hat{j}^{(in)\,\mu}(x). \tag{38}$$

Next, let's investigate the time evolution of $\hat{j}^{\bullet\,\mu}$ as a function of t_0.

$$\begin{aligned}
\partial_{t_0}\hat{j}^{\bullet\,\mu}(x;t_0) \;&=\; \{\partial_{t_0}\hat{U}^{-1}(t,t_0)\}\hat{j}^{(in)\,\mu}(x)\hat{U}(t,t_0) + \hat{U}^{-1}(t,t_0)\hat{j}^{(in)\,\mu}(x)\{\partial_{t_0}\hat{U}(t,t_0)\} \\
&=\; \frac{1}{i\hbar}\hat{V}^{(in)}(t_0)\hat{U}^{-1}(t,t_0)\hat{j}^{(in)\,\mu}(x)\hat{U}(t,t_0) + \hat{U}^{-1}(t,t_0)\hat{j}^{(in)\,\mu}(x)\hat{U}(t,t_0)\frac{-1}{i\hbar}\hat{V}^{(in)}(t_0) \\
&=\; \frac{-1}{i\hbar}\left[\hat{j}^{\bullet\,\mu}(x;t_0), \hat{V}^{(in)}(t_0)\right]
\end{aligned}$$

Integrating over $[t_0, t]$, approximating iteratively using Eq.(38), and changing the region of multi-integration, we obtain:

$$\begin{aligned}
\hat{j}^{\bullet\,\mu}(x;t_0) \;&=\; \hat{j}^{(in)\,\mu}(x) + \frac{1}{i\hbar}\int_{t_0}^{t}\mathrm{d}t_1\left[\hat{j}^{\bullet\,\mu}(x;t_1), \hat{V}^{(in)}(t_1)\right] \\
&=\; \hat{j}^{(in)\,\mu}(x) + \frac{1}{i\hbar}\int_{t_0}^{t}\mathrm{d}t_1\left[\hat{j}^{(in)\,\mu}(x), \hat{V}^{(in)}(t_1)\right] \\
&\qquad + \left(\frac{1}{i\hbar}\right)^2\int_{t_0}^{t}\mathrm{d}t_1\int_{t_1}^{t}\mathrm{d}t_2\left[\left[\hat{j}^{(in)\,\mu}(x), \hat{V}^{(in)}(t_2)\right], \hat{V}^{(in)}(t_1)\right] \\
&\qquad + \left(\frac{1}{i\hbar}\right)^3\int_{t_0}^{t}\mathrm{d}t_1\int_{t_1}^{t}\mathrm{d}t_2\int_{t_2}^{t}\mathrm{d}t_3\left[\left[\left[\hat{j}^{(in)\,\mu}(x), \hat{V}^{(in)}(t_3)\right], \hat{V}^{(in)}(t_2)\right], \hat{V}^{(in)}(t_1)\right] + \cdots \\
&=\; \hat{j}^{(in)\,\mu}(x) + \frac{1}{i\hbar}\int_{t_0}^{t}\mathrm{d}t_1\left[\hat{j}^{(in)\,\mu}(x), \hat{V}^{(in)}(t_1)\right] \\
&\qquad + \left(\frac{1}{i\hbar}\right)^2\int_{t_0}^{t}\mathrm{d}t_1\int_{t_0}^{t_1}\mathrm{d}t_2\left[\left[\hat{j}^{(in)\,\mu}(x), \hat{V}^{(in)}(t_1)\right], \hat{V}^{(in)}(t_2)\right] \\
&\qquad + \left(\frac{1}{i\hbar}\right)^3\int_{t_0}^{t}\mathrm{d}t_1\int_{t_0}^{t_1}\mathrm{d}t_2\int_{t_0}^{t_2}\mathrm{d}t_3\left[\left[\left[\hat{j}^{(in)\,\mu}(x), \hat{V}^{(in)}(t_1)\right], \hat{V}^{(in)}(t_2)\right], \hat{V}^{(in)}(t_3)\right] + \cdots
\end{aligned}$$

Then, taking the limit $t_0 \to -\infty$, the above equation yields the retarded product of the Heisenberg operators, as follows:

$$\begin{aligned}
\hat{j}^{\mu}(x) \;&=\; \hat{j}^{(in)\,\mu}(x) + \frac{1}{i\hbar c}\int_{ct_1\in(-\infty,ct]}\mathrm{d}^4x_{\,1}\left[\hat{j}^{(in)\,\mu}(x), \hat{v}^{(in)}(x_1)\right] \\
&\qquad + \left(\frac{1}{i\hbar c}\right)^2\int_{ct_1\in(-\infty,ct]}\mathrm{d}^4x_{\,1}\int_{ct_2\in(-\infty,ct_1]}\mathrm{d}^4x_{\,2}\left[\left[\hat{j}^{(in)\,\mu}(x), \hat{v}^{(in)}(x_1)\right], \hat{v}^{(in)}(x_2)\right] \\
&\qquad + \left(\frac{1}{i\hbar c}\right)^3\int_{ct_1\in(-\infty,ct]}\mathrm{d}^4x_{\,1}\int_{ct_2\in(-\infty,ct_1]}\mathrm{d}^4x_{\,2}\int_{ct_3\in(-\infty,ct_2]}\mathrm{d}^4x_{\,3}\left[\left[\left[\hat{j}^{(in)\,\mu}(x), \hat{v}^{(in)}(x_1)\right], \hat{v}^{(in)}(x_2)\right], \hat{v}^{(in)}(x_3)\right]
\end{aligned}$$

$$+\cdots \tag{39}$$

where $\hat{V}^{(in)}(t) = \int \mathrm{d}^3x\ \hat{v}^{(in)}(x)\,,$

$$\hat{v}^{(in)}(x) = \frac{1}{c}\Delta A^{\mu}(x)\,\hat{j}^{(in0)}_{\mu}(x) - \frac{q}{2mc^3}\,\tilde{\delta}_{\mu}^{\ \mu'}\Delta A^{\mu}(x)\Delta A_{\mu'}(x)\,\hat{j}^{(in0)}_{0}(x)\,, \tag{40}$$

$$\hat{j}^{(in)\,\mu}(x) = \hat{j}^{(in0)\,\mu}(x) - \frac{q}{mc^2}\,\tilde{\delta}^{\ \mu}_{\mu'}\Delta A^{\mu'}(x)\,\hat{j}^{(in0)\,0}(x)\,, \tag{41}$$

and $\hat{j}^{(in0)\,\mu}(x)$ is the current density in the interaction picture, that is, Eq.(36) with the VP being replaced by the non-perturbed system. Equation (40) is obtained from Eq.(32), replacing $\hat{\psi}_\alpha$, $\hat{\psi}^\dagger_\alpha$ by $\hat{\psi}^{(in)}_\alpha$, $\hat{\psi}^{(in)\,\dagger}_\alpha$, respectively. Next, let us derive the single susceptibility in the form of Heisenberg operator by the functional derivative of Eq.(39) with respect to the EM potential. In Equation (39), the dependence of the EM potential through $\hat{j}^{(in)\,\mu}(x)$ in Eq.(36) is of zeroth and first order for $\mu \in \{1,2,3\}$, and dependence through $\hat{v}^{(in)}(x_1)$ is of first and second order. The linear single susceptibility operator comes from the A^1-dependence, which exists in the first and second terms of Eq.(39) :

$$\begin{aligned}
\hat{\chi}^{\mu}_{\ \mu_1}(x,x_1) \ &= \ \left.\frac{\delta\hat{j}^{\mu}(x)}{\delta A^{\mu_1}(x_1)}\right|_{A=A^{(0)}} \\
&= \frac{-q}{mc^2}\,\tilde{\delta}^{\mu}_{\ \mu_1}\delta^4(x-x_1)\,\hat{j}^{(in0)\,0}(x) + \frac{1}{i\hbar c^2}\theta(ct-ct_1)\left[\hat{j}^{(in0)\,\mu}(x), \hat{j}^{(in0)}_{\ \mu_1}(x_1)\right], \qquad (42)\\
&\text{where} \qquad \hat{j}^{(in0)\,\mu}(x) = \left.\hat{j}^{(in)\,\mu}(x)\right|_{A=A^{(0)}}.
\end{aligned}$$

The Heisenberg operators of the nonlinear single susceptibilities, to second and higher order, are as follows. To avoid any confusion in the case of two times coinciding, the long and explicit expressions are given, without using the time ordering operator.

$$\begin{aligned}
2!\,\hat{\chi}^{\mu}_{\ \mu_1\mu_2}(x,x_1,x_2) &= \left.\frac{\delta^2\hat{j}^{\mu}(x)}{\delta A^{\mu_1}(x_1)\delta A^{\mu_2}(x_2)}\right|_{A=A^{(0)}} \\
&= \frac{1}{i\hbar c^2}\,\frac{-q}{mc^2} \quad \Big\{\delta(ct-ct_1)\theta(ct-ct_2) \quad \tilde{\delta}^{\mu}_{\ \mu_1}\delta^3(x-x_1)\left[\hat{j}^{(in0)\,0}(x), \hat{j}^{(in0)}_{\ \mu_2}(x_2)\right] \\
&\qquad\qquad +\delta(ct-ct_2)\theta(ct-ct_1) \quad \tilde{\delta}^{\mu}_{\ \mu_2}\delta^3(x-x_2)\left[\hat{j}^{(in0)\,0}(x), \hat{j}^{(in0)}_{\ \mu_1}(x_1)\right] \\
&\qquad\qquad + \theta(ct-ct_1)\delta(ct_1-ct_2)\tilde{\delta}_{\mu_1\,\mu_2}\delta^3(x_1-x_2)\left[\hat{j}^{(in0)\,\mu}(x), \hat{j}^{(in0)}_{\ 0}(x_1)\right]\Big\} \\
&+ \left(\frac{1}{i\hbar c^2}\right)^2 \quad \Big\{\theta(ct-ct_1)\theta(ct_1-ct_2)\left[\left[\hat{j}^{(in0)\,\mu}(x), \hat{j}^{(in0)}_{\ \mu_1}(x_1)\right], \hat{j}^{(in0)}_{\ \mu_2}(x_2)\right] \\
&\qquad\qquad + \theta(ct-ct_2)\theta(ct_2-ct_1)\left[\left[\hat{j}^{(in0)\,\mu}(x), \hat{j}^{(in0)}_{\ \mu_2}(x_2)\right], \hat{j}^{(in0)}_{\ \mu_1}(x_1)\right]\Big\}. \qquad (43)
\end{aligned}$$

$$
\begin{aligned}
3!\,\hat{\chi}^{\mu}{}_{\mu_1\mu_2\mu_3}(x,x_1,x_2,x_3) &= \left.\frac{\delta^3\hat{j}^{\mu}(x)}{\delta A^{\mu_1}(x_1)\delta A^{\mu_2}(x_2)\delta A^{\mu_3}(x_3)}\right|_{A=A^{(0)}} \\
&= \frac{1}{i\hbar c^2}\left(\frac{-q}{mc^2}\right)^2 \\
&\Big\{\theta(ct-ct_2)\delta(ct-ct_1)\delta(ct_2-ct_3)\tilde{\delta}^{\mu}{}_{\mu_1}\delta^3(x-x_1)\tilde{\delta}_{\mu_2\,\mu_3}\delta^3(x_2-x_3)\left[\hat{j}^{(in0)\,0}(x),\hat{j}^{(in0)}{}_0(x_2)\right] \\
&+\theta(ct-ct_3)\delta(ct-ct_2)\delta(ct_3-ct_1)\tilde{\delta}^{\mu}{}_{\mu_2}\delta^3(x-x_2)\tilde{\delta}_{\mu_3\,\mu_1}\delta^3(x_3-x_1)\left[\hat{j}^{(in0)\,0}(x),\hat{j}^{(in0)}{}_0(x_3)\right] \\
&+\theta(ct-ct_1)\delta(ct-ct_3)\delta(ct_1-ct_2)\tilde{\delta}^{\mu}{}_{\mu_3}\delta^3(x-x_3)\tilde{\delta}_{\mu_1\,\mu_2}\delta^3(x_1-x_2)\left[\hat{j}^{(in0)\,0}(x),\hat{j}^{(in0)}{}_0(x_1)\right]\Big\} \\
&+\left(\frac{1}{i\hbar c^2}\right)^2\frac{-q}{mc^2} \\
&\Big\{\delta(ct-ct_1)\theta(ct_1-ct_2)\theta(ct_2-ct_3)\tilde{\delta}^{\mu}{}_{\mu_1}\delta^3(x-x_1)\left[\left[\hat{j}^{(in0)\,0}(x),\hat{j}^{(in0)}{}_{\mu_2}(x_2)\right],\hat{j}^{(in0)}{}_{\mu_3}(x_3)\right] \\
&+\delta(ct-ct_1)\theta(ct_1-ct_3)\theta(ct_3-ct_2)\tilde{\delta}^{\mu}{}_{\mu_1}\delta^3(x-x_1)\left[\left[\hat{j}^{(in0)\,0}(x),\hat{j}^{(in0)}{}_{\mu_3}(x_3)\right],\hat{j}^{(in0)}{}_{\mu_2}(x_2)\right] \\
&+\delta(ct-ct_2)\theta(ct_2-ct_3)\theta(ct_3-ct_1)\tilde{\delta}^{\mu}{}_{\mu_2}\delta^3(x-x_2)\left[\left[\hat{j}^{(in0)\,0}(x),\hat{j}^{(in0)}{}_{\mu_3}(x_3)\right],\hat{j}^{(in0)}{}_{\mu_1}(x_1)\right] \\
&+\delta(ct-ct_2)\theta(ct_2-ct_1)\theta(ct_1-ct_3)\tilde{\delta}^{\mu}{}_{\mu_2}\delta^3(x-x_2)\left[\left[\hat{j}^{(in0)\,0}(x),\hat{j}^{(in0)}{}_{\mu_1}(x_1)\right],\hat{j}^{(in0)}{}_{\mu_3}(x_3)\right] \\
&+\delta(ct-ct_3)\theta(ct_3-ct_1)\theta(ct_1-ct_2)\tilde{\delta}^{\mu}{}_{\mu_3}\delta^3(x-x_3)\left[\left[\hat{j}^{(in0)\,0}(x),\hat{j}^{(in0)}{}_{\mu_1}(x_1)\right],\hat{j}^{(in0)}{}_{\mu_2}(x_2)\right] \\
&+\delta(ct-ct_3)\theta(ct_3-ct_2)\theta(ct_2-ct_1)\tilde{\delta}^{\mu}{}_{\mu_3}\delta^3(x-x_3)\left[\left[\hat{j}^{(in0)\,0}(x),\hat{j}^{(in0)}{}_{\mu_2}(x_2)\right],\hat{j}^{(in0)}{}_{\mu_1}(x_1)\right] \\
&+\theta(ct-ct_1)\delta(ct_1-ct_2)\theta(ct_2-ct_3)\tilde{\delta}_{\mu_1\,\mu_2}\delta^3(x_1-x_2)\left[\left[\hat{j}^{(in0)\,\mu}(x),\hat{j}^{(in0)}{}_0(x_1)\right],\hat{j}^{(in0)}{}_{\mu_3}(x_3)\right] \\
&+\theta(ct-ct_2)\delta(ct_2-ct_3)\theta(ct_3-ct_1)\tilde{\delta}_{\mu_2\,\mu_3}\delta^3(x_2-x_3)\left[\left[\hat{j}^{(in0)\,\mu}(x),\hat{j}^{(in0)}{}_0(x_2)\right],\hat{j}^{(in0)}{}_{\mu_1}(x_1)\right] \\
&+\theta(ct-ct_3)\delta(ct_3-ct_1)\theta(ct_1-ct_2)\tilde{\delta}_{\mu_3\,\mu_1}\delta^3(x_3-x_1)\left[\left[\hat{j}^{(in0)\,\mu}(x),\hat{j}^{(in0)}{}_0(x_3)\right],\hat{j}^{(in0)}{}_{\mu_2}(x_2)\right] \\
&+\theta(ct-ct_1)\theta(ct_1-ct_2)\delta(ct_2-ct_3)\tilde{\delta}_{\mu_2\,\mu_3}\delta^3(x_2-x_3)\left[\left[\hat{j}^{(in0)\,\mu}(x),\hat{j}^{(in0)}{}_{\mu_1}(x_1)\right],\hat{j}^{(in0)}{}_0(x_2)\right] \\
&+\theta(ct-ct_2)\theta(ct_2-ct_3)\delta(ct_3-ct_1)\tilde{\delta}_{\mu_3\,\mu_1}\delta^3(x_3-x_1)\left[\left[\hat{j}^{(in0)\,\mu}(x),\hat{j}^{(in0)}{}_{\mu_2}(x_2)\right],\hat{j}^{(in0)}{}_0(x_3)\right] \\
&+\theta(ct-ct_3)\theta(ct_3-ct_1)\delta(ct_1-ct_2)\tilde{\delta}_{\mu_1\,\mu_2}\delta^3(x_1-x_2)\left[\left[\hat{j}^{(in0)\,\mu}(x),\hat{j}^{(in0)}{}_{\mu_3}(x_3)\right],\hat{j}^{(in0)}{}_0(x_1)\right]\Big\} \\
&+\left(\frac{1}{i\hbar c^2}\right)^3 \\
&\Big\{\theta(ct-ct_1)\theta(ct_1-ct_2)\theta(ct_2-ct_3)\left[\left[\left[\hat{j}^{(in0)\,\mu}(x),\hat{j}^{(in0)}{}_{\mu_1}(x_1)\right],\hat{j}^{(in0)}{}_{\mu_2}(x_2)\right],\hat{j}^{(in0)}{}_{\mu_3}(x_3)\right] \\
&+\theta(ct-ct_1)\theta(ct_1-ct_3)\theta(ct_3-ct_2)\left[\left[\left[\hat{j}^{(in0)\,\mu}(x),\hat{j}^{(in0)}{}_{\mu_1}(x_1)\right],\hat{j}^{(in0)}{}_{\mu_3}(x_3)\right],\hat{j}^{(in0)}{}_{\mu_2}(x_2)\right] \\
&+\theta(ct-ct_2)\theta(ct_2-ct_3)\theta(ct_3-ct_1)\left[\left[\left[\hat{j}^{(in0)\,\mu}(x),\hat{j}^{(in0)}{}_{\mu_2}(x_2)\right],\hat{j}^{(in0)}{}_{\mu_3}(x_3)\right],\hat{j}^{(in0)}{}_{\mu_1}(x_1)\right] \\
&+\theta(ct-ct_2)\theta(ct_2-ct_1)\theta(ct_1-ct_3)\left[\left[\left[\hat{j}^{(in0)\,\mu}(x),\hat{j}^{(in0)}{}_{\mu_2}(x_2)\right],\hat{j}^{(in0)}{}_{\mu_1}(x_1)\right],\hat{j}^{(in0)}{}_{\mu_3}(x_3)\right] \\
&+\theta(ct-ct_3)\theta(ct_3-ct_1)\theta(ct_1-ct_2)\left[\left[\left[\hat{j}^{(in0)\,\mu}(x),\hat{j}^{(in0)}{}_{\mu_3}(x_3)\right],\hat{j}^{(in0)}{}_{\mu_1}(x_1)\right],\hat{j}^{(in0)}{}_{\mu_2}(x_2)\right]
\end{aligned}
$$

$$+\theta(ct-ct_3)\theta(ct_3-ct_2)\theta(ct_2-ct_1)\left[\left[\left[\hat{j}^{(in0)\,\mu}(x),\hat{j}^{(in0)}_{\mu_3}(x_3)\right],\hat{j}^{(in0)}_{\mu_2}(x_2)\right],\hat{j}^{(in0)}_{\mu_1}(x_1)\right]\Big\} \quad (44)$$

The charge conservation, Eq.(24) and gauge invariance, Eq.(25) are respected in Eqs.(42)-(44). This fact is successfully checked after long and tedious calculations; a supplementary document is provided for details.

V. THE GROUND STATE IN DENSITY FUNCTIONAL THEORY AND SINGLE SUSCEPTIBILITY

The linear and nonlinear single susceptibilities are the expectation values of the corresponding operators, Eqs.(42)-(44), using the ground state in the non-perturbed electron system, which is specified by the simplified conditions in this paper:

$$\mathbf{A}(x)=\mathbf{A}^{(0)}(x)=\mathbf{0},\quad \mathbf{j}^{(\mathrm{EXT})}(x)=\mathbf{0},\quad \phi(x)=\phi^{(0)}(x)\text{ and }\rho^{(\mathrm{EXT})}(x)\quad\text{are static.} \quad (45)$$

Let us explain how density functional theory[13, 14] may allow us to prepare the ground state and the complete set of the states in a many-electron system, refining the naive idea in Ref. [1]. For that purpose, we need the electron field operators together with the SP and VP satisfying the coupled equations, Eqs.(4)-(9). However, in the semiclassical treatment of the present theory, Eqs.(8) and (9) are replaced with their expectation values using the ground state, which we seek now on. Due to this procedure, the quantum many-electron effect, the so-called exchange-correlation effect is ignored. Therefore, the solution of Eqs.(4)-(9) as it is may not reproduce the electron charge density of the proper ground state, $\rho_{\mathrm{GS}}(\mathbf{r})$, which is obtained using the ordinary Hamiltonian including the two-body Coulomb interaction, converted from the SP under the Coulomb gauge. Such the electron density $\rho_{\mathrm{GS}}(\mathbf{r})$, in turn, brings about the proper SP $\phi^{(0)}(x)$ under the Coulomb gauge. Suppose that the proper electron charge density $\rho_{\mathrm{GS}}(\mathbf{r})$ is already known under the ordinary Hamiltonian.

Now, we like to seek for the ground state $|0\rangle$ in need, adjusting the auxiliary potential $v^{(\mathrm{AUX})}(\mathbf{r})$ to make the electron charge density fit the proper one:

$$\langle 0|\hat{\rho}(x)|0\rangle=\rho_{\mathrm{GS}}(\mathbf{r}). \quad (46)$$

Such a situation in Eq.(46) is assumed by Kohn and Sham in the density functional theory[14]. That is, Eqs.(4) and (5) are equivalent to Eq.(2.8) in Ref.[14] [the Kohn-Sham equation], if $v^{(\mathrm{AUX})}(\mathbf{r})$ is regarded as the so-called exchange-correlation potential.

For details, one may prepare the spin-orbital function $\varphi_k(\mathbf{r})$ (k, α stands for the orbital and spin states) as the eigenstate of the Kohn-Sham equation with the eigenenergy $\hbar\omega_k$. Under the conditions of Eq.(45), the Kohn-Sham equation is,

$$0 = \left(\hbar\omega_k - q\phi^{(0)}(\mathbf{r}) - \frac{1}{2m}\frac{\hbar}{i}\partial_i \cdot \frac{\hbar}{i}\partial_i - v^{(\mathrm{AUX})}(\mathbf{r}) \right) \varphi_k(\mathbf{r}), \tag{47}$$

where $v^{(\mathrm{AUX})}(\mathbf{r})$ is set to the exchange-correlation potential, that guarantees Eq.(46). Then, $\hat{\psi}_\alpha(x) = \hat{\psi}^{(in0)}_\alpha(x) = \sum_k \varphi_k(\mathbf{r})\, \hat{a}^{(in0)}_{k\alpha}(t)$ satisfies Eq.(4) under the condition Eq.(45), where $\hat{a}^{(in0)}_{k\alpha}$ is the operator to annihilate the electron associated with the spin-orbital $\varphi_k(\mathbf{r})$ in the non-perturbative system. Considering $\{\varphi_k(\mathbf{r})\}$ as a complete set of the one-electron functional space, the ground state with the electron number n in the present theory is constructed as the single Slater determinant,

$$|0\rangle = \lim_{t_0 \to -\infty} \frac{1}{\sqrt{n!}} \prod_{k\alpha} \hat{a}^{(in0)\,\dagger}_{k\alpha}(t_0)\, |\mathrm{vac}\rangle\,, \tag{48}$$

where $|\mathrm{vac}\rangle$ is the vacuum state, and the indecies $k\alpha$ scan over the n spin-orbitals from the lowest eigenenergies. Furthermore, under the fixed $v^{(\mathrm{AUX})}(\mathbf{r})$ and $\phi^{(0)}(\mathbf{r})$, one may consider all the possible combination of n spin-orbitals and obtain the normalized orthogonal complete set $\{|m\rangle | m = 0, 1, 2, \cdots\}$ in terms of all the possible single Slater determinants.

On the above logic, one should know the proper electron charge density $\rho_{\mathrm{GS}}(\mathbf{r})$ beforehand to determine $v^{(\mathrm{AUX})}(\mathbf{r})$, which is the universal functional of the electron density[13, 14]. In practice, however, one may solve the Kohn-Sham equation, possibly under the local density approximation for $v^{(\mathrm{AUX})}(\mathbf{r})$, and reconsider the resulting charge density as $\rho_{\mathrm{GS}}(\mathbf{r})$.

The expectation value of the single susceptibility operator is, $\langle 0|\hat{\chi}^{\mu}_{\mu_1\cdots}(x, x_1, \cdots)|0\rangle$, and, for example, the linear susceptibility becomes:

$$\begin{aligned}\langle 0|\hat{\chi}^{\mu}{}_{\mu_1}(x, x_1)|0\rangle =& \frac{-q}{mc^2}\, \tilde{\delta}^{\mu}{}_{\mu_1} \delta^4(x - x_1)\, \langle 0|\hat{j}^{(in0)\,0}(x)|0\rangle \\ &+ \frac{1}{i\hbar c^2}\theta(ct - ct_1)\langle 0| \left[\hat{j}^{(in0)\,\mu}(x), \hat{j}^{(in0)}_{\mu_1}(x_1) \right] |0\rangle\,. \end{aligned} \tag{49}$$

Next, to evaluate the products of two (or more) current density operators, e.g., the second term in Eq.(49), we may use the projection operator $\hat{1} = \sum_m |m\rangle\langle m|$. Now, the expectation

value in the second term of Eq.(49) becomes,

$$
\begin{aligned}
&\langle 0|\left[\hat{j}^{(in0)\,\mu}(x),\hat{j}^{(in0)}_{\ \ \mu_1}(x_1)\right]|0\rangle \\
&=\sum_m\Big\{\langle 0|\hat{j}^{(in0)\,\mu}(x)|m\rangle\langle m|\hat{j}^{(in0)}_{\ \ \mu_1}(x_1)|0\rangle-\langle 0|\hat{j}^{(in0)}_{\ \ \mu_1}(x_1)|m\rangle\langle m|\hat{j}^{(in0)\,\mu}(x)|0\rangle\Big\} \\
&=\sum_m\lim_{t_0\to\infty}\Big\{\langle 0|e^{\frac{-1}{i\hbar}\hat{H}^{(0)}(t-t_0)}\hat{j}^{(in0)\,\mu}(x)|_{t=t_0}e^{\frac{1}{i\hbar}\hat{H}^{(0)}(t-t_0)}|m\rangle\langle m|e^{\frac{-1}{i\hbar}\hat{H}^{(0)}(t_1-t_0)}\hat{j}^{(in0)}_{\ \ \mu_1}(x_1)|_{t_1=t_0}e^{\frac{1}{i\hbar}\hat{H}^{(0)}(t_1-t_0)}|0\rangle \\
&\qquad\qquad-\langle 0|e^{\frac{-1}{i\hbar}\hat{H}^{(0)}(t_1-t_0)}\hat{j}^{(in0)}_{\ \ \mu_1}(x_1)|_{t_1=t_0}e^{\frac{1}{i\hbar}\hat{H}^{(0)}(t_1-t_0)}|m\rangle\langle m|e^{\frac{-1}{i\hbar}\hat{H}^{(0)}(t-t_0)}\hat{j}^{(in0)\,\mu}(x)|_{t=t_0}e^{\frac{1}{i\hbar}\hat{H}^{(0)}(t-t_0)}|0\rangle\Big\} \\
&=\sum_m\Big\{e^{\frac{1}{i\hbar}(E_m-E_0)(t-t_1)}\langle 0|\hat{j}^{(in0)\,\mu}(x)|_{t=-\infty}|m\rangle\langle m|\hat{j}^{(in0)}_{\ \ \mu_1}(x_1)|_{t_1=-\infty}|0\rangle \\
&\qquad\qquad-e^{\frac{-1}{i\hbar}(E_m-E_0)(t-t_1)}\langle 0|\hat{j}^{(in0)}_{\ \ \mu_1}(x_1)|_{t_1=-\infty}|m\rangle\langle m|\hat{j}^{(in0)\,\mu}(x)|_{t=-\infty}|0\rangle\Big\}. \qquad (50)
\end{aligned}
$$

In the induced charge and current densities obtained from the convolution integral of Eq.(50) with the perturbative EM field, the energy denominator will appear as shown in §VI.

In the above theoretical framework, $|m\rangle$'s are simply the members of the complete set, and, in principle, do not carry physical meaning of excited states of a many-electron system. Considering that the density functional theory concerns only the ground state of the many-electron system, the above treatment is a sound application of density functional theory to the response theory adequate for NFO. Remark that the variational principle based on Eq.(1) cannot determine the auxiliary potential, $v^{(\mathrm{AUX})}(x)$ but is determined with the help of another theory, namely, the density functional theory.

As a summary, the quantum many-electron effect is temporally ignored in the present semiclassical theory, but is compensated with the support of the density functional theory. In other words, the SP inherently existing in the electron system is separated as $\phi^{(0)}(x)$ and $v^{(\mathrm{AUX})}(\mathbf{r})$, and the SP incidence may be treated equally with the VP incidence. Note that, $\phi^{(0)}(x)$ is under the Coulomb gauge but the SP and VP incidences may be gauge-free, that is, the present response theory is still free from gauge-fixing.

VI. APPLICATION: A LOGICAL FALLACY TO USE THE ELECTRIC FIELD IN NEAR-FIELD OPTICS

Under *non-resonant conditions* in the optical near field, *non-metallic materials* cause various phenomena not observed in conventional optics, such as highly efficient light emission from indirect-transition-type semiconductors (LED[17, 18] and Laser[18, 19]), chem-

ical reaction with insufficient photon energy (chemical vapor deposition[20], optical NF lithography[21], optical NF etching[22]), frequency up-conversion[23, 24], non-adiabatic effect beyond forbidden transition (local energy concentration[25], nano-photonic gate device[26]), and gigantic magneto-optical rotation of the LED[18, 27].

These experimental results draw attention to a fundamental role of the non-resonant condition in NFO. We have no complete answer at this stage but the application of the present response theory to a many-electron system in NFO shows a logical fallacy to use the electric field and the electric permittivity, and the necessity to use the EM potential and the associated single susceptibility. The discussion of the *one-electron* system appeared in Ref.[1], but is concisely reviewed below in §VI B-§VI E because the *many-electron* version in §VI F may be simply a recast of the one-electron version, owing to the density functional theory. For the readability, calculation details are given in Appendix B.

A. Classification of optical systems

First, let us classify the optical systems. The two systems under near- and far-field incidence conditions in FIG.1 are subdivided into two classes depending on the near- or far-field observation condition. These four classes are listed in TABLE I, together with a summary of the results mentioned below. In particular, the systems of (I′) and (II′) are the limiting cases of null longitudinal incidence of the systems (I) and (II), respectively. Thus, in the systems (I′) and (II′), the longitudinal response vanishes and the difference in response may not be observed. In the following, therefore, we focus mainly on systems (I) and (II), in which longitudinal incidence exists.

B. Susceptibilities associated with longitudinal and transverse electric fields

Applying the present linear response theory and the long wave approximation (LWA) to the spinless one-electron system with two levels on a small scale, the induced charge and current densities (*as a result of the response*), $\Delta\rho(\mathbf{r},t)$ and $\Delta\mathbf{j}(\mathbf{r},t)$, are described as the total derivative with respect to the longitudinal and transverse electric fields (*as the cause of the response*), $\Delta\mathbf{E}^{(\ell)}(\mathbf{0},t)$ and $\Delta\mathbf{E}^{(t)}(\mathbf{0},t)$, where $\mathbf{0}$ is the representative position in the

TABLE I: Classification of optical systems by distance from the target material to the light source and distance from that to the observation point, together with a summary of the results; the validity of the electric field as the cause of the response.

	Near-field observation Source:$\Delta\rho$ and $\Delta\mathbf{j}$	**Far-field observation** Source: $\overline{\Delta\mathbf{j}}$
Near-field incidence : $\Delta\mathbf{E}^{(\ell)} + \Delta\mathbf{E}^{(t)}$	**(I) NF optical system** non-resonant / resonant	**(II) NF optical system** non-resonant / resonant
Validity of the electric field	NG / OK	OK / OK
Far-field incidence : $\Delta\mathbf{E}^{(t)}$	**(I′) NF optical system** non-resonant / resonant	**(II′)conventional optical system** non-resonant / resonant
Validity of the electric field	OK / OK	OK / OK

electron system under the LWA. The derivations are given in §B 1 and the results are,

$$\Delta\rho(\mathbf{r},t) = \chi_j^{\rho\leftarrow(\ell)}(\mathbf{r},\omega)\,\Delta E_j^{(\ell)}(\mathbf{0},t) + \chi_j^{\rho\leftarrow(t)}(\mathbf{r},\omega)\,\Delta E_j^{(t)}(\mathbf{0},t)\,, \tag{51}$$

$$\Delta j_i(\mathbf{r},t) = \chi_{ij}^{\mathbf{j}\leftarrow(\ell)}(\mathbf{r},\omega)\,\Delta \dot{E}_j^{(\ell)}(\mathbf{0},t) + \chi_{ij}^{\mathbf{j}\leftarrow(t)}(\mathbf{r},\omega)\,\Delta \dot{E}_j^{(t)}(\mathbf{0},t)\,, \tag{52}$$

where the partial derivative coefficients, $\chi_{\cdots}^{\cdots}(\mathbf{r},\omega)$'s are susceptibilities associated with the longitudinal and transversal electric fields. In Eq.(52), the time derivatives of the two types of electric fields, namely, $\Delta\dot{E}_j^{(\ell)}(\mathbf{0},t)$ and $\Delta\dot{E}_j^{(t)}(\mathbf{0},t)$, are regarded as the causes, instead of the two types of electric fields themselves. The magnetic response will appear in the higher order of the LWA and vanishes in Eqs.(51) and (52) representing the leading order; see Refs.[4, 5] and §VI G. For the present spinless electron system, the electron field operators, $\hat{\psi}_\alpha^\dagger(x)$, $\hat{\psi}_\alpha(x)$ is reconsidered as $\hat{\psi}^\dagger(x)$, $\hat{\psi}(x)$, respectively, eliminating the index of the spin state, α.

To evaluate the susceptibilities in Eqs.(51) and (52), the two levels are assumed to be the ground and excited states in the non-perturbed system with eigenenergies, $\hbar\omega_0$ and $\hbar\omega_1$, and orbitals, $\varphi_0(\mathbf{r})$ and $\varphi_1(\mathbf{r})$, respectively. Those orbitals are assumed to be bound states expressed by real functions, carry well-defined and distinct spatial parities (even and odd parities), and form the normalized orthogonal complete set. The excitation energy is $\hbar\Delta\omega_1 \equiv \hbar\omega_1 - \hbar\omega_0 > 0$; this finite excitation energy means that the target is a non-metallic material, such as a molecule, nano-structured semiconductor and insulator.

The susceptibilities in Eqs.(51) and (52) are derived in §B 1, and those leading to the induced charge density result in the following:

$$\chi_j^{\rho\leftarrow(\ell)}(\mathbf{r},\omega) = \chi_j^{\rho\leftarrow(t)}(\mathbf{r},\omega) = 2q^2\,\frac{\eta}{\eta^2-1}\,\frac{1}{\hbar\omega}\,\mathcal{D}_j\,\varphi_0(\mathbf{r})\varphi_1(\mathbf{r})\,, \tag{53}$$

$$\text{where} \qquad \eta \equiv \frac{\hbar\Delta\omega_1}{\hbar\omega} = \frac{\text{excitation energy}}{\text{photon energy}}\,, \text{ and} \tag{54}$$

$$\mathcal{D}_i \equiv \int \mathrm{d}^3 r\;\; \varphi_1(\mathbf{r})\, r_i\, \varphi_0(\mathbf{r})\,. \tag{55}$$

This means that the responses to the longitudinal and transverse electric fields are common, such that the induced charge density has a linear relationship with *the total electric field*, namely, $\Delta\rho(\mathbf{r},t) = \chi_j^{\rho\leftarrow(\ell)\text{ or }(t)}(\mathbf{r},\omega)\left(\Delta E_j^{(\ell)}(\mathbf{0},t) + \Delta E_j^{(t)}(\mathbf{0},t)\right)$.

The susceptibilities leading to the induced current density are not so simple and result in the following:

$$\chi_{ij}^{\mathbf{j}\leftarrow(\ell)}(\mathbf{r},\omega) = \frac{q^2\hbar^2}{m}\,\frac{1}{\eta^2-1}\,\frac{1}{(\hbar\omega)^2}\,\mathcal{D}_j\;\left(\partial_i\varphi_1(\mathbf{r})\varphi_0(\mathbf{r}) - \varphi_1(\mathbf{r})\partial_i\varphi_0(\mathbf{r})\right)\,, \tag{56}$$

$$\chi_{ij}^{\mathbf{j}\leftarrow(t)}(\mathbf{r},\omega) = \eta^2\,\chi_{ij}^{\mathbf{j}\leftarrow(\ell)}(\mathbf{r},\omega) - \frac{q^2\hbar^2}{m}\,\frac{1}{(\hbar\omega)^2}\,\varphi_0(\mathbf{r})\varphi_0(\mathbf{r})\,. \tag{57}$$

The susceptibility to the transverse electric field, Eq.(57), is composed of two terms. The first term, namely, the resonant term, includes the energy denominator enhanced under the resonant condition, $\eta \simeq 1$, as in the susceptibility to the longitudinal electric field, Eq.(56). The second term, namely, the non-resonant term, does not include such a resonance factor.

C. Equal responses under the resonant condition

Under the condition $\eta \simeq 1$ in all cases in TABLE I, Eq.(57) is dominated by the resonant term (the first term) over the non-resonant term (the second term) and asymptotically equals Eq.(56).

$$\chi_{ij}^{\mathbf{j}\leftarrow(t)}(\mathbf{r},\omega) \simeq \chi_{ij}^{\mathbf{j}\leftarrow(\ell)}(\mathbf{r},\omega)\,. \tag{58}$$

Equation (58) together with Eq.(53) reveal the equivalency of the responses to the longitudinal and transverse electric fields, so that the total electric field is regarded as the cause of the response in all the optical systems under the resonant condition listed in TABLE I.

D. Equal responses under the far-field observation condition

In the system (Ⅱ) and (Ⅱ′) in TABLE I, the far field to be observed is insensitive to the details of the source but is determined by the spatial average of the source. Under the LWA, such an average can be achieved by the spatial average of the susceptibilities. Detailed calculations are shown in §B 2 and the results are as follows:

$$\overline{\chi_j^{\rho\leftarrow(\ell)}(\mathbf{r},\omega)} = \quad \overline{\chi_j^{\rho\leftarrow(t)}(\mathbf{r},\omega)} = 0\,, \tag{59}$$

$$\overline{\chi_{ij}^{\mathbf{j}\leftarrow(\ell)}(\mathbf{r},\omega)} = \overline{\chi_{ij}^{\mathbf{j}\leftarrow(t)}(\mathbf{r},\omega)} = \delta_{i\,j}\frac{q^2\hbar^2}{m\,\mathcal{V}}\frac{1}{(\hbar\Delta\omega_1)^{\,2}-(\hbar\omega)^2}\,, \tag{60}$$

where the overline represents the spatial average and $\mathcal{V}$ is the volume of the target material. From Eqs.(59) and (60), one may not observe different responses to the two types of incidences under the far-field observation condition. The null response represented in Eq.(59) is reasonable because the induced charge density yields the longitudinal electric field, which has a non-radiative nature and vanishes in the far-field regime.

E. Unequal responses under the non-resonant, NF incidence, and NF observation conditions

The different responses to the longitudinal and transverse electric fields claimed in §I B may be detected only in the system (I) in TABLE I under the non-resonant condition, which is just the compliment to the popular optical systems under the resonant condition or the far-field incidence condition or the far-field observation condition. In the NF optical system (I) with a non-metallic material under the non-resonant condition, *the total electric field* is not the cause of the response; therefore, the response may not be described by the ordinary constitutive equation, namely, the linear relationship between the polarization and "electric field" via the electric permittivity, so that the single susceptibility is essential to treat separately the longitudinal and transverse incidences.

F. Extension to the many-electron system

The above one-electron model is very simple and the responses may be modified in a many-electron system or a low-symmetry system. However, the difference in the responses

to the two types of electric fields originates in *the non-relativistic nature* of the system (as stated in §I B), and should survive in actual NF optical systems with non-metallic materials (the materials with finite excitation energy). Actually, the results revealed in §VI B-§VI E are applicable to the corresponding many-electron system, considering the auxiliary potential $v^{(\mathrm{AUX})}(x)$ to construct the orbitals using the Kohn-Sham equation (46), and replacing the complete orthogonal set composed of the one-electron ground and excited states, $\{\hat{a}_0^{(in0)\,\dagger}(-\infty)|\mathrm{vac}\rangle,\ \hat{a}_1^{(in0)\,\dagger}(-\infty)|\mathrm{vac}\rangle\}$ ($-\infty$ means the time of the infinite past) to the corresponding set, composed of two single Slater determinants, $\{|0\rangle,\ \hat{a}_1^{(in0)\,\dagger}(-\infty)\hat{a}_0^{(in0)}(-\infty)|0\rangle\}$, where $|0\rangle$ is the ground state in the density functional theory as defined in §V, and $\hat{a}_0^{(in0)}[,\ \hat{a}_0^{(in0)\,\dagger}]$ and $\hat{a}_1^{(in0)}[,\ \hat{a}_1^{(in0)\,\dagger}]$ are the annihilation [and creation] operators associated by the the highest occupied molecular orbital (HOMO) and the lowest unoccupied molecular orbital (LUMO), respectively, determined by the Kohn-Sham equation (46). Owing to the density functional theory, recasting the formulation in the one-electron system brings that in the many-electron system, if the HOMO and LUMO dominate the excitation.

As a result, the many-electron system of a non-metallic material under the non-resonant, NF incidence, and NF observation conditions may not be described in terms of the electric field and the associated permittivity. Instead, the EM potential and the single susceptibility are essential.

G. Comparison with the existing theories

In NFO, the response to the longitudinal electric field is discussed in Chap. 5 in Ref.[5] and Chap. 9 in Ref.[9], as mentioned in §I C. The present work is a further comparison of the responses to the two-types of electric field, considering *the non-resonant condition*.

Another logical fallacy to use the electric and magnetic fields is pointed out by Cho, as briefly mentioned in §I B. In Refs.[4, 5], Cho derived a Taylor series of the nonlocal response function[8] under the LWA, and assigned the electric permittivity and magnetic permeability in the macroscopic constitutive equation as the term of order $\mathcal{O}(ka)^0$ (the leading order) and $\mathcal{O}(ka)^2$, respectively, where $ka \ll 1$, $2\pi/k$ is the light wavelength, and a is the representative size of the material. Furthermore, he pointed out that the ordinary two susceptibilities are irrational because the separability of the electric and magnetic responses not applicable and the term of order $\mathcal{O}(ka)^1$ appears in a chiral symmetric system, including

a NF optical system with a low-symmetric nanostructure. The present demonstration is concerned with the logical fallacy, which appears in the electric response (the leading order from the viewpoint of Cho) in NFO under *a non-resonant condition*.

H. A remark on applying the finite differential time domain (FDTD) method to NF optical systems

The macroscopic constitutive equations in terms of the electron permittivity and magnetic permeability have been widely employed to calculate the optical near field in the FDTD method[16]. One may notice that the permittivity in the FDTD method carries a simple spatial dependence and leads to some quantitative error. Actually, the microscopic susceptibilities, for example, Eq.(53), Eq.(56), and Eq.(57), have rippling spatial distributions originating from the orbitals.

In the case of the NF optical system (I) in TABLE I with a non-metallic material under the non-resonant condition, the situation is more serious because the concept *electric field* is not available, such that it is a logical fallacy to use the macroscopic constitutive equation. Thus, a novel simulation method is necessary, in particular, for the NF optical system with a non-metallic material.

I. Why this fallacy has been missed for a long time?

Why has the comparison of responses to the two types of electric fields not been addressed in NF optical theory? First, in the long history of optics, the NF optical system (I) in TABLE I under a non-resonant condition has been out of focus. Such a system could not be resolved until the technical difficulty of NF observation was overcome. Additionally, resonance phenomena continue to attract attention. Furthermore, even in NFO, there has been less emphasis on non-metallic materials, as opposed to metallic materials, which are essential for plasmonics.

The second reason is that the ordinary Hamiltonian for a many-electron system does not include the longitudinal electric field, which is rewritten to the two-body Coulomb interaction, as stated in §I C. With this Hamiltonian, the non-linear response to the longitudinal electric field (the SP under the Coulomb gauge) incidence accompanies the Coulomb inter-

action, and is ignored or unequally treated compared with the response to the transverse electric field (the VP under the Coulomb gauge).

J. Summary of this section

In the NF optical system (I) in TABLE I, the responses to the longitudinal and transverse electric fields should be separately treated, and in a more general view point beyond the LWA and linear response theory, it is essential to employ the linear and nonlinear single susceptibilities, considering both of the SP and VP equally as the cause of response.

To the best of our knowledge, the NF optical system with non-metallic material under the non-resonant condition, namely, the system (I) in TABLE I, is the third example that cannot be described in terms of the electric field and/or magnetic field, after the superconductor system with the Meissner effect[2] and the electron system with the Aharonov-Bohm effect[3], as mentioned in §I A.

VII. SUMMARY

1. Aiming to investigate electron response in NFO, we define the linear and nonlinear single susceptibilities, equally considering the SP and VP as the cause of the response.

2. It is shown that the present single linear and nonlinear susceptibilities guarantee charge conservation and gauge invariance.

3. The linear and nonlinear susceptibilities in the form of Heisenberg operators are derived systematically by means of the functional derivatives of the action integral of the matter with respect to the SP and VP.

4. It is shown that the density functional theory may be used in the non-perturbed system and support to prepare the ground state and a complete set of states, which in turn are used to evaluate the expectation values of the operators of the linear and nonlinear susceptibilities.

5. Applying the present response theory to a simplified model system, it is shown that the single susceptibility is essential to describe the response of the optical system

with non-metallic material under the non-resonant, NF incidence, and NF observation conditions.

Some remaining problems meriting further investigation include:

1. Applying the present response theory to actual non-resonant NF optical systems with a non-metallic material in Refs.[17]-[27] to explore the mechanism leading to the outstanding experimental results such as the high-efficient light emission and gigantic magneto-optical effect, etc.

2. Developing a constitutive equation based on the single susceptibility which can aid experimentalists in NFO as a substitute for the electric permittivity and magnetic permeability of ordinary optics.

3. Developing a practical simulator for the many-electron system in NFO, using the present response theory with the support of the density functional theory, as the replacement of the FDTD simulation method,

4. Extending the response theory to treat the spin-polarization system in NFO, based on the Pauli or Dirac equation.

Acknowledgments

The author thanks Prof. K. Cho in Osaka Univ. for useful discussion about the single susceptibility. He also thanks Prof. M. Ohtsu (Univ. of Tokyo, Research Origin of Dressed Photon (RODreP)) and the members of his group in Univ. of Tokyo, Prof. T. Kawazoe (Tokyo Denki Univ.) for the comment from the experimental view point and dressed photons; Prof. I. Ojima (RODreP), Prof. H. Saigo (Nagahama Insitute of Bio-Science and Technology), Drs H. Sakuma (RODreP), K. Okamura (Nagoya Univ.), H. Ando (Chiba Univ.) for useful discussions on the context of dressed photon. This work is partially supported by JSPS KAKENHI Grant Number JP25610071 during 2013-2015, Research Foundation for Opto-Science and Technology during 2018-2019, and Research Origin for Dressed Photons.

Appendix A: Optimization of Electron Field Operators Under Arbitrary EM Potential

Under a given EM potential, A^ν, the electron field operator optimized to satisfy Eq.(4) is considered as the functional of A^ν, i.e., $\hat{\psi}_\alpha(x;[A^\nu]), \hat{\psi}^\dagger_\alpha(x;[A^\nu])$. Then, the next equation holds for $n = 0, 1, 2, \cdots$:

$$\frac{\delta^n}{\delta A^{\mu_n}(x_n)\cdots\delta A^{\mu_1}(x_1)}\delta\hat{\psi}^\dagger_\alpha(x')\backslash\delta\mathcal{I}_{\rm mat}\,\Big|_{A^\nu=A^{(0)\nu}} = 0, \tag{A1}$$

$$\frac{\delta^n}{\delta A^{\mu_n}(x_n)\cdots\delta A^{\mu_1}(x_1)}\delta\mathcal{I}_{\rm mat}/\delta\hat{\psi}_\alpha(x')\,\Big|_{A^\nu=A^{(0)\nu}} = 0. \tag{A2}$$

Proof: Equation (4) should be hold both under $A^{(0)\nu}$(non-perturbative EM potential) and under $A^{(0)\nu} + \Delta A^\nu$, therefore,

$$\delta\hat{\psi}^\dagger_\alpha(x')\backslash\delta\mathcal{I}_{\rm mat}\Big|_{(\hat{\psi}_\alpha,\hat{\psi}^\dagger_\alpha,A^\nu)=(\hat{\psi}_\alpha[A^{(0)\nu}+\Delta A^\nu],\hat{\psi}^\dagger_\alpha[A^{(0)\nu}+\Delta A^\nu],A^{(0)\nu}+\Delta A^\nu)} = 0,$$

Taylor expansion leads to:

$$\sum_{n=0}^{\infty}\frac{1}{n!}\int{\rm d}^4x_{\,n}\cdots\int{\rm d}^4x_{\,1}\,\frac{\delta^n\left(\delta\hat{\psi}^\dagger_\alpha(x')\backslash\delta\mathcal{I}_{\rm mat}\right)}{\delta A^{\mu_n}(x_n)\cdots\delta A^{\mu_1}(x_1)}\Big|_{(\hat{\psi}_\alpha,\hat{\psi}^\dagger_\alpha,A^\nu)=(\hat{\psi}_\alpha[A^{(0)\nu}],\hat{\psi}^\dagger_\alpha[A^{(0)\nu}],A^{(0)\nu})}\Delta A^{\mu_1}(x_1)\cdots\Delta A^{\mu_n}(x_n) = 0,$$

Considering this equation as the identity with respect to $\Delta A^\mu(x)$ results in Eq.(A1). Equation (A2) is proved in the same manner, starting from Eq.(5).

Appendix B: Calculation details in §VI

Here we provide the calculation details in §VI, including the derivation of the unfamiliar relationship Eq.(B14) between two types of dipole transition matrix elements.

1. Derivation of the constitutive equations, Eqs.(51) and (52), and the susceptibilities, Eq.(53), Eqs.(56) and (57)

The incident SP and VP, $\Delta\phi(\mathbf{r},t)$ and $\Delta A_i(\mathbf{r},t)$, are assumed to be monochromatic with the angular momentum ω, and are expressed using the Coulomb gauge and LWA as follows:

$$\Delta\phi(\mathbf{r},t) = \Delta\phi(\mathbf{r})\cos\omega t = \left(\Delta\phi(\mathbf{0}) - \Delta\mathbf{E}^{(\ell)}(\mathbf{0})\cdot\mathbf{r}\right)\cos\omega t\,, \tag{B1}$$

$$\Delta\mathbf{A}(\mathbf{r},t) = \Delta\mathbf{A}(\mathbf{r})\sin(\omega t+\xi) = -\frac{1}{\omega}\Delta\mathbf{E}^{(t)}(\mathbf{0})\sin(\omega t+\xi)\,, \tag{B2}$$

where ξ is the phase difference between the two incident potentials. In the spinless one-electron system, the linear response theory with Eqs.(20) and (42) leads to the Heisenberg operators of the induced charge and current densities, as follows in the three-element representation:

$$\Delta\hat{\rho}(\mathbf{r},t) = \int_{-\infty}^{t} \mathrm{d}t_1 \int \mathrm{d}^3 r_1 \left\{ \frac{1}{i\hbar} \left[\hat{\rho}^{(in0)}(\mathbf{r},t)\,,\, \hat{\rho}^{(in0)}(\mathbf{r}_1,t_1) \right] \Delta\phi(\mathbf{r}_1,t_1) \right. \\ \left. -\frac{1}{i\hbar} \left[\hat{\rho}^{(in0)}(\mathbf{r},t)\,,\, \hat{j}_{i_1}^{(in0)}(\mathbf{r}_1,t_1) \right] \Delta A_{i_1}(\mathbf{r}_1,t_1) \right\}, \tag{B3}$$

$$\Delta\hat{j}_i(\mathbf{r},t) = \int_{-\infty}^{t} \mathrm{d}t_1 \int \mathrm{d}^3 r_1 \left\{ \frac{1}{i\hbar} \left[\hat{j}_i^{(in0)}(\mathbf{r},t)\,,\, \hat{\rho}^{(in0)}(\mathbf{r}_1,t_1) \right] \Delta\phi(\mathbf{r}_1,t_1) \right. \\ \left. -\frac{1}{i\hbar} \left[\hat{j}_i^{(in0)}(\mathbf{r},t)\,,\, \hat{j}_{i_1}^{(in0)}(\mathbf{r}_1,t_1) \right] \Delta A_{i_1}(\mathbf{r}_1,t_1) \right\} - \frac{q}{m}\hat{\rho}^{(in0)}(\mathbf{r},t)\Delta A_i(\mathbf{r},t)\,. \tag{B4}$$

The last term in Eq.(B4) originates from *the non-relativistic nature* of the system and is needed to maintain charge conservation law.

Evaluating the expectation value of Eqs.(B3) and (B4) using the ground state [$\varphi_0(\mathbf{r})$ in Eq.(B8)] and substituting Eqs.(B1) and (B2) leads to Eqs.(51) and (52), in which the causes of the responses are the two types of electric fields and their temporal derivatives, defined as

$$\Delta E_j^{(\ell)}(\mathbf{0},t) \equiv \quad \Delta E_j^{(\ell)}(\mathbf{0})\cos\omega t\,, \quad \Delta E_j^{(t)}(\mathbf{0},t) \equiv \quad \Delta E_j^{(t)}(\mathbf{0})\cos(\omega t+\xi)\,, \tag{B5}$$

$$\Delta \dot{E}_j^{(\ell)}(\mathbf{0},t) \equiv \frac{\partial}{\partial t}\Delta E_j^{(\ell)}(\mathbf{0},t)\,, \qquad \Delta \dot{E}_j^{(t)}(\mathbf{0},t) \equiv \frac{\partial}{\partial t}\Delta E_j^{(t)}(\mathbf{0},t)\,. \tag{B6}$$

In the above, no magnetic response appears because it is the higher order in the LWA as revealed by Cho [4, 5]. To obtain susceptibilities, Eq.(53),Eqs.(56) and (57) using the two-level model, we take the expectation values of Eqs.(B3) and (B4) using the ground state $\varphi_0(\mathbf{r})$, insert the projection operator [the left side of the second equation in Eq.(B7)], between the two operators in the commutators, and integrate over the domains of t_1 and $\mathbf{r}_1$. We assume that the two orbitals are real functions, and form the normalized orthogonal complete set:

$$\int \mathrm{d}^3 r\, \varphi_m(\mathbf{r})\varphi_n(\mathbf{r}) = \delta_{m\,n}\,, \qquad \sum_m \varphi_m(\mathbf{r})\varphi_m(\mathbf{r}') = \delta^3(\mathbf{r}-\mathbf{r}')\,, \tag{B7}$$

where $\varphi_m(\mathbf{r})$ satisfies,

$$\hat{H}^{(0)}\varphi_m(\mathbf{r}) = \hbar\omega_m\,\varphi_m(\mathbf{r})\,, \quad (m=0,1)\,. \tag{B8}$$

Having real orbitals infers even temporal parity, such that there is a null VP (or magnetic field) in the non-perturbed system. To derive the susceptibilities associated with the transversal electric field in Eqs.(53) and (57), we use the well-known linear relationship between the two types of dipole transition matrix elements,

$$\mathcal{C}_i \equiv \int \mathrm{d}^3 r \; (\partial_i \varphi_1(\mathbf{r})\varphi_0(\mathbf{r}) - \varphi_1(\mathbf{r})\partial_i \varphi_0(\mathbf{r})) = \frac{2m}{\hbar^2}\hbar\Delta\omega_1 \, \mathcal{D}_i \, . \tag{B9}$$

Equation (B9) is derived from the matrix element of Heisenberg equation for dipole charge density:

$$\frac{\partial}{\partial t} \, r_j \hat{\rho}^{(in0)}(\mathbf{r}, t) = \frac{1}{i\hbar} \left[r_j \hat{\rho}^{(in0)}(\mathbf{r}, t) \, , \, \hat{H}^{(0)} \right] \, , \tag{B10}$$

using $\hat{\rho}^{(in0)}(\mathbf{r}, t) = e^{-\frac{\hat{H}^{(0)} t}{i\hbar}} \hat{\rho}^{(in0)}(\mathbf{r}, 0) e^{+\frac{\hat{H}^{(0)} t}{i\hbar}}$ and the projection operator, i.e., the second equation in Eq.(B7) satisfying Eq.(B8).

2. Derivation of the spatial average of the susceptibilities, Eqs.(59) and (60)

The following replacements in Eq.(53), Eqs.(56) and (57) lead to Eqs.(59) and (60):

$$\varphi_0(\mathbf{r})\varphi_1(\mathbf{r}) \quad \longrightarrow \quad \frac{1}{\mathcal{V}} \int \mathrm{d}^3 r \, \varphi_0(\mathbf{r})\varphi_1(\mathbf{r}) = 0 \, , \tag{B11}$$

$$\partial_i \varphi_1(\mathbf{r})\varphi_0(\mathbf{r}) - \varphi_1(\mathbf{r})\partial_i \varphi_0(\mathbf{r}) \quad \longrightarrow \quad \frac{1}{\mathcal{V}} \int \mathrm{d}^3 r \, \partial_i \varphi_1(\mathbf{r})\varphi_0(\mathbf{r}) - \varphi_1(\mathbf{r})\partial_i \varphi_0(\mathbf{r}) = \frac{1}{\mathcal{V}} \mathcal{C}_i \, , \tag{B12}$$

$$\varphi_0(\mathbf{r})\varphi_0(\mathbf{r}) \quad \longrightarrow \quad \frac{1}{\mathcal{V}} \int \mathrm{d}^3 r \, \varphi_0(\mathbf{r})\varphi_0(\mathbf{r}) = \frac{1}{\mathcal{V}} \, . \tag{B13}$$

To derive Eq.(60), we additionally use the trade-off relationship between the two types of dipole transition matrix elements,

$$\mathcal{D}_i \, \mathcal{C}_j = \delta_{i\,j}. \tag{B14}$$

This is effective in the two-level system with well-defined parity and derived from the quantum-mechanical commutation relationship:

$$[r_i \, , \, \frac{\hbar}{i}\partial_j] = i\hbar \, \delta_{ij} \, , \quad \text{i.e.,} \quad r_i \left(\frac{\hbar}{i}\partial_j \cdots \right) + \frac{\hbar}{-i}\partial_j \left(r_i \cdots \right) = i\hbar\delta_{ij} \cdots \, . \tag{B15}$$

Inserting the projection operator between r_i and $\frac{\hbar}{i}\partial_j$, and eliminating the null integrals caused by mismatched parity result in Eq.(B14). From Eq.(B9) and Eq.(B14), $\mathcal{D}_i$ and $\mathcal{C}_i$ are specified as

$$\mathcal{D}_i = \frac{1}{\mathcal{C}_i} = \frac{\hbar}{\sqrt{2m \, \hbar\Delta\omega_1}} \, . \tag{B16}$$

(We do not use Eq.(B16) in this paper.)

---

[1] I. Banno, in *Progress in Nanophotonics vol. 5* edited by T. Yatsui (Springer International Publishing, 2018) Chap. 6.

[2] F. London, *Superfluids vol.1, Macroscopic Theory of Superconductivity* (Dover Publications, Inc., New York, 1950).

[3] Y. Aharanov and D. Bohm, Phys. Rev. **115**, 485 (1959).

[4] K. Cho, J. Phys. Condens. Matter **20**, 175202 (2008).

[5] K. Cho, *Reconstruction of Macroscopic Maxwell Equations* (Springer-Verlag, Berlin, Heidelberg, 2010).

[6] F. I. Fedorov, Optics and Spectroscopy **6**, 49 (1959); *ibid.* **6**, 237(1959). [translated from Russian journal "Optika i Spectroskopiia"]; Ref.[5], §3.4.

[7] Y. Toyozawa, *The Physics of Elementary Excitations* edited by S. Nakajima, Y. Toyozawa, and R. Abe (Springer-Verlag, Berlin, Heidelberg, 1980). Chap. 2. [This book was translated from Japanese book "Bussei II" in Iwanami Series of Fundamental Physics (Iwanami Shoten,1978).]

[8] K. Cho, *Optical Response of Nanostructures* (Springer-Verlag, Berlin, Heidelberg, 2003).

[9] O. Keller, *Quantum Theory of Near-Field Electrodynamics* (Springer, Heidelberg, Dordrecht, London, New York, 2011) Chap. 10.

[10] C. Itzykson and J.-B. Zuber, *Quantum Field Theory (International Edition)* (MacGraw-Hill Book Co., 1985). Chap. 9. ; T. Kugo, *Gēgi-ba no Riron (Quantum Theory of Gauge Fields)* (in Japanese) (Baifukan, Tokyo, 1989) Chap. 1.

[11] The Mathematical Society of Japan and K. Ito eds. *Encyclopedic Dictionary of Mathematics 2nd Ed.* (MIT Press, 1993). [This book was translated from Japanese Dictionary "Iwanami Sūgaku Jiten 3rd Ed." (Iwanami Shoten, 1985).]

[12] K. Nishijima, *Fields and Particles* (W. A. Benjamin, Inc., 1969). Chap. 4.

[13] P. Hohenberg and W. Kohn, Phys. Rev. **136**, 3864 (1964).

[14] W. Kohn and L. J. Sham, Phys Rev. **140**, A1133 (1965).

[15] M. Levy, Proc. Natl. Acad. Sci. USA **76**, 6062 (1979).

[16] K. Yee, *IEEE Transactions on Antennas and Propagation* **14,** 302 (1966).

[17] T. Kawazoe, M. A. Mueed, and M. Ohtsu, Appl. Phys. B **104**, 747 (2011).

[18] M. Ohtsu, *Silicon Light-Emitting Diodes and Lasers* (Springer International Publishing, Switsland, 2016).

[19] T. Kawazoe, M. Ohtsu, K. Akahane, and N. Yamamoto, Appl. Phys. B **107**, 659 (2012).

[20] T. Kawazoe, Y. Yamamoto, and M. Ohtsu, Appl. Phys. Lett. **79**, 1184 (2001).

[21] H. Yonemitsu, T. Kawazoe, K. Kobayashi, and M. Ohtsu, J. Photolumin. **122**, 230 (2007).

[22] T. Yatsui, K. Hirata, W. Nomura, Y. Tabata, and M. Ohtsu, Appl. Phys. B **93**, 55 (2008).

[23] T. Kawazoe, H. Fujiwara, K. Kobayashi, and M. Ohtsu, IEEE J. of Selected Topics in Quantum Electronics **15**, 1380 (2009).

[24] H. Fujiwara, T. Kawazoe, and M. Ohtsu, Appl. Phys. B **100**, 85 (2010).

[25] T. Kawazoe, K. Kobayashi, and M. Ohtsu, Appl. Phys. Lett. **86**, 103102-1 (2005).

[26] T. Kawazoe, M. Ohtsu, S. Aso, Y. Sawado, Y. Hosoda, K. Yoshizawa, K. Akahane, N. Yamamoto, and M. Naruse, Appl. Phys. B **103**, 537 (2011).

[27] N. Tate, T. Kawazoe, W. Nomura, and M. Ohtsu, Scientific Reports **5**, 12762-1 (2015).

Supplementary Document for

"Theory of Single Susceptibility for Near-field Optics

Equally Associated with Scalar and Vector Potentials"

Check for Charge Conservation Law and Gauge Invariance

Itsuki Banno*

Interdisciplinary Graduate School of Medicine and Engineering,

University of Yamanashi, 4-3-11 Takeda,

Kofu, Yamanashi 400-8511, Japan

(Dated: September 28, 2018)

Abstract

Charge conservation law and gauge invariance are explicitly checked for the linear and nonlinear single susceptibilities derived in the main text.

PACS numbers: 78.67.-n, 78.20.Bh, 41.20.-q, 42.25.Ja

Keywords: single susceptibility, non-resonant effect, optical near field, response function, electromagnetic potential

*Electronic address: banno@yamanashi.ac.jp

S. CHARGE CONSERVATION LAW AND GAUGE INVARIANCE OF LINEAR AND NONLINEAR FOUR-ELEMENT SINGLE SUSCEPTIBILITY

S 1. Linear single susceptibility: Eq.(40) in the main text

To show that four-element linear single susceptibility guarantees the charge conservation law, Eq.(24) in the main text, suppose the four-element divergence of Eq.(40) in the main text, considering $\partial_\mu \hat{j}^{(in0)\,\mu}(x) = 0$,

$$\begin{aligned} \partial_\mu \hat{\chi}^{\mu}{}_{\mu_1}(x, x_1) &= \frac{-q}{mc^2}\,\delta(ct - ct_1)\tilde{\delta}^{\mu}{}_{\mu_1}\partial_\mu \left(\delta^3(x - x_1)\,\hat{j}^{(in0)\,0}(x)\right) \\ &\quad + \frac{1}{i\hbar c^2}\delta(ct - ct_1)\left[\hat{j}^{(in0)\,0}(x), \hat{j}^{(in0)}_{\mu_1}(x_1)\right] \\ &= 0. \end{aligned} \tag{S1}$$

In the second term of the second hand, we use the following commutation relationship at the same time :

$$\begin{aligned} \delta(ct - ct_1)\left[\hat{j}^{(in0)\,0}(x), \hat{j}^{(in0)}_{\mu_1}(x_1)\right] &= -ihc^2\frac{-q}{mc^2}\delta(ct - ct_1)\tilde{\delta}^{\mu}_{\mu_1}\partial_\mu\left(\delta^3(x - x_1)\hat{j}^{(in0)\,0}(x)\right) \\ &= -ihc^2\frac{-q}{mc^2}\delta(ct - ct_1)\tilde{\delta}^{\mu}_{\mu_1}\left(\partial_\mu\delta^3(x - x_1)\right)\hat{j}^{(in0)\,0}(x_1) \end{aligned} \tag{S2}$$

The proof of Eq.(S2) is as follows: If $\mu_1 = 0$ in the left hand side of Equation (S2), it is the commutator between charge density operator at the same time, and is zero.

$$\left[\hat{j}^{(in0)\,0}(x), \hat{j}^{(in0)}_{0}(x_1)\right]_{t_1=t} = c^2q^2\left[\hat{\psi}^\dagger_\alpha(x)\hat{\psi}_\alpha(x)\,,\,\hat{\psi}^\dagger_\alpha(x_1)\hat{\psi}_\alpha(x_1)\right]_{t_1=t} = 0. \tag{S3}$$

One may check Eq.(S3) by a straightforward calculation using the anti-commutation relation of electron field operators at the same time,

$$\left[\hat{\psi}_\alpha(x)\,,\,\hat{\psi}^\dagger_\alpha(x_1)\right]_{+,\,t_1=t} = \delta^3(x - x_1).$$

Next, if $\mu_1 = i \in \{1, 2, 3\}$ in the left hand side of Equation (S2), the commutator in three-element representation becomes as follows:

$$\begin{aligned} &\left[\hat{j}^{(in0)\,0}(x), \hat{j}^{(in0)}_{\mu_1=i}(x_1)\right]_{t_1=t} \\ &= -cq\frac{q}{2m}\left[\hat{\psi}^\dagger_\alpha(x)\hat{\psi}_\alpha(x)\,,\,\hat{\psi}^\dagger_\alpha(x_1)\left(\frac{\hbar}{i}\partial^1_i - qA^{(0)}_i(x_1)\right)\hat{\psi}_\alpha(x_1)\right. \\ &\qquad \left. + \left(\left(\frac{\hbar}{-i}\partial^1_i - qA^{(0)}_i(x_1)\right)\hat{\psi}^\dagger_\alpha(x_1)\right)\hat{\psi}_\alpha(x_1)\right]_{t_1=t} \end{aligned} \tag{S4}$$

As the term includes $qA_i^{(0)}(x_1)$ is zero following Eq.(S3), let us treat the term including the derivative.

$$
\begin{aligned}
&\left[\hat{j}^{(in0)\,0}(x), \hat{j}^{(in0)}_{\mu_1=i}(x_1)\right]_{t_1=t} \\
&= -\frac{cq}{2} i\hbar c^2 \frac{-q}{mc^2} \lim_{x_1^\bullet \to x_1} \partial_i^{1\bullet} \left[\hat{\psi}_\alpha^\dagger(x)\hat{\psi}_\alpha(x)\,,\, \hat{\psi}_\alpha^\dagger(x_1)\hat{\psi}_\alpha(x_1^\bullet) - \hat{\psi}_\alpha^\dagger(x_1^\bullet)\hat{\psi}_\alpha(x_1)\right]_{t_1=t} \\
&= -\frac{cq}{2} i\hbar c^2 \frac{-q}{mc^2} \\
&\quad \lim_{x_1^\bullet \to x_1} \partial_i^{1\bullet} \Big(\delta^3(x-x_1)\left(\hat{\psi}_\alpha^\dagger(x)\hat{\psi}_\alpha(x_1^\bullet) + \hat{\psi}_\alpha^\dagger(x_1^\bullet)\hat{\psi}_\alpha(x)\right) \\
&\qquad\qquad -\delta^3(x-x_1^\bullet)\left(\hat{\psi}_\alpha^\dagger(x)\hat{\psi}_\alpha(x_1) + \hat{\psi}_\alpha^\dagger(x_1)\hat{\psi}_\alpha(x)\right)\Big)_{t_1=t} \\
&= -\frac{cq}{2} i\hbar c^2 \frac{-q}{mc^2} \\
&\quad \delta^3(x-x_1)\partial_i\left(\hat{\psi}_\alpha^\dagger(x)\hat{\psi}_\alpha(x_1) + \hat{\psi}_\alpha^\dagger(x_1)\hat{\psi}_\alpha(x)\right) \\
&\qquad\qquad + \left(\partial_i\delta^3(x-x_1)\right)\left(\hat{\psi}_\alpha^\dagger(x)\hat{\psi}_\alpha(x_1) + \hat{\psi}_\alpha^\dagger(x_1)\hat{\psi}_\alpha(x)\right)_{t_1=t} \\
&= -\frac{cq}{2} i\hbar c^2 \frac{-q}{mc^2}\partial_i\left(\delta^3(x-x_1)\left(\hat{\psi}_\alpha^\dagger(x)\hat{\psi}_\alpha(x_1) + \hat{\psi}_\alpha^\dagger(x_1)\hat{\psi}_\alpha(x)\right)\right)_{t_1=t} \\
&= -cqi\hbar c^2 \frac{-q}{mc^2}\partial_i\left(\delta^3(x-x_1)\hat{\psi}_\alpha^\dagger(x)\hat{\psi}_\alpha(x)\right) = -i\hbar c^2 \frac{-q}{mc^2}\tilde{\delta}^{\,\mu}_{\mu_1}\partial_\mu\left(\delta^3(x-x_1)\hat{j}^{(in0)\,0}(x)\right) \qquad \text{(S5)} \\
&= -cqi\hbar c^2 \frac{-q}{mc^2}\partial_i\left(\delta^3(x-x_1)\hat{\psi}_\alpha^\dagger(x_1)\hat{\psi}_\alpha(x_1)\right)_{t_1=t} = -i\hbar c^2 \frac{-q}{mc^2}\tilde{\delta}^{\,\mu}_{\mu_1}\left(\partial_\mu\delta^3(x-x_1)\right)\hat{j}^{(in0)\,0}(x_1)_{t_1=t}\,, \qquad \text{(S6)}
\end{aligned}
$$

where the last two-way expressions Eqs.(S5) and (S6) are in four-element representation instead of three-element representation. Summarizing Eqs.(S3) and (S6) result in Eq.(S2). As a result, the present four-element linear susceptibility,Eq.(40) in the main text maintains the charge conservation law, Eq.(24) in the main text.

For the proof for the gauge invariance, Eq.(25) in the main text, of the linear susceptibility, suppose the four-element divergence with respect to x_1. Then, using Eq.(S2) with the replacement, $x \leftrightarrow x_1$ and the relation, $\tilde{\delta}^{\mu_1}_{\mu}\partial_{\mu_1} = -\tilde{\delta}^{\mu}_{\mu_1}\partial^{\mu_1}$, one may obtain:

$$
\begin{aligned}
\partial^{\mu_1}\hat{\chi}^{\mu}{}_{\mu_1}(x,x_1) &= \frac{-q}{mc^2}\,\delta(ct-ct_1)\left(\tilde{\delta}^{\mu}{}_{\mu_1}\partial^{\mu_1}\delta^3(x-x_1)\right)\hat{j}^{(in0)\,0}(x) \qquad \text{(S7)} \\
&\quad -\frac{1}{i\hbar c^2}\delta(ct-ct_1)\left[\hat{j}^{(in0)\,\mu}(x), \hat{j}^{(in0)}_{\;0}(x_1)\right] \\
&= 0.
\end{aligned}
$$

As shown above, the linear susceptibility Eq.(40) in the main text maintains the gauge invariance Eq.(25) in the main text.

S 2. Second order nonlinear single susceptibility: Eq.(41) in the main text

Next, let us show that the charge conservation law is satisfied by the second order nonlinear single susceptibility, Eq.(41) in the main text. Operating $\partial_\mu = \delta^0_\mu\partial_0 + \delta^1_\mu\partial_1 + \delta^2_\mu\partial_2 + \delta^3_\mu\partial_3$ to Eq.(41) in the main text and considering $\partial_\mu \hat{j}^{(in0)\,\mu}(x) = 0$ (the charge conservation law for the current density operator in the non-interacting system), the surviving terms are those the operator ∂_μ operates on the step function or delta function in front of the commutator, and operates on $\hat{j}^{(in0)\,0}(x)$ in the commutator.

$$
\begin{aligned}
&\partial_\mu\, 2!\,\hat{\chi}^{\mu}{}_{\mu_1\mu_2}(x,x_1,x_2) = \\
&\quad \frac{1}{i\hbar c^2}\frac{-q}{mc^2} \quad \Big\{\delta(ct-ct_1)\theta(ct-ct_2) \quad \tilde{\delta}^{\mu}{}_{\mu_1}\partial_\mu\left(\delta^3(x-x_1)\left[\hat{j}^{(in0)\,0}(x),\hat{j}^{(in0)}_{\ \mu_2}(x_2)\right]\right) && \text{(S8a)}\\
&\qquad\qquad +\delta(ct-ct_2)\theta(ct-ct_1) \quad \tilde{\delta}^{\mu}{}_{\mu_2}\partial_\mu\left(\delta^3(x-x_2)\left[\hat{j}^{(in0)\,0}(x),\hat{j}^{(in0)}_{\ \mu_1}(x_1)\right]\right) && \text{(S8b)}\\
&\qquad\qquad +\delta(ct-ct_1)\delta(ct_1-ct_2)\tilde{\delta}_{\mu_1\,\mu_2} \quad \delta^3(x_1-x_2)\left[\hat{j}^{(in0)\,0}(x),\hat{j}^{(in0)}_{\ 0}(x_1)\right]\Big\} && \text{(S8c)}\\
&+\left(\frac{1}{i\hbar c^2}\right)^2 \quad \Big\{\delta(ct-ct_1)\theta(ct_1-ct_2)\left[\left[\hat{j}^{(in0)\,0}(x),\hat{j}^{(in0)}_{\ \mu_1}(x_1)\right],\hat{j}^{(in0)}_{\ \mu_2}(x_2)\right] && \text{(S8d)}\\
&\qquad\qquad +\delta(ct-ct_2)\theta(ct_2-ct_1)\left[\left[\hat{j}^{(in0)\,0}(x),\hat{j}^{(in0)}_{\ \mu_2}(x_2)\right],\hat{j}^{(in0)}_{\ \mu_1}(x_1)\right]\Big\}. && \text{(S8e)}
\end{aligned}
$$

Applying Eq.(S2), the third term (S8c) vanishes, and the fourth and fifth terms (S8d) and (S8e) cancel the first and second terms (S8a) and (S8b), respectively.

As a result, the second order nonlinear single susceptibility operator Eq.(41) in the main text maintains the charge conservation law, Eq.(24) in the main text.

To check the gauge invariance of the second order nonlinear single susceptibility operator, let us operate ∂^{μ_1} to Eq.(41) in the main text.

$$
\begin{aligned}
&\partial^{\mu_1}\, 2!\,\hat{\chi}^{\mu}{}_{\mu_1\mu_2}(x,x_1,x_2) = \\
&\frac{1}{i\hbar c^2}\frac{-q}{mc^2} \quad \Big\{\delta(ct-ct_1)\theta(ct-ct_2) \quad \left(\tilde{\delta}^{\mu}{}_{\mu_1}\partial^{\mu_1}\delta^3(x-x_1)\right)\left[\hat{j}^{(in0)\,0}(x),\hat{j}^{(in0)}_{\ \mu_2}(x_2)\right] && \text{(S9a)}\\
&\qquad\qquad -\delta(ct-ct_2)\delta(ct-ct_1) \quad \tilde{\delta}^{\mu}{}_{\mu_2} \quad \delta^3(x-x_2) \qquad \left[\hat{j}^{(in0)\,0}(x),\hat{j}^{(in0)}_{\ 0}(x_1)\right] && \text{(S9b)}\\
&\qquad\qquad +\theta(ct-ct_1)\delta(ct_1-ct_2)\tilde{\delta}_{\mu_1\,\mu_2}\partial^{\mu_1}\left(\delta^3(x_1-x_2)\left[\hat{j}^{(in0)\,\mu}(x),\hat{j}^{(in0)}_{\ 0}(x_1)\right]\right)\Big\} && \text{(S9c)}\\
&+\left(\frac{1}{i\hbar c^2}\right)^2 \quad \{(-\delta(ct-ct_1)\theta(ct_1-ct_2)+\theta(ct-ct_1)\delta(ct_1-ct_2))\\
&\qquad\qquad\qquad\qquad \left[\left[\hat{j}^{(in0)\,\mu}(x),\hat{j}^{(in0)}_{\ 0}(x_1)\right],\hat{j}^{(in0)}_{\ \mu_2}(x_2)\right] && \text{(S9d)}\\
&\qquad\qquad -\theta(ct-ct_2)\delta(ct_2-ct_1)\left[\left[\hat{j}^{(in0)\,\mu}(x),\hat{j}^{(in0)}_{\ \mu_2}(x_2)\right],\hat{j}^{(in0)}_{\ 0}(x_1)\right]\Big\}. && \text{(S9e)}
\end{aligned}
$$

Replacing the fifth term (S9e) using the next Jacobi identity:

$$\begin{aligned}&\left[\left[\hat{j}^{(in0)\,\mu}(x),\hat{j}^{(in0)}_{\ \ \mu_2}(x_2)\right],\hat{j}^{(in0)}_{\ \ 0}(x_1)\right] \\ =\ &-\left[\left[\hat{j}^{(in0)}_{\ \ \mu_2}(x_2),\hat{j}^{(in0)}_{\ \ 0}(x_1)\right],\hat{j}^{(in0)\,\mu}(x)\right]-\left[\left[\hat{j}^{(in0)}_{\ \ 0}(x_1),\hat{j}^{(in0)\,\mu}(x)\right],\hat{j}^{(in0)}_{\ \ \mu_2}(x_2)\right],\end{aligned} \tag{S10}$$

then, the first term in the right hand side of Eq.(S10) with Eq.(S2) offsets the term (S9c), and the second term in the right hand side of Eq.(S10) offsets the second term in (S9d). The first term in (S9d) offsets the first term, (S9a), considering the commutation relation at the simultaneous time, $\delta(ct-ct_1)\left[\hat{j}^{(in0)\,\mu}(x),\hat{j}^{(in0)}_{\ \ 0}(x_1)\right]$ and Eq.(S2)(remark the change of upper or lower subscript). The second term (S9b) vanishes by means of Eq.(S2).

As a result, the second order nonlinear single susceptibility operator Eq.(41) in the main text maintains the gauge invariance, Eq.(25) in the main text.

S 3. Third order nonlinear single susceptibility: Eq.(42) in the main text

With respect to the third order nonlinear single susceptibility, let us check the charge conservation law. Operating ∂_μ to Eq.(42) in the main text,

$$\begin{aligned}&\partial_\mu\, 3!\,\hat{\chi}^{\mu}_{\ \mu_1\mu_2\mu_3}(x,x_1,x_2,x_3)= \\ &\frac{1}{i\hbar c^2}\left(\frac{-q}{mc^2}\right)^2 \\ &\Big\{\theta(ct-ct_2)\delta(ct-ct_1)\delta(ct_2-ct_3)\tilde{\delta}_{\mu_2\,\mu_3}\delta^3(x_2-x_3)\tilde{\delta}^{\mu}_{\ \ \mu_1}\partial_\mu\left(\delta^3(x-x_1)\left[\hat{j}^{(in0)\,0}(x),\hat{j}^{(in0)}_{\ \ 0}(x_2)\right]\right) && \text{(S11a)}\\ &+\theta(ct-ct_3)\delta(ct-ct_2)\delta(ct_3-ct_1)\tilde{\delta}_{\mu_3\,\mu_1}\delta^3(x_3-x_1)\tilde{\delta}^{\mu}_{\ \ \mu_2}\partial_\mu\left(\delta^3(x-x_2)\left[\hat{j}^{(in0)\,0}(x),\hat{j}^{(in0)}_{\ \ 0}(x_3)\right]\right) && \text{(S11b)}\\ &+\theta(ct-ct_1)\delta(ct-ct_3)\delta(ct_1-ct_2)\tilde{\delta}_{\mu_1\,\mu_2}\delta^3(x_1-x_2)\tilde{\delta}^{\mu}_{\ \ \mu_3}\partial_\mu\left(\delta^3(x-x_3)\left[\hat{j}^{(in0)\,0}(x),\hat{j}^{(in0)}_{\ \ 0}(x_1)\right]\right)\Big\} && \text{(S11c)}\\ &+\left(\frac{1}{i\hbar c^2}\right)^2\frac{-q}{mc^2} \\ &\Big\{\delta(ct-ct_1)\theta(ct_1-ct_2)\theta(ct_2-ct_3)\tilde{\delta}^{\mu}_{\ \ \mu_1}\partial_\mu\left(\delta^3(x-x_1)\left[\left[\hat{j}^{(in0)\,0}(x),\hat{j}^{(in0)}_{\ \ \mu_2}(x_2)\right],\hat{j}^{(in0)}_{\ \ \mu_3}(x_3)\right]\right) && \text{(S11d)}\\ &+\delta(ct-ct_1)\theta(ct_1-ct_3)\theta(ct_3-ct_2)\tilde{\delta}^{\mu}_{\ \ \mu_1}\partial_\mu\left(\delta^3(x-x_1)\left[\left[\hat{j}^{(in0)\,0}(x),\hat{j}^{(in0)}_{\ \ \mu_3}(x_3)\right],\hat{j}^{(in0)}_{\ \ \mu_2}(x_2)\right]\right) && \text{(S11e)}\\ &+\delta(ct-ct_2)\theta(ct_2-ct_3)\theta(ct_3-ct_1)\tilde{\delta}^{\mu}_{\ \ \mu_2}\partial_\mu\left(\delta^3(x-x_2)\left[\left[\hat{j}^{(in0)\,0}(x),\hat{j}^{(in0)}_{\ \ \mu_3}(x_3)\right],\hat{j}^{(in0)}_{\ \ \mu_1}(x_1)\right]\right) && \text{(S11f)}\\ &+\delta(ct-ct_2)\theta(ct_2-ct_1)\theta(ct_1-ct_3)\tilde{\delta}^{\mu}_{\ \ \mu_2}\partial_\mu\left(\delta^3(x-x_2)\left[\left[\hat{j}^{(in0)\,0}(x),\hat{j}^{(in0)}_{\ \ \mu_1}(x_1)\right],\hat{j}^{(in0)}_{\ \ \mu_3}(x_3)\right]\right) && \text{(S11g)}\\ &+\delta(ct-ct_3)\theta(ct_3-ct_1)\theta(ct_1-ct_2)\tilde{\delta}^{\mu}_{\ \ \mu_3}\partial_\mu\left(\delta^3(x-x_3)\left[\left[\hat{j}^{(in0)\,0}(x),\hat{j}^{(in0)}_{\ \ \mu_1}(x_1)\right],\hat{j}^{(in0)}_{\ \ \mu_2}(x_2)\right]\right) && \text{(S11h)}\\ &+\delta(ct-ct_3)\theta(ct_3-ct_2)\theta(ct_2-ct_1)\tilde{\delta}^{\mu}_{\ \ \mu_3}\partial_\mu\left(\delta^3(x-x_3)\left[\left[\hat{j}^{(in0)\,0}(x),\hat{j}^{(in0)}_{\ \ \mu_2}(x_2)\right],\hat{j}^{(in0)}_{\ \ \mu_1}(x_1)\right]\right) && \text{(S11i)}\\ &+\delta(ct-ct_1)\delta(ct_1-ct_2)\theta(ct_2-ct_3)\tilde{\delta}_{\mu_1\,\mu_2}\delta^3(x_1-x_2)\left[\left[\hat{j}^{(in0)\,0}(x),\hat{j}^{(in0)}_{\ \ 0}(x_1)\right],\hat{j}^{(in0)}_{\ \ \mu_3}(x_3)\right] && \text{(S11j)}\end{aligned}$$

$$+\delta(ct-ct_2)\delta(ct_2-ct_3)\theta(ct_3-ct_1)\tilde{\delta}_{\mu_2\,\mu_3}\delta^3(x_2-x_3)\left[\left[\hat{j}^{(in0)\,0}(x),\hat{j}^{(in0)}_{\ 0}(x_2)\right],\hat{j}^{(in0)}_{\ \mu_1}(x_1)\right] \tag{S11k}$$

$$+\delta(ct-ct_3)\delta(ct_3-ct_1)\theta(ct_1-ct_2)\tilde{\delta}_{\mu_3\,\mu_1}\delta^3(x_3-x_1)\left[\left[\hat{j}^{(in0)\,0}(x),\hat{j}^{(in0)}_{\ 0}(x_3)\right],\hat{j}^{(in0)}_{\ \mu_2}(x_2)\right] \tag{S11l}$$

$$+\delta(ct-ct_1)\theta(ct_1-ct_2)\delta(ct_2-ct_3)\tilde{\delta}_{\mu_2\,\mu_3}\delta^3(x_2-x_3)\left[\left[\hat{j}^{(in0)\,0}(x),\hat{j}^{(in0)}_{\ \mu_1}(x_1)\right],\hat{j}^{(in0)}_{\ 0}(x_2)\right] \tag{S11m}$$

$$+\delta(ct-ct_2)\theta(ct_2-ct_3)\delta(ct_3-ct_1)\tilde{\delta}_{\mu_3\,\mu_1}\delta^3(x_3-x_1)\left[\left[\hat{j}^{(in0)\,0}(x),\hat{j}^{(in0)}_{\ \mu_2}(x_2)\right],\hat{j}^{(in0)}_{\ 0}(x_3)\right] \tag{S11n}$$

$$+\delta(ct-ct_3)\theta(ct_3-ct_1)\delta(ct_1-ct_2)\tilde{\delta}_{\mu_1\,\mu_2}\delta^3(x_1-x_2)\left[\left[\hat{j}^{(in0)\,0}(x),\hat{j}^{(in0)}_{\ \mu_3}(x_3)\right],\hat{j}^{(in0)}_{\ 0}(x_1)\right]\Big\} \tag{S11o}$$

$$+\left(\frac{1}{i\hbar c^2}\right)^3$$

$$\Big\{\delta(ct-ct_1)\theta(ct_1-ct_2)\theta(ct_2-ct_3)\left[\left[\left[\hat{j}^{(in0)\,0}(x),\hat{j}^{(in0)}_{\ \mu_1}(x_1)\right],\hat{j}^{(in0)}_{\ \mu_2}(x_2)\right],\hat{j}^{(in0)}_{\ \mu_3}(x_3)\right] \tag{S11p}$$

$$+\delta(ct-ct_1)\theta(ct_1-ct_3)\theta(ct_3-ct_2)\left[\left[\left[\hat{j}^{(in0)\,0}(x),\hat{j}^{(in0)}_{\ \mu_1}(x_1)\right],\hat{j}^{(in0)}_{\ \mu_3}(x_3)\right],\hat{j}^{(in0)}_{\ \mu_2}(x_2)\right] \tag{S11q}$$

$$+\delta(ct-ct_2)\theta(ct_2-ct_3)\theta(ct_3-ct_1)\left[\left[\left[\hat{j}^{(in0)\,0}(x),\hat{j}^{(in0)}_{\ \mu_2}(x_2)\right],\hat{j}^{(in0)}_{\ \mu_3}(x_3)\right],\hat{j}^{(in0)}_{\ \mu_1}(x_1)\right] \tag{S11r}$$

$$+\delta(ct-ct_2)\theta(ct_2-ct_1)\theta(ct_1-ct_3)\left[\left[\left[\hat{j}^{(in0)\,0}(x),\hat{j}^{(in0)}_{\ \mu_2}(x_2)\right],\hat{j}^{(in0)}_{\ \mu_1}(x_1)\right],\hat{j}^{(in0)}_{\ \mu_3}(x_3)\right] \tag{S11s}$$

$$+\delta(ct-ct_3)\theta(ct_3-ct_1)\theta(ct_1-ct_2)\left[\left[\left[\hat{j}^{(in0)\,0}(x),\hat{j}^{(in0)}_{\ \mu_3}(x_3)\right],\hat{j}^{(in0)}_{\ \mu_1}(x_1)\right],\hat{j}^{(in0)}_{\ \mu_2}(x_2)\right] \tag{S11t}$$

$$+\delta(ct-ct_3)\theta(ct_3-ct_2)\theta(ct_2-ct_1)\left[\left[\left[\hat{j}^{(in0)\,0}(x),\hat{j}^{(in0)}_{\ \mu_3}(x_3)\right],\hat{j}^{(in0)}_{\ \mu_2}(x_2)\right],\hat{j}^{(in0)}_{\ \mu_1}(x_1)\right]\Big\}. \tag{S11u}$$

The term (S11p) offsets the term (S11d), applying Eq.(S2) to the most inner commutator in (S11p). In the same manner, the terms (S11q)-(S11u),respectively, offsets the terms (S11e)-(S11i), applying Eq.(S2). The terms (S11j)-(S11l) vanishes, applying Eq.(S2) to the inner commutator at the simultaneous time. The term (S11m) offsets the term (S11a), applying Eq.(S2) to the most inner commutator. In the same manner, the terms (S11n)-(S11o), respectively, offsets (S11b)-(S11c), using Eq.(S2).

As a result, the third order nonlinear single susceptibility operator Eq.(42) in the main text maintains the charge conservation law, Eq.(24) in the main text.

To check the gauge invariance of the third order nonlinear single susceptibility operator, let us operate ∂^{μ_1} to Eq.(42) in the main text.

$$\partial^{\mu_1}\,3!\,\hat{\chi}^{\mu}_{\ \mu_1\mu_2\mu_3}(x,x_1,x_2,x_3)=$$

$$\frac{1}{i\hbar c^2}\left(\frac{-q}{mc^2}\right)^2$$

$$\Big\{\theta(ct-ct_2)\delta(ct-ct_1)\delta(ct_2-ct_3)\left(\tilde{\delta}^{\mu}_{\ \mu_1}\partial^{\mu_1}\delta^3(x-x_1)\right)\tilde{\delta}_{\mu_2\,\mu_3}\delta^3(x_2-x_3)\left[\hat{j}^{(in0)\,0}(x),\hat{j}^{(in0)}_{\ 0}(x_2)\right] \tag{S12a}$$

$$+\theta(ct-ct_3)\delta(ct-ct_2)\delta(ct_3-ct_1)\tilde{\delta}^{\mu}_{\ \mu_2}\delta^3(x-x_2)\left(\tilde{\delta}_{\mu_3\,\mu_1}\partial^{\mu_1}\delta^3(x_3-x_1)\right)\left[\hat{j}^{(in0)\,0}(x),\hat{j}^{(in0)}_{\ 0}(x_3)\right] \tag{S12b}$$

$$+\,\theta(ct-ct_1)\delta(ct-ct_3)\delta(ct_1-ct_2)\tilde{\delta}^{\mu}_{\ \mu_3}\delta^3(x-x_3)\left(\tilde{\delta}_{\mu_1\,\mu_2}\partial^{\mu_1}\delta^3(x_1-x_2)\left[\hat{j}^{(in0)\,0}(x),\hat{j}^{(in0)}_{\ 0}(x_1)\right]\right)\Big\} \tag{S12c}$$

$$+\left(\frac{1}{i\hbar c^2}\right)^2\frac{-q}{mc^2}$$

$$\Big\{\delta(ct-ct_1)\theta(ct_1-ct_2)\theta(ct_2-ct_3)\left(\tilde{\delta}^{\mu}{}_{\mu_1}\partial^{\mu_1}\delta^3(x-x_1)\right)\left[\left[\hat{j}^{(in0)\,0}(x),\hat{j}^{(in0)}_{\mu_2}(x_2)\right],\hat{j}^{(in0)}_{\mu_3}(x_3)\right] \tag{S12d}$$

$$+\delta(ct-ct_1)\theta(ct_1-ct_3)\theta(ct_3-ct_2)\left(\tilde{\delta}^{\mu}{}_{\mu_1}\partial^{\mu_1}\delta^3(x-x_1)\right)\left[\left[\hat{j}^{(in0)\,0}(x),\hat{j}^{(in0)}_{\mu_3}(x_3)\right],\hat{j}^{(in0)}_{\mu_2}(x_2)\right] \tag{S12e}$$

$$-\delta(ct-ct_2)\theta(ct_2-ct_3)\delta(ct_3-ct_1)\tilde{\delta}^{\mu}{}_{\mu_2}\delta^3(x-x_2)\left[\left[\hat{j}^{(in0)\,0}(x),\hat{j}^{(in0)}_{\mu_3}(x_3)\right],\hat{j}^{(in0)}_{0}(x_1)\right] \tag{S12f}$$

$$+\left(-\delta(ct-ct_2)\delta(ct_2-ct_1)\theta(ct_1-ct_3)+\delta(ct-ct_2)\theta(ct_2-ct_1)\delta(ct_1-ct_3)\right)$$

$$\tilde{\delta}^{\mu}{}_{\mu_2}\delta^3(x-x_2)\left[\left[\hat{j}^{(in0)\,0}(x),\hat{j}^{(in0)}_{0}(x_1)\right],\hat{j}^{(in0)}_{\mu_3}(x_3)\right] \tag{S12g}$$

$$+\left(-\delta(ct-ct_3)\delta(ct_3-ct_1)\theta(ct_1-ct_2)+\delta(ct-ct_3)\theta(ct_3-ct_1)\delta(ct_1-ct_2)\right)$$

$$\tilde{\delta}^{\mu}{}_{\mu_3}\delta^3(x-x_3)\left[\left[\hat{j}^{(in0)\,0}(x),\hat{j}^{(in0)}_{0}(x_1)\right],\hat{j}^{(in0)}_{\mu_2}(x_2)\right] \tag{S12h}$$

$$-\delta(ct-ct_3)\theta(ct_3-ct_2)\delta(ct_2-ct_1)\tilde{\delta}^{\mu}{}_{\mu_3}\delta^3(x-x_3)\left[\left[\hat{j}^{(in0)\,0}(x),\hat{j}^{(in0)}_{\mu_2}(x_2)\right],\hat{j}^{(in0)}_{0}(x_1)\right] \tag{S12i}$$

$$+\theta(ct-ct_1)\delta(ct_1-ct_2)\theta(ct_2-ct_3)\tilde{\delta}_{\mu_1\,\mu_2}\partial^{\mu_1}\left(\delta^3(x_1-x_2)\left[\left[\hat{j}^{(in0)\,\mu}(x),\hat{j}^{(in0)}_{0}(x_1)\right],\hat{j}^{(in0)}_{\mu_3}(x_3)\right]\right) \tag{S12j}$$

$$-\theta(ct-ct_2)\delta(ct_2-ct_3)\delta(ct_3-ct_1)\tilde{\delta}_{\mu_2\,\mu_3}\delta^3(x_2-x_3)\left[\left[\hat{j}^{(in0)\,\mu}(x),\hat{j}^{(in0)}_{0}(x_2)\right],\hat{j}^{(in0)}_{0}(x_1)\right] \tag{S12k}$$

$$+\theta(ct-ct_3)\delta(ct_3-ct_1)\theta(ct_1-ct_2)\tilde{\delta}_{\mu_3\,\mu_1}\left(\partial^{\mu_1}\delta^3(x_3-x_1)\right)\left[\left[\hat{j}^{(in0)\,\mu}(x),\hat{j}^{(in0)}_{0}(x_3)\right],\hat{j}^{(in0)}_{\mu_2}(x_2)\right] \tag{S12l}$$

$$+\left(-\delta(ct-ct_1)\theta(ct_1-ct_2)\delta(ct_2-ct_3)+\theta(ct-ct_1)\delta(ct_1-ct_2)\delta(ct_2-ct_3)\right)$$

$$\tilde{\delta}_{\mu_2\,\mu_3}\delta^3(x_2-x_3)\left[\left[\hat{j}^{(in0)\,\mu}(x),\hat{j}^{(in0)}_{0}(x_1)\right],\hat{j}^{(in0)}_{0}(x_2)\right] \tag{S12m}$$

$$+\theta(ct-ct_2)\theta(ct_2-ct_3)\delta(ct_3-ct_1)\left(\tilde{\delta}_{\mu_3\,\mu_1}\partial^{\mu_1}\delta^3(x_3-x_1)\right)\left[\left[\hat{j}^{(in0)\,\mu}(x),\hat{j}^{(in0)}_{\mu_2}(x_2)\right],\hat{j}^{(in0)}_{0}(x_3)\right] \tag{S12n}$$

$$+\theta(ct-ct_3)\theta(ct_3-ct_1)\delta(ct_1-ct_2)\tilde{\delta}_{\mu_1\,\mu_2}\partial^{\mu_1}\left(\delta^3(x_1-x_2)\left[\left[\hat{j}^{(in0)\,\mu}(x),\hat{j}^{(in0)}_{\mu_3}(x_3)\right],\hat{j}^{(in0)}_{0}(x_1)\right]\right)\Big\} \tag{S12o}$$

$$+\left(\frac{1}{i\hbar c^2}\right)^3$$

$$\{\left(-\delta(ct-ct_1)\theta(ct_1-ct_2)\theta(ct_2-ct_3)+\theta(ct-ct_1)\delta(ct_1-ct_2)\theta(ct_2-ct_3)\right)$$

$$\left[\left[\left[\hat{j}^{(in0)\,\mu}(x),\hat{j}^{(in0)}_{0}(x_1)\right],\hat{j}^{(in0)}_{\mu_2}(x_2)\right],\hat{j}^{(in0)}_{\mu_3}(x_3)\right] \tag{S12p}$$

$$+\left(-\delta(ct-ct_1)\theta(ct_1-ct_3)\theta(ct_3-ct_2)+\theta(ct-ct_1)\delta(ct_1-ct_3)\theta(ct_3-ct_2)\right)$$

$$\left[\left[\left[\hat{j}^{(in0)\,\mu}(x),\hat{j}^{(in0)}_{0}(x_1)\right],\hat{j}^{(in0)}_{\mu_3}(x_3)\right],\hat{j}^{(in0)}_{\mu_2}(x_2)\right] \tag{S12q}$$

$$-\theta(ct-ct_2)\theta(ct_2-ct_3)\delta(ct_3-ct_1)\left[\left[\left[\hat{j}^{(in0)\,\mu}(x),\hat{j}^{(in0)}_{\mu_2}(x_2)\right],\hat{j}^{(in0)}_{\mu_3}(x_3)\right],\hat{j}^{(in0)}_{0}(x_1)\right] \tag{S12r}$$

$$+\left(-\theta(ct-ct_2)\delta(ct_2-ct_1)\theta(ct_1-ct_3)+\theta(ct-ct_2)\theta(ct_2-ct_1)\delta(ct_1-ct_3)\right)$$

$$\left[\left[\left[\hat{j}^{(in0)\,\mu}(x),\hat{j}^{(in0)}_{\mu_2}(x_2)\right],\hat{j}^{(in0)}_{0}(x_1)\right],\hat{j}^{(in0)}_{\mu_3}(x_3)\right] \tag{S12s}$$

$$+\left(-\theta(ct-ct_3)\delta(ct_3-ct_1)\theta(ct_1-ct_2)+\theta(ct-ct_3)\theta(ct_3-ct_1)\delta(ct_1-ct_2)\right)$$

$$\left[\left[\left[\hat{j}^{(in0)\,\mu}(x),\hat{j}^{(in0)}_{\mu_3}(x_3)\right],\hat{j}^{(in0)}_{0}(x_1)\right],\hat{j}^{(in0)}_{\mu_2}(x_2)\right] \tag{S12t}$$

$$-\theta(ct-ct_3)\theta(ct_3-ct_2)\delta(ct_2-ct_1)\left[\left[\left[\hat{j}^{(in0)\,\mu}(x),\hat{j}^{(in0)}_{\mu_3}(x_3)\right],\hat{j}^{(in0)}_{\mu_2}(x_2)\right],\hat{j}^{(in0)}_{0}(x_1)\right]\Big\}. \tag{S12u}$$

In the following, we prove the next equation, which leads to the gauge invariance.

$$\begin{aligned}
\text{(S12p)} + \text{(S12d)} + \text{(S12j)} + \text{(S12s)} + \text{(S12r)} + \text{(S12n)} &= 0, && \text{(S13)}\\
\text{(S12q)} + \text{(S12e)} + \text{(S12l)} + \text{(S12t)} + \text{(S12u)} + \text{(S12o)} &= 0, && \text{(S14)}\\
\text{(S12m)} + \text{(S12a)} + \text{(S12k)} &= 0, && \text{(S15)}\\
\text{(S12i)} + \text{(S12c)} + \text{(S12h)} &= 0, && \text{(S16)}\\
\text{(S12f)} + \text{(S12b)} + \text{(S12g)} &= 0. && \text{(S17)}
\end{aligned}$$

1. Eq.(S13): The first term of (S12p) offsets (S12d), using Eq.(S2). To the inner double commutator in the second term of (S12p), the nest Jacobi identity is applied:

$$\begin{aligned}
&\left[\left[\left[\hat{j}^{(in0)\,\mu}(x), \hat{j}^{(in0)}_{\ 0}(x_1)\right], \hat{j}^{(in0)}_{\ \mu_2}(x_2)\right], \hat{j}^{(in0)}_{\ \mu_3}(x_3)\right] \qquad \text{(S18)}\\
= &-\left[\left[\left[\hat{j}^{(in0)}_{\ 0}(x_1), \hat{j}^{(in0)}_{\ \mu_2}(x_2)\right], \hat{j}^{(in0)\,\mu}(x)\right], \hat{j}^{(in0)}_{\ \mu_3}(x_3)\right]\\
&-\left[\left[\left[\hat{j}^{(in0)}_{\ \mu_2}(x_2), \hat{j}^{(in0)\,\mu}(x)\right], \hat{j}^{(in0)}_{\ 0}(x_1)\right], \hat{j}^{(in0)}_{\ \mu_3}(x_3)\right].
\end{aligned}$$

   Furthermore, the inner commutator (, assuming at the simultaneous time) in the first term of Eq.(S18) , one may apply Eq.(S2). The part including this factor in the second term of (S12p) offsets the term (S12j). In the second term of (S12p), the part including the second term of Eq.(S18) offsets the first term of (S12s). Up to now, (S12p)+(S12d)+(S12j)+ the first term of (S12s)= 0 has been shown.

   Next, to the outer double commutator in the second term of (S12r), let us apply the next Jacobi identity,

$$\begin{aligned}
&\left[\left[\left[\hat{j}^{(in0)\,\mu}(x), \hat{j}^{(in0)}_{\ \mu_2}(x_2)\right], \hat{j}^{(in0)}_{\ \mu_3}(x_3)\right], \hat{j}^{(in0)}_{\ 0}(x_1)\right] \qquad \text{(S19)}\\
= &-\left[\left[\hat{j}^{(in0)}_{\ \mu_3}(x_3), \hat{j}^{(in0)}_{\ 0}(x_1)\right], \left[\hat{j}^{(in0)\,\mu}(x), \hat{j}^{(in0)}_{\ \mu_2}(x_2)\right]\right]\\
&+\left[\left[\left[\hat{j}^{(in0)\,\mu}(x), \hat{j}^{(in0)}_{\ \mu_2}(x_2)\right], \hat{j}^{(in0)}_{\ 0}(x_1)\right], \hat{j}^{(in0)}_{\ \mu_3}(x_3)\right].
\end{aligned}$$

   The commutator in the first term of Eq.(S19): $\left[\hat{j}^{(in0)}_{\ \mu_3}(x_3), \hat{j}^{(in0)}_{\ 0}(x_1)\right]$ is the commutator at the simultaneous time, therefore, we may use Eq.(S2). The part including this factor in (S12r) offsets the term (S12n). In (S12r), the part including the second term of Eq.(S19) offsets the second term of (S12s). Up to now, (S12r)+(S12n)+ the second term of (S12s)= 0 is shown.

   Together with the previous result, Eq.(S13) holds.

2. Eq.(S14): This equation is Eq.(S13) with the replacement $x_2 \leftrightarrow x_3$ and $\mu_2 \leftrightarrow \mu_3$, therefore, Eq.(S14) holds.

3. Eq.(S15): The first term of (S12m) offsets (S12a), using Eq.(S2).

   To the double commutator in the second term of (S12m), the nest Jacobi identity is applied:

$$\begin{aligned} & \left[\left[\hat{j}^{(in0)\,\mu}(x), \hat{j}^{(in0)}_{\ 0}(x_1)\right], \hat{j}^{(in0)}_{\ 0}(x_2)\right] \\ = & -\left[\left[\hat{j}^{(in0)}_{\ 0}(x_1), \hat{j}^{(in0)}_{\ 0}(x_2)\right], \hat{j}^{(in0)\,\mu}(x)\right] - \left[\left[\hat{j}^{(in0)}_{\ 0}(x_2), \hat{j}^{(in0)\,\mu}(x)\right], \hat{j}^{(in0)}_{\ 0}(x_1)\right] \\ = & \left[\left[\hat{j}^{(in0)\,\mu}(x), \hat{j}^{(in0)}_{\ 0}(x_2)\right], \hat{j}^{(in0)}_{\ 0}(x_1)\right] \end{aligned} \tag{S20}$$

   In the above, we use the inner commutator (at the simulatenesou time) in the first term of the second hand side becomes zero, using Eq.(S2). The second term of (S12m) includes the factor of Eq.(S20) and offsets (S12k).

   As a result, Eq.(S15) holds.

4. Eq.(S16): To the double commutator in (S12i), we apply the next Jacobi identity:

$$\begin{aligned} & \left[\left[\hat{j}^{(in0)\,0}(x), \hat{j}^{(in0)}_{\ \mu_2}(x_2)\right], \hat{j}^{(in0)}_{\ 0}(x_1)\right] \\ = & -\left[\left[\hat{j}^{(in0)}_{\ \mu_2}(x_2), \hat{j}^{(in0)}_{\ 0}(x_1)\right], \hat{j}^{(in0)\,0}(x)\right] - \left[\left[\hat{j}^{(in0)}_{\ 0}(x_1), \hat{j}^{(in0)\,0}(x)\right], \hat{j}^{(in0)}_{\ \mu_2}(x_2)\right]. \end{aligned} \tag{S21}$$

   The inner commutator in the first term of Eq.(S21) is the commutator at the simultaneous time, therefore, we may use Eq.(S2). The part including this factor in (S12i) offsets the term (S12c). In (S12i), the part including the second term of Eq.(S21) offsets the second term of (S12h). The first term of (S12h) is zero, because the inner commutator included in this term is commutator at the simultaneous time and leads to zero, using Eq.(S2).

   Therefore, Eq.(S16) holds.

5. Eq.(S17): This equation is Eq.(S16) with the replacement $x_2 \leftrightarrow x_3$ and $\mu_2 \leftrightarrow \mu_3$, therefore, Eq.(S17) holds.

As the summery, Eqs.(S13)-(S17) hold and the third order nonlinear single susceptibility Eq.(42) in the main text maintains the gauge invariance Eq.(25) in the main text.

Photon localization revisited

Izumi Ojima*
Otsu 520-0105, Japan
and
Hayato Saigo†
Nagahama Institute of Bio-Science and Technology
Nagahama 526-0829, Japan

Abstract

In the light of Newton-Wigner-Wightman theorem of localizability question, we have proposed before a typical generation mechanism of effective mass for photons to be localized in the form of polaritons owing to photon-media interactions. In this paper, the general essence of this example model is extracted in such a form as Quantum Field Ontology associated with Eventualization Principle, which enables us to explain the mutual relations, back and forth, between quantum fields and various forms of particles in the localized form of the former.

1 Introduction

Extending the scope of our joint paper [24] whose essense is summarized in 1) and 2) below, we discuss in this paper the following points:

1) Starting from a specific problem of photon localization in the light of Newton-Wigner-Wightman Theorem (Sec.2), we try here to clarify the mathematical and conceptual relations among spatial points, localization processes of physical systems into restricted regions in space (and time), in contrast to the usual formulation dependent directly on the concepts of particles and their masses (in a spacetime structure given in an *a priori* way). In this context, Wightman's mathematical formulation of the Newton-Wigner paper plays an important role: On the basis of an imprimitivity system on the 3-dimensional space, the absence of position observables is shown to follow from the vanishing mass $m = 0$ of a free photon.

2) We encounter here a sharp conflict between the mathematically clear-cut negative result and the actual existence of experimental devices for detecting photons in quantum optics which is impossible without the spatial

*E-mail: ojima@kurims.kyoto-u.ac.jp
†E-mail: h_saigoh@nagahama-i-bio.ac.jp

localization of detected photons. Fortunately, this conflict is resolved by the presence of coupled modes of photons with material media which generates non-trivial deviations of refractive index n from 1, or equivalently generates the mass $m > 0$, in such typical example cases as "polaritons", as will be shown later (Sec.3.4).

3) Through the model example of polaritons, we learn that such fundamental issues as related with mass and particles as its carriers should be viewed as something variable dependent on the contexts and situations surrounding them. Thus, we need and can elaborate on highly philosophical abstract questions like "what is a mass?" or "what are particles as mass points?", in mathematically accessible contexts. For this purpose, we certainly need to set up suitable theoretical and/or mathematical frameworks and models so that they allow us to systematically control the dynamics of our object systems coupled with their external systems. Once this coupling scheme is established, the external systems can be seen to serve as reference systems for the purpose of describing the object systems and the processes carried out by them. Such a framework and methodology are available in the form of the Tomita's integral decomposition theorem (Sec. 4.3) viewed from the standpoint of "quadrality scheme" based on "Micro-Macro duality" (Sec. 3.2 & Sec. 4.2).

4) For instance, the delicate choice between 4-dimensional spacetime and 3-dimensional spatial setting up involved in Wightman's theorem can be naturally understood as the choice of pertinent variables to a given context. In the light of Tomita's theorem this issue is seen in such a form as the choice between central vs. subcentral decomposition measures of a relevant state. A satisfactory understanding of fundamental concepts of space (and time) coordinates and velocities is attainable in the scheme and, at the same time, crucial premise underlying such comprehension is the understanding that these concepts are never among pre-existing attributes inherent in the object system but are epigenetic properties emerging through what is to be called the "eventualization processes" as will be explained in Sec.5. These epigenetic aspects are closely related with the choices of different contexts of placing an object system and the boundary conditions specifying various different choices of subalgebras of central observables, reflected in the choices of subcentral (or central) measures appearing in Tomita's theorem (Sec. 4.3).

5) While the above explanation guarantees the naturality and genericity of the polariton picture mentioned in 2), as one of the typical explicit examples for making photons localizable, the freedom in choices of subcentral measures clarifies their speciality in the *spatial homogeneity* of mass generation. In fact, under such conditions that the spatial homogeneity is *not* required, many such forms of photon localizations are allowed as Debye shielding, various forms of dressed photons, among which cavity QED can equally be understandable.

6) Along this line of thought, it becomes also possible to compare and unify various other forms of localizations and of their "leakages" at the same time: For instance, the presence of non-vanishing mass m can be viewed as an index of timelike and spacetime-homogeneous parameter of leakage from spatial localization as exhibited by the decay rate $\propto e^{-mr}$ of correlation functions in clustering limit. On the other hand, the decay width Γ in the energy spectrum can also be interpreted as a time-homogeneous parameter of leakage from chronological localizations of resonance modes (as exhibited through the decay rate $\propto e^{-\Gamma/2}$ of relaxation of correlations). (To be precise, it is more appropriate to regard the inverse of m and Γ as leakages.) The tunneling rate $\propto \sqrt{|E-V|}$ can be interpreted as the leakage rate of spatial localization materialized by the potential barrier V.

7) The universality, naturality and the necessity of the present standpoint is verified by the above considerations in terms of subcentral measures and of the corresponding commutative algebras $\mathcal{B}$. On the basis of the bidirectionality between quantum fields and particles, moreover, such a unified viewpoint will be meaningful that the microscopic quantum systems consisting of quantum fields can be controlled and designed from the macro side via the control of quantum fields.

8) To make sure of the above possibility, it would be important to recognize the constitution of the macroscopic levels in close relations with the microscopic quantum regimes. This question is answered in terms of the word, "eventualization processes", which can be mathematically described as the filtered "cones" to amplify the connections between Macro and Micro (which is analogous to the forcing method in the context of foudations of mathematics), with Micro ends given by the dynamics of quantum fields and Macro ones by the pointlike events as the apices of cones of eventualizations.

2 Newton-Wigner-Wightman Theorem

In 1949, Newton and Wigner [15] raised the question of localizability of single free particles. They attempted to formulate the properties of the localized states on the basis of natural requirements of relativistic covariance.

Physical quantities available in this formulation admitting direct physical meaning are restricted inevitably to the generators of Poincaré group $\mathcal{P}_+^\uparrow = \mathbb{R}^4 \rtimes L_+^\uparrow$ (with $L_+^\uparrow$ the orthochronous proper Lorentz group) which is locally isomorphic to the semi-direct product $\mathcal{H}_2(\mathbb{C}) \rtimes SL(2,\mathbb{C})$ of the Jordan algebra $\mathcal{H}_2(\mathbb{C})$ of hermitian (2×2)-matrices and $SL(2,\mathbb{C})$, consisting of the energy-momentum vector P_μ and of the Lorentz generators $M_{\mu\nu}$ (composed of angular momenta M_{ij} and of Lorentz boosts M_{0i}). The problem is then to find conditions under which "position operators" can naturally be derived from the Poincaré generators $(P_\mu, M_{\mu\nu})$. In [15], position operators

have been shown to exist in massive cases in an essentially unique way for "elementary" systems in the sense of the irreducibility of the corresponding representations of $\mathcal{P}_+^\uparrow$ so that localizability of a state can be defined in terms of such position operators. In massless cases, however, no localized states are found to exist in the above sense. That was the beginning of the story.

Wightman [25] clarified the situation by recapturing the concept of "localization" in quite a general form as follows. In place of the usual approaches with unbounded generators of position operators, he has formulated the problem in terms of their spectral resolution in the form of axioms (i)-(iii) :

(i) The spectral resolution of position operators: It is defined by a family $\mathcal{B}(\mathbb{R}^3) \ni \Delta \longmapsto E(\Delta) \in Proj(\mathfrak{H})$ of projection-valued measures $E(\Delta)$ in a Hilbert space $\mathfrak{H}$ defined for each Borel subset Δ of $\mathbb{R}^3$, characterized by the following properties (ia), (ib), (ic):

(ia) $E(\Delta_1 \cap \Delta_2) = E(\Delta_1)E(\Delta_2)$;

(ib) $E(\Delta_1 \cup \Delta_2) = E(\Delta_1) + E(\Delta_2)$, if $\Delta_1 \cap \Delta_2 = \phi$;

(ic) $E(\mathbb{R}^3) = 1$;

(ii) Physical interpretation of $E(\Delta)$: When the system is prepared in a state ω, the expectation value $\omega(E(\Delta))$ of a spectral measure $E(\Delta)$ gives the probability for the system to be found in a localized region Δ;

(iii) Covariance of the spectral resolution: Under a transformation $(\mathbf{a}, \mathcal{R})$ with a spatial rotation $\mathcal{R}$ followed by a spatial translation $\mathbf{a}$, a Borel subset Δ is transformed into $\mathcal{R}\Delta + \mathbf{a}$. The corresponding unitary implementer is given in $\mathfrak{H}$ by $U(\mathbf{a}, \mathcal{R})$, which represents $(\mathbf{a}, \mathcal{R})$ covariantly on E in such a way that

$$E(\Delta) \to E(\mathcal{R}\Delta + \mathbf{a}) = U(\mathbf{a}, \mathcal{R})E(\Delta)U(\mathbf{a}, \mathcal{R})^{-1}.$$

Note that, in spite of the relevance of the relativistic covariance, localizability discussed above is the *localization of states in space at a given time* formulated in terms of *spatial* translations $\mathbf{a}$ and rotations $\mathcal{R}$, respectively. To understand the reason, one should imagine the situation with the axioms (i)-(iii) replaced with those for the whole spacetime; then the CCR relations hold between 4-momenta p_μ and space-time coordinates x^ν, which implies the Lebesgue spectrum covering the whole $\mathbb{R}^4$ for both observables $\hat{p}_\mu$ and $\hat{x}^\nu$. Therefore any such physical requirements as the spectrum condition or as the mass spectrum cannot be imposed on the energy-momentum spectrum $\hat{p}_\mu$, and hence, the concept of localizability in space-time does not make sense.

According to Mackey's theory of induced representations, Wightman's formulation can easily be seen as the condition for the family of operators $\{E(\Delta)\}$ to constitute a *system of imprimitivity* ([12]) under the action of the unitary representation $U(\mathbf{a}, \mathcal{R})$ in $\mathfrak{H}$ of the three-dimensional Euclidean group $SE(3) := \mathbb{R}^3 \rtimes SO(3)$ given by the semi-direct product of the spatial translations $\mathbb{R}^3$ and the rotation group $SO(3)$. In a more algebraic form, the pair (E, U) can also be viewed as a *covariant W*-dynamical system* $L^\infty(\mathbb{R}^3) \underset{\tau}{\curvearrowleft} SE(3), [\tau_{(\mathbf{a},\mathcal{R})}(f)](\mathbf{x}) := f(\mathcal{R}^{-1}(\mathbf{x} - \mathbf{a}))$, given by the covariant *-representation $E : L^\infty(\mathbb{R}^3) \ni f \longmapsto E(f) = \int f(\mathbf{x}) dE(\mathbf{x}) \in B(\mathfrak{H})$, s.t. $E(\chi_\Delta) = E(\Delta)$, of the commutative algebra $L^\infty(\mathbb{R}^3)$ generated by the position operators acted on by $SE(3)$ characterized by the *covariance condition*:

$$E(\tau_{(\mathbf{a},\mathcal{R})}(f)) = U(a, \mathcal{R}) E(f) U(a, \mathcal{R})^{-1} \quad (1)$$
$$\text{for } f \in L^\infty(\mathbb{R}^3), (\mathbf{a}, \mathcal{R}) \in SE(3).$$

As will be seen later, this algebraic reformulation turns out to be useful for constructing coupled systems of photon degrees of freedom with matter systems, which play the crucial roles in observing or measuring the former in the actual situations. Thus Wightman's formulation of the Newton-Wigner localizability problem is just to examine whether the Hilbert space $\mathfrak{H}$ of the representation $(U, \mathfrak{H})$ of $SE(3)$ can accommodate a representation E of the algebra $L^\infty(\mathbb{R}^3)$ consisting of position operators, covariant under the action of $SE(3)$ in the sense of Eq. (1).

Applying Mackey's general theory to the case of three-dimensional Euclidean group $SE(3)$, Wightman proved the following fundamental result as a purely kinematical consequence:

Theorem 1 ([25], excerpt from theorem 6 and 7) *A Lorentz covariant massive system is always localizable. The only localizable massless elementary system (i.e. irreducible representation) has spin zero.*

Corollary 2 *A free photon is not localizable.*

The essential mechanism causing (non-)localizability in the sense of Newton-Wigner-Wightman can be found in the structure of Wigner's little groups, the stabilizer groups of standard 4-momenta on each type of $\mathcal{P}_+^\uparrow$-orbits in p-space.

When $m \neq 0$, the little group corresponding to the residual degrees of freedom in a rest frame is the group $SO(3)$ of spatial rotations. As a consequence, "the space of rest frames" becomes $SO(1,3)/SO(3) \cong \mathbb{R}^3$. The physical meaning of this homeomorphism is just a correspondence between a rest frame $r \in SO(1,3)/SO(3)$ for registering positions and a boost $k \in SO(1,3)$ required for transforming a fixed rest frame r_0 to the chosen one $r = kr_0$. The universality (or, independence for the choice the frame) of positions is recovered up to Compton wavelength $h/(mc)$, again due to massiveness.

Remark 3 *Here the coordinates of rest frames just plays the role of the order parameters (or, "sector parameters") on each $\mathcal{P}_+^\uparrow$-orbit as the space of "degenerate vacua" associated with certain of symmetry breaking, which should play the roles of position operators appearing in the imprimitivity system.*

In sharp contrast, there is *no* rest frame for a massless particle: Its little group is isomorphic to the two-dimensional Euclidean group $SE(2) = \mathbb{R}^2 \rtimes SO(2)$ (locally isomorphic to $\mathbb{C} \rtimes U(1)$), whose rotational generator corresponds to the helicity. Since the other two translation generators corresponding to gauge transformations span *non-compact* directions in distinction from the massive cases with a compact $SO(3)$, the allowed representation (without indefinite inner product) is only the trivial one which leaves the transverse modes invariant, and hence, the little group cannot provide position operators in the massless case.

After the papers by Newton and Wigner and by Wightman, many discussions have been developed around the photon localization problem. As far as we know, the arguments seem to be divided into two opposite directions, one relying on purely dynamical bases [8] and another on pure kinematics [2], where it is almost impossible to find any meaningful agreements. Below we propose an alternative strategy based on the concept of "effective mass", which can provide a reasonable reconciliation between these conflicting ideas because of its "kinematical" nature arising from some dynamical origin.

3 Polariton as a Typical Model of Effective Mass Generation

3.1 Physical roles played by coupled external system

In spite of the above theoretical difficulty in the localizability of photons, however, it is a plain fact that almost no experiments can be performed in quantum optics where photons must be registered by *localized* detectors. To elaborate on this problem, we will see that it is indispensable to reexamine the behaviour of a photon in composite systems coupled with some external system such as material media constituting apparatus without which any kind of measurement processes cannot make sense. For this purpose, the above group-theoretical analysis of localizability of kinematical nature should be extended to incorporate algebraic aspects involved in the formation of a coupled dynamics between photons to be detected and the measuring devices consisting of matters.

Our scheme of the localization for photons can be summarized as follows:

- Photons are coupled with external system into a composite system with a coupled dynamics.

- Positive effective mass emerges in the composite system.
- Once a positive effective mass appears, Wightman's theorem itself provides the "kinematical basis" for the localization of a photon.

From our point of view, therefore, this theorem of Wightman's interpreted traditionally as a no-go theorem against the localizability becomes actually an affirmative support for it. It conveys such a strongly selective meaning (which will be discussed in detail in Sec.4) that, whenever a photon is localized, it should carry a non-zero effective mass.

In the next subsection, we explain the meaning of our scheme from a physical point of view.

3.2 How to define effective mass of a photon

As a typical example of our scheme, we focus first on a photon interacting with homogeneous medium, in the case of the monochromatic light with angular frequency ω as a classical light wave. For simplicity, we neglect here the effect of absorption, that is, the imaginary part of refractive index. When a photon interacting with matter can be treated as a single particle, it is natural to identify its velocity $\mathbf{v}$ with the "signal velocity" of light in medium. The relativistic total energy E of the particle should be related to $v := \sqrt{\mathbf{v} \cdot \mathbf{v}}$ by its mass m_{eff}:

$$E = \frac{m_{\mathsf{eff}} c^2}{\sqrt{1 - \frac{v^2}{c^2}}} \tag{2}$$

Since v is well known to be smaller than the light velocity c (theoretically or experimentally), m_{eff} is positive (when the particle picture above is valid). Then we may consider m_{eff} as the relativistic "effective (rest) mass of a photon", and identify its momentum $\mathbf{p}$ with

$$\mathbf{p} = \frac{m_{\mathsf{eff}} \mathbf{v}}{\sqrt{1 - \frac{v^2}{c^2}}}. \tag{3}$$

Hence, as long as "an interacting photon" can be well approximated by a single particle, it should be massive, according to which its "localization problem" is resolved. The validity of this picture will be confirmed later in the next subsection.

The concrete forms of energy/momentum are related to the Abraham-Minkowski controversy [1, 14, 4] and modified versions of Einstein/de Broglie formulae [24].

Our argument itself, however, does not depend on the energy/momentum formulae. The only essential point is that a massless particle can be made massive through some interactions. That is, while a free photon satisfies

$$E_{\mathrm{free}}^2 - c^2 p_{\mathrm{free}}^2 = 0, \tag{4}$$

an interacting photon satisfies

$$E^2 - c^2p^2 = m_{\mathsf{eff}}^2 c^4 > 0. \tag{5}$$

To sum up, an "interacting photon" can gain a positive effective mass, while a "free photon" remains massless! This is the key we have sought for. We note, however, the present argument is based on the assumption that "a photon dressed with interactions" can be viewed as a single particle. We proceed to consolidate the validity of this picture, especially the existence of particles whose effective mass is produced by the interactions, analogous to Higgs mechanism: Such a universal model for photon localization certainly exists, which is based on the concept of polariton, well known in optical and solid physics.

3.3 Polariton picture

In these areas of physics, the propagation of light in a medium is viewed as follows: By the interaction between light and matter, creation of an "excition (an excited state of polarization field above the Fermi surface)" and annihilation of a photon will be followed by annihilation of an exciton and creation of a photon, $\cdots$, and so on. This chain of processes itself is often considered as the motion of particles called *polaritons* (in this case "exciton-polaritons"), which constitute particles associated with the coupled wave of the polarization wave and electromagnetic wave.

The concept of polariton has been introduced to develop a microscopic theory of electromagnetic interactions in materials ([6], [10]). Injected photons become polaritons by the interaction with matter. As exiton-phonon interaction is dissipative, the polariton picture gives a scenario of absorption. It has provided an approximation better than the scenarios without it. Moreover, the group velocity of polaritons discussed below gives another confirmation of the presence of an effective mass.

As is well known, permittivity $\epsilon(\omega)$ is given by the following equality,

$$\epsilon(\omega) = n^2 = \frac{c^2k^2}{\omega^2}, \tag{6}$$

and hence, we can determine the dispersion relation (between frequency and wave number) of polariton once the formula of permittivity is specified. In general, this dispersion relation implies branching, analogous to the Higgs mechanism. The signal pulse correponding to each branch can also be detected in many experiments, for example, in [13] cited below.

In the simple case, the permittivity is given by the transverse frequency ω_T of exciton's (lattice vibration) as follows:

$$\epsilon(\omega) = \epsilon_\infty + \frac{\omega_T^2(\epsilon_{st} - \epsilon_\infty)}{\omega_T^2 - \omega^2}, \tag{7}$$

where ϵ_∞ denotes $\lim_{\omega\to\infty}\epsilon(\omega)$ and $\epsilon_{st} = \epsilon(0)$ (static permittivity). With a slight improvement through the wavenumber dependence of the exciton energy, the theoretical result of polariton group velocity $\frac{\partial\omega}{\partial\mathbf{k}} < c$ based on the above dispersion relation can explain satisfactorily experimental data of the passing time of light in materials (for example, [13]). This strongly supports the validity of the polariton picture.

From the above arguments, polaritons can be considered as a universal model of the "interacting photons in a medium" in the previous section. The positive mass of a polariton gives a solution to its "localization problem". Conversely, as the "consequence" of Wightman's theorem, it follows that "all" physically accessible photons as particles which can be localized are more or less polaritons (or similar particles) because only the interaction can give a photon its effective mass, if it does not violate particle picture.

4 Effective Mass Generation in General

4.1 Toward general situations

In the last subsection we have discussed that the interaction of photons with media can cause their localization by giving effective masses to them. Then a natural question arises: Is the exsistence of media a necessary condition for the emergence of effectve photon mass? The answer is no: In fact, light beams with finite transvese size have group velocities less than c.

In a recent publication [7], Giovannni et al., show experimentally that even in vacuum photons (in the optical regime) travel at the speed less than c when it is transversally structured, such as Bessel beams or Gaussian beams, by measuring a change in the arrival time of time-correlated photon pairs. They show a reduction in the velocity of photons in both a Bessel beam and a focused Gaussian one. Their work highlights that, even in free space, the invariance of the speed of light only applies to plane waves, i.e., free photons.

From our viewpoint, this result can be understood quite naturally in the light of the Newton-Wigner-Wightman theorem. As we have seen, the theorem states that every localizable elementary system (particle) with spin must be massive. It implies that photons in the real world should travel less than c, in any conditions, which makes the probability distribution of its position well-defined without contradicting with the presence of spin. Hence, transversally structured photons should become slow.

The scenario also applies to more general settings. Any kinds of boundary conditions with finite volume (like cavity), or even nanoparticles in the context of dressed photons [17], will make photons heavier and slower, even without medium!

4.2 Wightman's theorem re-interpreted as the "basis" for localization

Our general scheme of the localization for photons can be depicted as follows, whose essense can be understood in accordance with the basic formulation of "quadrality scheme" [20] underlying the Micro-Macro duality [18, 19]:

$$\begin{array}{ccc} & & \text{Localization of photons} \\ & & \Uparrow \\ \text{Effective mass of photons} & \Longrightarrow & \text{Change in kinematics} \\ \Uparrow & & \\ \text{Dynamical interaction} & & \\ \text{between photons \& external system} & & \end{array}$$

In order to actualize the physical properties of a given system such as photons driven by an invisible microscopic dynamics, it is necessary for it to be coupled with some external measuring system through which a composite system is formed. According to this formation of coupled dynamics, the kinematics controlling the observed photons are modified and what can be actually observed is a result of this changed kinematics, realized in our case in the form of localized photons.

4.3 Tomita's theorem of integral decomposition of a state

Before going into the details of mass generation mechanisms, we examine here the theoretical framework relevant to our context. From the mathematical viewpoint, an idealized form of constructing a coupled system of the object system with an external reference one can be found conveniently in Tomita's theorem of integral decomposition of a state as follows:

Theorem 4 (Tomita [5]) *For a state ω of a unital C*-algebra $\mathcal{A}$, the following three sets are in a 1-to-1 correspondence:*

1. *subcentral measures μ (pseudo-)supported by the space $F_{\mathcal{A}}$ of factor states on $\mathcal{A}$;*
2. *abelian von Neumann subalgebras $\mathcal{B}$ of the centre $\mathfrak{Z}_{\pi_\omega}(\mathcal{A}) = \pi_\omega(\mathcal{A})'' \cap \pi_\omega(\mathcal{A})'$;*
3. *central projections C on $\mathfrak{H}_\omega$ such that*

$$C\Omega_\omega = \Omega_\omega, \qquad C\pi_\omega(\mathcal{A})C \subset \{C\pi_\omega(\mathcal{A})C\}'. \tag{8}$$

If μ, $\mathcal{B}$ and C are in the above correspondence, then the following relations hold:

(i) $\mathcal{B} = \{\pi_\omega(\mathcal{A}) \cup \{C\}\}'$*;*

(ii) $C = [\mathcal{B}\Omega_\omega]$*: projection operator onto the subspace spanned by* $\mathcal{B}\Omega_\omega$*;*

(iii) $\mu(\hat{A}_1\hat{A}_2\cdots\hat{A}_n) = \langle\Omega_\omega|\ \pi_\omega(A_1)C\ \pi_\omega(A_2)C\cdots C\pi_\omega(A_n)\Omega_\omega\rangle$ *for* $A_1, A_2, \cdots, A_n \in \mathcal{A}$*;*

(iv) The map $\kappa_\mu : L^\infty(E_\mathcal{A}, \mu) \to \mathcal{B}$ *defined by*

$$\langle\Omega_\omega|\ \kappa_\mu(f)\pi_\omega(A)\Omega_\omega\rangle = \int d\mu(\omega')f(\omega')\omega'(A) \tag{9}$$

for $f \in L^\infty(E_\mathcal{A}, \mu)$ *and* $A \in \mathcal{A}$ *is a *-isomorphism, satisfying the following equality for* $A, B \in \mathcal{A}$*:*

$$\kappa_\mu(\hat{A})\pi_\omega(B)\Omega_\omega = \pi_\omega(B)C\pi_\omega(A)\Omega_\omega. \tag{10}$$

Some vocabulary in the above need be explained: The space $F_\mathcal{A}$ of factor states on $\mathcal{A}$ is the set of all the factor states φ whose (GNS) representations π_φ have trivial centres: $\pi_\varphi(\mathcal{A})'' \cap \pi_\varphi(\mathcal{A})' = \mathbb{C}1_{\mathfrak{H}_\varphi}$. This $F_\mathcal{A}$ divided by the quasi-equivalence relation $\approx$ defined by the unitary equivalence up to multiplicity, $F_\mathcal{A}/\approx$ plays the role of sector-classifying space (or, sector space, for short) whose elements we call "sectors" mathematically or "pure phases" physically. Then Tomita's theorem plays a crucial role in verifying mathematically the so-called Born rule [22] postulated in quantum theory in physics.

Via the definition $\widehat{A}(\rho) := \rho(A)$, $\rho \in E_\mathcal{A}$, any element $A \in \mathcal{A}$ can be expressed by a continuous function $\widehat{A} : E_\mathcal{A} \to \mathbb{C}$ on the state space $E_\mathcal{A}$. Among measures on $E_\mathcal{A}$, a measure μ is called *barycentric* for a state $\omega \in E_\mathcal{A}$ if it satisfies $\omega = \int_{E_\mathcal{A}} \rho d\mu(\rho) \in E_\mathcal{A}$ and is said to be *subcentral* if linear functionals $\int_\Delta \rho d\mu(\rho)$ and $\int_{E_\mathcal{A}\setminus\Delta} \sigma d\mu(\sigma)$ on $\mathcal{A}$ are disjoint for any Borel set $\Delta \subset E_\mathcal{A}$, having no non-vanishing intertwiners between them: i.e., $T\int_\Delta \pi_\rho(A)d\mu(\rho) = \int_{E_\mathcal{A}\setminus\Delta} \pi_\sigma(A)d\mu(\sigma)T$ for $\forall A \in \mathcal{A}$ implies $T = 0$. If the abelian subalgebra $\mathcal{B}$ in the above theorem is equal to the centre $\mathcal{B} = \mathfrak{Z}_{\pi_\omega}(\mathcal{A})$, the measure μ is called the central measure of ω, determined uniquely by the state ω and the corresponding barycentric decomposition $\omega = \int_{F_\mathcal{A}} \rho d\mu(\rho)$ is called the central decomposition of ω. This last concept plays crucial roles in establishing precisely the bi-directional relations between microscopic and macroscopic aspects in quantum theory, as has been exhibited by the examples of "Micro-Macro duality" (see, for instance, [18, 19]).

At first sight, the distinction between central and subcentral may look too subtle, but it plays important roles in different treatments, for instance, between *spatial* and *spacetime* degrees of freedom in Wightman's theorem concerning the localizability, as mentioned already after the theorem. In this connection, we consider the problem as to how classically visible configurations of electromagnetic field can be specified in close relation with its

microscopic quantum behaviour, for the purpose of which most convenient concept seems to be the coherent state and the Segal-Bargmann transform associated with it. Since coherent states are usually treated within the framework of quantum mechancs for systems with the *finite degrees of freedom*, the aspect commonly discussed is the so-called *overcompleteness relations* due to the non-orthogonality, $\langle\alpha|\beta\rangle \neq 0$, between coherent states $\hat{a}|\alpha\rangle = \alpha|\alpha\rangle$ with different coherence parameters $\alpha \neq \beta$.

We note that, in connection with Tomita's theorem, a composite system arises in such a form as $\mathcal{A} \otimes C(\Sigma)$ consisting of the object system $\mathcal{A}$ and of the external system $\Sigma(\subset F_{\mathcal{A}})$ to which measured data are to be registered through measurement processes involving $\mathcal{A}$. In this scheme, the universal reference system Σ can be viewed naturally *emergent* from the object system $\mathcal{A}$ itself just as the classifying space of its sector structure. Then, via the *logical extension* [21] to parametrize the object system $\mathcal{A}$ by its sectors in Σ, an abstract model of *quantum fields* $\varphi : \Sigma \to \mathcal{A}$ can be created, constituting a crossed product $\varphi \in \mathcal{A} \rtimes \widehat{\mathcal{U}(\Sigma)}$ (via the co-action of the structure group $\mathcal{U}(\Sigma)$ of Σ). Thus, the above non-orthogonality can be resolved by the effects of the classifying parameters of sectors Σ in $F_{\mathcal{A}}$. As a result, we arrive at the quantum-probabilistic realization of coherent states in such a form as the "exponential vectors" treated by Obata [16] in the context of "Fock expansions" of white noises. What is important conceptually in this framework is the *analyticity* due to the Segal-Bargmann transform and the associated *reproducing kernel* (RS) to be identified through the projection operator P in $L^2(\Sigma, d\mu)$ onto its subspace $\mathcal{H}L^2(\Sigma, d\mu)$ of coherent states expressed by holomorphic functions on Σ [9], where $d\mu$ denotes the Gaussian measure.

As commented briefly above, we can find various useful relations and connections of quantum theory in terms of the concept of "quantum fields". From this viewpoint, we elaborate on its roles in attaining a transparent understanding of the mutual relations among fields, particles and mass in the next section.

5 Quantum Field Ontology

5.1 From particles to fields

As we have discussed in Sec.4, the effective mass generating scenario applies to general settings. Any kinds of boundary conditions with finite volume (like cavity) will make photons heavier and slower, even without medium. This fact itself leads to a paradoxical physical question — how can the boundary condition affect a particle traveling in vacua? What is a spooky action through vacua?

Our answer is quite simple: In fact a photon is not "a particle traveling in vacua". It is just a field filling the space time, before it "becomes" a

particle, or more rigorously, before it appears in a particle-like event caused via the interaction (energy-momentum exchange with external system). As we will discuss in this section, it is quite unreasonable to imagine a photon as a traveling particle unless any kinds of interaction is there.

Based on the arguments above, we discuss the limitation of particle concept in connection with a new physical interpretation of Newton-Wigner-Wightman analysis.

To begin with, we should mention that this concept involves a strong inconsistency with particle concept which seems to have been forgotten at some stage in history. In fact, the concept of a classical massless point particle with non-zero spin cannot survive special relativity with the worldline of such a particle obscured by the spin: Instead of being a purely "internal" degree of freedom, the spin causes kinematical extensivity of the particle which is exhibited in a boost transformation, as is pointed out by Bacry in [3].

The result of Newton-Wigner-Wightman analysis can be understood to show that this inconsistency cannot be eliminated by generalizing the problem in the context of quantum theory: A massless particle cannot be localized unless the spin is zero. Even in the massive case, the concept of localization is not independent of the choice of reference frames. There is no well-defined concept of "spacetime localization" as we have mentioned.

These facts are consistent with the idea that the position is not a clear cut a priori concept but an emergent property. Instead of a point particle, therefore, we should find something else having spacetime structure to accommodate events in point-like forms, which is nothing but the quantum field. In other words, the Newton-Wigner-Wightman analysis should be re-interpreted as "the existence proof of a quantum field", showing its inevitability.

5.2 From fields to particles: Principle of eventualization

This does not mean that particle-like property is artificial nor fictional. On the contrary, point-like events do take place in any kind of elementary processes of quantum measurement such as exposure on a film, photon counting, and so on.

This apparent contradiction is solved if we adopt the universality of the indeterminate processes emerging point-like events (energy-momentum exchanges) from quantum fields via formation of composite system with external systems (like media or systems giving boundary conditions), even the latter coming from the part of the degrees of freedom of quantum fields. Let us call these fundamental processes as *eventualization*. From our viewpoint, the most radical implication of Newton-Wigner-Wightman analysis is that we should abandon the ontology based on naïve particle picture and replace it by the one based on quantum fields with their eventualizations.

The idea of eventualization may appear to be just a palliative to avoid the contradiction between abstract theory of localization and the concrete localization phenomena, but actually, it opens the door to quite natural formulation of quantum physics. In fact, the notion of measurement process can be considered as a special kind of eventualization process with amplification. As we will discuss in a forthcoming paper [23], a glossary of "quantum paradoxes" is solved by just posing an axiom we call "eventualization principle".

> **Eventualization Principle:** Quantum fields can effect macroscopic systems only through eventualization.

In other words, we hypothesize that the notion of "macroscopic systems"— including a Schrödinger cat— can be characterized, or defined, by the collection of events, formed by perpertual eventualization.

Acknowledgments

We would like to express our sincere gratitudes to Prof. P. Jorgensen for inviting us to the opportunity of contributing this paper to a Special Issue "Mathematical Physics" in the Journal "Mathematics". We are grateful to Prof. S. M. Barnett, Dr. T. Brougham, Dr. V. Potoček and Dr. M. Sonnleitner for enlightening discussions on the occasion of one of us (H.S.) to visit Glasgow. Similarly, we thank Prof. M. Bożejko, Prof. G. Hofer-Szabó and Prof. M. Rédei for encouraging discussions in Wrocław and Budapest. We are grateful to Prof. M. Ohtsu, Prof. M. Naruse and Prof. T. Yatsui for their interests in our work and instructive discussions in Tokyo. Last but not least, we cordially thank Prof. H. Sako and Dr. K. Okamura for inspiring and continuing collaboration.

References

[1] Abraham, M., Zur Elektrodynamik bewegter Körper. Rend. Circ. Mat. Palermo **28**, 1 (1909).

[2] Angelopuolos, E., Bayen, F. and Flato, M., On the localizability of massless particles, Physica Scripta 9, 173 (1974).

[3] Bacry, H., *Localizability and Space in Quantum Physics*, Lect. Notes in Phys. Vol. 308, Springer-Verlag, 1988.

[4] Barnett, S.M., Resolution of the Abraham-Minkowski Dilemma. Phys. Rev. Lett. 104, 070401 (2010).

[5] Bratteli, O. and Robinson, D.W., *Operator Algebras and Quantum Statistical Mechanics* (vol.1) (2nd printing of 2nd ed.), Springer-Verlag, 2002.

[6] Fano, U., Atomic theory of electromagnetic interactions in dense materials. Phys. Rev. **103**, 1202 (1956)

[7] Giovannni, D. et al., Spatially structured photons that travel in free space slower than the speed of light. Science **347**, 857 (2015).

[8] Haag, R. *Local Quantum Physics –Fields, Particles, Algebras–* 2nd ed., Springer-Verlag, 1996.

[9] Hall, B., Holomorphic methods in analysis and mathematical physics, *in* "First Summer School in Analysis and Mathematical Physics," (S. Pérez-Esteva and C. Villegas-Blas, Eds.), Contemp. Math. Vol. 260, Amer. Math. Soc., Providence, RI, 2000, pp. 1-59.

[10] Hopfield, J.J., Theory of the contribution of excitons to the complex dielectric constant of crystals. Phys. Rev. **112**, 1555 (1958).

[11] Landau, L.D., Über die Bewegung der Elektronen in Kristalgitter. Phys. Z. Sowjetunion **3**, 644 (1933).

[12] Mackey, G.W., *Induced representations and quantum mechanics*, Benjamin/Cummings, 1968.

[13] Masumoto,Y., Unuma, Y., Tanaka, Y. and Shionoya, S., Picosecond time of flight measurements of excitonic polariton in CuCl. J. Phys. Soc. Jpn. **47**, 1844 (1979).

[14] Minkowski, H., Die Grundgleichungen für die elektromagnetischen Vorgänge in bewegten Körpern. Nach. Königl. Ges. Wiss. Göttingen 53 (1908); Math. Ann. **68** 472 (Reprinted 1910).

[15] Newton, T.D. and Wigner, E.P. Localized states for elementary systems. Rev. Mod. Phys. **21**, 400 (1949).

[16] Obata, N., *White Noise Calculus and Fock Space*, Lect. Notes in Math. Vol. 1577, Springer-Verlag, 1994.

[17] Ohtsu, M., *Dressed Photons*, Springer-Verlag, 2013.

[18] Ojima, I., A unified scheme for generalized sectors based on selection criteria –Order parameters of symmetries and of thermality and physical meanings of adjunctions–, Open Systems and Information Dynamics, **10**, 235-279 (2003) (math-ph/0303009); Temperature as order parameter of broken scale invariance, Publ. RIMS (Kyoto Univ.) **40**, 731-756 (2004) (math-ph0311025). arXiv:math-ph/0502038.

[19] Ojima, I., Micro-Macro Duality in Quantum Physics, pp.143–161, in Proc. Intern. Conf. "Stochastic Analysis: Classical and Quantum", World Scientific, 2005; Micro-Macro duality and emergence of macroscopic levels, Quantum Probability and White Noise Analysis, **21**, 217 – 228 (2008)

[20] Ojima, I. Meaning of Non-Extensive Entropies in Micro-Macro Duality, J. Phys.: Conf. Ser. 201 012017 (2010): Invited talk at RIMS International Workshop, "Mathematical Aspects of Generalized Entropies and their Applications", July 2009.

[21] Ojima, I. and Ozawa, M., Unitary representations of the hyperfinite Heisenberg group and the logical extension methods in physics, Open Systems and Information Dynamics **2**, 107-128 (1993).

[22] Ojima, I., Okamura, K. and Saigo, H., Derivation of Born Rule from Algebraic and Statistical Axioms, Open Sys. Information Dyn. **21**, 1450005 (2014).

[23] Ojima, I., Okamura, K. and Saigo, H., in preparation.

[24] Ojima, I., and Saigo, H., Who has seen a free photon?, Open Sys. Information Dyn. **19**, 1250008 (2012).

[25] Wightman, A.S., On th localizability of quantum mechanical systems. Rev. Mod Phys. **34**, 845 (1962).

Theory of Single Susceptibility for Near-field Optics Equally Associated with Scalar and Vector Potentials

Itsuki Banno*

Interdisciplinary Graduate School of Medicine and Engineering,

University of Yamanashi, 4-3-11 Takeda,

Kofu, Yamanashi 400-8511, Japan

(Dated: July 31, 2018)

Abstract

A response theory was developed to describe a small-scale many-electron system within the neighborhood of a nanostructure radiating longitudinal and transverse electric fields, essentially the full degrees of freedom of the scalar and vector potentials (SP and VP). The coexistence of the SP and VP incidents distinguishes such a near-field optical system from the ordinary optical system, and is the motivation for equal treatment of both potentials as the cause of the response in the electron system. Furthermore, the low symmetry of the system makes the electric and magnetic responses indistinguishable, so it is essential to use a single susceptibility, instead of the ordinary two susceptibilities, i.e., the electric permittivity and the magnetic permeability. Therefore, the present theory developed a single susceptibility relating the scalar and vector potentials (as the cause) to the charge and current densities (as the result). The Heisenberg operators of both linear and nonlinear single susceptibilities are systematically given in terms of functional derivatives of the action integral with respect to the SP and VP, and proofs for charge conservation and gauge invariance are given in a general manner; this theory is free from gauge-fixing. To make the ground state bounded in the non-perturbed system, it is essential to consider the quantum many electron effect (exchange-correlation effect), and this is done by employing the fundamental idea of density functional theory, instead of the ordinary unequal treatment of the SP and VP, i.e., remaking the SP into a Coulomb interaction between electron charges.

PACS numbers: 78.67.-n, 78.20.Bh, 41.20.-q, 42.25.Ja

Keywords: single susceptibility, non-resonant effect, optical near field, response function, electromagnetic potential

*Electronic address: banno@yamanashi.ac.jp

I. INTRODUCTION

Suppose that a small-scale many-electron system, a molecule for example, is exposed to the longitudinal electric field and the transverse electromagnetic (EM) field radiated by a neighboring nanostructure. Using the Coulomb gauge for a while, the scalar potential and vector potential represent the longitudinal electric field and transverse EM field, respectively. The coexistence of these two types of incident fields distinguishes such a near-field (NF) optical system from the ordinary optical system; in the ordinary optical system, the electron system of interest is located far from the light source and is exposed only to the transverse EM field incident. As the first stage of investigation, it was assumed that the nanostructure serves as a robust light source, which is insensible to the electron system of interest.

Here, the longitudinal electric field originates from the charge density on the nanostructure, obeys Coulomb's law, has a non-radiative nature, and is localized around the nanostructure, while the transverse EM field originates from the transverse current density on the nanostructure, obeys Ampere-Maxwell's law and Faraday's law, has a radiative nature, and may propagate far from the light source. Therefore, the longitudinal and transverse incident fields are qualitatively different and should be treated separately and equally as the cause of the response of the many-electron system in NF optics.

Up to now, there has been no such theoretical framework for equally treating the scalar and vector potentials (the longitudinal electric field and transverse EM field). The reason for this lies in the the many-body problem inevitably related to the NF optics via the scalar potential (the longitudinal electric field). This fact has not been well recognized in NF optics, although the problem of how to separate the cause of excitation from the Coulomb interaction has remained for a long time[1]. In the usual Hamiltonian for a many-electron system, the scalar potential in the Coulomb gauge (the longitudinal electric field)

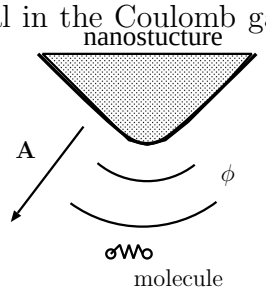

FIG. 1: A nanostructure yields a scalar potential, $\phi(\mathbf{r},t)$ and a vector potential, $\mathbf{A}(\mathbf{r},t)$ and these potentials irradiate the neighboring many-electron system, e.g., a molecule.

is rewritten as the interaction between the electron charge density operators, and only the vector potential is considered as the cause of the response. This unequal treatment of the scalar and vector potentials is needed to consider the quantum many-electron effect (the so-called exchange-correlation effect) to construct the ground and excited states as the proper bound states in a many-electron system. This is the usual procedure and is compatible with ordinary optical systems, where the electron system of interest is far from the light source, and the scalar potential incident is negligible. By contrast, in an NF optical system, this approach results in a difficulty of understanding the response to the scalar potential incident, because both the scalar potential incident (radiated by the nanostructure) and the inherent scalar potential (originating from the particle charge) are built into the two-body Coulomb interaction, and the two contributions are indistinguishable. To make matters worse, the Coulomb interaction in itself is so difficult to treat that it is often ignored, without considering it includes the effect of the scalar potential incident.

To best understand the fundamental physics in NFO, it is essential to develop an adequate response theory. For this purpose, this paper defines and characterizes a *single* susceptibility equally associated with the scalar and vector potentials based on the action integral from scratch.

The single susceptibility introduced below relates the EM potential (as the cause) to the induced charge and current densities (as the result) , while the two ordinary susceptibilities, i.e., the electric permittivity and magnetic permeability, relate the total electric and magnetic fields (as the cause) to the polarization and magnetization (as the result), respectively. There are two motives for employing a single susceptibility: (1) The usual constitutive equations with the two susceptibilities gives relationships between redundant degrees of freedom. (2) In low-symmetry systems, such as in NF optical systems with nanostructures, it is essential to use the single susceptibility instead of the two ordinary susceptibilities. A detailed explanation of the two points is as follows.

(1) The inapplicability of the two susceptibilities may be explained from a naive view point. The essential source of the EM field is the three components of charge density and the transverse current density. The longitudinal current density is excluded because it can be determined through the charge conservation law, once the charge density is known. However, the redundant components of the polarization and magnetization are introduced as the source of the EM field, so that the associated constitutive equations using the two

susceptibilities include the constraint condition for the redundancy, of which the physical meaning is not declared. This situation is physically unreasonable and should be fixed by the constitutive equation using a single susceptibility associated with the proper degrees of freedom.

(2) The need for a single susceptibiity in low-symmetry optical systems as first claimed by Cho[2, 3], who is one of the pioneers of non-local response theory from first principles and who formulated a single susceptibility using the usual Hamiltonian for a many-electron system. He derived a Taylor expansion for his single susceptibility, using the long wavelength approximation ($ka \ll 1$, where $2\pi/k$ is the light wavelength and a is the representative size of the material) and has shown the term of leading order, $\mathcal{O}(ka)^0$, gives the electric permittivity, and the term of order $\mathcal{O}(ka)^2$ gives the magnetic permeability. This separability of the electric and magnetic responses holds only in systems with non-chiral symmetry. In a system exhibiting chiral symmetry, however, this separability does not hold and there exists a mixing of electric dipole (E1) transitions with magnetic dipole (M1) and/or electric quadrupole (E2) transitions in the term of order $\mathcal{O}(ka)^1$. Furthermore, the term of order $\mathcal{O}(ka)^1$is incompatible with the so-called Drude-Born-Fedorov theory, which extends the two susceptibilities, adding the cross terms of the electric-field-induced magnetization and the magnetic-field-induced polarization. Consequently, in low-symmetry systems, the two susceptibilities including the Drude-Born-Fedorov-extension are irrational, and a single susceptibility is essential.

The above two points mean that the two ordinary susceptibilities are logically unreasonable in NF optics, although these has been practically used, for example, in numerical calculations using the Finite-Difference Time-Domain method. For NF optics, there are two approaches for the single susceptibility (or the non-local response function).

Cho formulated a single susceptibility that relates the transverse vector potential (as the cause) to the current density (as the result), and applied it to various optical systems[4]. Additionally, a modification that considers the scalar potential incident (longitudinal electric field incident) in NF optical systems has been proposed[5]. Keller formulated another single susceptibility within the non-local linear response theory, and it relates the transverse electric field and the incident part of the longitudinal electric field (as the cause) to the current density (as the result) [6].

In the above two formulations, the gauge is fixed, and the scalar potential (or the longitu-

dinal electric field), except the incident contribution, is rewritten as the two-body Coulomb interaction in the usual manner. Therefore, the response to the scalar potential, in principle, can be rigorously considered via the Coulomb interaction if the many-body problem is properly solved, whereas the response to the vector potential incident is treated in the perturbative manner. In this approach, it is essential to solve the many-body problem, in particular, for the nonlinear process related with the scalar potential (the longitudinal electric field). Even if the Coulomb interaction is properly considered, unequal treatment may make it difficult to regulate the perturbation order of the responses and to understand the role of the scalar potential incident.

The purpose of this paper is to define and characterize the single susceptibility of a many-electron system, equally treating the scalar and vector potentials to explore the physics in NF optics.

The contents of this paper are as follows: §II defines the linear and nonlinear single susceptibilities equally associated with the scalar and vector potentials, as functional derivatives of the action integral. §III shows that the present susceptibility respects both charge conservation and gauge invariance, in a general manner. §IV derives the Heisenberg operators of the linear and nonlinear single susceptibilities. §V shows that the present theoretical scheme may be supported by density functional theory to prepare the non-perturbed state as well as a complete set of many-electron states. §VI provides a summary of this work. Two appendices are included: §A provides some details of a calculation in §II. §B gives an explicit check for the charge conservation and gauge invariance of the linear and nonlinear single susceptibilities.

II. DEFINITION OF NEW SINGLE SUSCEPTIBILITY

Based on the Lagrangian formulation of non-relativistic quantum electrodynamics, we define the single susceptibility, which relates the scalar and vector potentials (the cause) to the induced charge and current densities (the result). Furthermore, it is shown that this susceptibility guarantees that charge conservation and gauge invariance hold; see the next section. The action integral for non-relativistic quantum electrodynamics is:

$$\mathcal{I}[\hat{\psi}^\dagger_\alpha, \hat{\psi}_\alpha, \phi, \mathbf{A}] \equiv \mathcal{I}_{\rm mat}[\hat{\psi}^\dagger_\alpha, \hat{\psi}_\alpha, \phi, \mathbf{A}] + \mathcal{I}_{\rm EM}[\phi, \mathbf{A}], \tag{1}$$

$$\mathcal{I}_{\rm mat}[\hat{\psi}^\dagger_\alpha,\hat{\psi}_\alpha,\phi,\mathbf{A}] \equiv \frac{1}{c}\int {\rm d}^4x\ \Big\{\hat{\psi}^\dagger_\alpha(x)(i\hbar\partial_t - q\phi(x))\hat{\psi}_\alpha(x)$$
$$-\frac{1}{2m}\left(\frac{\hbar}{-i}\partial_i - qA_i(x)\right)\hat{\psi}^\dagger_\alpha(x)\cdot\left(\frac{\hbar}{i}\partial_i - qA_i(x)\right)\hat{\psi}_\alpha(x)$$
$$-\phi(x)\rho^{\rm (EXT)}(x) + A_i(x)j^{\rm (EXT)}_i(x) - \hat{\psi}^\dagger_\alpha(x)v^{\rm (AUX)}(x)\hat{\psi}_\alpha(x)\Big\} \quad (2)$$
$$\mathcal{I}_{\rm EM}[\phi,\mathbf{A}] \equiv \frac{1}{c}\int {\rm d}^4x\ \Big\{\frac{\epsilon_0}{2}\left(\partial_t A_i(x) + \partial_i\phi(x)\right)\left(\partial_t A_i(x) + \partial_i\phi(x)\right)$$
$$-\frac{\epsilon_0 c^2}{2}\epsilon_{ijk}\partial_j A_k(x)\epsilon_{ilm}\partial_l A_m(x)\Big\}, \quad (3)$$

where m and $q(=-e)$ are the electron mass and charge, c is the speed of light, $\phi, \mathbf{A}$ are the scalar and vector potentials, $\hat{\psi}^\dagger_\alpha, \hat{\psi}_\alpha$ are the electron field operators with the spin state α (one of the two spin states; so called "up" and "down" states), and $\rho^{\rm (EXT)}, \mathbf{j}^{\rm (EXT)}$ are the nuclear or other charge and the current densities, which yield the external electric and magnetic fields, respectively. A static auxiliary potential $v^{\rm (AUX)}(x)$ is null for now, but is introduced here for later discussion of the density functional theory to consider effectively the quantum many-electron effect (the exchange-correlation effect) ; see §V. ϵ_{ijk} is an antisymmetric tensor, and the Einstein rule is used for indices of vector and Grassmann fields, that is, summation should be executed over repeated indices. At this first stage of investigation, the interaction between spin polarization and the EM field is ignored. The soundness of the above action integral is confirmed by its Euler equations, which will soon be derived.

The electron field operators are considered as quantized Grassmann fields. The Grassmann field satisfies $[\hat{\psi}_\alpha(\mathbf{r},t),\hat{\psi}^\dagger_\beta(\mathbf{r}',t')]_+ = 0$ [8], and corresponds to the "classical" field of the electron. These operators become the creation and annihilation operators of the electron in quantum theory (the quantized Grassmann fields) if one introduces the anti-commutation relation: $[\hat{\psi}_\alpha(\mathbf{r},t),\hat{\psi}^\dagger_\beta(\mathbf{r}',t)]_+ = \delta^3(\mathbf{r}-\mathbf{r}')\delta_{\alpha\beta}$.

The action integral is composed of two parts: one is the action for the matter (including the interaction between matter and the EM field) $\mathcal{I}_{\rm mat}[\hat{\psi}^\dagger_\alpha,\hat{\psi}_\alpha,\phi,\mathbf{A}]$, and the other is the action for the EM field $\mathcal{I}_{\rm EM}[\phi,\mathbf{A}]$. Applying the extremal (optimizing) conditions with respect to $\hat{\psi}_\alpha(x)\,,\hat{\psi}^\dagger_\alpha(x)$ leads to Heisenberg's equation, and optimizing with respect to $\phi(x)$, $\mathbf{A}(x)$ leads to Maxwell's wave equations:

$$0 = c\,\delta\hat{\psi}^\dagger_\alpha(x)\backslash\delta\mathcal{I} = c\,\delta\hat{\psi}^\dagger_\alpha(x)\backslash\delta\mathcal{I}_{\rm mat}$$
$$= \left(i\hbar\partial_t - q\phi(x) - \frac{1}{2m}\left(\frac{\hbar}{i}\partial_i - qA_i(x)\right)\cdot\left(\frac{\hbar}{i}\partial_i - qA_i(x)\right) - v^{\rm (AUX)}(x)\right)\hat{\psi}_\alpha(x), \quad (4)$$
$$0 = c\,\delta\mathcal{I}/\delta\hat{\psi}_\alpha(x) = c\,\delta\mathcal{I}_{\rm mat}/\delta\hat{\psi}_\alpha(x)$$

$$= \left(-i\hbar\partial_t - q\phi(x) - \frac{1}{2m}\left(\frac{\hbar}{-i}\partial_i - qA_i(x)\right)\cdot\left(\frac{\hbar}{-i}\partial_i - qA_i(x)\right) - v^{(\mathrm{AUX})}(x)\right)\hat{\psi}^\dagger_\alpha(x), \tag{5}$$

$$0 = c\,\frac{\delta\mathcal{I}}{\delta A_i(x)} = \epsilon_0 c^2\left(-\epsilon_{ijk}\partial_j\epsilon_{klm}\partial_l A_m(x) - \frac{1}{c^2}\partial_t^2 A_i(x) - \frac{1}{c^2}\partial_t\partial_i\phi(x) + \frac{1}{\epsilon_0 c^2}(\hat{j}_i(x) + j_i^{(EXT)}(x))\right), \tag{6}$$

$$0 = c\,\frac{\delta\mathcal{I}}{\delta\phi(x)} = \epsilon_0\left(-\partial_i\partial_i\phi(x) - \partial_t\partial_i A_i(x) - \frac{1}{\epsilon_0}(\hat{\rho}(x) + \rho^{(EXT)}(x))\right). \tag{7}$$

In Eqs.(4) and (5), the left- and right-hand functional derivatives with respect to the Grassmann field are executed, respectively[8]. In Eqs.(6) and (7), the following definitions are introduced for the electron charge and current densities, respectively:

$$\hat{\rho}(x) \equiv -c\frac{\delta}{\delta\phi(x)}\mathcal{I}_{\mathrm{mat}} = q\hat{\psi}^\dagger_\alpha(x)\hat{\psi}_\alpha(x), \tag{8}$$

$$\hat{j}_i(x) \equiv +c\frac{\delta}{\delta A_i(x)}\mathcal{I}_{\mathrm{mat}} = \frac{q}{2m}\hat{\psi}^\dagger_\alpha(x)\left(\frac{\hbar}{i}\partial_i - qA_i(x)\right)\hat{\psi}_\alpha(x) + \mathrm{h.c.}. \tag{9}$$

The charge-conservation law below holds, and is checked through explicit calculation:

$$\partial_t\hat{\rho}(x) + \partial_i\hat{j}_i(x) = 0. \tag{10}$$

In the four-element representation, Eqs.(6) and (7) become:

$$\left(\delta^\mu{}_\nu\Box - \partial^\mu\partial_\nu\right)A^\nu(x) = \frac{1}{\epsilon_0 c}(\hat{j}^\mu(x) + j^{\mu(EXT)}(x)), \tag{11}$$

$$\begin{aligned}
\text{where}\quad & \hat{j}^\mu = (c\hat{\rho}, \hat{\mathbf{j}}),\ \hat{j}_\mu = (c\hat{\rho}, -\hat{\mathbf{j}}),\\
& A^\mu = (\phi, c\mathbf{A}),\ A_\mu = (\phi, -c\mathbf{A}),\\
& \partial^\mu = (1/c\,\partial_t, -\nabla),\ \partial_\mu = (1/c\,\partial_t, \nabla),\\
& \Box = \partial^\mu\partial_\mu = 1/c^2\,\partial_t^2 - \Delta\ \text{etc.}
\end{aligned} \tag{12}$$

Although Lorentz invariance is not maintained in the non-relativistic theory, we use the four-element notation to simply represent charge conservation and gauge invariance. For example, Eqs.(8)-(10) become:

$$\hat{j}^\mu(x) = -c^2\frac{\delta}{\delta A_\mu(x)}\mathcal{I}_{\mathrm{mat}}, \tag{13}$$

$$\partial_\mu\,\hat{j}^\mu(x) = 0. \tag{14}$$

The action integral, Eq.(1) is invariant under the following gauge transformation:

$$\begin{aligned}
& A^\mu(x) \to A^\mu(x) + c\,\partial^\mu\eta(x),\\
& \hat{\psi}_\alpha(x) \to e^{\frac{i}{\hbar}q\eta(x)}\hat{\psi}_\alpha(x), \quad \hat{\psi}^\dagger_\alpha(x) \to \hat{\psi}^\dagger_\alpha(x)e^{\frac{-i}{\hbar}q\eta(x)}.
\end{aligned} \tag{15}$$

From the point of view of Noether's theorem[7], the gauge invariance of the action integral is the cause of the charge conservation law, Eq.(10) or Eq.(14).

Let us separate the EM field into two parts:

$$A^{\mu}(x) = A^{(0)\mu}(x) + \Delta A^{\mu}(x), \tag{16}$$

where $A^{(0)\mu}$ is the static, initial EM potential satisfying Eqs.(6) and (7), and $\Delta A^{\mu}(x)$ is the perturbative EM potential. Under this variation of the EM field, let us re-optimize the action for matter, $\mathcal{I}_{\rm mat}[\hat{\psi}^{\dagger}_{\alpha}, \hat{\psi}_{\alpha}, A^{\mu}]$. That is, we re-optimize the electron field operator satisfying Eqs.(4) and (5) under $A^{(0)\mu} + \Delta A^{\mu}(x)$. In the above procedure, the variation of the action for the matter is expressed by the total functional derivative of $A^{\mu}(x)$:

$$\begin{aligned}
&\frac{\delta}{\delta A_{\mu}(x)} \mathcal{I}_{\rm mat}[\hat{\psi}^{\dagger}_{\alpha}[A^{\nu}], \hat{\psi}_{\alpha}[A^{\nu}], A^{\nu}] \\
&= \left.\frac{\delta}{\delta A_{\mu}(x)}\right|_{\rm explicit} \mathcal{I}_{\rm mat} + \int \mathrm{d}^4x' \frac{\delta \hat{\psi}^{\dagger}_{\alpha}(x')}{\delta A_{\mu}(x)} \delta \hat{\psi}^{\dagger}_{\alpha}(x') \backslash \delta \mathcal{I}_{\rm mat} + \int \mathrm{d}^4x' \delta \mathcal{I}_{\rm mat} / \delta \hat{\psi}_{\alpha}(x') \frac{\delta \hat{\psi}_{\alpha}(x')}{\delta A_{\mu}(x)} \\
&= \frac{-1}{c^2} \hat{j}^{\mu}(x; [A^{(0)\nu}]).
\end{aligned} \tag{17}$$

where the first term in the second expression is the variation explicitly caused by the perturbative EM field, and the second and third terms are the implicit variations, created through re-optimization of the field operator to satisfy Eqs.(6) and (7) under the perturbative EM field. The last expression is derived using Eq.(13), Eqs.(4) and (5). The above equation reveals that the first order total functional derivative of the action of matter is simply the current density. Furthermore, the second order total functional derivative is calculated as follows:

$$\begin{aligned}
&\frac{\delta}{\delta A^{\mu_1}(x_1)} \frac{\delta}{\delta A_{\mu}(x)} \mathcal{I}_{\rm mat}[\hat{\psi}^{\dagger}_{\alpha}[A^{\nu}], \hat{\psi}_{\alpha}[A^{\nu}], A^{\nu}] \\
&= \frac{\delta}{\delta A^{\mu_1}(x_1)} \left(\left.\frac{\delta}{\delta A_{\mu}(x)}\right|_{\rm explicit} \mathcal{I}_{\rm mat} \right) + \int \mathrm{d}^4x' \frac{\delta}{\delta A^{\mu_1}(x_1)} \left(\frac{\delta \hat{\psi}^{\dagger}_{\alpha}(x')}{\delta A_{\mu}(x)} \delta \hat{\psi}^{\dagger}_{\alpha}(x') \backslash \delta \mathcal{I}_{\rm mat} \right) \\
&\qquad + \int \mathrm{d}^4x' \frac{\delta}{\delta A^{\mu_1}(x_1)} \left(\delta \mathcal{I}_{\rm mat} / \delta \hat{\psi}_{\alpha}(x') \frac{\delta \hat{\psi}_{\alpha}(x')}{\delta A_{\mu}(x)} \right) \\
&= \frac{-1}{c^2} \left. \frac{\delta \hat{j}^{\mu}(x; [A^{\nu}])}{\delta A^{\mu_1}(x_1)} \right|_{A^{\nu} = A^{(0)\nu}},
\end{aligned} \tag{18}$$

where the second and third terms in the second expression are 0. Actually, the integrand of

the second term is:

$$\left(\frac{\delta}{\delta A^{\mu_1}(x_1)}\frac{\delta\hat{\psi}^\dagger_\alpha(x')}{\delta A_\mu(x)}\right)\delta\hat{\psi}^\dagger_\alpha(x')\backslash\delta\mathcal{I}_{\rm mat}+\frac{\delta\hat{\psi}^\dagger_\alpha(x')}{\delta A_\mu(x)}\left(\frac{\delta}{\delta A^{\mu_1}(x_1)}\delta\hat{\psi}^\dagger_\alpha(x')\backslash\delta\mathcal{I}_{\rm mat}\right),$$

The first term in this equation is 0 because of Eq.(4) under the initial EM potential, and the second term is 0 because of the re-optimization of the field operators under the perturbative EM potential. That is, Heisenberg's equation holds for any EM potential. In the same manner as for higher order total functional derivatives of the action of matter, the following extension of Eq.(18) holds (see Appendix A for details):

$$\left.\frac{\delta^{n+1}\mathcal{I}_{\rm mat}[\hat{\psi}^\dagger_\alpha[A^\nu],\hat{\psi}_\alpha[A^\nu],A^\nu]}{\delta A^{\mu_n}(x_n)\cdots\delta A^{\mu_1}(x_1)\delta A_\mu(x)}\right|_{A^\nu=A^{(0)\nu}}=\frac{-1}{c^2}\left.\frac{\delta^n\hat{j}^\mu(x;[A^\nu])}{\delta A^{\mu_n}(x_n)\cdots\delta A^{\mu_1}(x_1)}\right|_{A^\nu=A^{(0)\nu}}. \tag{19}$$

To define the single susceptibility, suppose the system under the initial EM field $A^{(0)\mu}(x)$ is exposed to the perturbative EM field $\Delta A^\mu(x)$. The initial EM field $A^{(0)\mu}$ is a solution of the coupled equations Eqs.(4) and (7), i.e., Heisenberg's equation and Maxwell's wave equations, and is assumed to be a static solution existing in the ground state. On the other hand, the total EM field $A^{(0)\mu}+\Delta A^\mu$ is not necessarily a solution of Maxwell's wave equations, Eqs.(6) and (7), that is, ΔA^μ is introduced as a virtual variation. The induced current density is the variation from the current density under the initial EM field:

$$\begin{aligned}
&\hat{j}^\mu(x;[A^{(0)\nu}+\Delta A^\nu])-\hat{j}^\mu(x;[A^{(0)\nu}])\\
=&\int\mathrm{d}^4x_1\left.\frac{\delta\hat{j}^\mu(x;[A^\nu]))}{\delta A^{\mu_1}(x_1)}\right|_{A^\nu=A^{(0)\nu}}\Delta A^{\mu_1}(x_1)\\
+&\frac{1}{2!}\int\mathrm{d}^4x_1\int\mathrm{d}^4x_2\left.\frac{\delta^2\hat{j}^\mu(x;[A^\nu])}{\delta A^{\mu_1}(x_1)\delta A^{\mu_2}(x_2)}\right|_{A^\nu=A^{(0)\nu}}\Delta A^{\mu_1}(x_1)\Delta A^{\mu_2}(x_2)\\
+&\frac{1}{3!}\int\mathrm{d}^4x_1\int\mathrm{d}^4x_2\int\mathrm{d}^4x_3\left.\frac{\delta^3\hat{j}^\mu(x;[A^\nu])}{\delta A^{\mu_1}(x_1)\delta A^{\mu_2}(x_2)\delta A^{\mu_3}(x_3)}\right|_{A^\nu=A^{(0)\nu}}\Delta A^{\mu_1}(x_1)\Delta A^{\mu_2}(x_2)\Delta A^{\mu_3}(x_3)\\
+&\cdots.
\end{aligned}\tag{20}$$

From Eq.(19), the linear and nonlinear single susceptibility operators are defined as:

$$\begin{aligned}
\hat{\chi}^\mu{}_{\mu_1}(x,x_1)&\equiv\left.\frac{\delta\hat{j}^\mu(x;[A^\nu])}{\delta A^{\mu_1}(x_1)}\right|_{A^\nu=A^{(0)\nu}}\\
&=-c^2\left.\frac{\delta^2\mathcal{I}_{\rm mat}}{\delta A_\mu(x)\delta A^{\mu_1}(x_1)}\right|_{A^\nu=A^{(0)\nu}},\\
\hat{\chi}^\mu{}_{\mu_1\,\mu_2}(x,x_1,x_2)&\equiv\frac{1}{2!}\left.\frac{\delta^2\hat{j}^\mu(x;[A^\nu])}{\delta A^{\mu_1}(x_1)\delta A^{\mu_2}(x_2)}\right|_{A^\nu=A^{(0)\nu}},
\end{aligned}\tag{21}$$

$$= \frac{-c^2}{2!} \left. \frac{\delta^3 \mathcal{I}_{\rm mat}}{\delta A_\mu(x)\delta A^{\mu_1}(x_1)\delta A^{\mu_2}(x_2)} \right|_{A^\nu = A^{(0)\nu}} \tag{22}$$

$$\hat{\chi}^{\mu}{}_{\mu_1\cdots\mu_n}(x, x_1, \cdots, x_n) \equiv \frac{1}{n!} \left. \frac{\delta^n \hat{j}^\mu(x; [A^\nu])}{\delta A^{\mu_1}(x_1)\cdots\delta A^{\mu_n}(x_n)} \right|_{A^\nu = A^{(0)\nu}}$$

$$= \frac{-c^2}{n!} \left. \frac{\delta^{n+1} \mathcal{I}_{\rm mat}}{\delta A_\mu(x)\delta A^{\mu_1}(x_1)\cdots\delta A^{\mu_n}(x_n)} \right|_{A^\nu = A^{(0)\nu}}, \tag{23}$$

The susceptibility is defined using a small amount of the virtual variation, ΔA^μ. That is, the EM field does not in general satisfy its Euler equation, Eq.(11), while the electron field operators satisfy Eqs.(4) and (5). To evaluate the real EM field, ΔA^μ must be determined and a further procedure is required to solve the coupled equations, with the constitutive equations in terms of the susceptibility and Maxwell's wave equations Eqs.(6) and (7). This procedure is provided in a self-consistent manner, established by K.Cho[4].

III. CHARGE CONSERVATION LAW AND GAUGE INVARIANCE OF THE SINGLE SUSCEPTIBILITY

In the last expressions in Eqs.(21)-(23) the coordinates $x_1, x_2, \cdots$ for the cause (the perturbative EM field) and the coordinates x for the result (the induced current density) are symmetric. Charge conservation for the induced charge density holds to each order of the perturbation; this is described by the derivative of the coordinate for the result, x:

$$\partial_\mu \hat{\chi}^{\mu}{}_{\mu_1\cdots}(x, x_1, \cdots) = 0. \tag{24}$$

This symmetry of the coordinates between the result and the cause leads to the following equation concerning the derivative of the coordinate for the cause, e.g., x_1 :

$$\partial^{\mu_1} \hat{\chi}^{\mu}{}_{\mu_1\cdots}(x, x_1, \cdots) = 0. \tag{25}$$

Equation (25) means that the susceptibility guarantees that gauge invariance is respected. That is, the resultant charge and current densities are independent of the chosen gauge. To confirm this fact, consider the convolution integral with the single susceptibility and the perturbative EM field, in a certain gauge, e.g.,

$$\int \mathrm{d}^4 x_1 \ \hat{\chi}^{\mu}{}_{\mu_1\cdots}(x, x_1, \cdots)\Delta A^{\mu_1}(x_1). \tag{26}$$

A gauge transformation of ΔA to $\Delta A'$ in another gauge is expressed as :

$$\Delta A^{\mu_1}(x_1) = \Delta A'^{\mu_1}(x_1) + c\,\partial^{\mu_1}\eta(x_1), \tag{27}$$

where η is the gauge function. Equation (26) leads to:

$$\begin{aligned} & \int \mathrm{d}^4x_1 \;\; \hat{\chi}^{\mu}{}_{\mu_1\cdots}(x, x_1, \cdots)\Delta A^{\mu_1}(x_1) \\ = & \int \mathrm{d}^4x_1 \;\; \hat{\chi}^{\mu}{}_{\mu_1\cdots}(x, x_1, \cdots)\Delta A'^{\mu_1}(x_1) - c\int \mathrm{d}^4x_1 \;\; \partial^{\mu_1}\hat{\chi}^{\mu}{}_{\mu_1\cdots}(x, x_1, \cdots)\eta(x_1) \\ = & \int \mathrm{d}^4x_1 \;\; \hat{\chi}^{\mu}{}_{\mu_1\cdots}(x, x_1, \cdots)\Delta A'^{\mu_1}(x_1). \end{aligned} \tag{28}$$

The contribution of the gauge function vanishes in the convolution integral. Thus, the gauge of the perturbative EM field may be freely selected. This means that the susceptibility is independent of the chosen gauge and, in practice, one may select a gauge that is most convenient for calculation.

IV. HEISENBERG OPERATOR OF THE SINGLE SUSCEPTIBILITY

In this section, the formula for Heisenberg operators of the linear and nonlinear single susceptibilities is given using an expansion of the retarded product in Hamiltonian formulation[9]. The Heisenberg operator of four-element current density, i.e., $\hat{j}^{\mu}(x) = (c\hat{\rho}(x), \hat{\mathbf{j}}(x))$ is:

$$\hat{j}^{\mu}(x) \;=\; \begin{cases} cq\hat{\psi}^{\dagger}_{\alpha}(x)\hat{\psi}_{\alpha}(x) & \text{for} \quad \mu = 0, \\ \hat{\psi}^{\dagger}_{\alpha}(x)\dfrac{q}{2m}\left(\dfrac{\hbar}{i}\partial^{\mu} - \dfrac{q}{c}A^{\mu}(x)\right)\hat{\psi}_{\alpha}(x) + \text{h.c.} & \text{for} \quad \mu = 1, 2, 3\,. \end{cases} \tag{29}$$

In Eq.(2), if the factor $i\hbar\hat{\psi}^{\dagger}_{\alpha}(x)$ of the first term is regarded as the canonical momentum of $\hat{\psi}_{\alpha}(x)$, then the Hamiltonian density may be determined as the Legendre transformation from the Lagrangian density, that is:

$$\hat{H} \quad \equiv \int \mathrm{d}^3x \;\; \frac{1}{2m}\left(\frac{\hbar}{-i}\partial_i - qA_i(x)\right)\hat{\psi}^{\dagger}_{\alpha}(x) \;\; \left(\frac{\hbar}{i}\partial_i - qA_i(x)\right)\hat{\psi}_{\alpha}(x) + q\phi(x)\;\hat{\psi}^{\dagger}_{\alpha}(x)\hat{\psi}_{\alpha}(x). \tag{30}$$

This Hamiltonian governs the motion of electron field operators. Assuming that the initial EM field $\phi^{(0)}, \mathbf{A}^{(0)}$ is the static EM field existing in the ground state of a many-electron

system, the Hamiltonian, $\hat{H}$ may be separated into a non-perturbative part, $\hat{H}^{(0)}$ and a perturbative part, $\hat{V}$ as follows:

$$\begin{aligned}
\hat{H}^{(0)} \equiv & \int \mathrm{d}^3x \ \frac{1}{2m}\left(\frac{\hbar}{-i}\partial_i - qA_i^{(0)}(x)\right)\hat{\psi}_\alpha^\dagger(x)\cdot\left(\frac{\hbar}{i}\partial_i - qA_i^{(0)}(x)\right)\hat{\psi}_\alpha(x) + q\phi^{(0)}(x)\,\hat{\psi}_\alpha^\dagger(x)\hat{\psi}_\alpha(x) \\
& + v^{(\mathrm{AUX})}(x)\,\hat{\psi}_\alpha^\dagger(x)\hat{\psi}_\alpha(x), \qquad (31) \\
\hat{V}(t) \equiv & \hat{H} - \hat{H}^{(0)} = \int \mathrm{d}^3x\,\hat{v}(x), \\
= & \int \mathrm{d}^3x \ \Big\{\big(\phi(x) - \phi^{(0)}(x)\big)\ q\hat{\psi}_\alpha^\dagger(x)\hat{\psi}_\alpha(x) \\
& - \Big(A_i(x) - A_i^{(0)}(x)\Big)\left(\hat{\psi}_\alpha^\dagger(x)\,\frac{q}{2m}\left(\frac{\hbar}{i}\partial_i - qA_i^{(0)}(x)\right)\hat{\psi}_\alpha(x) + \mathrm{h.c.}\right) \\
& + \frac{q}{2m}\Big(A_i(x) - A_i^{(0)}(x)\Big)\Big(A_i(x) - A_i^{(0)}(x)\Big)\ q\hat{\psi}_\alpha^\dagger(x)\hat{\psi}_\alpha(x)\Big\} \\
= & \int \mathrm{d}^3x \ \left\{\frac{1}{c}\left(A^\mu(x) - A^{(0)\,\mu}(x)\right)\hat{j}_\mu(x)\Big|_{A=A^{(0)}}\right. \\
& \left. - \frac{q}{2mc^3}\,\tilde{\delta}_\mu^{\ \mu'}\left(A^\mu(x) - A^{(0)\,\mu}(x)\right)\Big(A_{\mu'}(x) - A_{\mu'}^{(0)}(x)\Big)\,\hat{j}_0(x)\right\}, \qquad (32) \\
& \text{where } \tilde{\delta}_\mu^{\ \mu'} = \begin{cases} 1 & \text{for } \mu = \mu' = 1,2,3\,, \\ 0 & \text{otherwise}\,. \end{cases} \qquad (33)
\end{aligned}$$

The auxiliary potential, $v^{(\mathrm{AUX})}(x)$ effectively represents for the quantum many-electron effect (the exchange-correlation effect), ; this fact will be explained in the next section. The tensor Eq.(33) represents the non-relativistic effect. Actually, this tensor is the analogue of the four-element Kronecker delta, but the time and spatial coordinates are inequivalent.

Here, the field operators in the interaction picture (the asymptotic field operators) $\hat{\psi}_\alpha^{(in)\dagger}, \hat{\psi}_\alpha^{(in)}$ are governed by the non-perturbative Hamiltonian $\hat{H}^{(0)}$ and coincide with the field operators in the Heisenberg picture, $\hat{\psi}_\alpha^\dagger, \hat{\psi}_\alpha$ at the infinite past time, $t \to -\infty$, assuming the adiabatic switch-on. The time-evolution operator $\hat{U}(t, -\infty)$ relates the operators in the two pictures as follows:

$$\begin{aligned}
\hat{\psi}_\alpha(x) &= \hat{U}^{-1}(t,-\infty)\hat{\psi}_\alpha^{(in)}(x)\hat{U}(t,-\infty), \qquad (34) \\
\hat{\psi}_\alpha^\dagger(x) &= \hat{U}^{-1}(t,-\infty)\hat{\psi}_\alpha^{(in)\dagger}(x)\hat{U}(t,-\infty), \\
\text{where} \quad & \hat{U}(t,-\infty) = \lim_{t_0\to-\infty}\hat{U}(t,t_0) = \lim_{t_0\to-\infty}\hat{T}e^{\frac{1}{i\hbar}\int_{t_0}^t \mathrm{d}t'\hat{V}^{(in)}(t')}, \\
& \hat{V}^{(in)}(t') \equiv \hat{V}([\hat{\psi}_\alpha^{(in)\,\dagger}, \hat{\psi}_\alpha^{(in)}]; t')
\end{aligned}$$

Combining Eq.(34) and Eq.(29), the four-element current density operator in the interaction picture may be defined as: $\hat{j}^{(in)\,\mu}(x) = (c\hat{\rho}^{(in)}(x), \hat{\mathbf{j}}^{(in)}(x))$. These charge and current

densities do not satisfy the charge conservation law, except for $A = A^{(0)}$, and are merely convenient tools used for obtaining the expansion of the retarded product of the Heisenberg operator.

$$\hat{j}^{\mu}(x) = \hat{U}^{-1}(t,-\infty)\hat{j}^{(in)\,\mu}(x)\hat{U}(t,-\infty), \tag{35}$$

$$\hat{j}^{(in)\,\mu}(x) = \begin{cases} c\,q\hat{\psi}^{(in)\dagger}_{\alpha}(x)\,\hat{\psi}^{(in)}_{\alpha}(x) & \text{for} \quad \mu = 0, \\ \hat{\psi}^{(in)\dagger}_{\alpha}(x)\dfrac{q}{2m}\left(\dfrac{\hbar}{i}(-\partial^{\mu}) - \dfrac{q}{c}A^{\mu}(x)\right)\hat{\psi}^{(in)}_{\alpha}(x) + \text{h.c.} & \text{for} \quad \mu = 1,2,3\,. \end{cases} \tag{36}$$

To obtain the perturbative expansion (the retarded product series) of the Heisenberg operator, let us introduce an operator in the intermediate picture, where $\hat{U}(t,t_0)$ will be used instead of $\hat{U}(t,-\infty)$:

$$\begin{aligned} \hat{\rho}^{\bullet}(x;t_0) &= \hat{U}^{-1}(t,t_0)\,q\,\hat{\psi}^{(in)\dagger}_{\alpha}(x)\,\hat{\psi}^{(in)}_{\alpha}(x)\hat{U}(t,t_0), \\ \hat{j}^{\bullet}_{i}(x;t_0) &= \hat{U}^{-1}(t,t_0)\frac{q}{2m}\hat{\psi}^{(in)\dagger}_{\alpha}(x)\left(\frac{\hbar}{i}\partial_i - qA_i(x)\right)\hat{\psi}^{(in)}_{\alpha}(x)\hat{U}(t,t_0) + \text{h.c.}. \end{aligned}$$

The corresponding four-element current density is

$$\hat{j}^{\bullet\,\mu}(x;t_0) = (c\hat{\rho}^{\bullet}(x;t_0),\,\hat{\mathbf{j}}^{\bullet}(x;t_0))$$

As $t_0 \to -\infty$, these operators coincide with those of the Heisenberg picture, while at $t_0 = t$, they coincide with those of the interaction picture:

$$\hat{j}^{\bullet\,\mu}(x;-\infty) = \hat{j}^{\mu}(x), \tag{37}$$

$$\hat{j}^{\bullet\,\mu}(x;t) = \hat{j}^{(in)\,\mu}(x). \tag{38}$$

Next, let's investigate the time evolution of $\hat{j}^{\bullet\,\mu}$ as a function of t_0.

$$\begin{aligned} \partial_{t_0}\hat{j}^{\bullet\,\mu}(x;t_0) &= \{\partial_{t_0}\hat{U}^{-1}(t,t_0)\}\hat{j}^{(in)\,\mu}(x)\hat{U}(t,t_0) + \hat{U}^{-1}(t,t_0)\hat{j}^{(in)\,\mu}(x)\{\partial_{t_0}\hat{U}(t,t_0)\} \\ &= \frac{1}{i\hbar}\hat{V}^{(in)}(t_0)\hat{U}^{-1}(t,t_0)\hat{j}^{(in)\,\mu}(x)\hat{U}(t,t_0) + \hat{U}^{-1}(t,t_0)\hat{j}^{(in)\,\mu}(x)\hat{U}(t,t_0)\frac{-1}{i\hbar}\hat{V}^{(in)}(t_0) \\ &= \frac{-1}{i\hbar}\left[\hat{j}^{\bullet\,\mu}(x;t_0), \hat{V}^{(in)}(t_0)\right] \end{aligned}$$

Integrating over $[t_0, t]$, approximating iteratively using Eq.(38), and changing the region of

multi-integration, we obtain:

$$
\begin{aligned}
\hat{j}^{\bullet\,\mu}(x;t_0) &= \hat{j}^{(in)\,\mu}(x) + \frac{1}{i\hbar}\int_{t_0}^{t}\mathrm{d}t_1\left[\hat{j}^{\bullet\,\mu}(x;t_1),\hat{V}^{(in)}(t_1)\right] \\
&= \hat{j}^{(in)\,\mu}(x) + \frac{1}{i\hbar}\int_{t_0}^{t}\mathrm{d}t_1\left[\hat{j}^{(in)\,\mu}(x),\hat{V}^{(in)}(t_1)\right] \\
&\quad + \left(\frac{1}{i\hbar}\right)^2\int_{t_0}^{t}\mathrm{d}t_1\int_{t_1}^{t}\mathrm{d}t_2\left[\left[\hat{j}^{(in)\,\mu}(x),\hat{V}^{(in)}(t_2)\right],\hat{V}^{(in)}(t_1)\right] \\
&\quad + \left(\frac{1}{i\hbar}\right)^3\int_{t_0}^{t}\mathrm{d}t_1\int_{t_1}^{t}\mathrm{d}t_2\int_{t_2}^{t}\mathrm{d}t_3\left[\left[\left[\hat{j}^{(in)\,\mu}(x),\hat{V}^{(in)}(t_3)\right],\hat{V}^{(in)}(t_2)\right],\hat{V}^{(in)}(t_1)\right] + \cdots \\
&= \hat{j}^{(in)\,\mu}(x) + \frac{1}{i\hbar}\int_{t_0}^{t}\mathrm{d}t_1\left[\hat{j}^{(in)\,\mu}(x),\hat{V}^{(in)}(t_1)\right] \\
&\quad + \left(\frac{1}{i\hbar}\right)^2\int_{t_0}^{t}\mathrm{d}t_1\int_{t_0}^{t_1}\mathrm{d}t_2\left[\left[\hat{j}^{(in)\,\mu}(x),\hat{V}^{(in)}(t_1)\right],\hat{V}^{(in)}(t_2)\right] \\
&\quad + \left(\frac{1}{i\hbar}\right)^3\int_{t_0}^{t}\mathrm{d}t_1\int_{t_0}^{t_1}\mathrm{d}t_2\int_{t_0}^{t_2}\mathrm{d}t_3\left[\left[\left[\hat{j}^{(in)\,\mu}(x),\hat{V}^{(in)}(t_1)\right],\hat{V}^{(in)}(t_2)\right],\hat{V}^{(in)}(t_3)\right] + \cdots
\end{aligned}
$$

Then, taking the limit $t_0 \to -\infty$, the above equation yields the retarded product of the Heisenberg operator, as follows:

$$
\begin{aligned}
\hat{j}^{\mu}(x) &= \hat{j}^{(in)\,\mu}(x) + \frac{1}{i\hbar c}\int_{ct_1\in(-\infty,ct]}\mathrm{d}^4x_{\,1}\left[\hat{j}^{(in)\,\mu}(x),\hat{v}^{(in)}(x_1)\right] \\
&\quad + \left(\frac{1}{i\hbar c}\right)^2\int_{ct_1\in(-\infty,ct]}\mathrm{d}^4x_{\,1}\int_{ct_2\in(-\infty,ct_1]}\mathrm{d}^4x_{\,2}\left[\left[\hat{j}^{(in)\,\mu}(x),\hat{v}^{(in)}(x_1)\right],\hat{v}^{(in)}(x_2)\right] \\
&\quad + \left(\frac{1}{i\hbar c}\right)^3\int_{ct_1\in(-\infty,ct]}\mathrm{d}^4x_{\,1}\int_{ct_2\in(-\infty,ct_1]}\mathrm{d}^4x_{\,2}\int_{ct_3\in(-\infty,ct_2]}\mathrm{d}^4x_{\,3}\left[\left[\left[\hat{j}^{(in)\,\mu}(x),\hat{v}^{(in)}(x_1)\right],\hat{v}^{(in)}(x_2)\right],\hat{v}^{(in)}(x_3)\right] \\
&\quad + \cdots
\end{aligned}
\tag{39}
$$

where $\hat{V}^{(in)}(t) = \int \mathrm{d}^3x\ \hat{v}^{(in)}(x)$.

The quantity $\hat{V}^{(in)}$, $\hat{v}^{(in)}$ in the above formula is Eq.(32), with $\hat{\psi}_\alpha$, $\hat{\psi}^\dagger_\alpha$ being replaced by $\hat{\psi}^{(in)}_\alpha$, $\hat{\psi}^{(in)\,\dagger}_\alpha$. Next, let us derive the Heisenberg operator of susceptibility, by means of the functional derivative of Eq.(39) by the EM potential. In Equation (39), the dependence of the EM potential through $\hat{j}^{(in)\,\mu}(x)$ in Eq.(36) is of zeroth and first order($\mu \in \{1,2,3\}$), and dependence through $\hat{v}^{(in)}(x_1)$ is of first and second order. The linear single susceptibility operator comes from the A^1-dependence, which exists in the first and second terms of Eq.(39) :

$$
\hat{\chi}^{\mu}{}_{\mu_1}(x,x_1) = \left.\frac{\delta\hat{j}^{\mu}(x)}{\delta A^{\mu_1}(x_1)}\right|_{A=A^{(0)}}
$$

$$= \frac{-q}{mc^2}\,\tilde{\delta}^{\mu}{}_{\mu_1}\delta^4(x-x_1)\,\hat{j}^{(in0)\,0}(x) + \frac{1}{i\hbar c^2}\theta(ct-ct_1)\left[\hat{j}^{(in0)\,\mu}(x), \hat{j}^{(in0)}_{\mu_1}(x_1)\right], \quad (40)$$

where $\quad \hat{j}^{(in0)\,\mu}(x) = \hat{j}^{(in)\,\mu}(x)\Big|_{A=A^{(0)}}$.

The Heisenberg operators of the nonlinear single susceptibilities, to second and higher order, are as follows. To avoid any confusion in the case of two times coinciding, the long and explicit expressions are given, without making use of the time ordering operator.

$$\begin{aligned}
2!\,\hat{\chi}^{\mu}{}_{\mu_1\mu_2}(x,x_1,x_2) &= \left.\frac{\delta^2\hat{j}^{\mu}(x)}{\delta A^{\mu_1}(x_1)\delta A^{\mu_2}(x_2)}\right|_{A=A^{(0)}} \\
&= \frac{1}{i\hbar c^2}\,\frac{-q}{mc^2} \quad \Big\{\delta(ct-ct_1)\theta(ct-ct_2) \quad \tilde{\delta}^{\mu}{}_{\mu_1}\delta^3(x-x_1)\left[\hat{j}^{(in0)\,0}(x), \hat{j}^{(in0)}_{\mu_2}(x_2)\right] \\
&\qquad +\delta(ct-ct_2)\theta(ct-ct_1) \quad \tilde{\delta}^{\mu}{}_{\mu_2}\delta^3(x-x_2)\left[\hat{j}^{(in0)\,0}(x), \hat{j}^{(in0)}_{\mu_1}(x_1)\right] \\
&\qquad + \theta(ct-ct_1)\delta(ct_1-ct_2)\tilde{\delta}_{\mu_1\,\mu_2}\delta^3(x_1-x_2)\left[\hat{j}^{(in0)\,\mu}(x), \hat{j}^{(in0)}_{0}(x_1)\right]\Big\} \\
&+\left(\frac{1}{i\hbar c^2}\right)^2 \quad \Big\{\theta(ct-ct_1)\theta(ct_1-ct_2)\left[\left[\hat{j}^{(in0)\,\mu}(x), \hat{j}^{(in0)}_{\mu_1}(x_1)\right], \hat{j}^{(in0)}_{\mu_2}(x_2)\right] \\
&\qquad + \theta(ct-ct_2)\theta(ct_2-ct_1)\left[\left[\hat{j}^{(in0)\,\mu}(x), \hat{j}^{(in0)}_{\mu_2}(x_2)\right], \hat{j}^{(in0)}_{\mu_1}(x_1)\right]\Big\}\,.
\end{aligned} \quad (41)$$

$$\begin{aligned}
3!\,\hat{\chi}^{\mu}{}_{\mu_1\mu_2\mu_3}(x,x_1,x_2,x_3) &= \left.\frac{\delta^3\hat{j}^{\mu}(x)}{\delta A^{\mu_1}(x_1)\delta A^{\mu_2}(x_2)\delta A^{\mu_3}(x_3)}\right|_{A=A^{(0)}} \\
= \frac{1}{i\hbar c^2}\left(\frac{-q}{mc^2}\right)^2 & \quad (42) \\
&\Big\{\theta(ct-ct_2)\delta(ct-ct_1)\delta(ct_2-ct_3)\tilde{\delta}^{\mu}{}_{\mu_1}\delta^3(x-x_1)\tilde{\delta}_{\mu_2\,\mu_3}\delta^3(x_2-x_3)\left[\hat{j}^{(in0)\,0}(x), \hat{j}^{(in0)}{}_{0}(x_2)\right] \\
&+\theta(ct-ct_3)\delta(ct-ct_2)\delta(ct_3-ct_1)\tilde{\delta}^{\mu}{}_{\mu_2}\delta^3(x-x_2)\tilde{\delta}_{\mu_3\,\mu_1}\delta^3(x_3-x_1)\left[\hat{j}^{(in0)\,0}(x), \hat{j}^{(in0)}{}_{0}(x_3)\right] \\
&+ \theta(ct-ct_1)\delta(ct-ct_3)\delta(ct_1-ct_2)\tilde{\delta}^{\mu}{}_{\mu_3}\delta^3(x-x_3)\tilde{\delta}_{\mu_1\,\mu_2}\delta^3(x_1-x_2)\left[\hat{j}^{(in0)\,0}(x), \hat{j}^{(in0)}{}_{0}(x_1)\right]\Big\} \\
&+\left(\frac{1}{i\hbar c^2}\right)^2\frac{-q}{mc^2} \\
&\Big\{\delta(ct-ct_1)\theta(ct_1-ct_2)\theta(ct_2-ct_3)\tilde{\delta}^{\mu}{}_{\mu_1}\delta^3(x-x_1)\left[\left[\hat{j}^{(in0)\,0}(x), \hat{j}^{(in0)}_{\mu_2}(x_2)\right], \hat{j}^{(in0)}_{\mu_3}(x_3)\right] \\
&+\delta(ct-ct_1)\theta(ct_1-ct_3)\theta(ct_3-ct_2)\tilde{\delta}^{\mu}{}_{\mu_1}\delta^3(x-x_1)\left[\left[\hat{j}^{(in0)\,0}(x), \hat{j}^{(in0)}_{\mu_3}(x_3)\right], \hat{j}^{(in0)}_{\mu_2}(x_2)\right] \\
&+\delta(ct-ct_2)\theta(ct_2-ct_3)\theta(ct_3-ct_1)\tilde{\delta}^{\mu}{}_{\mu_2}\delta^3(x-x_2)\left[\left[\hat{j}^{(in0)\,0}(x), \hat{j}^{(in0)}_{\mu_3}(x_3)\right], \hat{j}^{(in0)}_{\mu_1}(x_1)\right] \\
&+\delta(ct-ct_2)\theta(ct_2-ct_1)\theta(ct_1-ct_3)\tilde{\delta}^{\mu}{}_{\mu_2}\delta^3(x-x_2)\left[\left[\hat{j}^{(in0)\,0}(x), \hat{j}^{(in0)}_{\mu_1}(x_1)\right], \hat{j}^{(in0)}_{\mu_3}(x_3)\right] \\
&+\delta(ct-ct_3)\theta(ct_3-ct_1)\theta(ct_1-ct_2)\tilde{\delta}^{\mu}{}_{\mu_3}\delta^3(x-x_3)\left[\left[\hat{j}^{(in0)\,0}(x), \hat{j}^{(in0)}_{\mu_1}(x_1)\right], \hat{j}^{(in0)}_{\mu_2}(x_2)\right] \\
&+\delta(ct-ct_3)\theta(ct_3-ct_2)\theta(ct_2-ct_1)\tilde{\delta}^{\mu}{}_{\mu_3}\delta^3(x-x_3)\left[\left[\hat{j}^{(in0)\,0}(x), \hat{j}^{(in0)}_{\mu_2}(x_2)\right], \hat{j}^{(in0)}_{\mu_1}(x_1)\right]
\end{aligned}$$

$$
\begin{aligned}
&+\theta(ct-ct_1)\delta(ct_1-ct_2)\theta(ct_2-ct_3)\tilde{\delta}_{\mu_1\,\mu_2}\delta^3(x_1-x_2)\left[\left[\hat{j}^{(in0)\,\mu}(x),\hat{j}^{(in0)}_{\quad 0}(x_1)\right],\hat{j}^{(in0)}_{\quad\mu_3}(x_3)\right]\\
&+\theta(ct-ct_2)\delta(ct_2-ct_3)\theta(ct_3-ct_1)\tilde{\delta}_{\mu_2\,\mu_3}\delta^3(x_2-x_3)\left[\left[\hat{j}^{(in0)\,\mu}(x),\hat{j}^{(in0)}_{\quad 0}(x_2)\right],\hat{j}^{(in0)}_{\quad\mu_1}(x_1)\right]\\
&+\theta(ct-ct_3)\delta(ct_3-ct_1)\theta(ct_1-ct_2)\tilde{\delta}_{\mu_3\,\mu_1}\delta^3(x_3-x_1)\left[\left[\hat{j}^{(in0)\,\mu}(x),\hat{j}^{(in0)}_{\quad 0}(x_3)\right],\hat{j}^{(in0)}_{\quad\mu_2}(x_2)\right]\\
&+\theta(ct-ct_1)\theta(ct_1-ct_2)\delta(ct_2-ct_3)\tilde{\delta}_{\mu_2\,\mu_3}\delta^3(x_2-x_3)\left[\left[\hat{j}^{(in0)\,\mu}(x),\hat{j}^{(in0)}_{\quad\mu_1}(x_1)\right],\hat{j}^{(in0)}_{\quad 0}(x_2)\right]\\
&+\theta(ct-ct_2)\theta(ct_2-ct_3)\delta(ct_3-ct_1)\tilde{\delta}_{\mu_3\,\mu_1}\delta^3(x_3-x_1)\left[\left[\hat{j}^{(in0)\,\mu}(x),\hat{j}^{(in0)}_{\quad\mu_2}(x_2)\right],\hat{j}^{(in0)}_{\quad 0}(x_3)\right]\\
&+\theta(ct-ct_3)\theta(ct_3-ct_1)\delta(ct_1-ct_2)\tilde{\delta}_{\mu_1\,\mu_2}\delta^3(x_1-x_2)\left[\left[\hat{j}^{(in0)\,\mu}(x),\hat{j}^{(in0)}_{\quad\mu_3}(x_3)\right],\hat{j}^{(in0)}_{\quad 0}(x_1)\right]\Big\}\\
&+\left(\frac{1}{i\hbar c^2}\right)^3\\
&\Big\{\theta(ct-ct_1)\theta(ct_1-ct_2)\theta(ct_2-ct_3)\left[\left[\left[\hat{j}^{(in0)\,\mu}(x),\hat{j}^{(in0)}_{\quad\mu_1}(x_1)\right],\hat{j}^{(in0)}_{\quad\mu_2}(x_2)\right],\hat{j}^{(in0)}_{\quad\mu_3}(x_3)\right]\\
&+\theta(ct-ct_1)\theta(ct_1-ct_3)\theta(ct_3-ct_2)\left[\left[\left[\hat{j}^{(in0)\,\mu}(x),\hat{j}^{(in0)}_{\quad\mu_1}(x_1)\right],\hat{j}^{(in0)}_{\quad\mu_3}(x_3)\right],\hat{j}^{(in0)}_{\quad\mu_2}(x_2)\right]\\
&+\theta(ct-ct_2)\theta(ct_2-ct_3)\theta(ct_3-ct_1)\left[\left[\left[\hat{j}^{(in0)\,\mu}(x),\hat{j}^{(in0)}_{\quad\mu_2}(x_2)\right],\hat{j}^{(in0)}_{\quad\mu_3}(x_3)\right],\hat{j}^{(in0)}_{\quad\mu_1}(x_1)\right]\\
&+\theta(ct-ct_2)\theta(ct_2-ct_1)\theta(ct_1-ct_3)\left[\left[\left[\hat{j}^{(in0)\,\mu}(x),\hat{j}^{(in0)}_{\quad\mu_2}(x_2)\right],\hat{j}^{(in0)}_{\quad\mu_1}(x_1)\right],\hat{j}^{(in0)}_{\quad\mu_3}(x_3)\right]\\
&+\theta(ct-ct_3)\theta(ct_3-ct_1)\theta(ct_1-ct_2)\left[\left[\left[\hat{j}^{(in0)\,\mu}(x),\hat{j}^{(in0)}_{\quad\mu_3}(x_3)\right],\hat{j}^{(in0)}_{\quad\mu_1}(x_1)\right],\hat{j}^{(in0)}_{\quad\mu_2}(x_2)\right]\\
&+\theta(ct-ct_3)\theta(ct_3-ct_2)\theta(ct_2-ct_1)\left[\left[\left[\hat{j}^{(in0)\,\mu}(x),\hat{j}^{(in0)}_{\quad\mu_3}(x_3)\right],\hat{j}^{(in0)}_{\quad\mu_2}(x_2)\right],\hat{j}^{(in0)}_{\quad\mu_1}(x_1)\right]\Big\}.
\end{aligned}
$$

The charge conservation,Eq.(24), and gauge invariance are respected in Equations (40)-(42). This fact is successfully checked in §B.

V. A REPRESENTATION OF THE SINGLE SUSCEPTIBILITY USING EIGENSTATES BASED ON DENSITY FUNCTIONAL THEORY

The linear and nonlinear single susceptibilities are the expectation values of the corresponding operators, Eqs.(40)-(42), using the ground state in the non-perturbed electron system, which is specified by the simplified conditions in this paper:

$$
\mathbf{A}(x)=\mathbf{A}^{(0)}(x)=\mathbf{0},\quad \mathbf{j}^{(\mathrm{EXT})}(x)=\mathbf{0},\quad \phi(x)=\phi^{(0)}(x)\text{ and }\rho^{(\mathrm{EXT})}(x)\quad\text{are static.}\tag{43}
$$

Let us explain how density functional theory[10, 11] may allow us to prepare such the ground state and the complete set of the states in the electron system. For that purpose, we need the electron field operators together with the scalar and vector potentials satisfying the coupled equations, Eqs.(4)-(9). However, in the semiclassical treatment of the present theory, Eqs.(8)

and (9) are replaced with their expectation values using the ground state(, which we seek now on). Due to this procedure, the quantum many-electron effect, the so-called exchange correlation effect is ignored. Therefore, the solution of Eqs.(4)-(9) as it is may not reproduce the electron charge density of the proper ground state, $\rho_{\rm GS}(\mathbf{r})$, which is obtained using the ordinary Hamiltonian including the two-body Coulomb interaction, eliminating the scalar potential under the Coulomb gauge. Such the electron density $\rho_{\rm GS}(\mathbf{r})$, in turn, brings about the proper scalar potential $\phi^{(0)}(x)$ under the Coulomb gauge. Suppose that the proper electron charge density $\rho_{\rm GS}(\mathbf{r})$ is already known under the ordinary Hamiltonian.

Now, we like to seek for the ground state $|0\rangle$ in need, adjusting the auxiliary potential $v^{(\rm AUX)}(\mathbf{r})$ to make the electron charge density fit the proper one:

$$\langle 0|\hat{\rho}(x)|0\rangle = \rho_{\rm GS}(\mathbf{r}). \tag{44}$$

Such a situation in Eq.(44) is assumed by Kohn and Sham in the density functional theory[11]. That is, Eqs.(4) and (5) are equivalent to Eq.(2.8) in Ref.[11] [the Kohn-Sham equation (KS equation)], if $v^{(\rm AUX)}(\mathbf{r})$ is regarded as the so-called exchange-correlation potential.

For details, one may prepare the spin-orbit function $\varphi_{k\alpha}(\mathbf{r},\sigma)$ (k,α stands for the orbit and spin states, σ is the spin coordinate) as the eigenstate of the KS equation with the eigenenergy $\hbar\omega_k$. Under the conditions,Eq.(43), the KS equation is,

$$0 = \left(\hbar\omega_k - q\phi^{(0)}(\mathbf{r}) - \frac{1}{2m}\frac{\hbar}{i}\partial_i \cdot \frac{\hbar}{i}\partial_i - v^{(\rm AUX)}(\mathbf{r})\right)\varphi_{k\alpha}(\mathbf{r},\sigma), \tag{45}$$

where $v^{(\rm AUX)}(\mathbf{r})$ is set to the exchange-correlation potential. Then, $\hat{\psi}_\alpha(x) = \sum_k \varphi_{k\alpha}(\mathbf{r},\sigma)\hat{a}_{k\alpha}$ satisfies Eq.(4) under the condition Eq.(43), where $\hat{a}_{k\alpha}$ is the operator to annihilate the electron belonging to the spin-orbit $\varphi_{k\alpha}(\mathbf{r},\sigma)$. Then, the ground state with the electron number n in the present theory is constructed as the single Slater determinant,

$$|0\rangle = \frac{1}{\sqrt{n!}}\prod_{k\alpha}\hat{a}^\dagger_{k\alpha}|{\rm vac}\rangle\,, \tag{46}$$

where $|{\rm vac}\rangle$ is the vacuum state, and the indecies $k\alpha$ scan over the n spin-orbits from the lowest eigenenergies. Furthermore, under the fixed $v^{(\rm AUX)}(\mathbf{r})$ and $\phi^{(0)}(\mathbf{r})$, one may consider all the possible combination of n spin-orbits and obtain the normalized orthogonal complete set $\{|m\rangle|m=0,1,2,\cdots\}$ in terms of single Slater determinants.

On the above logic, one should know the proper electron charge density $\rho_{\rm GS}(\mathbf{r})$ beforehand to determine $v^{(\rm AUX)}(\mathbf{r})$, which is the universal functional of the electron density[10, 11]. In practice, however, one may solve the KS equation, possibly under the local density approximation for $v^{(\rm AUX)}(\mathbf{r})$, and reconsider the resulting charge density as $\rho_{\rm GS}(\mathbf{r})$.

The expectation value of the single susceptibility operator is, $\langle 0|\hat{\chi}^{\mu}_{\mu_1\cdots}(x,x_1,\cdots)|0\rangle$, and, for example, the linear susceptibility becomes:

$$\begin{aligned}\langle 0|\hat{\chi}^{\mu}{}_{\mu_1}(x,x_1)|0\rangle =& \frac{-q}{mc^2}\,\tilde{\delta}^{\mu}{}_{\mu_1}\delta^4(x-x_1)\,\langle 0|\hat{j}^{(in0)\,0}(x)|0\rangle \\ &+\frac{1}{i\hbar c^2}\theta(ct-ct_1)\langle 0|\left[\hat{j}^{(in0)\,\mu}(x),\hat{j}^{(in0)}_{\ \ \mu_1}(x_1)\right]|0\rangle\,. \end{aligned} \tag{47}$$

Next, to evaluate the products of two (or more) current density operators, e.g., the second term in Eq.(47), we may use the projection operator $\hat{1}=\sum_m|m\rangle\langle m|$. Now, the expectation value in the second term of Eq.(47) becomes,

$$\begin{aligned}&\langle 0|\left[\hat{j}^{(in0)\,\mu}(x),\hat{j}^{(in0)}_{\ \ \mu_1}(x_1)\right]|0\rangle \\ &=\sum_m\left\{\langle 0|\hat{j}^{(in0)\,\mu}(x)|m\rangle\langle m|\hat{j}^{(in0)}_{\ \ \mu_1}(x_1)|0\rangle-\langle 0|\hat{j}^{(in0)}_{\ \ \mu_1}(x_1)|m\rangle\langle m|\hat{j}^{(in0)\,\mu}(x)|0\rangle\right\} \\ &=\sum_m\lim_{t_0\to\infty}\Big\{\langle 0|e^{\frac{-1}{i\hbar}\hat{H}^{(0)}(t-t_0)}\hat{j}^{(in0)\,\mu}(x)|_{t=t_0}e^{\frac{1}{i\hbar}\hat{H}^{(0)}(t-t_0)}|m\rangle\langle m|e^{\frac{-1}{i\hbar}\hat{H}^{(0)}(t_1-t_0)}\hat{j}^{(in0)}_{\ \ \mu_1}(x_1)|_{t_1=t_0}e^{\frac{1}{i\hbar}\hat{H}^{(0)}(t_1-t_0)}|0\rangle \\ &\qquad-\langle 0|e^{\frac{-1}{i\hbar}\hat{H}^{(0)}(t_1-t_0)}\hat{j}^{(in0)}_{\ \ \mu_1}(x_1)|_{t_1=t_0}e^{\frac{1}{i\hbar}\hat{H}^{(0)}(t_1-t_0)}|m\rangle\langle m|e^{\frac{-1}{i\hbar}\hat{H}^{(0)}(t-t_0)}\hat{j}^{(in0)\,\mu}(x)|_{t=t_0}e^{\frac{1}{i\hbar}\hat{H}^{(0)}(t-t_0)}|0\rangle\Big\} \\ &=\sum_m\Big\{e^{\frac{1}{i\hbar}(E_m-E_0)(t-t_1)}\langle 0|\hat{j}^{(in0)\,\mu}(x)|_{t=-\infty}|m\rangle\langle m|\hat{j}^{(in0)}_{\ \ \mu_1}(x_1)|_{t_1=-\infty}|0\rangle \\ &\qquad-e^{\frac{-1}{i\hbar}(E_m-E_0)(t-t_1)}\langle 0|\hat{j}^{(in0)}_{\ \ \mu_1}(x_1)|_{t_1=-\infty}|m\rangle\langle m|\hat{j}^{(in0)\,\mu}(x)|_{t=-\infty}|0\rangle\Big\}\,. \end{aligned} \tag{48}$$

If the convolution integral with the perturbative EM field is performed, the energy denominator will appear.

In the above theoretical framework, $|m\rangle$'s are simply members of the complete set, and do not carry any physical meaning of excited states of the many-electron system. Considering that the density functional theory concerns only the ground state of the many-electron system, the above treatment is a sound application of density functional theory to the response theory adequate for near-field optics.

As a summary, the quantum many-electron effect is temporally ignored in the present semiclassical theory, but is compensated with the support of the density functional theory. In other words, the scalar potential inherently existing in the electron system is separated

as $\phi^{(0)}(x)$ and $v^{(\mathrm{AUX})}(\mathbf{r})$, and the scalar potential incident may be treated equally with the vector potential incident. Note that, $\phi^{(0)}(x)$ is under the Coulomb gauge but the scalar and vector potential incidents may be gauge-free, that is, the present response theory is still free from gauge-fixing.

For further refinements in the future, the prerequisites for the density functional theory is worth noting:

- The electron density can be considered as the elementary variable of the universal functional determining the ground state energy in the many-electron system[10], if the electron density belongs to the domain, where the density is represented by a wavefunction of n electron state. How to specify such the domain is known as the representability problem[12].

- In principle, the exchange-correlation potential, e.g., that under the local density approximation, can be defined in the system with the slowly-varying electron charge density[11].

VI. SUMMARY

1. Aiming to investigate electron response in NFO, we define the linear and nonlinear single susceptibilities, equally considering the scalar and vector potentials as the cause of the response.

2. It is shown that the present single linear and nonlinear susceptibilities satisfy charge conservation and gauge invariance.

3. The linear and nonlinear susceptibilities in the form of Heisenberg operators are derived by means of the functional derivatives of the action integral of the matter with respect to the scalar and vector potential.

4. It is shown, in principle, that the density functional theory may be used in the non-perturbed system and support to prepare the ground state and a complete set of states, which in turn are used to evaluate the expectation values of the operators of the linear and nonlinear susceptibilities.

Some remaining problems meriting further investigation include:

1. Applying the present linear response theory to a NF optical sysem to show a difference in response to the longitudinal electric field (the scalar potential) and to the transverse electric field (the vector potential).

2. Developing a practical simulator for the many-electron system in NFO, using the present response theory with the support of the density functional theory.

3. Extending the response theory to treat the spin-polarization system in NFO, based on the Pauli or Dirac equation.

4. Developing a phenomenological theory of the single susceptibility, which can aid experimentalists in NFO, providing a substitute for the electric permittivity and magnetic permeability of ordinary optics.

Acknowledgments

The author thanks Professor Kikuo Cho in Osaka Univ. and Professor Motoichi Ohtsu and the members of his group in Univ. of Tokyo for useful discussions. A part of this work is supported by JSPS KAKENHI Grant Number JP25610071 during 2013-2015, and Research Origin for Dressed Photons.

Appendix A: Optimization of Electron Field Operators Under Arbitrary EM Potential

Under a given EM potential, A^ν, the electron field operator optimized to satisfy Eq.(4) is considered as the functional of A^ν, i.e., $\hat{\psi}_\alpha(x;[A^\nu]), \hat{\psi}^\dagger_\alpha(x;[A^\nu])$. Then, the next equation holds for $n = 0, 1, 2, \cdots$:

$$\left.\frac{\delta^n}{\delta A^{\mu_n}(x_n)\cdots\delta A^{\mu_1}(x_1)}\right|_{A^\nu=A^{(0)\nu}} \delta\hat{\psi}^\dagger_\alpha(x')\backslash\delta\mathcal{I}_{\rm mat} = 0, \tag{A1}$$

$$\left.\frac{\delta^n}{\delta A^{\mu_n}(x_n)\cdots\delta A^{\mu_1}(x_1)}\right|_{A^\nu=A^{(0)\nu}} \delta\mathcal{I}_{\rm mat}/\delta\hat{\psi}_\alpha(x') = 0. \tag{A2}$$

Proof: Equation (4) should be hold both under $A^{(0)\nu}$(non-perturbative EM potential) and under $A^{(0)\nu} + \Delta A^\nu$, therefore,

$$\delta\hat{\psi}^\dagger_\alpha(x')\backslash\delta\mathcal{I}_{\rm mat}\Big|_{(\hat{\psi}_\alpha,\hat{\psi}^\dagger_\alpha,A^\nu)=(\hat{\psi}_\alpha[A^{(0)\nu}+\Delta A^\nu],\hat{\psi}^\dagger_\alpha[A^{(0)\nu}+\Delta A^\nu],A^{(0)\nu}+\Delta A^\nu)} = 0,$$

Taylor expansion leads to:

$$\sum_{n=0}^{\infty}\frac{1}{n!}\int \mathrm{d}^4x_{\,n}\cdots\int \mathrm{d}^4x_{\,1}\,\frac{\delta^n\left(\delta\hat{\psi}^{\dagger}_{\alpha}(x')\backslash\delta\mathcal{I}_{\mathrm{mat}}\right)}{\delta A^{\mu_n}(x_n)\cdots\delta A^{\mu_1}(x_1)}\bigg|_{(\hat{\psi}_\alpha,\hat{\psi}^{\dagger}_{\alpha},A^{\nu})=(\hat{\psi}_\alpha[A^{(0)\nu}],\hat{\psi}^{\dagger}_{\alpha}[A^{(0)\nu}],A^{(0)\nu})}\Delta A^{\mu_1}(x_1)\cdots\Delta A^{\mu_n}(x_n)=0,$$

Considering this equation as the identity with respect to $\Delta A^{\mu}(x)$ results in Eq.(A1). Equation (A2) is proved in the same manner.

Appendix B: Charge Conservation Law and Gauge Invariance of Linear and Nonlinear Four-Element Single Susceptibility

To show that four-element linear single susceptibility guarantees the charge conservation law Eq.(24), suppose the four-element divergence of Eq.(40), considering $\partial_{\mu}\hat{j}^{(in0)\,\mu}(x)=0$,

$$\begin{aligned}\partial_{\mu}\hat{\chi}^{\mu}{}_{\mu_1}(x,x_1) &= \frac{-q}{mc^2}\,\delta(ct-ct_1)\tilde{\delta}^{\mu}{}_{\mu_1}\partial_{\mu}\left(\delta^3(x-x_1)\,\hat{j}^{(in0)\,0}(x)\right)\\ &\quad+\frac{1}{i\hbar c^2}\delta(ct-ct_1)\left[\hat{j}^{(in0)\,0}(x),\hat{j}^{(in0)}_{\mu_1}(x_1)\right]\\ &= 0.\end{aligned}\tag{B1}$$

In the second term of the second hand, we use the following commutation relationship at the same time :

$$\begin{aligned}\delta(ct-ct_1)\left[\hat{j}^{(in0)\,0}(x),\hat{j}^{(in0)}_{\mu_1}(x_1)\right] &= -ihc^2\frac{-q}{mc^2}\delta(ct-ct_1)\tilde{\delta}^{\mu}_{\mu_1}\partial_{\mu}\left(\delta^3(x-x_1)\hat{j}^{(in0)\,0}(x)\right)\\ &= -ihc^2\frac{-q}{mc^2}\delta(ct-ct_1)\tilde{\delta}^{\mu}_{\mu_1}\left(\partial_{\mu}\delta^3(x-x_1)\right)\hat{j}^{(in0)\,0}(x_1)\end{aligned}\tag{B2}$$

The proof of Eq.(B2) is as follows: If $\mu_1=0$ in the left hand side of Equation (B2), it is the commutator between charge density operator at the same time, and is zero.

$$\left[\hat{j}^{(in0)\,0}(x),\hat{j}^{(in0)}_{\;0}(x_1)\right]_{t_1=t}=c^2q^2\left[\hat{\psi}^{\dagger}_{\alpha}(x)\hat{\psi}_{\alpha}(x)\,,\,\hat{\psi}^{\dagger}_{\alpha}(x_1)\hat{\psi}_{\alpha}(x_1)\right]_{t_1=t}=0.\tag{B3}$$

One may check Eq.(B3) by a straightforward calculation using the anti-commutation relation of electron field operators at the same time,

$$\left[\hat{\psi}_{\alpha}(x)\,,\,\hat{\psi}^{\dagger}_{\alpha}(x_1)\right]_{+,\,t_1=t}=\delta^3(x-x_1).$$

Next, if $\mu_1=i\in\{1,2,3\}$ in the left hand side of Equation (B2), the commutator in

three-element representation becomes as follows:

$$
\begin{aligned}
&\left[\hat{j}^{(in0)\,0}(x), \hat{j}^{(in0)}_{\mu_1=i}(x_1)\right]_{t_1=t} \\
&= -cq\frac{q}{2m}\left[\hat{\psi}^\dagger_\alpha(x)\hat{\psi}_\alpha(x)\,,\, \hat{\psi}^\dagger_\alpha(x_1)\left(\frac{\hbar}{i}\partial^1_i - qA^{(0)}_i(x_1)\right)\hat{\psi}_\alpha(x_1)\right. \\
&\qquad\left. + \left(\left(\frac{\hbar}{-i}\partial^1_i - qA^{(0)}_i(x_1)\right)\hat{\psi}^\dagger_\alpha(x_1)\right)\hat{\psi}_\alpha(x_1)\right]_{t_1=t} \qquad \text{(B4)}
\end{aligned}
$$

As the term includes $qA^{(0)}_i(x_1)$ is zero following Eq.(B3), let us treat the term including the derivative.

$$
\begin{aligned}
&\left[\hat{j}^{(in0)\,0}(x), \hat{j}^{(in0)}_{\mu_1=i}(x_1)\right]_{t_1=t} \\
&= -\frac{cq}{2}i\hbar c^2\frac{-q}{mc^2}\lim_{x^\bullet_1\to x_1}\partial^{1\,\bullet}_i\left[\hat{\psi}^\dagger_\alpha(x)\hat{\psi}_\alpha(x)\,,\, \hat{\psi}^\dagger_\alpha(x_1)\hat{\psi}_\alpha(x^\bullet_1) - \hat{\psi}^\dagger_\alpha(x^\bullet_1)\hat{\psi}_\alpha(x_1)\right]_{t_1=t} \\
&= -\frac{cq}{2}i\hbar c^2\frac{-q}{mc^2} \\
&\quad \lim_{x^\bullet_1\to x_1}\partial^{1\,\bullet}_i\left(\delta^3(x-x_1)\left(\hat{\psi}^\dagger_\alpha(x)\hat{\psi}_\alpha(x^\bullet_1) + \hat{\psi}^\dagger_\alpha(x^\bullet_1)\hat{\psi}_\alpha(x)\right)\right. \\
&\qquad\qquad \left. -\delta^3(x-x^\bullet_1)\left(\hat{\psi}^\dagger_\alpha(x)\hat{\psi}_\alpha(x_1) + \hat{\psi}^\dagger_\alpha(x_1)\hat{\psi}_\alpha(x)\right)\right)_{t_1=t} \\
&= -\frac{cq}{2}i\hbar c^2\frac{-q}{mc^2} \\
&\quad \delta^3(x-x_1)\partial_i\left(\hat{\psi}^\dagger_\alpha(x)\hat{\psi}_\alpha(x_1) + \hat{\psi}^\dagger_\alpha(x_1)\hat{\psi}_\alpha(x)\right) \\
&\qquad\qquad + \left(\partial_i\delta^3(x-x_1)\right)\left(\hat{\psi}^\dagger_\alpha(x)\hat{\psi}_\alpha(x_1) + \hat{\psi}^\dagger_\alpha(x_1)\hat{\psi}_\alpha(x)\right)_{t_1=t} \\
&= -\frac{cq}{2}i\hbar c^2\frac{-q}{mc^2}\partial_i\left(\delta^3(x-x_1)\left(\hat{\psi}^\dagger_\alpha(x)\hat{\psi}_\alpha(x_1) + \hat{\psi}^\dagger_\alpha(x_1)\hat{\psi}_\alpha(x)\right)\right)_{t_1=t} \\
&= -cqi\hbar c^2\frac{-q}{mc^2}\partial_i\left(\delta^3(x-x_1)\hat{\psi}^\dagger_\alpha(x)\hat{\psi}_\alpha(x)\right) = -i\hbar c^2\frac{-q}{mc^2}\tilde{\delta}^{\,\mu}_{\mu_1}\partial_\mu\left(\delta^3(x-x_1)\hat{j}^{(in0)\,0}(x)\right) \qquad \text{(B5)} \\
&= -cqi\hbar c^2\frac{-q}{mc^2}\partial_i\left(\delta^3(x-x_1)\hat{\psi}^\dagger_\alpha(x_1)\hat{\psi}_\alpha(x_1)\right)_{t_1=t} = -i\hbar c^2\frac{-q}{mc^2}\tilde{\delta}^{\,\mu}_{\mu_1}\left(\partial_\mu\delta^3(x-x_1)\right)\hat{j}^{(in0)\,0}(x_1)_{t_1=t}\,, \\
&\qquad\qquad \text{(B6)}
\end{aligned}
$$

where the last two-way expressions Eqs.(B5) and (B6) are in four-element representation instead of three-element representation. Summarizing Eqs.(B3) and (B6) result in Eq.(B2). As the result, the present four-element linear susceptibility,Eq.(40) maintains the charge conservation law ,Eq.(24).

For the proof for the gauge invariance, Eq.(25), of the linear susceptibility, suppose the four-element divergence with respect to x_1. Then, using Eq.(B2) with the replacement,

$x \leftrightarrow x_1$ and the relation, $\tilde{\delta}^{\mu_1}_{\mu}\partial_{\mu_1} = -\tilde{\delta}^{\mu}_{\mu_1}\partial^{\mu_1}$, one may obtain:

$$\begin{aligned}\partial^{\mu_1}\hat{\chi}^{\mu}{}_{\mu_1}(x,x_1) &= \frac{-q}{mc^2}\,\delta(ct-ct_1)\left(\tilde{\delta}^{\mu}{}_{\mu_1}\partial^{\mu_1}\delta^3(x-x_1)\right)\hat{j}^{(in0)\,0}(x) \\ &\quad -\frac{1}{i\hbar c^2}\delta(ct-ct_1)\left[\hat{j}^{(in0)\,\mu}(x),\hat{j}^{(in0)}_{\ 0}(x_1)\right] \\ &= 0.\end{aligned} \tag{B7}$$

As shown above, the linear susceptibility Eq.(40) maintains gauge invariance Eq.(25).

Next, let us show that the charge conservation law is satisfied by the 2nd order nonlinear single susceptibility, Eq.(41). Operating $\partial_\mu = \delta^0_\mu\partial_0 + \delta^1_\mu\partial_1 + \delta^2_\mu\partial_2 + \delta^3_\mu\partial_3$ to Eq.(41) and considering $\partial_\mu\hat{j}^{(in0)\,\mu}(x) = 0$ (the charge conservation law for the current density operator in the non-interacting system), the surviving terms are those the operator ∂_μ operates on the step function or delta function in front of the commutator, and operates on $\hat{j}^{(in0)\,0}(x)$ in the commutator.

$$\begin{aligned}&\partial_\mu\, 2!\,\hat{\chi}^{\mu}{}_{\mu_1\mu_2}(x,x_1,x_2) = \\ &\frac{1}{i\hbar c^2}\frac{-q}{mc^2}\quad\Big\{\delta(ct-ct_1)\theta(ct-ct_2)\quad\tilde{\delta}^{\mu}{}_{\mu_1}\partial_\mu\left(\delta^3(x-x_1)\left[\hat{j}^{(in0)\,0}(x),\hat{j}^{(in0)}_{\ \mu_2}(x_2)\right]\right) &\text{(B8a)}\\ &\qquad +\delta(ct-ct_2)\theta(ct-ct_1)\quad\tilde{\delta}^{\mu}{}_{\mu_2}\partial_\mu\left(\delta^3(x-x_2)\left[\hat{j}^{(in0)\,0}(x),\hat{j}^{(in0)}_{\ \mu_1}(x_1)\right]\right) &\text{(B8b)}\\ &\qquad +\delta(ct-ct_1)\delta(ct_1-ct_2)\tilde{\delta}_{\mu_1\,\mu_2}\quad\delta^3(x_1-x_2)\left[\hat{j}^{(in0)\,0}(x),\hat{j}^{(in0)}_{\ 0}(x_1)\right]\Big\} &\text{(B8c)}\\ &+\left(\frac{1}{i\hbar c^2}\right)^2\quad\Big\{\delta(ct-ct_1)\theta(ct_1-ct_2)\left[\left[\hat{j}^{(in0)\,0}(x),\hat{j}^{(in0)}_{\ \mu_1}(x_1)\right],\hat{j}^{(in0)}_{\ \mu_2}(x_2)\right] &\text{(B8d)}\\ &\qquad +\delta(ct-ct_2)\theta(ct_2-ct_1)\left[\left[\hat{j}^{(in0)\,0}(x),\hat{j}^{(in0)}_{\ \mu_2}(x_2)\right],\hat{j}^{(in0)}_{\ \mu_1}(x_1)\right]\Big\}. &\text{(B8e)}\end{aligned}$$

Applying Eq.(B2), the third term (B8c) vanishes, and the fourth and fifth terms (B8d) and (B8e) cancel the first and second terms (B8a) and (B8b), respectively.

As a result, the second order nonlinear single susceptibility operator Eq.(41) maintains the charge conservation law, Eq.(24).

To check the gauge invariance of the second order nonlinear single susceptibility operator, let us operate ∂^{μ_1} to Eq.(41).

$$\begin{aligned}&\partial^{\mu_1}\, 2!\,\hat{\chi}^{\mu}{}_{\mu_1\mu_2}(x,x_1,x_2) = \\ &\frac{1}{i\hbar c^2}\frac{-q}{mc^2}\quad\Big\{\delta(ct-ct_1)\theta(ct-ct_2)\quad\left(\tilde{\delta}^{\mu}{}_{\mu_1}\partial^{\mu_1}\delta^3(x-x_1)\right)\left[\hat{j}^{(in0)\,0}(x),\hat{j}^{(in0)}_{\ \mu_2}(x_2)\right] &\text{(B9a)}\\ &\qquad -\delta(ct-ct_2)\delta(ct-ct_1)\quad\tilde{\delta}^{\mu}{}_{\mu_2}\quad\delta^3(x-x_2)\qquad\left[\hat{j}^{(in0)\,0}(x),\hat{j}^{(in0)}_{\ 0}(x_1)\right] &\text{(B9b)}\\ &\qquad +\theta(ct-ct_1)\delta(ct_1-ct_2)\tilde{\delta}_{\mu_1\,\mu_2}\partial^{\mu_1}\left(\delta^3(x_1-x_2)\left[\hat{j}^{(in0)\,\mu}(x),\hat{j}^{(in0)}_{\ 0}(x_1)\right]\right)\Big\} &\text{(B9c)}\end{aligned}$$

$$+\left(\frac{1}{i\hbar c^2}\right)^2 \quad \{(-\delta(ct-ct_1)\theta(ct_1-ct_2)+\theta(ct-ct_1)\delta(ct_1-ct_2))$$

$$\left[\left[\hat{j}^{(in0)\,\mu}(x),\hat{j}^{(in0)}_{\ 0}(x_1)\right],\hat{j}^{(in0)}_{\ \mu_2}(x_2)\right] \tag{B9d}$$

$$-\theta(ct-ct_2)\delta(ct_2-ct_1)\left[\left[\hat{j}^{(in0)\,\mu}(x),\hat{j}^{(in0)}_{\ \mu_2}(x_2)\right],\hat{j}^{(in0)}_{\ 0}(x_1)\right]\Big\}. \tag{B9e}$$

Replacing the fifth term (B9e) using the next Jacobi identity:

$$\left[\left[\hat{j}^{(in0)\,\mu}(x),\hat{j}^{(in0)}_{\ \mu_2}(x_2)\right],\hat{j}^{(in0)}_{\ 0}(x_1)\right] \tag{B10}$$
$$=-\left[\left[\hat{j}^{(in0)}_{\ \mu_2}(x_2),\hat{j}^{(in0)}_{\ 0}(x_1)\right],\hat{j}^{(in0)\,\mu}(x)\right]-\left[\left[\hat{j}^{(in0)}_{\ 0}(x_1),\hat{j}^{(in0)\,\mu}(x)\right],\hat{j}^{(in0)}_{\ \mu_2}(x_2)\right],$$

then, the first term in the right hand side of Eq.(B10) with Eq.(B2) offsets the term (B9c), and the second term in the right hand side of Eq.(B10) offsets the second term in (B9d). The first term in (B9d) offsets the first term, (B9a), considering the commutation relation at the simultaneous time, $\delta(ct-ct_1)\left[\hat{j}^{(in0)\,\mu}(x),\hat{j}^{(in0)}_{\ 0}(x_1)\right]$ and Eq.(B2)(remark the change of upper or lower subscript). The second term (B9b) vanishes by means of Eq.(B2).

As a result, the second order nonlinear single susceptibility operator Eq.(41) maintains the gauge invariance, Eq.(25).

With respect to the third order nonlinear single susceptibility, let us check the charge conservation law. Operating ∂_μ to Eq.(42),

$$\partial_\mu\, 3!\,\hat{\chi}^{\mu}_{\ \mu_1\mu_2\mu_3}(x,x_1,x_2,x_3)=$$
$$\frac{1}{i\hbar c^2}\left(\frac{-q}{mc^2}\right)^2$$
$$\Big\{\theta(ct-ct_2)\delta(ct-ct_1)\delta(ct_2-ct_3)\tilde{\delta}_{\mu_2\,\mu_3}\delta^3(x_2-x_3)\tilde{\delta}^{\mu}_{\ \mu_1}\partial_\mu\left(\delta^3(x-x_1)\left[\hat{j}^{(in0)\,0}(x),\hat{j}^{(in0)}_{\ 0}(x_2)\right]\right) \tag{B11a}$$
$$+\theta(ct-ct_3)\delta(ct-ct_2)\delta(ct_3-ct_1)\tilde{\delta}_{\mu_3\,\mu_1}\delta^3(x_3-x_1)\tilde{\delta}^{\mu}_{\ \mu_2}\partial_\mu\left(\delta^3(x-x_2)\left[\hat{j}^{(in0)\,0}(x),\hat{j}^{(in0)}_{\ 0}(x_3)\right]\right) \tag{B11b}$$
$$+\,\theta(ct-ct_1)\delta(ct-ct_3)\delta(ct_1-ct_2)\tilde{\delta}_{\mu_1\,\mu_2}\delta^3(x_1-x_2)\tilde{\delta}^{\mu}_{\ \mu_3}\partial_\mu\left(\delta^3(x-x_3)\left[\hat{j}^{(in0)\,0}(x),\hat{j}^{(in0)}_{\ 0}(x_1)\right]\right)\Big\} \tag{B11c}$$
$$+\left(\frac{1}{i\hbar c^2}\right)^2\frac{-q}{mc^2}$$
$$\Big\{\delta(ct-ct_1)\theta(ct_1-ct_2)\theta(ct_2-ct_3)\tilde{\delta}^{\mu}_{\ \mu_1}\partial_\mu\left(\delta^3(x-x_1)\left[\left[\hat{j}^{(in0)\,0}(x),\hat{j}^{(in0)}_{\ \mu_2}(x_2)\right],\hat{j}^{(in0)}_{\ \mu_3}(x_3)\right]\right) \tag{B11d}$$
$$+\delta(ct-ct_1)\theta(ct_1-ct_3)\theta(ct_3-ct_2)\tilde{\delta}^{\mu}_{\ \mu_1}\partial_\mu\left(\delta^3(x-x_1)\left[\left[\hat{j}^{(in0)\,0}(x),\hat{j}^{(in0)}_{\ \mu_3}(x_3)\right],\hat{j}^{(in0)}_{\ \mu_2}(x_2)\right]\right) \tag{B11e}$$
$$+\delta(ct-ct_2)\theta(ct_2-ct_3)\theta(ct_3-ct_1)\tilde{\delta}^{\mu}_{\ \mu_2}\partial_\mu\left(\delta^3(x-x_2)\left[\left[\hat{j}^{(in0)\,0}(x),\hat{j}^{(in0)}_{\ \mu_3}(x_3)\right],\hat{j}^{(in0)}_{\ \mu_1}(x_1)\right]\right) \tag{B11f}$$
$$+\delta(ct-ct_2)\theta(ct_2-ct_1)\theta(ct_1-ct_3)\tilde{\delta}^{\mu}_{\ \mu_2}\partial_\mu\left(\delta^3(x-x_2)\left[\left[\hat{j}^{(in0)\,0}(x),\hat{j}^{(in0)}_{\ \mu_1}(x_1)\right],\hat{j}^{(in0)}_{\ \mu_3}(x_3)\right]\right) \tag{B11g}$$
$$+\delta(ct-ct_3)\theta(ct_3-ct_1)\theta(ct_1-ct_2)\tilde{\delta}^{\mu}_{\ \mu_3}\partial_\mu\left(\delta^3(x-x_3)\left[\left[\hat{j}^{(in0)\,0}(x),\hat{j}^{(in0)}_{\ \mu_1}(x_1)\right],\hat{j}^{(in0)}_{\ \mu_2}(x_2)\right]\right) \tag{B11h}$$
$$+\delta(ct-ct_3)\theta(ct_3-ct_2)\theta(ct_2-ct_1)\tilde{\delta}^{\mu}_{\ \mu_3}\partial_\mu\left(\delta^3(x-x_3)\left[\left[\hat{j}^{(in0)\,0}(x),\hat{j}^{(in0)}_{\ \mu_2}(x_2)\right],\hat{j}^{(in0)}_{\ \mu_1}(x_1)\right]\right) \tag{B11i}$$

$$+\delta(ct-ct_1)\delta(ct_1-ct_2)\theta(ct_2-ct_3)\tilde{\delta}_{\mu_1\,\mu_2}\delta^3(x_1-x_2)\left[\left[\hat{j}^{(in0)\,0}(x),\hat{j}^{(in0)}_{\;\;0}(x_1)\right],\hat{j}^{(in0)}_{\;\;\mu_3}(x_3)\right] \tag{B11j}$$

$$+\delta(ct-ct_2)\delta(ct_2-ct_3)\theta(ct_3-ct_1)\tilde{\delta}_{\mu_2\,\mu_3}\delta^3(x_2-x_3)\left[\left[\hat{j}^{(in0)\,0}(x),\hat{j}^{(in0)}_{\;\;0}(x_2)\right],\hat{j}^{(in0)}_{\;\;\mu_1}(x_1)\right] \tag{B11k}$$

$$+\delta(ct-ct_3)\delta(ct_3-ct_1)\theta(ct_1-ct_2)\tilde{\delta}_{\mu_3\,\mu_1}\delta^3(x_3-x_1)\left[\left[\hat{j}^{(in0)\,0}(x),\hat{j}^{(in0)}_{\;\;0}(x_3)\right],\hat{j}^{(in0)}_{\;\;\mu_2}(x_2)\right] \tag{B11l}$$

$$+\delta(ct-ct_1)\theta(ct_1-ct_2)\delta(ct_2-ct_3)\tilde{\delta}_{\mu_2\,\mu_3}\delta^3(x_2-x_3)\left[\left[\hat{j}^{(in0)\,0}(x),\hat{j}^{(in0)}_{\;\;\mu_1}(x_1)\right],\hat{j}^{(in0)}_{\;\;0}(x_2)\right] \tag{B11m}$$

$$+\delta(ct-ct_2)\theta(ct_2-ct_3)\delta(ct_3-ct_1)\tilde{\delta}_{\mu_3\,\mu_1}\delta^3(x_3-x_1)\left[\left[\hat{j}^{(in0)\,0}(x),\hat{j}^{(in0)}_{\;\;\mu_2}(x_2)\right],\hat{j}^{(in0)}_{\;\;0}(x_3)\right] \tag{B11n}$$

$$+\delta(ct-ct_3)\theta(ct_3-ct_1)\delta(ct_1-ct_2)\tilde{\delta}_{\mu_1\,\mu_2}\delta^3(x_1-x_2)\left[\left[\hat{j}^{(in0)\,0}(x),\hat{j}^{(in0)}_{\;\;\mu_3}(x_3)\right],\hat{j}^{(in0)}_{\;\;0}(x_1)\right]\Big\} \tag{B11o}$$

$$+\left(\frac{1}{i\hbar c^2}\right)^3$$

$$\Big\{\delta(ct-ct_1)\theta(ct_1-ct_2)\theta(ct_2-ct_3)\left[\left[\left[\hat{j}^{(in0)\,0}(x),\hat{j}^{(in0)}_{\;\;\mu_1}(x_1)\right],\hat{j}^{(in0)}_{\;\;\mu_2}(x_2)\right],\hat{j}^{(in0)}_{\;\;\mu_3}(x_3)\right] \tag{B11p}$$

$$+\delta(ct-ct_1)\theta(ct_1-ct_3)\theta(ct_3-ct_2)\left[\left[\left[\hat{j}^{(in0)\,0}(x),\hat{j}^{(in0)}_{\;\;\mu_1}(x_1)\right],\hat{j}^{(in0)}_{\;\;\mu_3}(x_3)\right],\hat{j}^{(in0)}_{\;\;\mu_2}(x_2)\right] \tag{B11q}$$

$$+\delta(ct-ct_2)\theta(ct_2-ct_3)\theta(ct_3-ct_1)\left[\left[\left[\hat{j}^{(in0)\,0}(x),\hat{j}^{(in0)}_{\;\;\mu_2}(x_2)\right],\hat{j}^{(in0)}_{\;\;\mu_3}(x_3)\right],\hat{j}^{(in0)}_{\;\;\mu_1}(x_1)\right] \tag{B11r}$$

$$+\delta(ct-ct_2)\theta(ct_2-ct_1)\theta(ct_1-ct_3)\left[\left[\left[\hat{j}^{(in0)\,0}(x),\hat{j}^{(in0)}_{\;\;\mu_2}(x_2)\right],\hat{j}^{(in0)}_{\;\;\mu_1}(x_1)\right],\hat{j}^{(in0)}_{\;\;\mu_3}(x_3)\right] \tag{B11s}$$

$$+\delta(ct-ct_3)\theta(ct_3-ct_1)\theta(ct_1-ct_2)\left[\left[\left[\hat{j}^{(in0)\,0}(x),\hat{j}^{(in0)}_{\;\;\mu_3}(x_3)\right],\hat{j}^{(in0)}_{\;\;\mu_1}(x_1)\right],\hat{j}^{(in0)}_{\;\;\mu_2}(x_2)\right] \tag{B11t}$$

$$+\delta(ct-ct_3)\theta(ct_3-ct_2)\theta(ct_2-ct_1)\left[\left[\left[\hat{j}^{(in0)\,0}(x),\hat{j}^{(in0)}_{\;\;\mu_3}(x_3)\right],\hat{j}^{(in0)}_{\;\;\mu_2}(x_2)\right],\hat{j}^{(in0)}_{\;\;\mu_1}(x_1)\right]\Big\}. \tag{B11u}$$

The term (B11p) offsets the term (B11d), applying Eq.(B2) to the most inner commutator in (B11p). In the same manner, the terms (B11q)-(B11u),respectively, offsets the terms (B11e)-(B11i), applying Eq.(B2). The terms (B11j)-(B11l) vanishes, applying Eq.(B2) to the inner commutator at the simultaneous time. The term (B11m) offsets the term (B11a), applying Eq.(B2) to the most inner commutator. In the same manner, the terms (B11n)-(B11o), respectively, offsets (B11b)-(B11c), using Eq.(B2).

As a result, the third order nonlinear single susceptibility operator Eq.(42) maintains the charge conservation law, Eq.(24).

To check the gauge invariance of the third order nonlinear single susceptibility operator, let us operate ∂^{μ_1} to Eq.(42).

$$\partial^{\mu_1}\,3!\,\hat{\chi}^{\mu}_{\;\;\mu_1\mu_2\mu_3}(x,x_1,x_2,x_3)=$$

$$\frac{1}{i\hbar c^2}\left(\frac{-q}{mc^2}\right)^2$$

$$\Big\{\theta(ct-ct_2)\delta(ct-ct_1)\delta(ct_2-ct_3)\left(\tilde{\delta}^{\mu}_{\;\;\mu_1}\partial^{\mu_1}\delta^3(x-x_1)\right)\tilde{\delta}_{\mu_2\,\mu_3}\delta^3(x_2-x_3)\left[\hat{j}^{(in0)\,0}(x),\hat{j}^{(in0)}_{\;\;0}(x_2)\right] \tag{B12a}$$

$$+\theta(ct-ct_3)\delta(ct-ct_2)\delta(ct_3-ct_1)\tilde{\delta}^{\mu}_{\;\;\mu_2}\delta^3(x-x_2)\left(\tilde{\delta}_{\mu_3\,\mu_1}\partial^{\mu_1}\delta^3(x_3-x_1)\right)\left[\hat{j}^{(in0)\,0}(x),\hat{j}^{(in0)}_{\;\;0}(x_3)\right] \tag{B12b}$$

$$+\,\theta(ct-ct_1)\delta(ct-ct_3)\delta(ct_1-ct_2)\tilde{\delta}^{\mu}_{\;\;\mu_3}\delta^3(x-x_3)\left(\tilde{\delta}_{\mu_1\,\mu_2}\partial^{\mu_1}\delta^3(x_1-x_2)\left[\hat{j}^{(in0)\,0}(x),\hat{j}^{(in0)}_{\;\;0}(x_1)\right]\right)\Big\} \tag{B12c}$$

$$+\left(\frac{1}{i\hbar c^2}\right)^2\frac{-q}{mc^2}$$

$$\Big\{\delta(ct-ct_1)\theta(ct_1-ct_2)\theta(ct_2-ct_3)\left(\tilde{\delta}^{\mu}{}_{\mu_1}\partial^{\mu_1}\delta^3(x-x_1)\right)\left[\left[\hat{j}^{(in0)\,0}(x),\hat{j}^{(in0)}_{\mu_2}(x_2)\right],\hat{j}^{(in0)}_{\mu_3}(x_3)\right] \tag{B12d}$$

$$+\delta(ct-ct_1)\theta(ct_1-ct_3)\theta(ct_3-ct_2)\left(\tilde{\delta}^{\mu}{}_{\mu_1}\partial^{\mu_1}\delta^3(x-x_1)\right)\left[\left[\hat{j}^{(in0)\,0}(x),\hat{j}^{(in0)}_{\mu_3}(x_3)\right],\hat{j}^{(in0)}_{\mu_2}(x_2)\right] \tag{B12e}$$

$$-\delta(ct-ct_2)\theta(ct_2-ct_3)\delta(ct_3-ct_1)\tilde{\delta}^{\mu}{}_{\mu_2}\delta^3(x-x_2)\left[\left[\hat{j}^{(in0)\,0}(x),\hat{j}^{(in0)}_{\mu_3}(x_3)\right],\hat{j}^{(in0)}_{0}(x_1)\right] \tag{B12f}$$

$$+\left(-\delta(ct-ct_2)\delta(ct_2-ct_1)\theta(ct_1-ct_3)+\delta(ct-ct_2)\theta(ct_2-ct_1)\delta(ct_1-ct_3)\right)$$

$$\tilde{\delta}^{\mu}{}_{\mu_2}\delta^3(x-x_2)\left[\left[\hat{j}^{(in0)\,0}(x),\hat{j}^{(in0)}_{0}(x_1)\right],\hat{j}^{(in0)}_{\mu_3}(x_3)\right] \tag{B12g}$$

$$+\left(-\delta(ct-ct_3)\delta(ct_3-ct_1)\theta(ct_1-ct_2)+\delta(ct-ct_3)\theta(ct_3-ct_1)\delta(ct_1-ct_2)\right)$$

$$\tilde{\delta}^{\mu}{}_{\mu_3}\delta^3(x-x_3)\left[\left[\hat{j}^{(in0)\,0}(x),\hat{j}^{(in0)}_{0}(x_1)\right],\hat{j}^{(in0)}_{\mu_2}(x_2)\right] \tag{B12h}$$

$$-\delta(ct-ct_3)\theta(ct_3-ct_2)\delta(ct_2-ct_1)\tilde{\delta}^{\mu}{}_{\mu_3}\delta^3(x-x_3)\left[\left[\hat{j}^{(in0)\,0}(x),\hat{j}^{(in0)}_{\mu_2}(x_2)\right],\hat{j}^{(in0)}_{0}(x_1)\right] \tag{B12i}$$

$$+\theta(ct-ct_1)\delta(ct_1-ct_2)\theta(ct_2-ct_3)\tilde{\delta}_{\mu_1\,\mu_2}\partial^{\mu_1}\left(\delta^3(x_1-x_2)\left[\left[\hat{j}^{(in0)\,\mu}(x),\hat{j}^{(in0)}_{0}(x_1)\right],\hat{j}^{(in0)}_{\mu_3}(x_3)\right]\right) \tag{B12j}$$

$$-\theta(ct-ct_2)\delta(ct_2-ct_3)\delta(ct_3-ct_1)\tilde{\delta}_{\mu_2\,\mu_3}\delta^3(x_2-x_3)\left[\left[\hat{j}^{(in0)\,\mu}(x),\hat{j}^{(in0)}_{0}(x_2)\right],\hat{j}^{(in0)}_{0}(x_1)\right] \tag{B12k}$$

$$+\theta(ct-ct_3)\delta(ct_3-ct_1)\theta(ct_1-ct_2)\tilde{\delta}_{\mu_3\,\mu_1}\left(\partial^{\mu_1}\delta^3(x_3-x_1)\right)\left[\left[\hat{j}^{(in0)\,\mu}(x),\hat{j}^{(in0)}_{0}(x_3)\right],\hat{j}^{(in0)}_{\mu_2}(x_2)\right] \tag{B12l}$$

$$+\left(-\delta(ct-ct_1)\theta(ct_1-ct_2)\delta(ct_2-ct_3)+\theta(ct-ct_1)\delta(ct_1-ct_2)\delta(ct_2-ct_3)\right)$$

$$\tilde{\delta}_{\mu_2\,\mu_3}\delta^3(x_2-x_3)\left[\left[\hat{j}^{(in0)\,\mu}(x),\hat{j}^{(in0)}_{0}(x_1)\right],\hat{j}^{(in0)}_{0}(x_2)\right] \tag{B12m}$$

$$+\theta(ct-ct_2)\theta(ct_2-ct_3)\delta(ct_3-ct_1)\left(\tilde{\delta}_{\mu_3\,\mu_1}\partial^{\mu_1}\delta^3(x_3-x_1)\right)\left[\left[\hat{j}^{(in0)\,\mu}(x),\hat{j}^{(in0)}_{\mu_2}(x_2)\right],\hat{j}^{(in0)}_{0}(x_3)\right] \tag{B12n}$$

$$+\theta(ct-ct_3)\theta(ct_3-ct_1)\delta(ct_1-ct_2)\tilde{\delta}_{\mu_1\,\mu_2}\partial^{\mu_1}\left(\delta^3(x_1-x_2)\left[\left[\hat{j}^{(in0)\,\mu}(x),\hat{j}^{(in0)}_{\mu_3}(x_3)\right],\hat{j}^{(in0)}_{0}(x_1)\right]\right)\Big\} \tag{B12o}$$

$$+\left(\frac{1}{i\hbar c^2}\right)^3$$

$$\{\left(-\delta(ct-ct_1)\theta(ct_1-ct_2)\theta(ct_2-ct_3)+\theta(ct-ct_1)\delta(ct_1-ct_2)\theta(ct_2-ct_3)\right)$$

$$\left[\left[\left[\hat{j}^{(in0)\,\mu}(x),\hat{j}^{(in0)}_{0}(x_1)\right],\hat{j}^{(in0)}_{\mu_2}(x_2)\right],\hat{j}^{(in0)}_{\mu_3}(x_3)\right] \tag{B12p}$$

$$+\left(-\delta(ct-ct_1)\theta(ct_1-ct_3)\theta(ct_3-ct_2)+\theta(ct-ct_1)\delta(ct_1-ct_3)\theta(ct_3-ct_2)\right)$$

$$\left[\left[\left[\hat{j}^{(in0)\,\mu}(x),\hat{j}^{(in0)}_{0}(x_1)\right],\hat{j}^{(in0)}_{\mu_3}(x_3)\right],\hat{j}^{(in0)}_{\mu_2}(x_2)\right] \tag{B12q}$$

$$-\theta(ct-ct_2)\theta(ct_2-ct_3)\delta(ct_3-ct_1)\left[\left[\left[\hat{j}^{(in0)\,\mu}(x),\hat{j}^{(in0)}_{\mu_2}(x_2)\right],\hat{j}^{(in0)}_{\mu_3}(x_3)\right],\hat{j}^{(in0)}_{0}(x_1)\right] \tag{B12r}$$

$$+\left(-\theta(ct-ct_2)\delta(ct_2-ct_1)\theta(ct_1-ct_3)+\theta(ct-ct_2)\theta(ct_2-ct_1)\delta(ct_1-ct_3)\right)$$

$$\left[\left[\left[\hat{j}^{(in0)\,\mu}(x),\hat{j}^{(in0)}_{\mu_2}(x_2)\right],\hat{j}^{(in0)}_{0}(x_1)\right],\hat{j}^{(in0)}_{\mu_3}(x_3)\right] \tag{B12s}$$

$$+\left(-\theta(ct-ct_3)\delta(ct_3-ct_1)\theta(ct_1-ct_2)+\theta(ct-ct_3)\theta(ct_3-ct_1)\delta(ct_1-ct_2)\right)$$

$$\left[\left[\left[\hat{j}^{(in0)\,\mu}(x),\hat{j}^{(in0)}_{\mu_3}(x_3)\right],\hat{j}^{(in0)}_{0}(x_1)\right],\hat{j}^{(in0)}_{\mu_2}(x_2)\right] \tag{B12t}$$

$$-\theta(ct-ct_3)\theta(ct_3-ct_2)\delta(ct_2-ct_1)\left[\left[\left[\hat{j}^{(in0)\,\mu}(x),\hat{j}^{(in0)}_{\mu_3}(x_3)\right],\hat{j}^{(in0)}_{\mu_2}(x_2)\right],\hat{j}^{(in0)}_{0}(x_1)\right]\Big\}. \tag{B12u}$$

In the following, we prove the next equation, which leads to the gauge invariance.

$$\begin{aligned}
\text{(B12p)} + \text{(B12d)} + \text{(B12j)} + \text{(B12s)} + \text{(B12r)} + \text{(B12n)} &= 0, && \text{(B13)}\\
\text{(B12q)} + \text{(B12e)} + \text{(B12l)} + \text{(B12t)} + \text{(B12u)} + \text{(B12o)} &= 0, && \text{(B14)}\\
\text{(B12m)} + \text{(B12a)} + \text{(B12k)} &= 0, && \text{(B15)}\\
\text{(B12i)} + \text{(B12c)} + \text{(B12h)} &= 0, && \text{(B16)}\\
\text{(B12f)} + \text{(B12b)} + \text{(B12g)} &= 0. && \text{(B17)}
\end{aligned}$$

Eq.(B13): The first term of (B12p) offsets (B12d), using Eq.(B2). To the inner double commutator in the second term of (B12p), the nest Jacobi identity is applied:

$$\begin{aligned}
&\left[\left[\left[\hat{j}^{(in0)\,\mu}(x), \hat{j}^{(in0)}_{\ 0}(x_1)\right], \hat{j}^{(in0)}_{\ \mu_2}(x_2)\right], \hat{j}^{(in0)}_{\ \mu_3}(x_3)\right] \qquad \text{(B18)}\\
= &-\left[\left[\left[\hat{j}^{(in0)}_{\ 0}(x_1), \hat{j}^{(in0)}_{\ \mu_2}(x_2)\right], \hat{j}^{(in0)\,\mu}(x)\right], \hat{j}^{(in0)}_{\ \mu_3}(x_3)\right]\\
&-\left[\left[\left[\hat{j}^{(in0)}_{\ \mu_2}(x_2), \hat{j}^{(in0)\,\mu}(x)\right], \hat{j}^{(in0)}_{\ 0}(x_1)\right], \hat{j}^{(in0)}_{\ \mu_3}(x_3)\right].
\end{aligned}$$

Furthermore, the inner commutator (, assuming at the simultaneous time) in the first term of Eq.(B18) , one may apply Eq.(B2). The part including this factor in the second term of (B12p) offsets the term (B12j). In the second term of (B12p), the part including the second term of Eq.(B18) offsets the first term of (B12s). Up to now, (B12p)+(B12d)+(B12j)+ the first term of (B12s)= 0 has been shown.

Next, to the outer double commutator in the second term of (B12r), let us apply the next Jacobi identity,

$$\begin{aligned}
&\left[\left[\left[\hat{j}^{(in0)\,\mu}(x), \hat{j}^{(in0)}_{\ \mu_2}(x_2)\right], \hat{j}^{(in0)}_{\ \mu_3}(x_3)\right], \hat{j}^{(in0)}_{\ 0}(x_1)\right] \qquad \text{(B19)}\\
= &-\left[\left[\hat{j}^{(in0)}_{\ \mu_3}(x_3), \hat{j}^{(in0)}_{\ 0}(x_1)\right], \left[\hat{j}^{(in0)\,\mu}(x), \hat{j}^{(in0)}_{\ \mu_2}(x_2)\right]\right]\\
&+\left[\left[\left[\hat{j}^{(in0)\,\mu}(x), \hat{j}^{(in0)}_{\ \mu_2}(x_2)\right], \hat{j}^{(in0)}_{\ 0}(x_1)\right], \hat{j}^{(in0)}_{\ \mu_3}(x_3)\right].
\end{aligned}$$

The commutator in the first term of Eq.(B19): $\left[\hat{j}^{(in0)}_{\ \mu_3}(x_3), \hat{j}^{(in0)}_{\ 0}(x_1)\right]$ is the commutator at the simultaneous time, therefore, we may use Eq.(B2). The part including this factor in (B12r) offsets the term (B12n). In (B12r), the part including the second term of Eq.(B19) offsets the second term of (B12s). Up to now, (B12r)+(B12n)+ the second term of (B12s)= 0 is shown.

Together with the previous result, Eq.(B13) holds.

Eq.(B14): This equation is Eq.(B13) with the replacement $x_2 \leftrightarrow x_3$ and $\mu_2 \leftrightarrow \mu_3$, therefore, Eq.(B14) holds.

Eq.(B15): The first term of (B12m) offsets (B12a), using Eq.(B2).

To the double commutator in the second term of (B12m), the nest Jacobi identity is applied:

$$\begin{aligned} & \left[\left[\hat{j}^{(in0)\,\mu}(x), \hat{j}^{(in0)}_{\ 0}(x_1)\right], \hat{j}^{(in0)}_{\ 0}(x_2)\right] \\ = & -\left[\left[\hat{j}^{(in0)}_{\ 0}(x_1), \hat{j}^{(in0)}_{\ 0}(x_2)\right], \hat{j}^{(in0)\,\mu}(x)\right] - \left[\left[\hat{j}^{(in0)}_{\ 0}(x_2), \hat{j}^{(in0)\,\mu}(x)\right], \hat{j}^{(in0)}_{\ 0}(x_1)\right] \\ = & \left[\left[\hat{j}^{(in0)\,\mu}(x), \hat{j}^{(in0)}_{\ 0}(x_2)\right], \hat{j}^{(in0)}_{\ 0}(x_1)\right] \end{aligned} \tag{B20}$$

In the above, we use the inner commutator (at the simulatenesou time) in the first term of the second hand side becomes zero, using Eq.(B2). The second term of (B12m) includes the factor of Eq.(B20) and offsets (B12k).

As a result, Eq.(B15) holds.

Eq.(B16): To the double commutator in (B12i), we apply the next Jacobi identity:

$$\begin{aligned} & \left[\left[\hat{j}^{(in0)\,0}(x), \hat{j}^{(in0)}_{\ \mu_2}(x_2)\right], \hat{j}^{(in0)}_{\ 0}(x_1)\right] \\ = & -\left[\left[\hat{j}^{(in0)}_{\ \mu_2}(x_2), \hat{j}^{(in0)}_{\ 0}(x_1)\right], \hat{j}^{(in0)\,0}(x)\right] - \left[\left[\hat{j}^{(in0)}_{\ 0}(x_1), \hat{j}^{(in0)\,0}(x)\right], \hat{j}^{(in0)}_{\ \mu_2}(x_2)\right]. \end{aligned} \tag{B21}$$

The inner commutator in the first term of Eq.(B21) is the commutator at the simultaneous time, therefore, we may use Eq.(B2). The part including this factor in (B12i) offsets the term (B12c). In (B12i), the part including the second term of Eq.(B21) offsets the second term of (B12h). The first term of (B12h) is zero, because the inner commutator included in this term is commutator at the simultaneous time and leads to zero, using Eq.(B2).

Therefore, Eq.(B16) holds.

Eq.(B17): This equation is Eq.(B16) with the replacement $x_2 \leftrightarrow x_3$ and $\mu_2 \leftrightarrow \mu_3$, therefore, Eq.(B17) holds.

As the summery, Eqs.(B13)-(B17) hold and the third order nonlinear single susceptibility

Eq.(42) maintains the gauge invariance Eq.(25).

---

[1] Y. Toyozawa, *The Physics of Elementary Excitations* eds. S. Nakajima, Y. Toyozawa, R. Abe (Springer-Verlag, Berlin, Heidelberg, 1980) Chap. 2; this book was translated from Japanese book "Bussei II" in Iwanami Series of Fundamental Physics (1978).

[2] Kikuo Cho, J. Phys. Condens. Matter., **20**, 175202 (2008);

[3] Kikuo Cho, *Reconstruction of Macroscopic Maxwell Equations* (Springer-Verlag, Berlin, Heidelberg, 2010).

[4] Kikuo Cho, *Optical Response of Nanostructures* (Springer-Verlag, Berlin, Heidelberg, 2003).

[5] Kikuo Cho, Ref.[3] Chap. 5.

[6] O. Keller, *Quantum Theory of Near-Field Electrodynamics*Springer, Heidelberg, Dordrecht, London, New York, 2011Chap. 10.

[7] T. Kugo, *Quantum Theory of Gauge Fields* (in Japanese) (Baifukan, Tokyo, 1989) Chap. 1.

[8] T. Kugo, Ref.[7] Chap. 2.

[9] K. Nishijima, *Field Theory* (in Japanese)Kinokuniya-Shoten, Tokyo,1987Chap.5.

[10] P. Hohenberg and W. Kohn, Phys. Rev. **136**, 3864 (1964);

[11] W. Kohn and L. J. Sham, Phys Rev. **140**, A1133 (1965).

[12] M. Levy, Proc. Natl. Acad. Sci. USA **76**, 6062-6065 (1979)

Chapter 2
Virtual Photon Model by Spatio-Temporal Vortex Dynamics

Hirofumi Sakuma

Abstract The issue on theoretical foundation of optical near field or dressed photon (DP) as its quantum mechanical representation in the field of nanophotonics remains unsettled. Experimental data accumulated so far seem to suggest that DP possesses characteristics of off-shell virtual photons. On the basis of this observation and critical reviews of classical as well as quantum theory of light, we are now developing a novel theory describing DP. A unique feature of the theory explained here is that it takes an important role played by spacelike momentum to describe field interactions into consideration and hence it provides an extended picture of conventional virtual photon dynamics on spacetime. We show here that the new model is closely related to so-called "scalar photon" and longitudinal mode of free electromagnetic waves that are eliminated as unphysical modes in a covariant quantization of electromagnetic wave field. So, as an important preliminary step toward constructing a new model of virtual photons, we first discuss that the above prevailing claim made by a covariant quantization theory only reflects dynamical requirement on the micro quantum world and overlooks the emergence of condensed classical modes which can be understood in the framework of Ojima's Micro-Macro Duality Scheme (MMDS) providing a mathematically derived quantum-classical correspondence. As a matter of fact, the existence of those eliminated "unphysical" modes are clearly reported in the field of classical electromagnetic theory in addition to the fact that those modes are directly related to Coulomb modes playing a significant role in electromagnetic interactions. As a central theme of this article, a newly introduced Clebsch dual field of electromagnetic wave field as an extension of conventional electromagnetic one is shown to be a promising new model of DP as virtual photons. We also point out an intriguing property that extended virtual photons with spacelike property carry negative scalar curvature similar to enigmatic dark energy discussed in cosmology.

H. Sakuma (✉)
Research Origin for Dressed Photon, c/o Yokohama Technology center,
NICHIA Corporation, 3-13-19 Moriya-cho, Kanagawa-ku, Yokohama
221-0022, Japan
e-mail: sakuma@rodrep.or.jp

T. Yatsui (ed.), *Progress in Nanophotonics 5*, Nano-Optics and Nanophotonics,
https://doi.org/10.1007/978-3-319-98267-0_2

Chapter 3
Quantum Probability for Dressed Photons: The Arcsine Law in Nanophotonics

Hayato Saigo

Abstract In the present paper we propose a new framework for the investigation of dressed photon from the viewpoint of quantum probability. As a result, we show that a probability measure called the Arcsine law plays crucial roles in nanophotonics. For instance, a concrete formula for the probability density of dressed photon in a fiber probe and a new prediction in photon breeding phenomena are given in terms of the Arcsine law.

3.1 Introduction

Dressed Photon (DP) is an essential concept for the investigation of many phenomena which cannot be explained in conventional optics, especially of the phenomena arising in the interaction between light and nano-scale matter [1]. This concept provides the fundamental reflections on physics and engineering and the interesting examples motivating the reformulation of the concept such as the composite systems or the micro-macro relationships.

In this paper we investigate some mathematical/physical aspects of the DP in terms of *Quantum Probability* (QP), the generalization of probability theory which includes whole quantum (and classical) physics as a subtheory.

As a result, it is shown that an important probability distribution called the *Arcsine law* plays fundamental roles in the phenomena of DP, and a new mathematical/physical interpretation is given for the universal phenomenon that DP occurs at the extreme points of a material system such as the tip of a fiber probe.

In the Sect. 3.2 we define the notion of DP from the author's viewpoint which clarifies why DP is related to the fundamental notions of physics such as *quantum-*

H. Saigo (✉)
Nagahama Institute of Bio-Science and Technology, Nagahama, Japan
e-mail: harmoniahayato@gmail.com

T. Yatsui (ed.), *Progress in Nanophotonics 5*, Nano-Optics and Nanophotonics,
https://doi.org/10.1007/978-3-319-98267-0_3

Chapter 4
Control over Off-Shell QFT via Induction and Imprimitivity

Izumi Ojima

Abstract In the framework of Micro–Macro duality with quadrality scheme, the mutual relations between Micro and Macro are considered in a systematic way. On this basis, many interesting aspects of symmetry breaking are discussed, according to which the classifying space of sectors is shown to have the structure of symmetric spaces characterized by the condition similar to Maxwell and Einstein equations. Applying these results to the attempts for constructing a theory of dressed photons, we are naturally led to the idea of the relevance of automorphic forms which have close connections with number theory.

4.1 Micro–Macro Duality + Quadrality Scheme

When we integrate a mathematical approach to the dynamical aspects of the system in question, together with the geometric description of the relevant structure in terms of invariants which are generated by the dynamical processes and which implement the classification of the processes and structures, then we arrive at the category-theoretical framework of "Micro–Macro duality + quadrality scheme" ([1]; "Quantum Fields and Micro–Macro Duality [2], a book by Ojima, 2013 in Japanese and also see [3]) by incorporating categorically the natural duality between the dynamical processes and the classifying spaces.

By analyzing closely in this framework the dynamical processes and the classifying scheme based on geometric invariants generated by the former processes, we can understand that both of the invisible Micro doman corresponding to the dynamical processes and of the visible Macro structure to the classifying structure in terms of geometric invariants constitute the duality structure, to be called "***Micro–Macro duality***" [4]. According to such general feature, the description in terms of momenta p corresponds to the inivisible Micro domain and the familiar concept of "spacetime

I. Ojima (✉)
Research Origin for Dressed Photon, c/o Nichia Corp., 3-13-19 Moriya-cho, Kanagawa-ku, Yokohama, Kanagawa 221-0022, Japan
e-mail: ojima@za.ztv.ne.jp

T. Yatsui (ed.), *Progress in Nanophotonics 5*, Nano-Optics and Nanophotonics,
https://doi.org/10.1007/978-3-319-98267-0_4

Chapter 5
An Approach from Measurement Theory to Dressed Photon

Kazuya Okamura

Abstract In this review, we discuss quantum measurement theory to develop that for dressed photons. Algebraic quantum theory is based on the theory of operator algebras, especially, C*-algebras. Our formulation of quantum measurement theory stands on von Neumann algebras, a special class of C*-algebra, and treats processes of measurements both in the Schrödinger picture and in the Heisenberg picture.

5.1 Introduction

In this review, we discuss quantum measurement theory in algebraic quantum theory to develop that for dressed photons. Algebraic quantum theory is based on the theory of operator algebras, especially, C*-algebras. The advantage of C*-algebraic quantum theory is that it can explicitly describe macroscopic classical levels of quantum systems. A sector, a quasi-equivalence class of a factor state, is a macroscopic unit of quantum system. And we can describe the statistical aspect of sectors in the measure-theoretical probability theory. In terms of sectors, we axiomatically formulate algebraic quantum theory and discuss symmetry breaking.

Our formulation of quantum measurement theory stands on von Neumann algebras, a special class of C*-algebra, and is applicable to local measurements in algebraic quantum field theory. In the Schrödinger picture, processes of measurements are described by the notion of completely positive instrument defined on von Neumann algebras. On the other hand, we can consider quantum mechanical modelings of measuring appratuses, called measuring processes. It is shown that there exists a one-to-one correspondence between completely positive instruments with "the normal extension property" and "statistical equivalence classes" of measuring

K. Okamura (✉)
Graduate School of Infomatics, Nagoya University, Furo-cho, Chikusa-ku, Nagoya, Aichi 464-8601, Japan
e-mail: okamura@math.cm.is.nagoya-u.ac.jp

T. Yatsui (ed.), *Progress in Nanophotonics 5*, Nano-Optics and Nanophotonics,
https://doi.org/10.1007/978-3-319-98267-0_5

Chapter 6
Response Theory Supporting Dressed Photons

Itsuki Banno

Abstract For a theoretical description of the dressed photon (DP) introduced in Chap. 1, it is essential to develop a novel method different from those applied to conventional optics. The difficulties lie in the facts that the familiar concepts such as the electric field, electric permittivity, and polarization become irrational in near-field optics (NFO), and that NFO is inevitably related to the many-electron problem. Starting from the redefinition the DP in a general manner, this chapter is devoted to explain above mentioned difficulties and develops the linear response theory applicable to the optical near field and the DP. The derived linear single susceptibility relates the scalar and vector potentials (as the cause) to the induced charge and current densities (as the result), guarantees the gauge invariance and the charge conservation law, and is soundly applicable to the many-electron system in NFO as the replacement of ordinary two susceptibilities, namely, the electric permittivity and magnetic permeability that relate the electric and magnetic fields (as the cause) to the polarization and magnetization (as the result), respectively. The present formulation will be extensible to the nonlinear single susceptibility, which is essential for a future challenge to describe the DP.

6.1 Introduction

A series of experiments in near-field optics (NFO) utilizing non-metallic materials was performed under non-resonant conditions and/or forbidden-transition conditions, and showed various phenomena which have not been observed in conventional optics. Such the NF optical phenomena are:

I. Banno (✉)
Graduate Faculty of Interdisciplinary Research Faculty of Engineering,
University of Yamanashi, 4-3-11 Takeda, Kofu, Yamanashi 400-8511, Japan
e-mail: banno@yamanashi.ac.jp

T. Yatsui (ed.), *Progress in Nanophotonics 5*, Nano-Optics and Nanophotonics,
https://doi.org/10.1007/978-3-319-98267-0_6

ドレスト光子への測定理論的アプローチ

An approach from measurement theory to dressed photon

○(PC) 岡村 和弥 [1] (1. 名大情報)

○(PC)Kazuya Okamura[1] (1. Nagoya Univ.)

E-mail: okamura@math.cm.is.nagoya-u.ac.jp

量子測定理論の定式化を拡張することによって，電磁場と物質の相互作用により生じるドレスト光子のモデリングがより柔軟に行える可能性について本講演では議論する。

量子系での測定について Heisenberg 以来の伝統的な枠組みの中で「測定は対象の状態を乱す」などと言われてきた。γ 線顕微鏡の例では，有限の時間の間だけ相互作用で γ 線により被測定系である粒子の位置と運動量が変化することが知られている。概ねこれまで量子測定理論が対象として想定してきたのは，この例のように測定前は独立な被測定系と測定系（測定装置のミクロ端）を有限の時間相互作用させ測定系の物理量の変化をメーターに用いる場合である [2, 3]。量子場の測定理論での有界時空領域における局所測定は相対論的な状況を含む形に従来の量子測定理論の定式化を拡張したものである [4]。

近接場光学・ドレスト光子を対象とした測定はその現象のあり方から，系によっては遠方での放射光に頼った測定だけでは不十分で，測定装置と被測定系が近接した事実上その 2 つが区別不可能な状況での測定を取り扱わなければならない。それ故先行研究通りに測定理論を適用できない。本講演ではドレスト光子の現象で想定されるタイプの測定の一般的な定式化を代数的量子論の枠組みにおいて行う。局所ネット (local net) の概念にもとづいて時空領域の物理量の指定を行うが，メーターに関与しうる部分がこれまでの測定理論での扱いとは異なるのが本質的で，測定しない状況と測定する状況の比較がマクロに可能な記述をしなければならない。同時に，Heisenberg 描像での測定理論 [5] を参考にした記述にも触れる。

謝辞 この研究は日本学術振興会科研費 No. 26247016, No. 16K17641,（社）ドレスト光子研究起点ならびに住友財団基礎科学研究助成の支援を受けています。

参考文献

[1] 大津 元一,『ドレスト光子』,（朝倉書店, 2013）.

[2] J. von Neumann, *Mathematische Grundlagen der Quantenmechanik*, (Springer, Berlin, 1932); *Mathematical Foundations of Quantum Mechanics*, (Princeton UP, Princeton, 1955).

[3] M. Ozawa, Uncertainty relations for noise and disturbance in generalized quantum measurements, Ann. Phys. (N.Y.) **331**, 350–416 (2004).

[4] K. Okamura and M. Ozawa, Measurement theory in local quantum physics, J. Math. Phys. **57**, 015209 (2016), doi: 10.1063/1.4935407.

[5] K. Okamura, Measuring processes and the Heisenberg picture, (2018) arXiv:1511.09228 [math-ph].

ドレスト光子の局在性を理解する為の数理モデルの検討

On a mathematical model describing the localization property of dressed photons

○ 安藤 浩志 (千葉大理)

○Hiroshi Ando

E-mail: hiroando@math.s.chiba-u.ac.jp

ドレスト光子はナノメートル寸法の領域で電子や電子・正孔対と光子が結合して出来た準粒子であり, 自由空間を伝搬する光とは本質的に異なる振る舞いを示す. またその性質が伝搬光を用いては実現できなかった様々な光デバイスの設計に活用されている [8]. その性質の数理的側面を研究する事は大切であるが, その為に量子化された電磁場とナノ寸法の結晶中の電子等との相互作用を記述する理論が必要である [1, 2]. 形式的には量子化された電磁場は無限個の調和振動子の集まりの様に見えるが, そこには無限自由度の力学変数を持つ系の量子化を考えると現れる非同値な表現達を考察する必要が現れ, 具体的モデルを構築し, その解析を行う事と並行して作用素代数的考察も重要になる [3, 4, 6, 7]. またドレスト光子の存在を直接観測す事は出来ず, 伝搬光の散乱の様子からその様子を推測する必要性から, ミクロ・マクロ双対性の観点が鍵となる [6]. 本講演では電磁場の作用素のつくる代数系の性質を調べ, そこから局在するという性質をどのように導く事が可能かを検討する. 巨視的物質と電磁場に囲まれたナノ物質間のドレスト光子を介した相互作用は [5] により, 湯川関数で与えられる有効ポテンシャルの形をしている事が示されている. 本講演では作用素代数の観点からドレスト光子の有効相互作用の形について議論し, [5] との関連について, 分かった事を報告する.

謝辞

本研究は (社) ドレスト光子研究起点の助成を受けています.

参考文献

[1] 新井朝雄, フォック空間と量子場 上・下 (日本評論社), 2000.

[2] 新井朝雄・河東泰之・原隆・廣島文生, 量子場の数理 (数学書房), 2016.

[3] Ola Bratteli and Derek William Robinson, Operator Algebras and Quantum Statistical Mechanics I, II (Springer), 1986.

[4] Rudolf Haag, Local quantum physics (Springer), 1992.

[5] K. Kobayashi and M. Ohtsu, J. Microscopy 202, 279 (2001).

[6] 岡村和弥・小嶋泉, 無限量子系の物理と数理 (SGC), 2013.

[7] 小嶋泉, 量子場とミクロ・マクロ双対性 (丸善出版), 2013.

[8] 大津元一, ドレスト光子 (朝倉書店), 2013.

量子確率論の見地からみたドレスト光子

Dressed Photons from the Viewpoint of Quantum Probability

○ 西郷　甲矢人 (長浜バイオ大学)

○Hayato Saigo (Nagahama Institute of Bio-Science and Technology)

E-mail: h_saigoh@nagahama-i-bio.ac.jp

ドレスト光子 (Dressed Photon, DP）[4] は、ナノスケールにおける光と物質の相互作用において新規に発見された多くの現象を理解するために不可欠な概念である。この概念は、物理学および一般的な工学における基本概念についての再吟味を促す。特に、「合成系」の概念およびミクロ・マクロの関係の定式化の概念的・数学的発展に役立つと考えられる（その際、「ミクロ・マクロ双対性」[5] の考えが重要な指針となる)。

本講演では、ドレスト光子の数理物理学的側面を、量子確率論（Quantum Probability)[1, 3] という観点から考察する。量子確率論は、コルモゴロフが定式化した現代の（古典）確率論 [2] と、量子論の双方をその一部として包含する、「一般化された確率論」の枠組みである。

講演者は、酒匂宏樹博士（新潟大学）とともに、量子古典対応の数理をこの量子確率論の枠組みでとらえる研究を行ってきた [6]。その結果、量子古典対応における「逆正弦法則」とよばれる確率分布が果たす重要な役割が明らかになってきた。さらにこの間講演者は、この数理がドレスト光子の理解にも役立つことを発見し、現在その内容を深化させつつある。

本講演では、ドレスト光子を量子確率論を通じてとらえることにより、この逆正弦法則がドレスト光子現象においても重要な役割を果たすことを示す。その応用として、ドレスト光子が「尖端」に生ずる機構の普遍的な理解と、そこから示唆される新しい現象の予言について提起する。

Acknowledgments

本研究は（社）ドレスト光子研究起点の助成を得た。また、本研究の一部は JST CREST(JPMJCR17N2)、JSPS 科研費 (JP17H01277)、Core-to-Core の支援を受けた。

参考文献

[1] 明出伊類似 (L. Accardi), 尾畑伸明: 量子確率論の基礎 (牧野書店, 東京 2003)

[2] A. Kolmogorov: *Grundbegriffe der Wahrscheinlichkeitsrechnung*(Springer, Berlin 1933)

[3] A. Hora, N. Obata: *Quantum Probability and Spectral Analysis of Graphs* (Springer, Berlin Heiderberg 2007)

[4] M. Ohtsu: *Dressed Photons* (Springer, Berlin Heidelberg 2014)

[5] I. Ojima: *Proc. Intern. Conf. of Stochastic Analysis*, ed. by T. Hida (World Scientific, 2005)

[6] H. Saigo, H. Sako: Ann. Inst. Henri Poincaré Comb. Phys. Interact. **3**, 405 (2016)

第79回応用物理学会秋季学術講演会 講演予稿集 (2018 名古屋国際会議場 (愛知県名古屋市))

波長変換膜を目的とした EVA 樹脂への酸化亜鉛量子ドット−色素分散手法の開発

Development of dispersing method of ZnO quantum dots and dye in EVA resin for wavelength conversion film

電機大[1]，ナノフォト推進機構[2] ○野村 航[1]，山岸 亙[2]，川添 忠[1]

TDU[1], NPEO[2] ○Wataru Nomura[1], Wataru Yamagishi[2], Tadashi Kawazoe[1]

E-mail: wnomura@mail.dendai.ac.jp

我々の研究グループではこれまでに光波長変換膜として、酸化亜鉛量子ドット(ZnO-QD)と有機色素を含有するシリコーン樹脂膜の製造手法を確立し、結晶系 Si 太陽電池のエネルギー変換効率向上や紫外光を白色光に変換する薄膜の作製と評価を行ってきた[1,2]。これは ZnO-QD から色素分子へドレスト光子を介したエネルギー移動[3]が起こることで高効率に光の波長変換が行われるもので、紫外光から可視光への変換において 90%以上の量子効率を達成している。今回、同原理に基づく波長変換材料の適用範囲をより広げるべく、透明性や耐候性に優れ接着剤などに応用可能なプラスチック材料であるエチレン酢酸ビニル共重合体(EVA)樹脂のペレットに ZnO-QD と色素を分散させる手法を開発したのでこれを報告する。

実験のための EVA ペレットには東ソー(株)ウルトラセン 710 を用いた。ペレット形状を破壊しない変換膜の作製プロセスとして、まずトルエン中で亜鉛錯体と過酸化水素水を常温で混合し、反応熱のみで ZnO-QD の前駆体を作製した。この前駆体溶液に EVA ペレットと色素(Exciton 社、Coumarin 545)を混合し静置することで、膨潤した EVA に ZnO-QD と色素を内包させることに成功した。また比較のため同手法で色素のみを内包させたペレットも作製した。

作製した試料と、QD、色素を含有させる前の EVA ペレットの外観写真を Fig.1a に示す。色素を含む 2 試料は白色光下ではほぼ同等の外観を示し、内包する色素量も同程度と考えられるが、Fig.1b に示す水銀ランプ照射下では ZnO-QD を内包する試料がより明るい蛍光を示した。分光蛍光光度計(日本分光(株)、FP-8300)により取得した蛍光スペクトルを Fig.2 に示す。赤線で示す ZnO-QD を内包する試料では 525 nm のピークが強調され、特定のエネルギー準位からの発光強度が増加したことから、これは ZnO-QD からのエネルギー移動を示す結果と言える。

参考文献 [1] 山岸他、2016 年秋応物講演会、16a-B12-6、 [2] 川添他、2017 年秋応物講演会、15a-F202-10、 [3] 大津元一著「ドレスト光子」朝倉書店(2013)

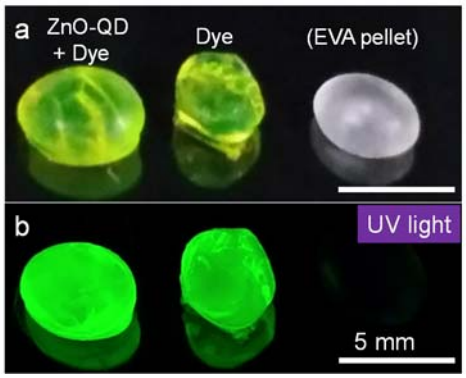

Fig.1 Photos of EVA pellets under (a) white light and (b) mercury lamp.

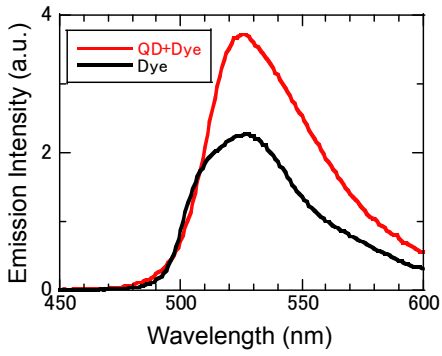

Fig.2 Emission spectra of wavelength conversion resins.

第79回応用物理学会秋季学術講演会 講演予稿集 (2018 名古屋国際会議場 (愛知県名古屋市))

積層型 Si-LED の作製と評価

Fabrication and demonstration of stacked Si-LED connected in series

電機大[1], NPEO[2], ○川添 忠[1]、橋本和信[2]、杉浦聡[2]
TDU[1], NPEO[2], ○T. Kawazoe[1], K. Hashimoto[2], S. Sugiura
E-mail: kawazoe@mail.dendai.ac.jp

我々はドレスト光子フォノン(DPP)アニールによって間接遷移型半導体であるシリコン(Si)を用いた発光素子の開発を行っている[1-5]。Si の pn 接合における電子正孔再結合による発光は極めて弱い。これは Si の伝導体の底と価電子帯の頂上の電子の波数が大きく異なり、光子放出の際満たされるべき波数保存則が成り立たないからである。DPP アニールにより特定の規則性を持つドーパント対を Si 結晶中に形成するとこの性質は変化する。ドーパント原子は周囲の Si 原子と質量の異なり格子振動(フォノン)の反射境界となる。その結果、2つのドーパント対には特定のモードのフォノンが局在する。この局在フォノンの波数が Si の伝導体の底と価電子帯の頂上の波数の差と一致する場合、ドーパント対周辺の電子正孔対はフォノンから波数を受け取り光子を放出する。

DPP アニールでは外部から照射する光による誘導放出を利用している。このため、作製された LED はレーザーのような閾値特性を示す。通常の使用にはこの閾値の存在は障害にはならないが、例えば細かなパワー調整が必要な場合、PWM 制御等が必須になること、閾値の存在が発光強度の不安定性をもたらすことなどが危惧される。今回の発表では非常に微小な Si-LED を積層した素子試作し、通常の動作範囲には閾値が現れないことを確認したので報告する。

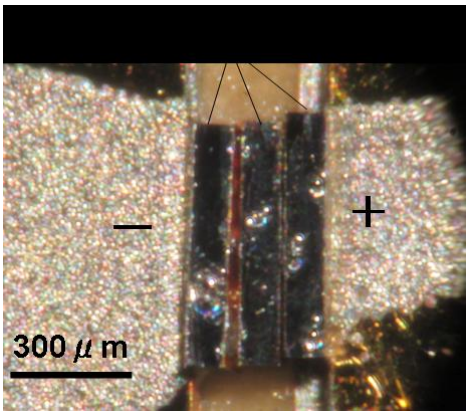

Fig.1.

Fig.1.に今回作製した素子の拡大写真を示す。1つの Si チップサイズは 1mm×0.2mm×0.1mm である。3 つの素子を直接接触させて並べ直列接続させる方法で作製した。Fig.2 に作製した素子の電流電圧特性および DPP アニール後に撮影した発光の赤外写真を示す。また Fig.2 の写真に示すように DPP アニール後には素子間の出力光強度の大きなバラツキは見られなかった。

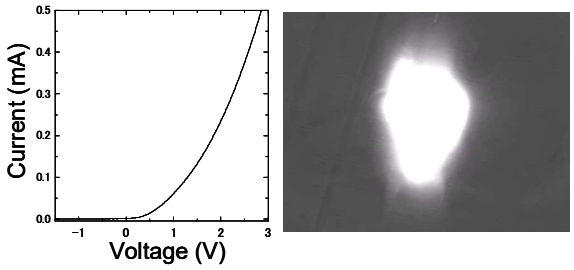

Fig.2.

Fug.3 に光出力の注入電流依存性を示す。従来の Si-LED のように指数関数的な閾値は見られず、比較的滑らかな立ち上がりになった。この理由は素子が 3 つの領域に分断されているため、誘導放出の影響が小さくなったためだと思われる。

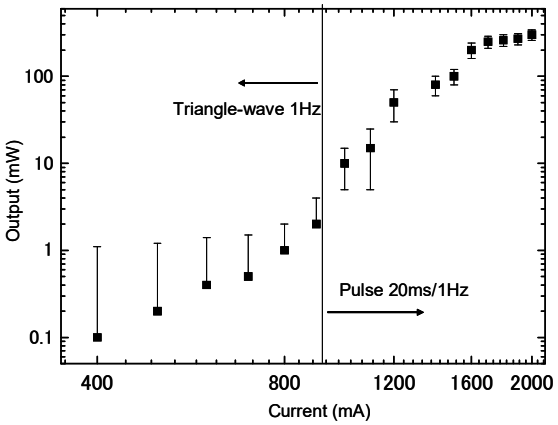

Fig.3

[1] T. Kawazoe & M. Ohtsu, Appl. Phys. A, **115**, 127-133, (2014).
[2] T. Kawazoe, et al., Appl. Phys. B-Lasers and Optics, **98**, 5-11 (2010). also **107**, 659-663 (2012).
[3] H. Tanaka, et al., Appl. Phys. B-Lasers and Optics, **108**, 51-56 (2012).
[4]Y. Tanaka, K. Kobayashi, J. Microscopy **229** 228-232(2008).
[5] 川添忠、橋本和信、杉浦聡、大津 元一、2017年第 78 回秋季応用物理学会、福岡 講演番号 7a-A405-5.

高出力ホモ接合シリコンレーザー

High power Homojunction Silicon Laser

電機大[1], NPEO[2], ○川添 忠[1]、橋本和信[2]、杉浦聡[2]
TDU[1], NPEO[2], ○T. Kawazoe[1], K. Hashimoto[2], S. Sugiura
E-mail: kawazoe@mail.dendai.ac.jp

我々はドレスト光子フォノン(DPP)アニールによって間接遷移型半導体であるシリコン(Si)を用いたLED，レーザーなど発光素子の開発を行っている[1-3]。これらの素子は通常の直接遷移過程半導体を用いた素子とは異なり発光遷移過程はドレスト光子フォノンと呼ばれる中間状態を介する。

通常の pn 接合 Si では注入電流による発光は極めて弱い。注入された電子と正孔のエネルギーは非発光再結合する。これは Si の伝導体の底と価電子帯の頂上の電子の波数が大きく異なり、光子放出の際満たされるべき波数保存則が成り立たないからである。ここで特定の規則性を持つドーパント対が Si 結晶中に存在すると状況は一変する。周囲の Si 原子と質量の異なるドーパント原子は格子振動すなわちフォノンの反射境界となる。その結果、2つのドーパント対には特定のモードのフォノンが集中する[4]。この局在フォノンの波数が Si の伝導体の底と価電子帯の頂上の波数の差と一致する場合、ドーパント対周辺の電子正孔対は速やかにフォノン散乱され光子を放出すると予想される。このような特異なドーパント対配列を作り出す方法は DPP アニールと呼ばれる[1-3]。

DPP アニールされた Si の pn 接合部はレーザーの活性層としても機能する。前回、この DPP アニールの効果を大きくするためにこれまで用いていたドーパント種を変更し、原子の質量数の Si との違いがより大きな新しいドーパントを用いて Si レーザーを作製した(Fig.1)[5]。

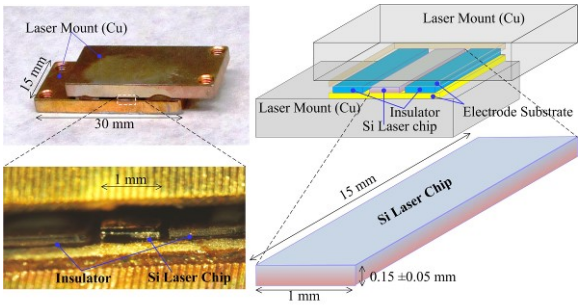

Fig.1

その結果、これまでよりも低い電圧で動作する Si レーザーの動作検証に成功した。Si レーザーチップは閾値以下でチップ全体が発光し、やがて閾値付近でその一部が輝点のように発光を強める。さらに電流を増やすと素子全体のレーザー発振が確認される(Fig.2)。

Fig.2

Fig.3 にドーパント種や構造の異なる 4 種の Si レーザーの光出力に対する注入電流依存性を示す。この結果から素子長を 30mm に増やし、素子冷却の強化やパルス動作にする事で注入電流を 3～5 倍に増やすことが出来れば 100W 級の Si レーザーが実現可能であることが分かったので、作製した素子長 30mm の Si レーザーについて動作報告を行う予定である。

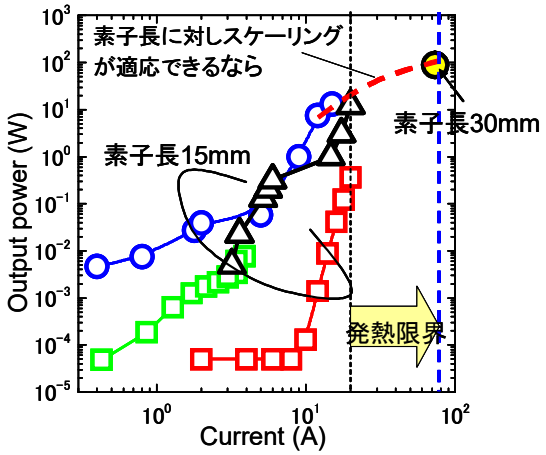

Fig.3

[1] T. Kawazoe & M. Ohtsu, Appl. Phys. A, **115**, 127-133, (2014).
[2] T. Kawazoe, et al., Appl. Phys. B-Lasers and Optics, **98**, 5-11 (2010). also **107**, 659-663 (2012).
[3] H. Tanaka, et al., Appl. Phys. B-Lasers and Optics, **108**, 51-56 (2012).
[4]Y. Tanaka, K. Kobayashi, J. Microscopy **229** 228-232(2008).
[5] 川添忠、橋本和信、杉浦聡、大津 元一、2017 年第 78 回秋季応用物理学会、福岡 講演番号 7a-A405-5.